Oceanographic Information for Engineering Submarine Cable Systems*

By C. H. ELMENDORF and BRUCE C. HEEZEN

(Manuscript received June 4, 1957)

Information on the environment in which submarine cable systems are placed is of vital interest in designing, selecting routes for, placing, and repairing this type of communications facility. Existing data are summarized and evaluated, and their application to submarine cable systems is considered.

I. INTRODUCTION

1.1 *General*

Oceanography, broadly defined, includes the study of all aspects of the oceans. As a science, it is concerned with gathering data and devising theories which describe and explain the past, present, and the future of the oceans. Oceanography includes physical description of the topography, sediments, and temperature of the ocean bottom; investi-

---

* This is Lamont Geological Observatory Contribution No. 251. Dr. Heezen is a member of the Lamont Geological Observatory of Columbia University. Additional information on this subject is being presented by Dr. Heezen in a publication by the Geological Society of America.

gation of currents and circulation; study of the geology of the earth's crust under the ocean; and investigation of biological factors.

In designing, in finding the best route for, in laying, and in repairing a submarine cable system one can benefit from as detailed a knowledge of the ocean floor as can be obtained. However, the vastness, complexity, and inaccessibility of the ocean bottom make its study difficult. One must depend on limited data, interpreted with the aid of a knowledge of the earth sciences. The acquisition of specific engineering information is further complicated by the inaccuracies of much of the existing data, and the rudimentary nature of many present theories. Yet, by culling, codifying, interpolating, and interpreting the data gathered during the past hundred years, much can be learned that is applicable to particular cable routes. Further, methods now exist for surveying and describing a route with a thoroughness and accuracy that will permit many refinements in the engineering of future submarine cable systems.

In this paper specific problems of immediate interest in the engineering of submarine cable systems are discussed in order to give a perspective of the use of such data in current applications. Emphasis is placed on the state of existing knowledge and on the accuracy of available data. The work reported forms a foundation for more detailed studies of specific routes and for the application of knowledge which will be derived from rapidly expanding oceanographic studies to the particular problems of submarine cable systems.

1.2 *Application To Submarine Cable Systems*

How are oceanographic information and technique applied in the selection and description of the detailed path of a new cable? First, variations on a direct route must be examined to avoid ocean bottom conditions which may result in cable failures. Studies of telegraph cable fault records indicate that many of the deep sea cable breaks occur where cables pass over sea mounts, canyons and areas susceptible to turbidity currents, and an effort must be made to avoid such hazards. Topographic studies form the basis for both initial route selection planning and for a preliminary description of the selected route.

This description will include, where data are available, an exaggerated depth profile uncorrected for angle of the sound beam of the sonic depth recorder, a corrected 1:1 depth profile where necessary, and a temperature profile. Also, bottom characteristics, including photographs, can be collected for the particular route. These data will be essential in planning a detailed survey of the route, and they will provide

preliminary information for the determination of the amount of cable required, for system transmission planning and for studies of cable-placing techniques.

One of the fundamental requirements in cable laying is the deposit of a sufficient amount of cable to cover irregularities of the bottom without introducing dangerous suspensions and without laying a wasteful amount of excess slack. Satisfaction of this requirement will require the most detailed possible knowledge of bottom topography, coupled with knowledge of the kinematics of the cable laying process.[1]

A determination of required cable strength does not directly call for an extremely accurate knowledge of bottom depth and contour. The required cable strength is determined by cable tension during recovery, which is two or more times that experienced during laying. Although the required strength is directly proportional to the depth, it is also affected to a major degree by the ship speed, cable angle during recovery, and the ship motion caused by waves. The ship motion can be controlled to some extent by seamanship and choice of the time at which the recovery is to be made.

Further, the design strength of the cable is in large measure determined by the strength of available steel and the amount of steel that can be accommodated in an economical over-all design. Thus, uncertainties of 5 to 10 per cent in the maximum depth of the water on a route would not affect the cable design. Yet, during a critical recovery situation, a more accurate knowledge of depth would be useful in planning and executing the operation.

The integrity of the cable will depend on the choice of materials to withstand biological factors and wear on the ocean bottom. A companion paper[2] discusses the resistance of likely cable-sheath materials to attack by marine borers and bacteria.

II. TOPOGRAPHY

2.1 *General*

Mapping the ocean bottom involves depth measurements coupled with a knowledge of the location on the earth's surface of the points at which these measurements are made. There exists a vast store of data on the depths of the oceans taken by hundreds of observers and expeditions over the past hundred years. It is not surprising that many of these data are of questionable accuracy due to errors in navigation, soundings, plotting, and interpretation. Thus, before existing data can be used for the engineering of submarine cable systems, it is essential

TABLE I — MARINE NAVIGATION SYSTEMS

Name	Description	Range	Accuracy	Coverage
LORAN	Measures time difference between pulses transmitted by two or more shore station groups.	900 miles*	$\pm\frac{1}{2}$ mile at short range	Good over N. Atlantic steamer routes; spotty elsewhere.
SHORAN	Radar system: shipboard equipment triggers two shore stations to determine position.	Line of sight	±50 feet	Nil
DECCA NAVIGATOR	Measures phase difference in continuous waves transmitted by two or more shore stations.	240 miles	±100 yards	Good around British Isles practically nil elsewhere.
LORAC	Measures phase difference in continuous waves transmitted by three shore stations.	100 miles	±50 yards	Used as a temporary installation for special purposes.
CONSOL	Radio determination of great circle bearing of transmitting station.	1500 miles	±0.2° to 1°	Eastern North Atlantic
SOFAR	Experimental underwater sound system; shore stations determine distance to under-water explosion.	4000 miles†	±4 miles	Eastern Pacific only
E. P. I.	An electronic position indicator which measures distances from ship to each of two shore stations, using a pulse technique.	350 to 500 miles (max.)	±75 yards (in measured distances)	Developed by U.S.C. & G.S. for surveying purposes, temporary installations.
TACAN	Provides range and bearing from transmitter.	Line of sight	Range $\pm\frac{1}{2}$ mile, bearing $\pm\frac{3}{4}°$	Experimental only

* Ground wave; Sky wave range up to 1400 miles with decreased accuracy (15 miles at max. range).
† Range limited by size of basin and topographic obstructions.

that it be compiled, evaluated, and culled with due regard for the sources, inherent errors, and possible misinterpretations. The data remaining after this type of review can then be combined with other knowledge from the earth sciences to provide the best available maps and profiles.

2.2 *Instrumentation for Topographic Studies*

2.2.1 *Navigation*

Celestial navigation, depending on hand sextant sights of heavenly bodies and subsequent solution of an astronomical triangle, is the only method available in all parts of the world. It is, of course, useless during periods of poor visibility. Positional accuracy of $\pm\frac{1}{2}$ mile can be obtained, although the usual accuracy is ± 2 to 5 miles. During the interval between sights, an estimated position is computed by dead-reckoning methods, assuming the ship's speed and course to be known. Speed determined by propeller revolutions or by a pitometer log is subject to the influence of winds, seas, and currents. The ship's heading is indicated by compass, but the course actually traveled by the vessel is affected by all the same variables that affect the speed. Starting from a celestial or radio fix, a good navigator can plot a dead-reckoning track with little error over short periods of time under ideal conditions. The probable error increases rapidly with elapsed time under less than ideal conditions.

Some of the existing radio navigational systems and their limitations are listed in Table I.

2.2.2 *Echo Sounding Errors and Corrections*

Present-day echo sounders, operating with a total beam angle of about 60 degrees, indicate the distance to the best reflectors within the effective cone of sound. Neglecting scattering layers, which can usually be eliminated from consideration by interpretation, the best reflector will coincide with the bottom immediately below the transducer if the bottom is horizontal or if the highest point on the bottom is immediately below the transducer. Under any other condition the echo sounder indicates less than the true depth. Where the bottom is very uneven or rocky, a multiplicity of echoes are returned and recorded. These considerations necessitate careful evaluation of the data and its correction for slope.

Since the echo sounder actually measures the time interval between transmission of a pulse and receipt of an echo, the timing mechanism

is the heart of the indicating and recording equipment. However, many types of echo sounders have poor timing mechanisms which depend upon mechanical governors, poorly regulated AC power supplies, and friction drives. Recently, a Precision Depth Recorder (PDR) having an instrument accuracy of better than one fathom in 3,000 has been developed.[3] The equipment is used with standard deep-sea sounding equipment. This PDR will perform the timing function with an accuracy better than one part in a million.

After obtaining a record of the time between the outgoing and received pulses the data must be converted to depth, employing velocity corrections and slope corrections. True sound velocity is obtained by
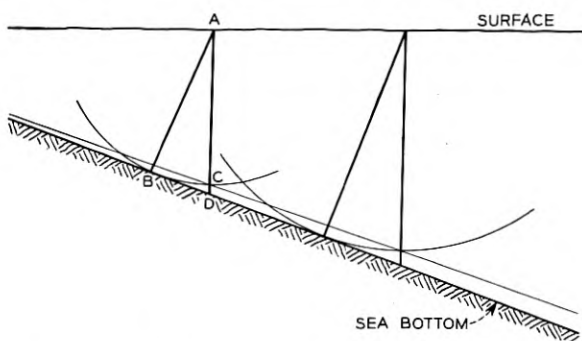

Fig. 1 — Slope correction of echo soundings.

reference to tables, or by computation based on simultaneous sea water temperature and salinity measurements. The distance traveled by the echo, obtained from the velocity-corrected data, is converted to depth by the slope correction.

The PDR sends out a ping and records an echo once each second. If the sounding vessel is under way at 10 knots, the individual soundings are about 17 feet apart. When the outgoing ping exactly coincides with the returning echo, a gating circuit reduces the frequency of soundings to once in 2 seconds corresponding to a spacing of about 34 feet at 10 knots.

Fig. 1 illustrates the problem of slope correction on an ideal slope, where the ship is steaming at right angles to the slope. At sounding position A, the echo is returned from B, the nearest point on the bottom. On the uncorrected profile, this would be interpreted as a vertical sounding AC. To obtain the true vertical depth at A, an amount CD must

be added to the depth read from the echo trace. This is done graphically by swinging arcs representing the echo distances, using the distance between soundings as the arc center spacings. The envelope of a succession of such arcs is the best approximation to the actual bottom configuration that can be made. This method, of course, requires that the sounding track be run approximately at right angles to the slope, and thus, that the trend of the topography be determined. In addition, when the relief becomes more complicated, constructing and interpreting the envelope becomes much more difficult. Although all hills are shown on echograms, small valleys are often completely missed because their width is much less than the breadth of the cone of sound. This problem is partly eliminated by the use of a PDR, where second echoes indicate the existence of valleys not recognized on standard echo sounders.

Fig. 2 (a) shows the trace made by a PDR in passing over a rugged slope in mid-Atlantic. The multiple echo on the left hand side of the figure illustrates how echoes from the wide sound cone are returned from different parts of a steep slope. Similarly, the multiple echoes in the center show a deep valley with energy from the same pulse reflected from the steep slopes as well as the bottom. Fig. 2 (b) shows a corrected profile constructed from the echogram illustrated in Fig. 2 (a), and Fig. 2 (c) is a profile of the same track with 40:1 vertical exaggeration, which is typically used in describing bottom topography.

To construct a profile and interpret each sounding taken would require a prohibitive amount of work. Thus, in preparing contours and uncorrected profiles for ordinary mapping purposes, a sufficient number of the initial echoes are taken to allow a reasonably accurate profile to be constructed. Where 1:1 corrected profiles are required, all the echoes are used and the best possible envelope representing the bottom is constructed.

2.3 CHARACTERISTICS OF AVAILABLE INFORMATION

2.3.1 *Sources of Data*

The vast majority of data for a study of submarine topography are obtained as a series of "soundings," or depths below sea level.* Prior to the development of echo sounding apparatus, soundings were made by measuring the length of either a weighted piano wire or hemp line which was lowered to the bottom. This method of line or wire sounding

---

* Features to be studied by detailed soundings can often be located by measurements of the earth's magnetic and gravitational fields and by acoustic methods.
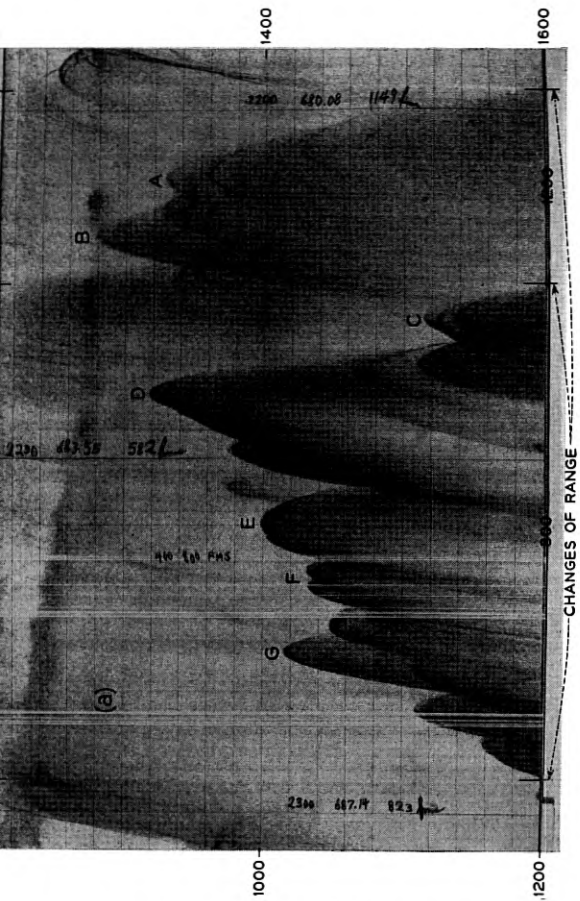
Fig. 2 — (a) Precision-Depth-Recorder record of a peak in the Mid-Atlantic Ridge. Record shows multiple 400-fathom scales. On original record 400-fathom range is represented by 18 inches and one hour or about 10 miles by 24 inches. Light horizontal lines are at 20-fathom intervals. (b) Same profile with no vertical exaggeration, with corrections for slope. (c) Profile at 40:1 exaggeration plotted from first echoes shown in (a).

1054
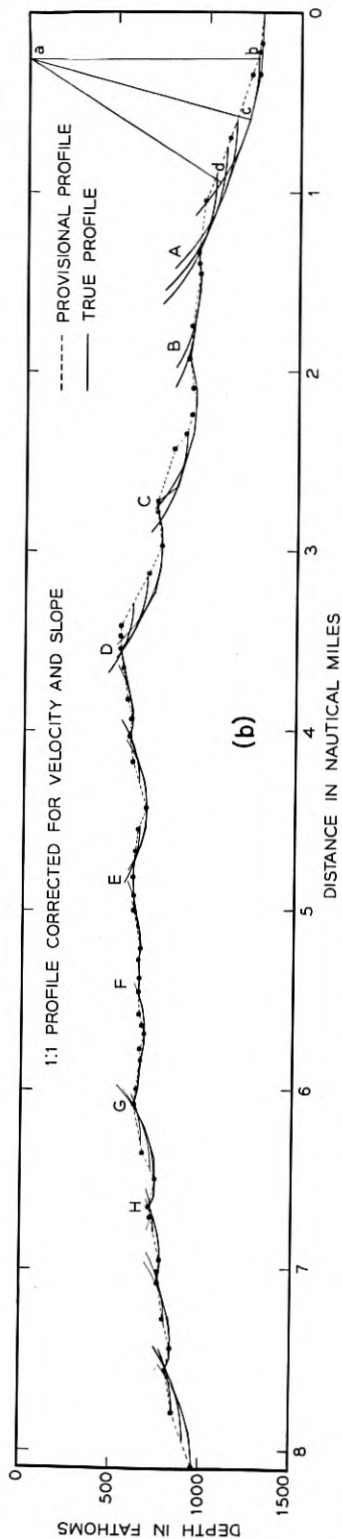
was fraught with error because there was no adequate sensing device to indicate when the bottom was reached, and because the sounding line might be swept far from a true vertical by the action of currents between the surface and the bottom. These difficulties could cause errors as great as 50 per cent. Echo sounding was thus a tremendous improvement despite its own inherent inaccuracies.

Ocean bottom soundings are available from a number of sources including, in this country, government agencies such as the Navy's Hydrographic Office and the U. S. Coast and Geodetic Survey, and private oceanographic institutions. Abroad, national hydrographic offices, such as the British Admiralty's Hydrographic Department, the Japanese Hydrographic Office, and the International Hydrographic Bureau, collect and publish soundings.

Depending upon the organization which compiles the soundings, various corrections are applied to the raw data, each organization selecting both the corrections it wishes to apply and the method of application. If all soundings for an area off the continental shelf of the United States were compiled, there might be available soundings in feet, corrected for velocity, supplied by the U. S. Coast and Geodetic Survey; uncorrected soundings in fathoms supplied by the U. S. Navy Hydrographic Office; similar soundings supplied by Lamont Geological Observatory; corrected soundings in fathoms supplied by the British Admiralty; and corrected soundings in meters supplied by the International Hydrographic Bureau. In addition, there would be a quantity of hemp, wire and discrete echo soundings on published charts. One difficulty in using the soundings printed on the published charts arises from the fact that hemp line, wire, and echo soundings of all types, both corrected and uncorrected, are all plotted on the same chart usually without designation as to method or corrections.

Table II summarizes the methods of presenting sounding data used by various agencies.

Several methods of recording continuous depth records are used. The most common, and least satisfactory, is to read the echo sounder and plot the sounding at the appropriate point on the chart at discrete intervals, say every 10 or 20 minutes. This achieves an orderliness in printing but has the disadvantage that canyons, mountains, or other features which cannot be adequately represented by such spacing are ignored and obscured in the plotted soundings. Better results are obtained by use of the "texture method," where soundings are recorded at each crest, valley, or change of slope, and soundings at uniform time intervals are only used in areas where a continuous slope extends for

TABLE II — METHODS OF PRESENTING SOUNDING DATA

Source	Depth Units	Sounding Velocity	Velocity Correction	Slope Correction
Coast and Geodetic Survey, U. S. Dept. of Commerce............	Fathoms	820 or 800 fm/sec	Note A	Note B
Hydrographic Office, U. S. Navy...	Fathoms	800 fm/sec	No	No
Lamont Geological Observatory......	Fathoms	800 fm/sec	No — Note E	No — Note E
British Admiralty Hydrographic Dept.............	Fathoms	820 fm/sec	Yes — Note C	No
International Hydrographic Bureau.............	Meters	Note D	Yes	Note D
Japanese Hydrographic Office....	Meters	1500 meters/sec	?	?

1. All agencies use Mercator projection charts.

2. All deep sea soundings on 4″ = 1° longitude charts; various larger scales used near shore.

A. USC & GS usually makes velocity correction according to data taken at time of sounding.

B. USC & GS makes slope and drift corrections where deemed necessary.

C. Admiralty data velocity corrections are made according to D. J. Matthews.[4]

D. International Hydrographic Bureau takes no data of its own, but publishes data received from various surveyors.

E. Although corrections are made in surveys of specific areas, soundings are first compiled in uncorrected form.

many miles. This produces an uneven spacing of numbers on the chart, and in some areas the soundings have to be crowded together to show all crests and valleys. In this method the sounding is written alongside a dot which represents the location of the sounding. Another method is to write the sounding without a dot but centered over the place where the sounding was taken. This produces a more pleasing drawing but all detail must be left out in complicated areas since the physical size of the letters limits the number of soundings that can be so recorded on the chart.

2.3.2 Methods of Evaluation

Evaluation of topographic data starts with a comparison of data from all the different sources, with all the soundings plotted to the same scale on one set of charts. Soundings from different sources must be reduced to a common base.

When the soundings from all sources are compiled on the same sheet, many obvious discrepancies will be noted. A great number of these

cases can be traced to either gross mistakes in plotting or poor accuracy in navigation which may cause errors in position of up to 25 miles. Usually these gross errors are fairly easy to spot. For example, a large shoal area was shown for many years in deep water east of Georgia, but it now appears that this particular shoal resulted from the misplotting, by one-half degree of longitude, of a series of continental shelf soundings.

Lines of soundings from different sources should indicate the same depth at their intersections, providing a check on the reliability of both or an indication that one or both is suspect. Where there is lack of agreement the sounding and navigational methods should be checked in an effort to find a basis for choosing one set of soundings rather than the other. However, without special knowledge about the individual sounding lines, it is often impossible to decide which line is correct. Uncertainties of 2 to 25 miles in position combined with possible errors in depth determination of 10 per cent and possible gross errors in plotting are indicative of the difficulties that may be encountered.

The extent of the coverage of the Atlantic Ocean with precision sounding tracks is shown on Fig. 3. Sounding tracks taken by the Lamont staff prior to the availability of the PDR are shown on Fig. 4.

2.3.3 *Methods of Presentation*

Relief is usually indicated on maps and charts by any one of a number of devices, including contour lines, profile views, and physiographic sketches. In contouring, after surveying a number of control points and obtaining their exact elevations, the land surveyor sketches in the contour lines between control points while standing on a vantage point such that he can actually see the terrain. In contrast, the oceanographer must sketch contour lines by applying his own interpretation of the submarine processes responsible for the relief in the areas between soundings. The accuracy of contour is, of course, determined by both the number, spacing, and accuracy of the soundings, and the skill and knowledge of the oceanographer.

The International Hydrographic Bureau in Monaco publishes a colored contour chart for the entire world on a scale of 1:10 million, individual sheets of which are revised and republished at 10–25 year intervals.

Profiles, or elevation views along particular tracks, provide a detailed outline of the bottom. The usual practice is to construct exaggerated profiles (40:1 or greater vertical to horizontal scale ratio), such as those illustrated in Figs. 2(c) and 5. Where accuracy of the highest order
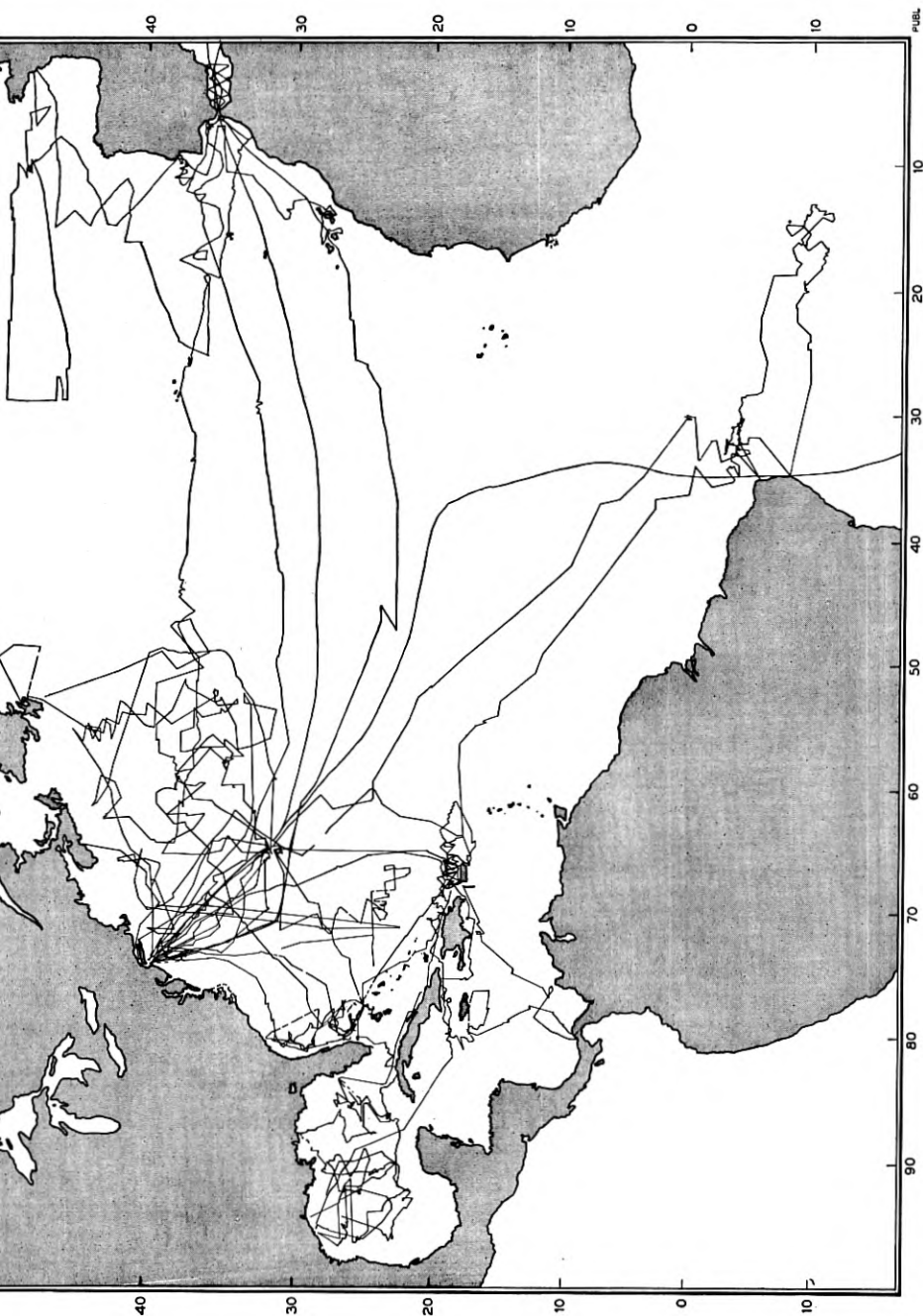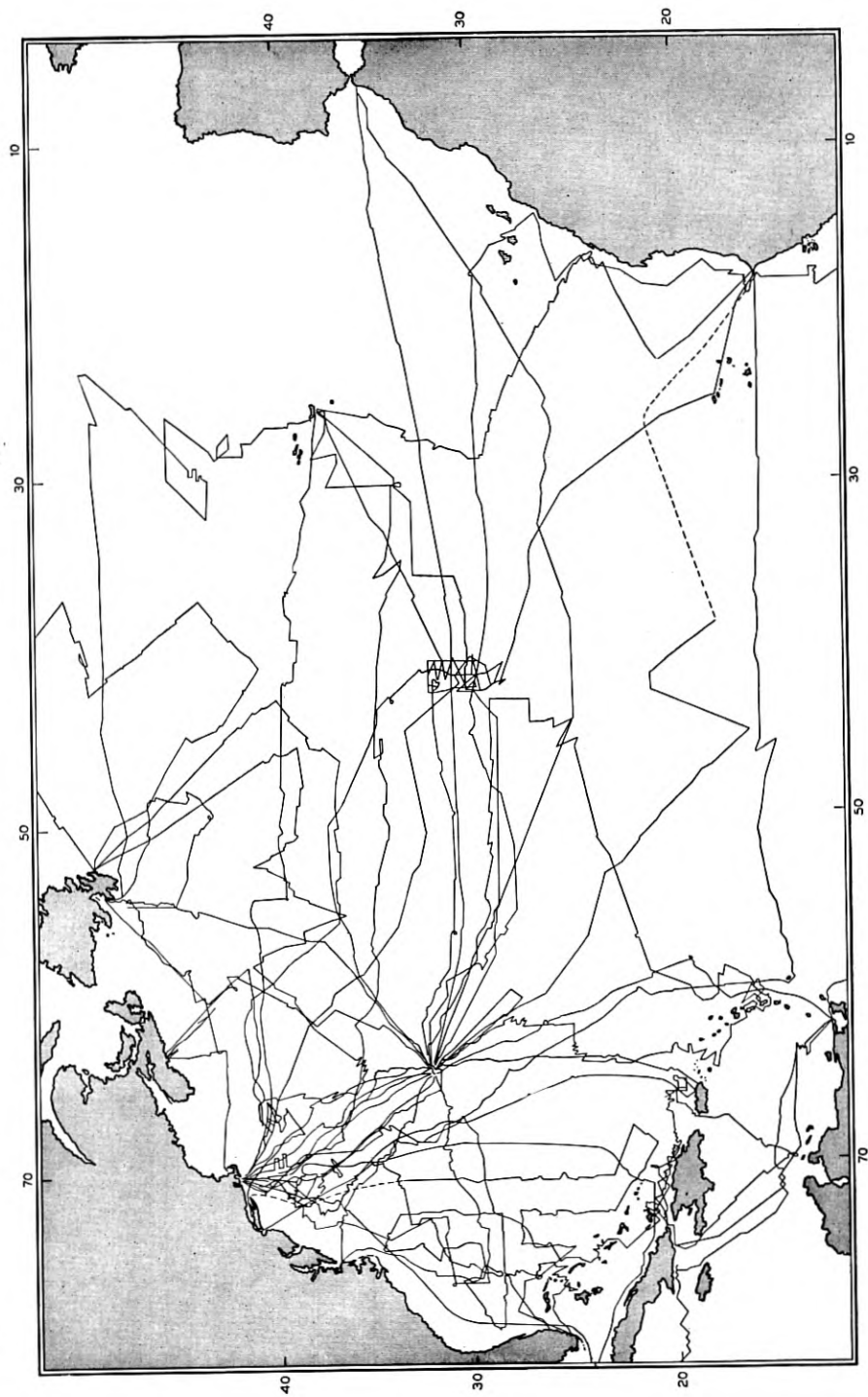
Fig. 4 — Tracks of research vessels employing fairly good but nonprecision depth recorders. Tracks mainly of R. V. *Atlantis*, 1946–1952.
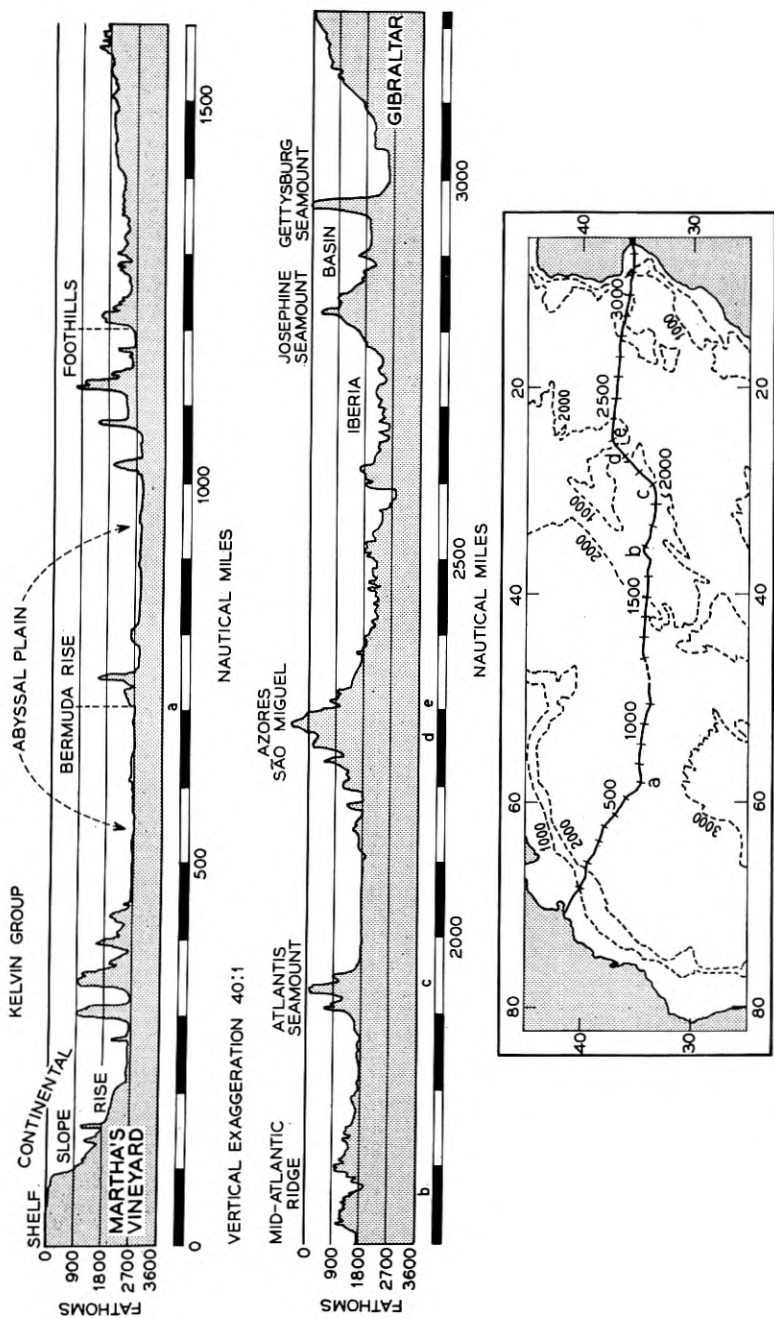
Fig. 5 — Transatlantic topographic profile, Massachusetts to Gibraltar. Vertical exaggeration 40:1.

is required, 1:1 profiles as illustrated in Fig. 2(b) are prepared by careful interpretation of precision depth records and their correction for actual sound velocity and slope.

The physiographic diagram (in envelope inside rear cover) was prepared by combining evaluated and corrected depth measurements with all other ocean bottom and geological information. The construction of these diagrams is preceded by the preparation of 40:1 exaggerated profiles along all available sounding tracks through the region under consideration. After study and evaluation of the profiles, areas of different texture are defined, and the various physiographic provinces are outlined. The relief shown on the profiles is then drawn in perspective view along the appropriate track of the chart. After all available tracks have been drawn, the remaining blank areas are sketched in, basing the interpretation on geological information.

Fig. 6 shows the physiographic provinces of the North Atlantic and the existing submarine cables on a great circle chart. A plot such as this is useful in preliminary studies of new routes. More detailed charts to a scale of 1:1 million showing contours, actual sounding tracks, existing cable routes and cable fault records can be prepared for specific engineering of new cable routes.

2.4 *North Atlantic Topography*

The relief of the continents naturally divides itself into mountain ranges, plateaus, and plains — physiographic provinces which can be recognized by distinct differences in topography, form and texture. Geologists recognize these differences as directly related to underlying geological structures. The topography of the ocean floor can also be divided into physiographic provinces similar to those familiar on land. In general, the relief of the deep sea topography is greater than on land due to the fact that the smoothing effects of erosion are less under the deep sea. Fig. 7 shows the relief along a continuous line extending from Peru across South America and thence across the South Atlantic.

The three major divisions of the Atlantic Ocean — Continental Margins, Ocean Basins, and Mid-Atlantic Ridge — each occupy about one third of the ocean floor. Since detailed topographic information is available for so little of the area covered by the oceans, the following descriptions of the relief must of necessity be general. Where specific details are available, they are presented as examples. The area to be described, the North Atlantic, is well outlined on the Physiographic Diagram. Frequent reference to this illustration should help to make the word descriptions more meaningful.
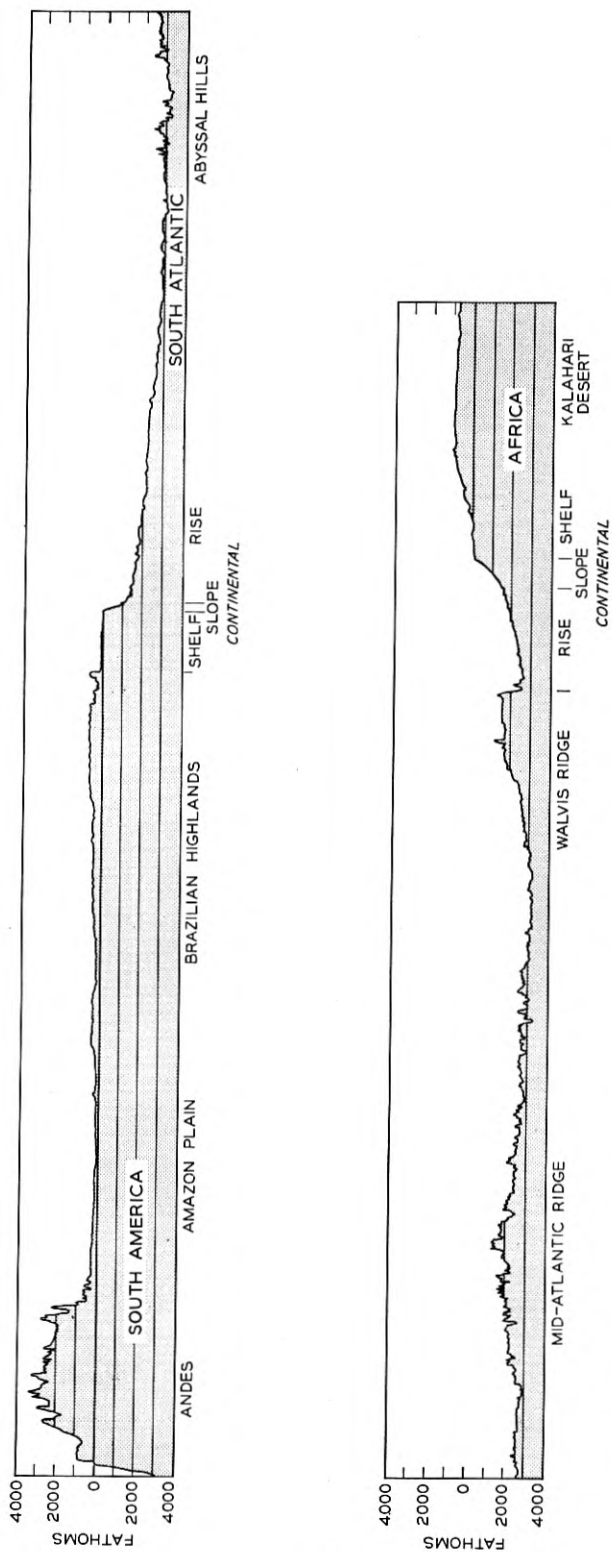
Fig. 7 — Topographic profile from the Pacific across South America and the South Atlantic to Africa. 40:1 exaggeration.
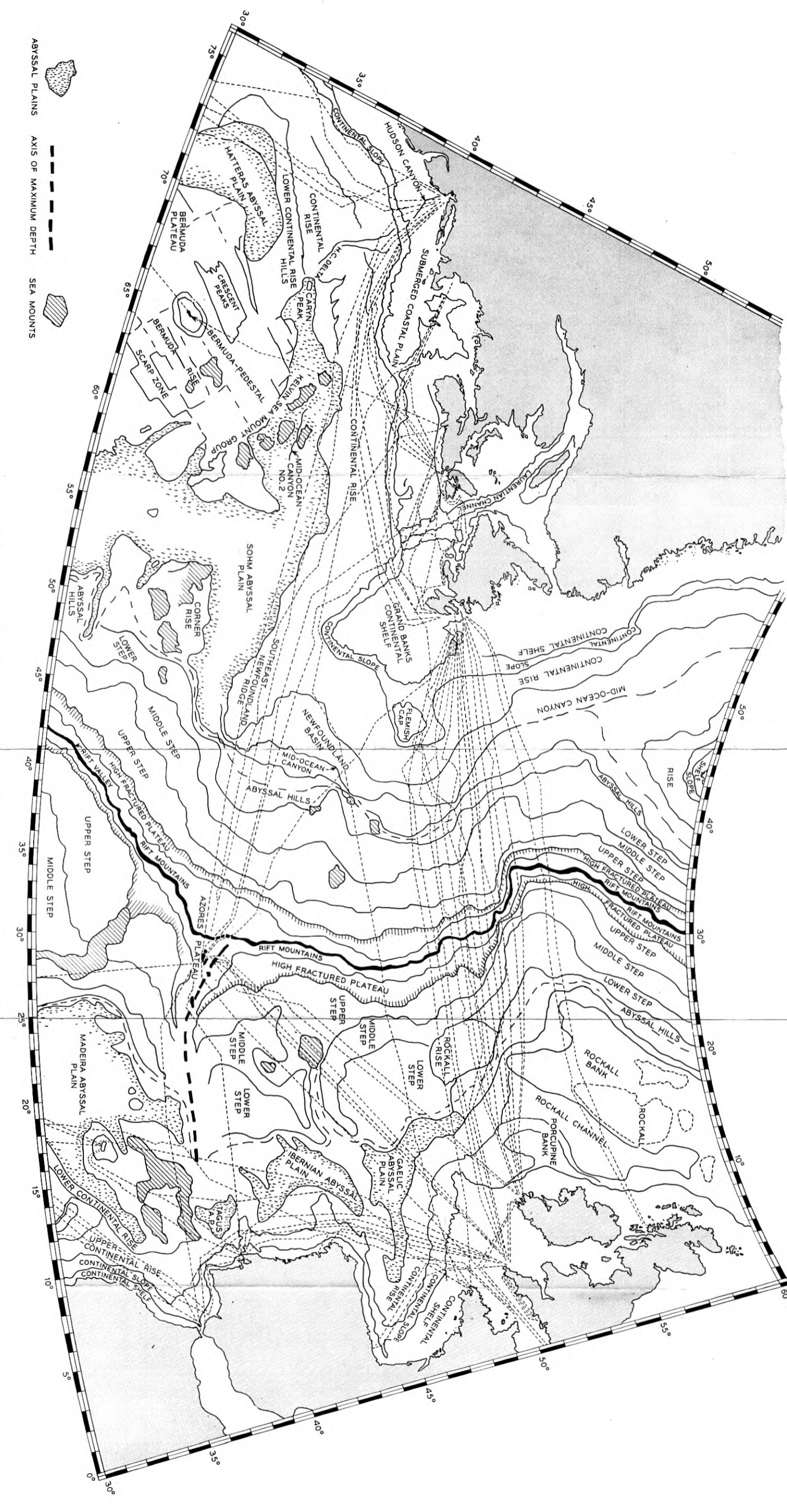
Fig. 6 — Great-circle chart showing physiographic provinces and existing submarine cable routes (dotted lines). (On this chart any straight line represents a great circle.)

Legend:

ABYSSAL PLAINS

AXIS OF MAXIMUM DEPTH

SEA MOUNTS

Map labels:

BERMUDA PLATEAU
HATTERAS ABYSSAL PLAIN
LOWER CONTINENTAL RISE HILLS
CONTINENTAL RISE
CONTINENTAL SLOPE
HUDSON CANYON
SUBMERGED COASTAL PLAIN
CRESCENT PEAKS
CAIRN
KELVIN SEA MOUNT GROUP
BERMUDA PEDESTAL
BERMUDA RISE
BERMUDA SCARP ZONE
MID-OCEAN CANYON NO. 2
CONTINENTAL RISE
LAURENTIAN CHANNEL
ABYSSAL HILLS
LOWER STEP
CORNER RISE
SOHM ABYSSAL PLAIN
SOUTHEAST NEWFOUNDLAND RIDGE
CONTINENTAL SLOPE
GRAND BANKS CONTINENTAL SHELF
CONTINENTAL SLOPE
CONTINENTAL SHELF
CONTINENTAL RISE
MID-OCEAN CANYON
MIDDLE STEP
UPPER STEP
HIGH FRACTURED PLATEAU
RIFT VALLEY
RIFT MOUNTAINS
NEWFOUNDLAND BASIN
MID-OCEAN CANYON
ABYSSAL HILLS
FLEMISH CAP
SHELF SLOPE
RISE
ABYSSAL HILLS
LOWER STEP
MIDDLE STEP
HIGH FRACTURED PLATEAU
RIFT MOUNTAINS
HIGH FRACTURED PLATEAU
UPPER STEP
MIDDLE STEP
LOWER STEP
ABYSSAL HILLS
UPPER STEP
MIDDLE STEP
AZORES
RIFT MOUNTAINS
HIGH FRACTURED PLATEAU
UPPER STEP
MIDDLE STEP
LOWER STEP
ROCKALL RISE
ROCKALL BANK
ROCKALL CHANNEL
PORCUPINE BANK
ROCKALL
AZORES PLATEAU
MADEIRA ABYSSAL PLAIN
MIDDLE STEP
LOWER STEP
IBERNIAN ABYSSAL PLAIN
GAELIC ABYSSAL PLAIN
CONTINENTAL SHELF
CONTINENTAL SLOPE
CONTINENTAL RISE
TAGUS A.P.
LOWER CONTINENTAL RISE
UPPER CONTINENTAL RISE
CONTINENTAL SLOPE
CONTINENTAL SHELF
CONTINENTAL SHELF
CONTINENTAL SLOPE
CONTINENTAL RISE

2.4.1 *Continental Margins*

The first area considered is the continental shelf which may be characterized as the shallow (0–100 fathoms) submarine terrace bordering the continents, extending seaward hundreds of miles in some localities. The shelf terminates where the bottom gradient increases suddenly from the shelf average of approximately 0.1° to the continental slope average of more than 4°. This change occurs in depths ranging from 20 to more than 100 fathoms. The shelf is a continuation of the coastal plain and displays the same numerous small irregularities as the plain. For example, off the United States east coast — from Cape Cod south — the shelf is relatively flat, but with many small (10-fathom) hills and ridges. This shelf varies in width from about 150 miles off Cape Cod to its virtual disappearance off the east coast of Florida. This region of smooth shelf terminates in depths of about 60 fathoms between Cape Cod and Cape Hatteras, but in only 20–30 fathoms south of Hatteras. It is crossed by at least three submerged valleys, off the Hudson River and Delaware and Chesapeake Bays.

North of Cape Cod the shelf presents a somewhat different pattern with many basins and troughs pitting the shelf whose width increases to 240 miles off Newfoundland. Characteristic of this region are the extensive off-shore shoals (the "Banks"), with depths of about 30 fathoms, which are found to seaward of areas with depths up to 100 fathoms.

Outside the continental shelf the bottom drops comparatively rapidly down the continental slope. The top of the continental slope usually lies near the 100-fathom contour but the base lies in depths varying from 700–2,000 fathoms, depending on the area. The typical slope has a gradient of approximately 1:13 (about $4\frac{1}{4}$°). The base is marked by a sharp change in the seaward gradient, from values greater than 1:50 (1°) to values less than 1:200 ($\frac{1}{4}$°). The continental slope is dissected by numerous submarine canyons, comparable in dimensions to the canyons of mountain slopes. In some cases these canyons connect with shelf channels but generally just slightly indent the shelf edge. Some of the canyons continue across the continental rise (at the foot of the slope), but most of them apparently flatten out and disappear in the rise.

The continental rise located at the foot of the continental slope is a gently sloping apron with gradients varying from about 1:200 (0°17′) to nearly 1:1,000 (0°3$\frac{1}{2}$′). Minor relief features are rare although there are submarine canyons and occasional protruding seamounts. The submarine canyons having steep, V-shaped walls which may approach the

vertical generally resemble land canyons cut in the sides of mountain ranges. These canyons, some with tributaries, usually follow gently curving to straight courses down the slope from their origins on the shelf and gradually disappear on the ocean floor. Most exhibit sediment filling on their floors, and many have rocky walls. In some areas the base of the continental rise is marked by a range of hills 100 fathoms or less in height and one mile wide or less at the base.

2.4.2 *Ocean Basins*

The continental rise gives way to the abyssal plains which occupy a sizable proportion of the ocean basins. The smooth, nearly flat topography of the abyssal plains was apparently produced by deposition of sands and silts which were carried by turbidity currents from the continental margins via the submarine canyons.

Sea mounts which rise from the abyssal plain have an appearance of being partially buried. The small sea mounts and hills which protrude from the abyssal plain increase in number toward the seaward limit of the plain. The seaward extremity of the abyssal plains frequently occurs where the small hills become so numerous that they occupy the entire area. The margin of the abyssal plain along certain positive features such as the east or west margin of the Bermuda Rise is marked by a sharp rise of the sea floor where the depositional floor has built up against the topographic rise. The larger sea mounts that occur scattered through the abyssal plain also show the same partially buried appearance.

Besides the two lines of large sea mounts which parallel the Mid-Atlantic Ridge on the east and west, there is another major trend of sea mounts, the Kelvin Group, running southeast from New England.

The eastern and western basins of the Atlantic are quite similar but there are several significant differences. The European continental slopes are in general higher, steeper, and more rugged and irregular than those off the North American coast. The continental rise is often absent or poorly developed; in some areas the continental slope descends almost directly to the abyssal plain. In the area north of the Azores the abyssal plains are less well developed than on the west side of the ridge. Rockall, Bill Bailey's, and Lousy Banks, rocky spines running south from the Iceland-Faeroe Ridge, represent features which have no direct analogies in the western basin. In the area between the Azores and Gibraltar numerous sea mounts of large size are encountered more frequently than in the western basin. The northwest margin of Africa bears the closest similarity to the northeast coast of the United States, with an extensive abyssal plain and a well-developed continental rise.

A mid-ocean canyon three miles wide with precipitous walls which drop fifty fathoms to the canyon floor runs down the length of the Labrador and Newfoundland Basins as shown on Fig. 8. Profiles across this canyon are shown in Fig. 9. Other mid-ocean canyons have recently been discovered in the equatorial Atlantic as well as in the basin south of Nova Scotia. Studies of sediments obtained in these canyons suggest that they were cut by turbidity currents.

2.4.3 *Mid-Atlantic Ridge*

The principal topographic feature of the Atlantic is the Mid-Atlantic Ridge which runs the entire length of the Atlantic and continues into the Indian and Arctic Oceans. The ridge is about 1,200 miles wide and can be thought of as a broad swell or arch with varied and generally extremely irregular topography. Along the axis of the ridge is a narrow crest about 60 miles wide with a characteristic median depression which cleaves the crest zone. Depths in the median depression exceed the maximum depths of the adjacent flanks of the ridge out to 100 miles or more. In some cases they reach depths equal to those of the abyssal plains. The tops of the highest peaks of the ridge, excluding those which emerge as islands, lie at about 800 fathoms while the median rift falls to depths of about 2,000 fathoms and locally to depths as great as 2,800 fathoms.

Near the outer margins of the ridge there is a discontinuous line of sea mounts which rise as isolated peaks. The major part of the ridge lies at depths intermediate between the abyssal plains and the central highlands, with extensive areas of flat intermountain basins, particularly in the area just south of the Azores. The earthquake epicenter belt accurately follows the median rift throughout the length of the ridge.

Other areas of the Atlantic which have topography similar to the Mid-Atlantic Ridge include an oval area trending northeast-southwest from Bermuda with a long axis of about 800 miles and a short axis of about 500 miles. The area is characterized, in part, by low irregular relief, but with a number of large sea mounts.

III. NATURE OF THE SEA BOTTOM

3.1 *Methods of Investigation*

There are four principal methods of investigating the nature of the bottom:

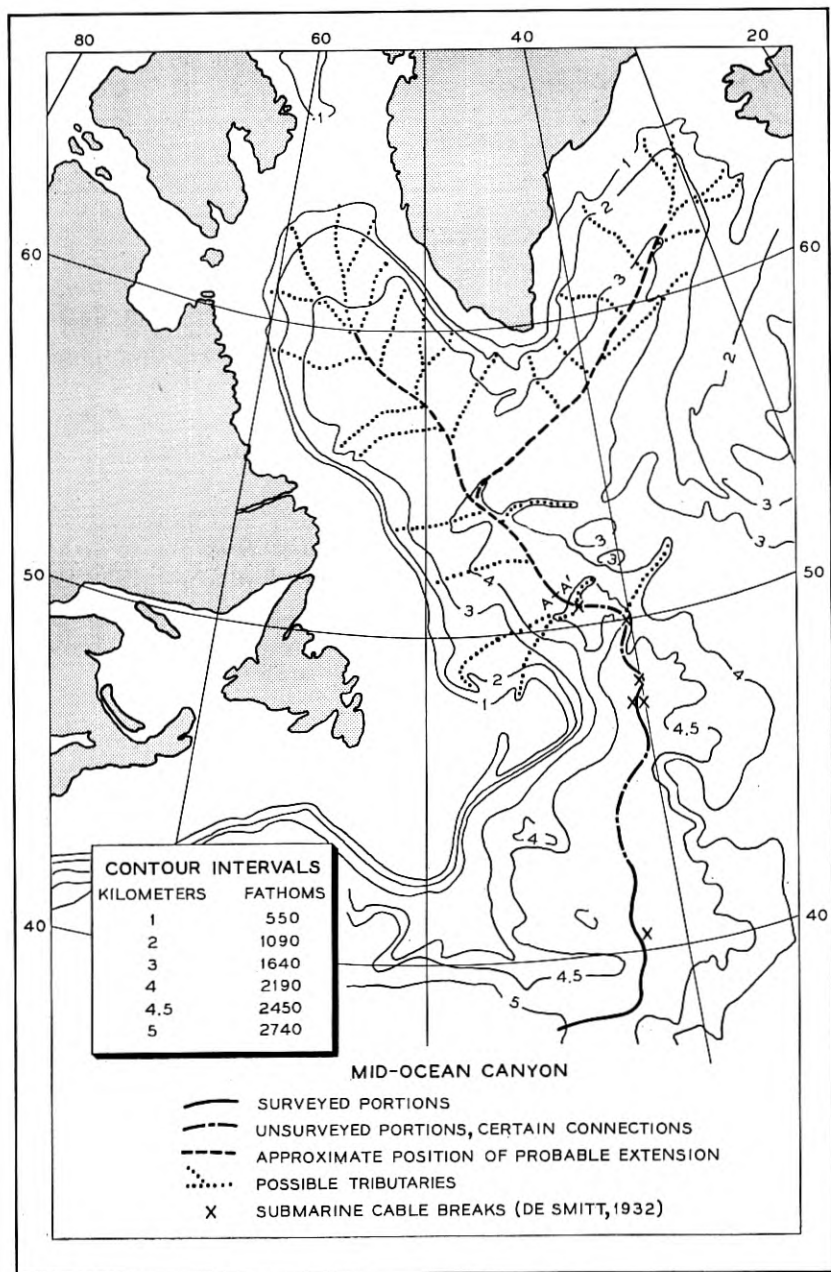(a) Visual inspections and photographs.

(b) Physical sampling.
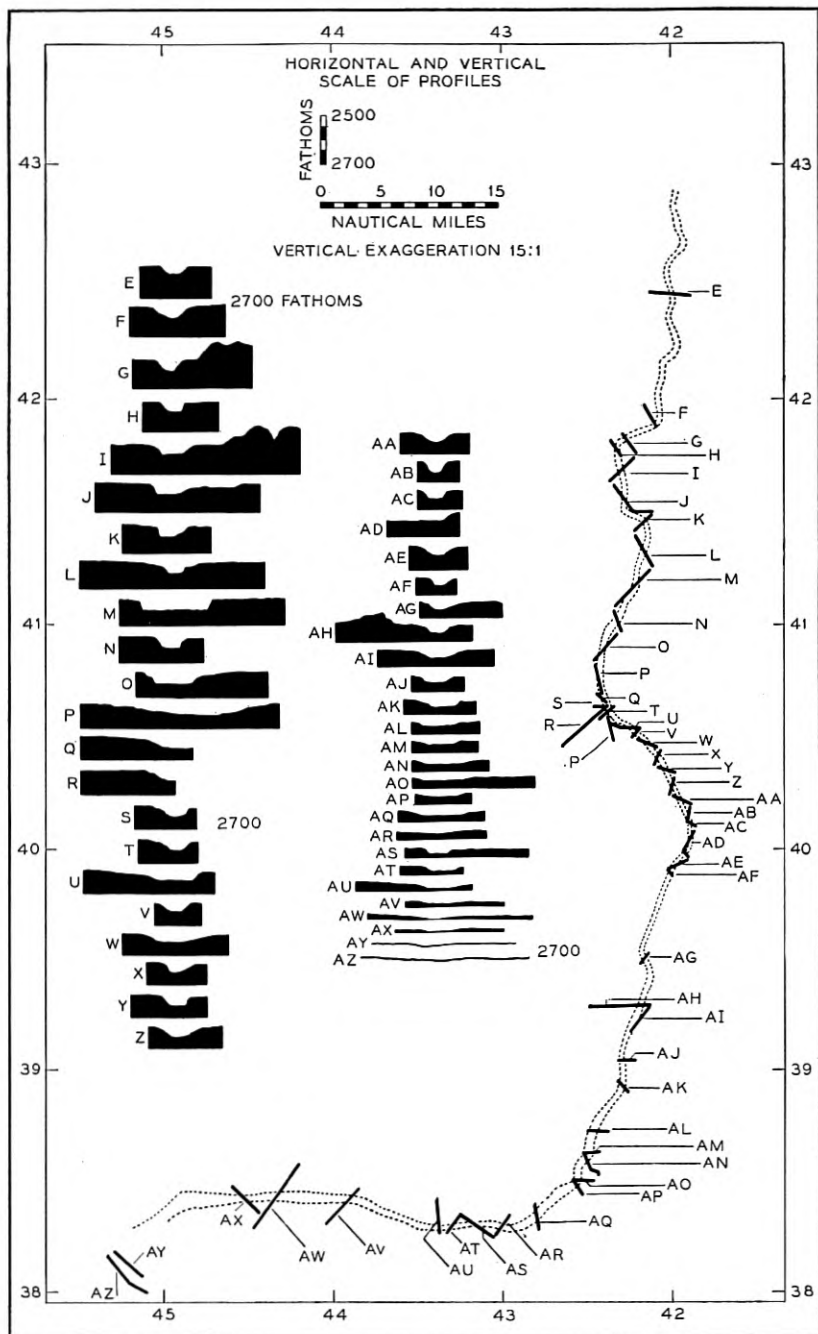
Fig. 8 — Mid-ocean canyon of the Northwest Atlantic.

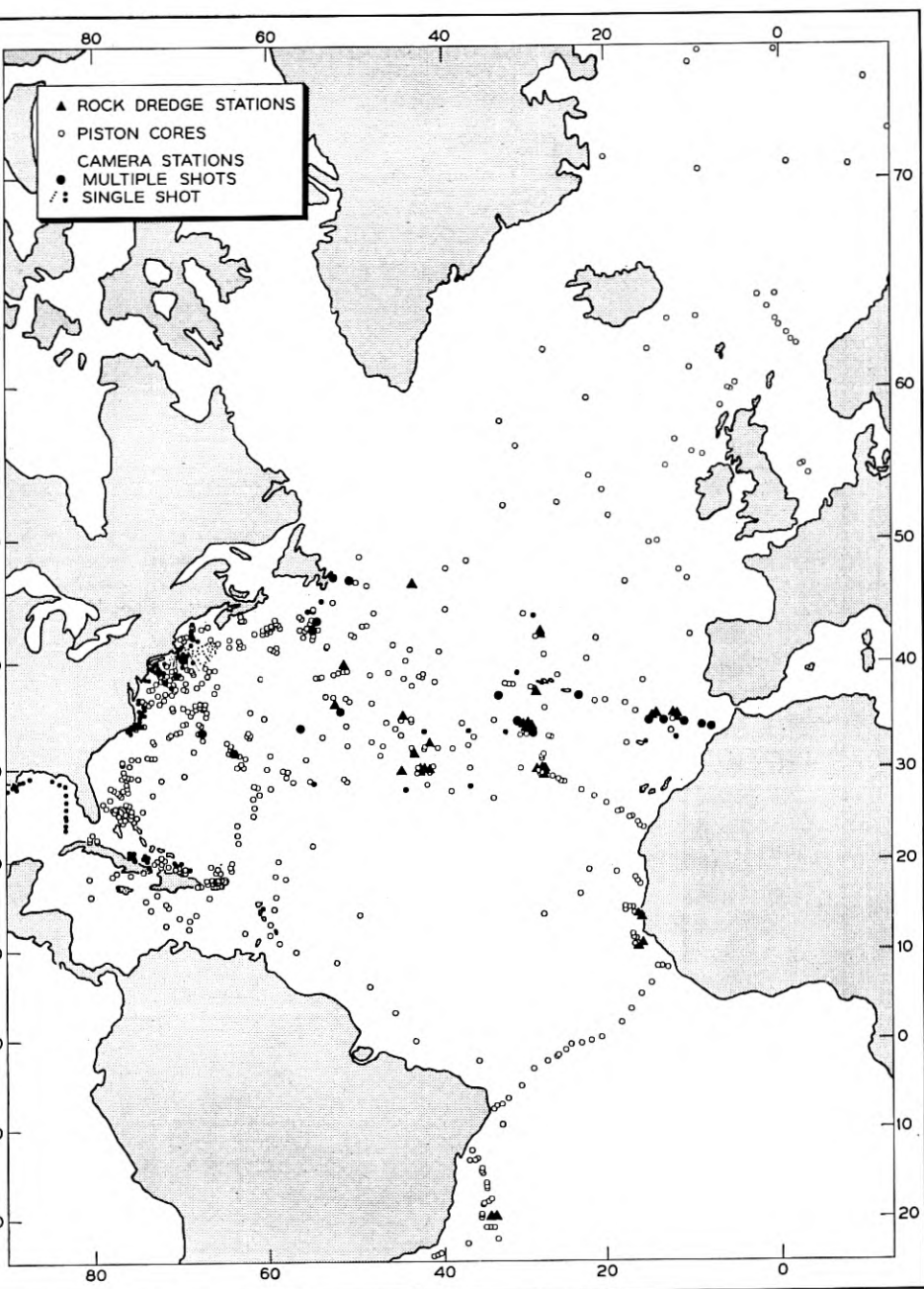Fig. 9 — Profiles across the mid-ocean canyon.

1067

Fig. 10 — Location of cores, rock dredges, and bottom-photograph sites of Columbia University expeditions in the North Atlantic, 1946–1956.

(c) Sound investigations.

(d) Investigations of magnetic and gravity fields, and heat flow.

Visual inspections have been performed by divers in depths up to only about two hundred feet. Vessels such as the bathyscaphe must be employed for greater depths but their design precludes any extensive observation of the sea floor.

Bottom photographs in shallow waters are fairly numerous but those taken in depths greater than 1,000 fathoms are still rare. Good photographs usually show an area approximately 5 ft by 8 ft and are focussed well enough to make objects and organisms $\frac{1}{8}$ inch in diameter clearly identifiable. A compass and a current indicator are often lowered with the camera and included in the photograph. These provide indications of current velocity and direction and a means of orienting the bottom features. Locations of almost all deep water photograph stations in the Atlantic are shown on Fig. 10, and a typical deep sea camera rig is depicted in Fig. 11.
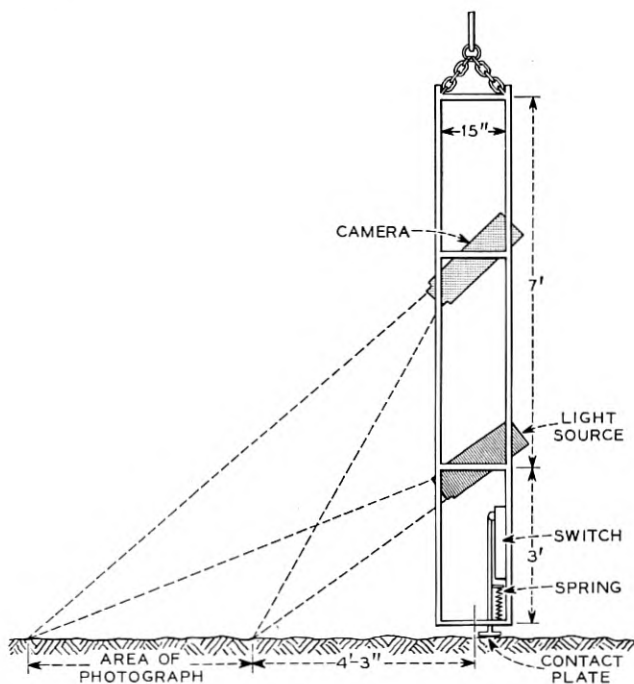
Fig. 11 — Diagram of multiple-shot underwater camera taking a bottom picture.

Television is being used in shallow waters by various organizations. However, picture resolution is poorer than that obtained photographically, and nothing has been done in depths greater than 110 fathoms.

Physical sampling is accomplished by corers, grab samplers, and rock dredgers. Earliest samples were obtained by "arming" a sounding lead with tallow, to which some of the bottom sediment would adhere. Coring is the most important source of bottom composition data. Specimens up to 70 feet in length are obtained by dropping a weighted tube vertically into the bottom sediments. About 1,200 sediment cores have been obtained in the Atlantic. The locations of most of these stations are shown in Fig. 10. Rock dredging has produced much evidence on the nature of the continental slope, the Mid-Atlantic Ridge, and on the various seamounts. Lamont's rock dredge stations are shown in Fig. 10. Not shown are a large number taken by French workers off the Bay of Biscay and off Georges Banks.

Sounding data can provide a wealth of detail in addition to the depth if an experienced operator evaluates the fathogram. The least skilled operator can differentiate between rough and smooth bottoms, while the most experienced can interpret a fathogram in terms of bottom smoothness, sediment thickness, and the location of interfaces in the sediment.

3.2 *Present Knowledge*

3.2.1 *General Characteristics*

Navigation charts sometimes include a short notation alongside a sounding, indicating the type of bottom, ranging from common terms such as sand, mud, or ooze, through the less familiar foraminifera or globigerina ooze (shells of microscopic marine life). These notations are most abundant in shallow coastal waters where they provide information for piloting and anchorages. In the less frequented depths, bottom notations on navigation charts are very rare—charts of bottom sediments commonly published are based on sparse and incomplete data and, as a result, are generalized.

Deep sea sediments have been divided into two main classes, terrigenous and pelagic. Terrigenous sediments are those derived from the erosion of the land and are found adjacent to the land masses, while the pelagic deposits are found in the deep sea and are distinguished as either organic ooze or inorganic clay. The organic oozes are composed principally of fossil remains of planktonic animals. Distribution of types of sediment is by no means static. Such factors as deposition by turbidity currents, land slides or slumps, bottom scour by ocean currents, and climatic changes continually cause changes.

3.2.2 *Sediment Densities*

Quite accurate density determination can be made by laboratory analysis of sediment from core tubes. Densities of 1.35 to 1.55 gm/cc are characteristic of the gray and red clays which cover most of the deeper parts of the ocean. The globigerina oozes which are abundant on the Mid-Atlantic ridge have densities from 1.60 to 1.75 gm/cc. Sand layers which may occur in abyssal plains at or near the sediment surface range in density from 1.65 to 2.00 gm/cc.

An increase in density as a function of depth in the core would be expected. However, after an initial increase in the first 1 or 2 meters the density usually fails to show further regular increase in cores up to 10 meters in length, and deep in the core the density often falls to within 0.1 gm/cc of the initial value.

The sediment averages about 300 fathoms in thickness over the deep ocean floor, except for the bare rock surfaces on the steeper parts of the continental slopes and submarine peaks where sediment is thin or absent. Thicknesses exceeding 100 fathoms may be reached on the continental rises.
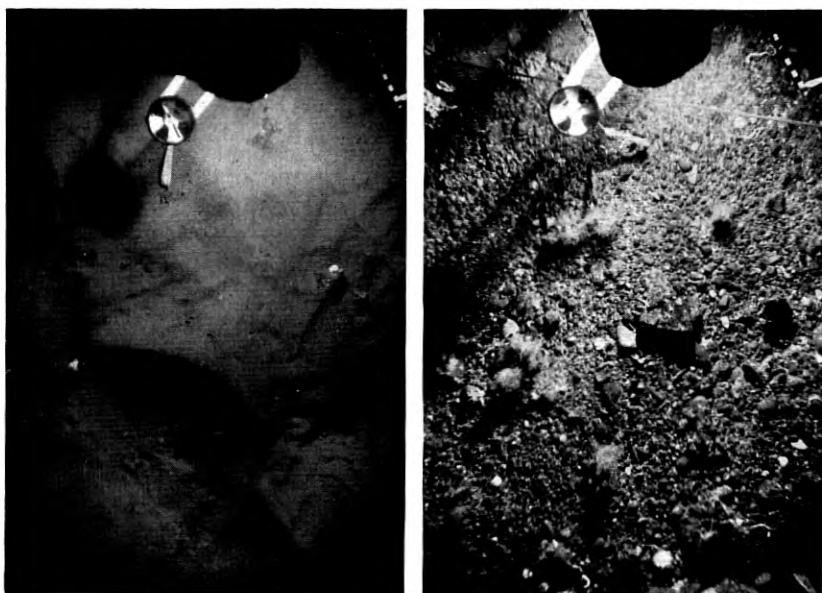
Fig. 12 — Continental-shelf photographs taken off Cape Cod. Each photograph shows an area of approximately 2.4 ft by 3.3 ft. Dials are compasses. Tassel beneath dial indicates current. Note small ripple marks in left photograph. Depths: 64 and 54 fathoms, respectively.
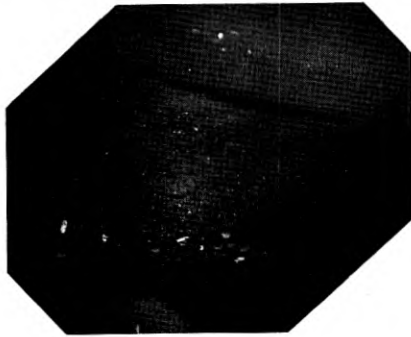
Fig. 13 — Continental-slope photograph taken at 550-fathom depth at 44°43′N, 54°30′W. Area shown in each photograph in Figs. 13–16 is about 40 square feet.

3.2.3 *The Bottom in the North Atlantic*

The continental shelf at depths less than about 70 fathoms was dry land for a considerable period prior to 11,000 years ago. Thus, the sediments of the continental shelf resembled the sediments of the coastal plain from Cape Hatteras to Cape Cod. A deposit of sand continues along the shelf edge and is generally thought to be an old beach. Landward of this is a series of irregularities generally considered to be old dunes and beaches. Photographs of the continental shelf are shown in Fig. 12.

Hardened sandstones and limestone have been recovered from the walls of submarine canyons off Georges, Browns and Banquero Banks. A rock outcrop has been photographed at a depth of 500 fathoms in a small gully south of Block Island. In other areas the continental slope is covered with low-density gray clay in which the coring rig completely buries itself. Gravel and sand form the floors of some continental slope canyons while others are deeply covered with low density mud. In many areas ancient, partly consolidated clay crops out on canyon walls.

The Western Union Company, when plowing in their continental-slope cables, had widely different experience along closely parallel cables.[5] Presumably the differences in the depth to which the plow would penetrate were due to differences between ancient and recent compaction of sediments. Although rock was probably not encountered on these runs, it is known from dredging experience that rock can be expected.

A photograph (Fig. 13) of the bottom at 550 fathoms depth south of the Grand Banks reveals huge ripple marks. It is not difficult to imagine that cable chafe would be appreciable in such an area.

Beneath the nearly flat abyssal plains alternate layers of sand, silt,

and red clay make up the approximately 300 fathoms of sediment. A photograph (Fig. 14) shows the bottom at a depth of 3,000 fathoms in the abyssal hills. This remarkable shot shows ball-shaped objects that have been identified as manganese nodules. The most interesting feature of this photo is the scour marks around the objects, implying an appreciable current at a depth of 3,000 fathoms.

Seamounts present extremely varied conditions. Rocks, from crystalline basalt through hardened limestone to soft marl, are encountered. Sediments, including sticky ancient formations, deep sea oozes, and shell sand are found. Photographs show all types from tranquil mud bottom through wave-rippled silt and sand to craggy rock. Some of these types are illustrated in Fig. 15.

The flanks of the Mid-Atlantic Ridge are areas of irregular topography. The steeper slopes are probably bare rock and the sediment removed from these slopes probably is deposited in the intermountain basins. Cores are usually of globigerina ooze, but the different rates of sedimentation on steep slopes and on basin floors cause changes in thickness of sediment and relatively great changes in physical properties over short distances. The deeper flanks of the ridge are covered by red clay. A very similar bottom is found on the Bermuda Rise.

Fig. 14 — Abyssal-hills photograph taken at 3,190-fathom depth at 29°17'N, 57°22'W.
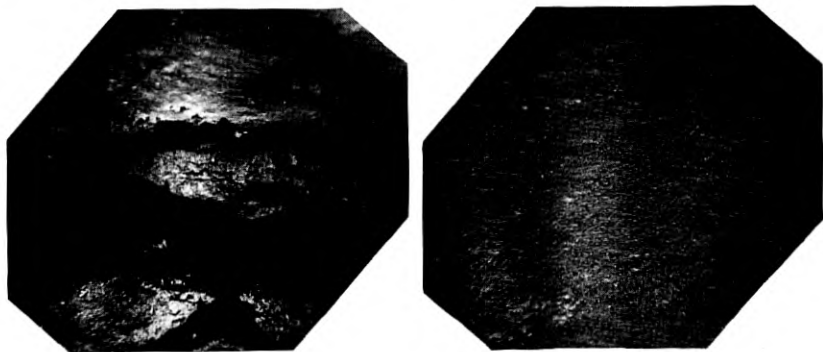
Fig. 15 — Seamount photographs taken near summit of seamount on Bermuda Rise at 34°38′N, 56°53′W at depth of 1,370 fathoms. The two photos were taken about 100 feet apart, indicating the rapid alternation of ooze and rock bottom over short distances.

The crest of the Mid-Atlantic Ridge is similar, as a bottom type, to the seamounts previously described. Dredge hauls have brought up mostly basalt, although a few fragments of limestone have also been retrieved. The photographs shown in Fig. 16 were taken about 60 feet apart on the Mid-Atlantic Ridge. They illustrate a change from smooth to rocky conditions in this short distance.
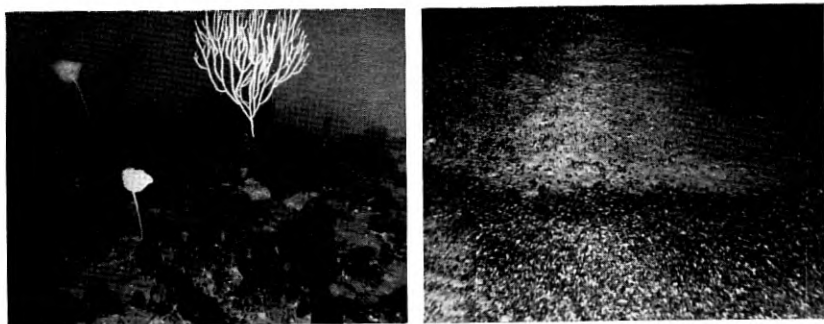
Fig. 16 — Mid-Atlantic Ridge photographs (1,500-fathom depth at 48°30′N, 28°48′W). The two pictures were taken about 60 feet apart. Out of 60 photographs taken at similar intervals in this location three were similar to that on the left and the remainder resembled that on the right. The dark band in the right-hand picture is probably composed of gravel and sand of the dark-colored rock of the peaks, while the white underlying layer is clay or ooze. The dark band was produced by a current which swept the dark material over the light-colored material.

IV. TEMPERATURES*

4.1 *General*

The temperature of a given point on the deep sea floor is determined by the system of ocean circulation. Study of deep sea circulation is still in an early stage and theories which would permit prediction of changes are still in a rudimentary form. In addition, observations of actual bottom temperature are few. Thus, a study of the temperature environment of submarine cables must proceed by evaluating those data that exist and striving for increased understanding of the underlying circulation processes.

The new electronic thermometer under development at the Lamont Geological Observatory determines temperature with an accuracy of 0.01°C by the frequency of an oscillator employing thermistors in an RC network. The oscillator is lowered on the end of a cable and its frequency is monitored by equipment installed aboard ship.

Bottom-temperature changes might be predicted if the rate and direction of circulation of the sea water could be determined. This is being studied by sonar tracking of a submerged blimp designed so that it has negative buoyancy at the surface but is neutrally buoyant at the level where the measurement is desired. This method has been used down to depths of 3,000 meters. Results have indicated much higher velocities than hitherto suspected. Near the base of the continental slope off the eastern United States near-bottom currents of $\frac{1}{3}$ knot have recently been observed by this method.

Another method depends on the measurement of the time elapsed since a given water mass was at the surface by radiocarbon dating of sea-water samples. At the surface, water is in free exchange with the atmosphere and acquires a radiocarbon concentration in equilibrium with that of the atmosphere. As the water sinks from the surface to enter the deep sea circulation system, it is cut off from the supply of fresh radiocarbon, and radioactive decay reduces the content of Carbon 14 at a rate given by its half life. Thus, the measurement of the radiocarbon content of a given sea water sample ideally will give the time at which this sample left the surface of the ocean.

---

* In this section dealing with temperature, depths are given in meters rather than in fathoms. Temperature has largely been of interest in physical oceanography where volume is of concern. This has led to the use of meters. Since a nautical mile is approximately 1,000 fathoms, the fathom has been widely used in topographic work. One fathom equals approximately two meters.

4.2 *Characteristics of Available Information*

4.2.1 *Sources of Data*

Observations of temperature in the deep sea were first made in the mid-nineteenth century. The early observations were made with crude instruments and are now of purely historical value. The *Challenger* expedition of 1872–1876 made several hundred observations but with maximum-minimum thermometers unprotected from pressure. In the late nineteenth century the Richter reversing thermometer was invented and by the turn of the century they were used by nearly all scientific expeditions. Cable ships have taken many observations but almost always with maximum-minimum thermometers.

Major expeditions have published volumes which included tabulated lists of temperature, salinity, oxygen, etc., for each station occupied, while the shorter expeditions and those institutions which continually collect oceanographic data in the North Atlantic publish their observations in the "Bulletin Hydrographique," a journal published by the International Commission for the Exploration of the Sea, Copenhagen. In addition, unpublished data are available from the files of oceanographic institutions.

Expedition reports give estimates of the reliability and accuracy of their data and usually describe the calibration tests used to determine the accuracy. The "Bulletin Hydrographique" merely publishes the data without comment. The scarcity of data and the tendency to systematic errors in single sets of data coupled with the temperature changes now being demonstrated for deep ocean water masses tend to frustrate efforts to evaluate the accuracy of data.

4.2.2 *Methods of Evaluation*

Evaluation of temperature data involves comparison of nearby observations, verification of the original data sheet, and checking for errors in computation. The calibration of the thermometers is ordinarily done with great care, and observations are generally accurate to $\pm.05°C$. When the thermometer fails to function properly, the temperature is usually so far off that the observation is not reported. The main error comes in the determination of depth of observations. The length of wire paid out to reach a stated depth varies with the magnitude of winds and currents in the area. On early expeditions this led to large errors in observation. The use of two thermometers, one in a pressure case and one unprotected from pressure, allows the calculation of depth of observations with relatively great accuracy.

One method of understanding temperature changes is to consider the movement of the water masses. These movements depend on density gradients which are directly dependent on the salinity and temperature. This type of study is applicable in shallow water where circulation of the surface layers is brisk. For the deep sea, however, dynamic calculations are ambiguous; different investigators using the same data not only arrive at different values for velocity but often arrive at opposite directions of flow. Thus, continuity considerations and the conservation of volume are the primary factors in studies of the deep-water circulation. It is important when evaluating temperature data and studying temperature change and rate of bottom water circulation to study the entire process and not be limited to temperature observations, even though the temperature is the desired final answer.

4.3 *Temperature in the North Atlantic*

4.3.1 *General*

Ocean-bottom temperatures in shallow water (less than 200 meters deep) are affected by seasonal air temperatures and movements of local masses of water. Thus, each specific area exhibits its own pattern of temperature changes. Data are fairly abundant in shallow water areas, so that despite the large and often erratic changes, it is generally possible to determine roughly the bottom-temperature cycle from existing data. However, the local nature of the phenomena makes it desirable to concentrate any detailed studies on areas of immediate interest rather than to attempt broad generalizations.

In deep water (depth greater than 200 meters) bottom temperatures and their variations result from large-scale, oceanwide topographical and circulation phenomena. At the same time, the paucity of data makes an analysis of any particular locale quite difficult. Thus, a general study of deep-water bottom temperatures in the North Atlantic presents the best hope of obtaining at least some useful data.

4.3.2 *Shallow Water (Depth less than 200 Meters)*

In many shallow-water areas near shore (depth less than 50 meters) there are predictable seasonal changes in temperature of the order of 10°C. In harbors and bays where interchange with open ocean water is restricted the seasonal temperature curve will approximate the seasonal air-temperature curves except that the amplitude of the sea bottom temperature changes will be smaller and the peaks and troughs will be

slightly retarded. In the open water of the continental shelf there is often a strong stratification of water masses and the vernal cycle is either strongly retarded (by several months) or completely obscured.

On the open shelf the bottom-temperature cycle is controlled by shifting currents and wedges of water which flow in along the bottom from the open ocean. In some areas these changes go through essentially the same cycle each year. The Irish Sea and the continental shelf west of Scotland are areas where the cycle is so regular that one can safely predict the bottom temperature for a given month within an accuracy of ±1.5–2°C. On the other hand, the bottom temperature on the Grand Banks changes radically from day to day and week to week. It is possible to show that on the Grand Banks summer temperatures are on an average 2° colder than winter bottom temperatures. The day-to-day temperature changes can amount to 5°C or more.

In one particularly well-studied area off Halifax, Nova Scotia, an interesting complication has been discovered. In this 10,000-square mile area the bottom temperatures had been studied for about twenty-five years, observations having been taken at different times of the year. The bottom temperature was considered known to 1°C. It has more recently been found that on occasion, the 8°C water is displaced upward by an underflow (incursion) of 2°C water which suddenly lowers the bottom temperature by 6°C. However, after a few weeks the bottom temperature again approaches the usual value of 8°C. Such incursions of contrasting water (both cold and warm) from the open ocean are as yet only partially understood.

The maximum amplitude of temperature changes in bays and near shore areas of both seasonal and erratic nature often approaches 20°C. On the outer shelves 8°C would be the maximum change expected.

It is now well established that the average temperature over wide areas in the North Atlantic has undergone a gradual increase for the past one hundred and fifty years. The average bottom temperature on the Nova Scotian shelf increased 2°C between the early and mid-nineteen thirties and the late nineteen forties. Similar changes have been reported for the area near Iceland. At present, no sure way of predicting the future longterm changes of temperature is available. Changes of 1° per decade may be experienced.

4.3.3 Deep Water (Depth more than 200 Meters)

A search was made for all deep sea temperature measurements taken with accurate thermometers in depths greater than 2,000 meters, from
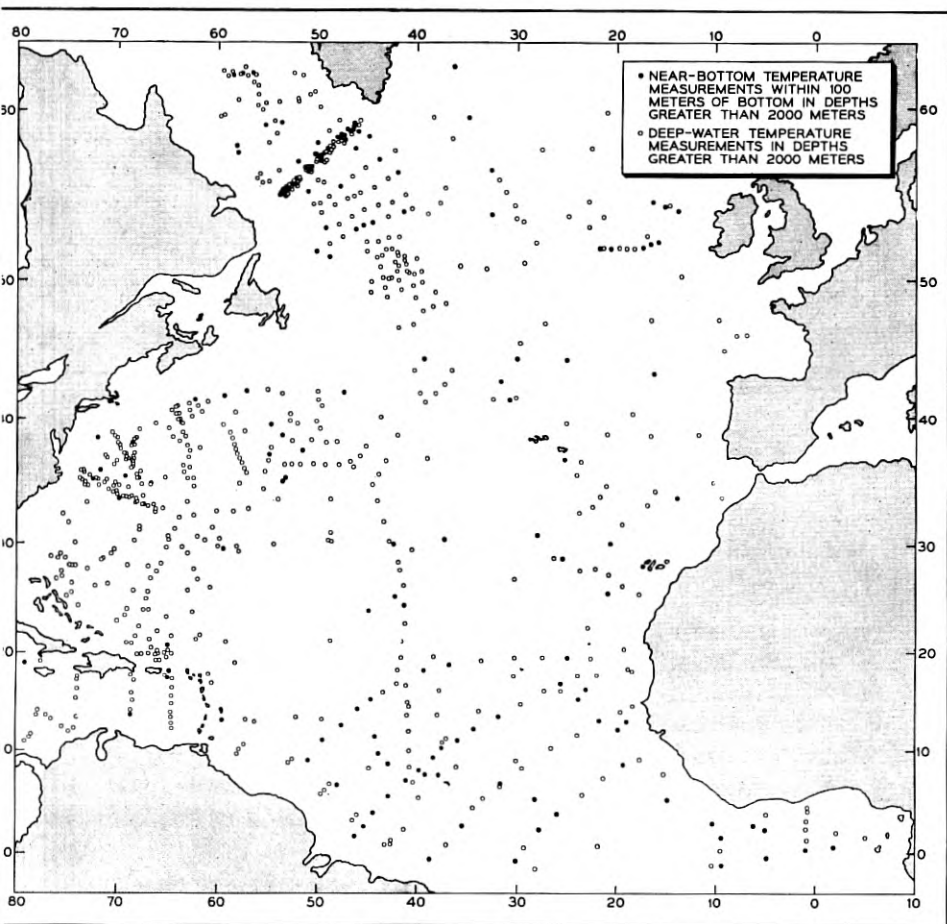
Fig. 17 — Accurate deep-water temperature measurements in depths greater than 2,000 eters. Points marked by solid circles indicate observations within 100 meters of the bottom.

the Equator to the Iceland-Faeroe-Greenland Ridge (which divides the Atlantic Ocean from the Norwegian Sea). Approximately 600 observations (Fig. 17) were found after a search of all data up to 1950 and much of the data up to 1954. (The "Bulletin Hydrographique" is 5 to 6 years behind in publication.) Since the temperature at intermediate depths is of interest to the cable engineer only to the extent that he can use it to determine bottom temperatures, the observations in depths greater than 2,000 meters which lay within 100 meters of the bottom were sorted out. Only about 150 observations (Fig. 17) were found in this
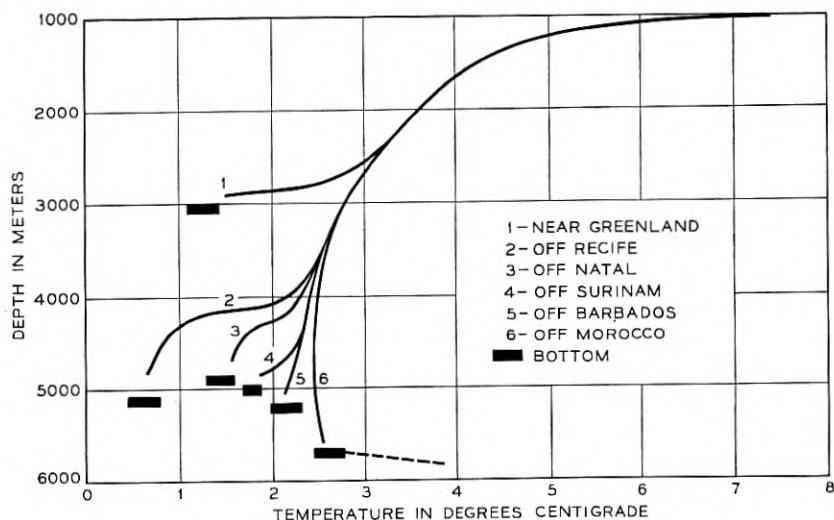
Fig. 18 — Deep-sea temperature gradients. Mean gradient in the sediments is indicated by the dashed line.

category and most of these were either between Greenland and Labrador or near the Equator. The number of actual bottom observations is limited by inability to determine when the bottom was reached and a reluctance on the part of observers to risk losing expensive equipment by having it snagged on the bottom.

At the present time there are insufficient data or knowledge of the mechanism involved to permit reliable extrapolation of bottom temperatures from a series of mid-depth observations. Fig. 18 illustrates the problem. Here are six different near-bottom gradients observed in different parts of the Atlantic. Assuming these gradients terminated 500 meters above the bottom (as do many of the observed data), it is apparent that extrapolating such data to the bottom is not feasible. Measurements of gradients to the bottom at stations for which near-bottom data exist, coupled with a knowledge of the processes causing the gradient, may make it possible in the future to make use of many of the old mid-depth observations in studying bottom temperature.

From the compilation of available data, the three profiles (Figs. 20–22) whose locations are shown in Fig. 19 were prepared. More recent studies indicating that deep water temperatures may vary a few tenths of a degree Centigrade with time make it probable that some of the ripples in the isotherms are not real but instead reflect the fact that the data were taken at widely different times. The data for Profile 1 were

taken in the same year and do not show these effects. The large fluc-
tuation on Profile 3 is probably due to variations with time.

At a certain depth, often about 1,200 meters, a sharp change in tem-
perature takes place. An interface known as the main thermocline
separates the warm surface waters from the cold (2°–4°C) deep water.
This boundary shifts slightly from time to time and is affected by sub-
surface (internal) tidal waves. Thus, cable laid near the main thermo-
cline may undergo temperature changes of a few degrees. These changes
may be of different periods depending on their causes, e.g., subsurface
waves, seasonal changes, or long term changes in ocean regime. It is not
known if a long-term change in depth of the thermocline has occurred
but such change seems probable.

The greatest percentage of any transatlantic cable route lies in depths
greater than 2,000 meters and thus the temperature changes in the
deep sea are of primary importance to the engineering of a cable. The
temperatures are low, averaging 3°C, and the temperature changes are
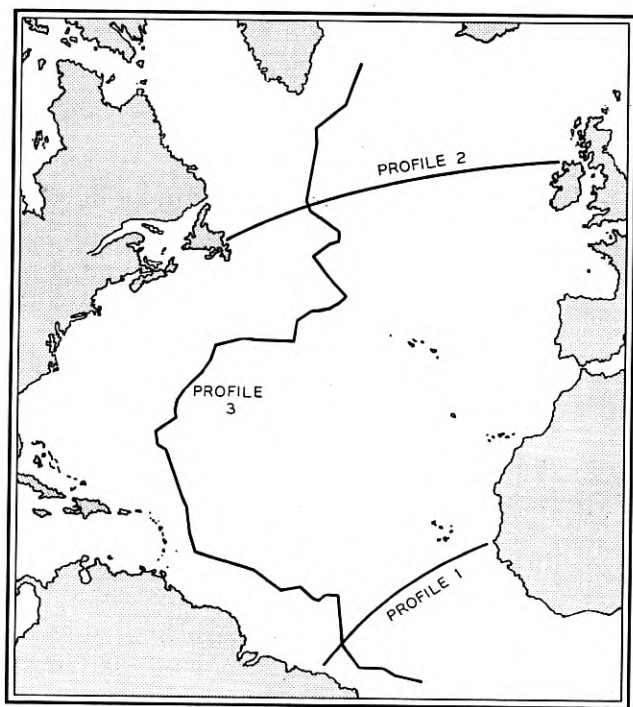
Fig. 19 — Positions of Temperature Profiles 1, 2, and 3.
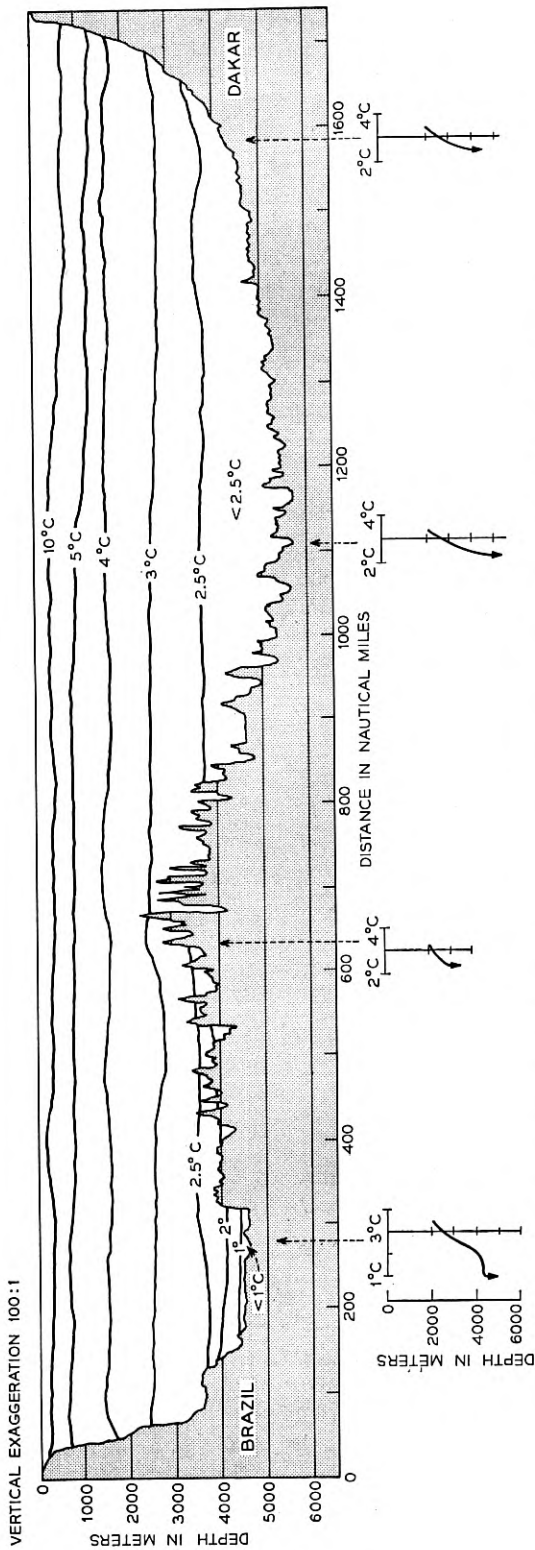
VERTICAL EXAGGERATION 100:1

Fig. 20 — Profile 1, Northeast Brazil to Dakar, Africa. Isotherms in degrees Centigrade. Data from 1928.
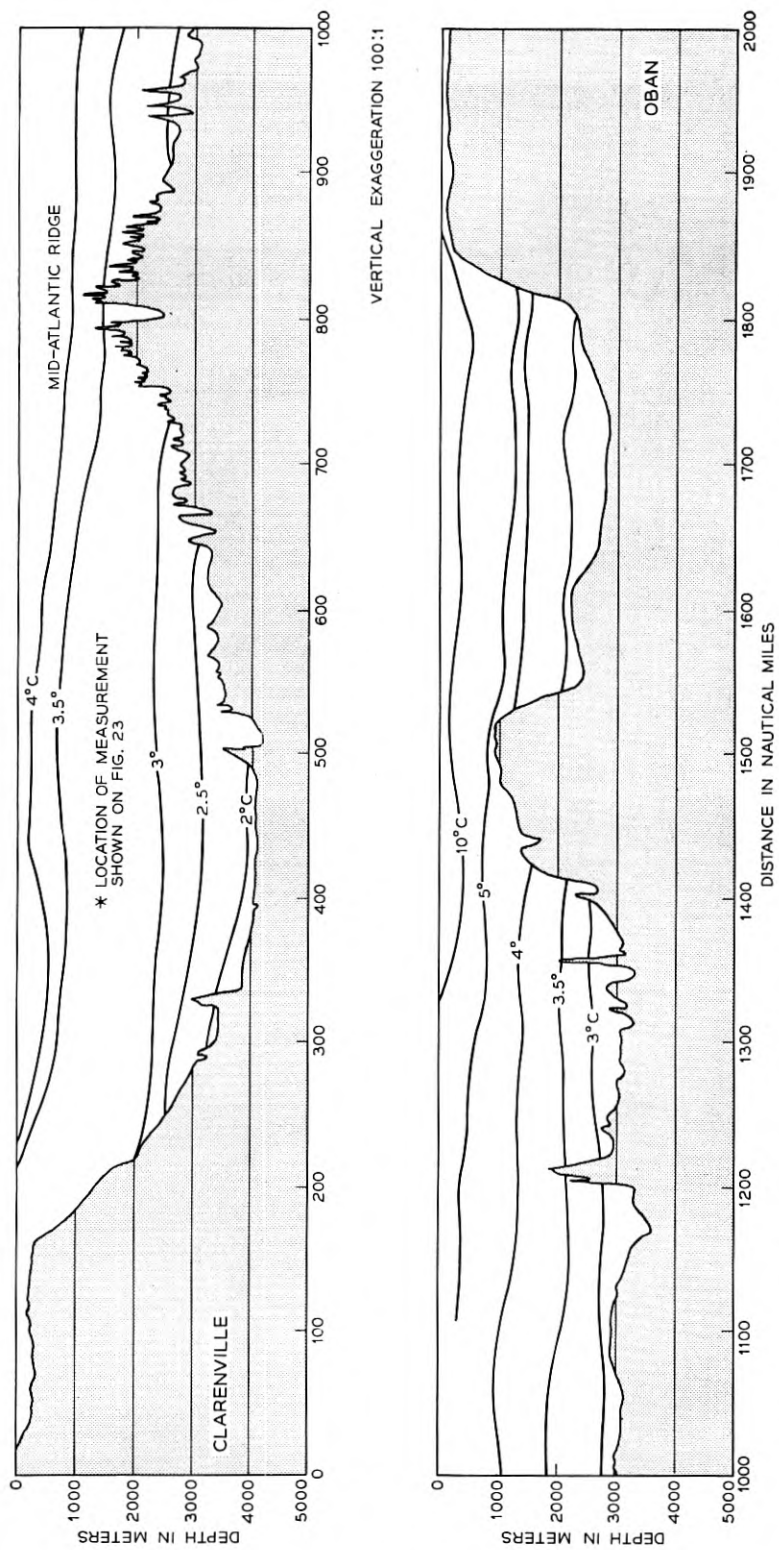
Fig. 21 — Profile 2, Clarenville, Newfoundland, to Oban, Scotland. Isotherms in degrees Centigrade. Data from several years.
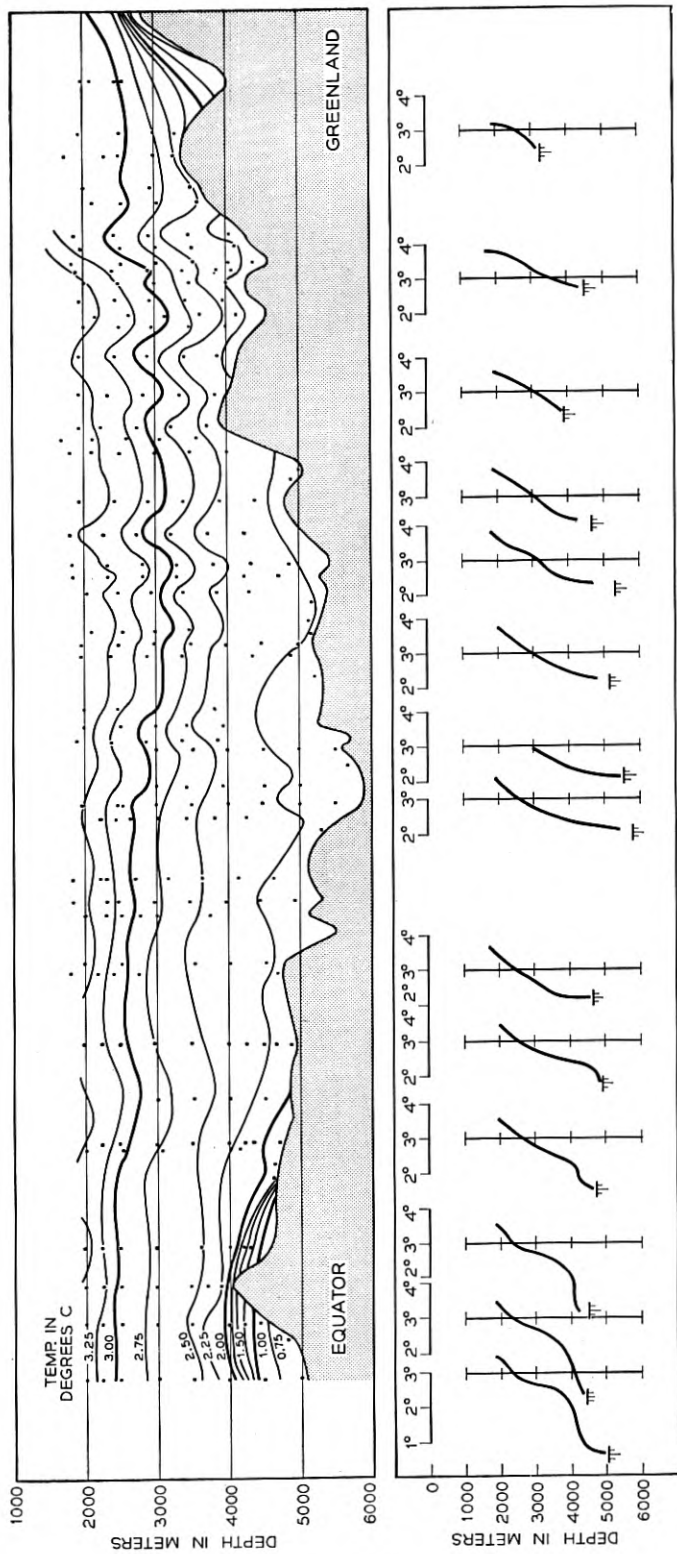
Fig. 22 — Profile 3, Equator to Greenland west of Mid-Atlantic Ridge. Top, isotherms in degrees Centigrade; bottom, gradients at corresponding locations. Data from 1920 to 1955.
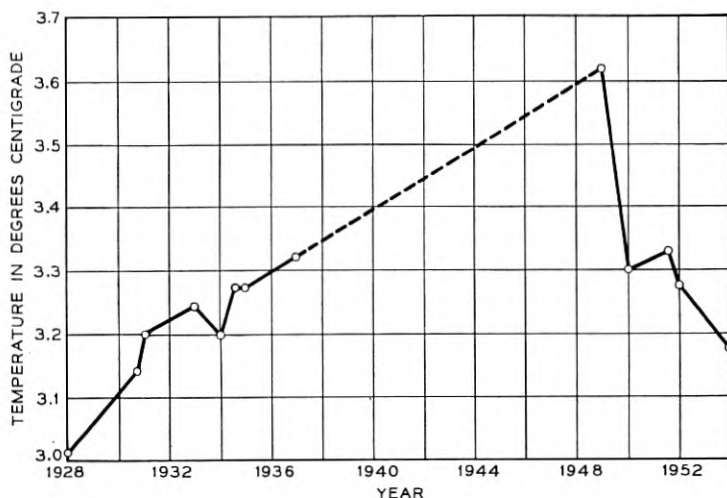
1084

Fig. 23 — Variation of mean temperature at 1,500-meter depth in the southern Labrador Sea at about the point indicated in Profile 2, Fig. 21.

probably small. At one time it was assumed that the ocean temperature in depths exceeding 1,000 meters remained constant. As more information is gathered it is becoming evident that changes in temperatures have occurred in deep water, but neither the mechanism nor the time scale of the changes is as yet completely understood.

Due to the virtual absence of deep sea bottom temperature observations it is not possible to determine changes in temperatures by comparison of repeated measurements at approximately the same position. In a few limited areas repeated observations have been taken to depths of about 3,000 meters. All observations for one such area northeast of Newfoundland have been studied in search of long-term trends. It has been found that the water temperature between 500 and 2,000 meters in this area is nearly constant, both vertically and laterally over a wide area during any one year. It is thus meaningful to compare the temperature at 1,500 meters depth for a series of years. Fig. 23 shows the results of this comparison which indicates a 0.6°C increase between 1928 and 1949, and a 0.4°C drop from 1949 to 1954. This curve resembles the air- and sea-surface temperature averages for Atlantic-coast stations during the same years.

In the area between Labrador and Greenland a moderate number of near-bottom temperature measurements have been made since 1928. No systematic curve can be drawn but it seems fairly certain that bot-

tom-temperature changes of 1°C have occurred in this area. These temperature changes are apparently caused by cold water cascading down the continental slope from the shelf off Greenland. It can be presumed that this water will flow south along the deep ocean basin. Depending on its velocity it will be more or less displaced towards the western margin of the basin. As the water masses flow south, lateral mixing should reduce the temperature contrast with the surrounding water.

In one area south of Newfoundland a study of scattered temperature observations made since the year 1900 indicates that water above 3,000 meters has shown a temperature increase and that the water below 3,000 meters has gradually decreased in temperature. The decrease at the bottom at a depth of 5,000 meters appears to have amounted to 0.2°C in fifty years and the maximum increase at depths less than 3,000 meters to about 0.5°C. In the high latitudes of the North Atlantic, temperature changes probably rarely exceed 1°C at depths greater than 2,000 meters and changes of a few tenths of a degree are more common.

V. CATASTROPHIC CHANGES IN THE OCEAN BOTTOM

5.1 *Earthquakes*

Earthquakes may cause damage to submarine cables by triggering the movements of rock and sediments (turbidity currents) and possibly through the effect of the actual earth vibration itself. The most serious threat to cables arises not from the direct effect of the earthquake's energy on the cable but from its ability to generate slumps, slides, and turbidity currents. It can be shown that, in an area of high seismic activity, the slopes will be nearly bare of loose sediment so that earthquakes in such an area will not result in gravitational displacements of sufficient size to cause serious damage to cable.

However, in areas such as the continental slopes of the Atlantic where few shocks have been recorded and where loose sediment has therefore accumulated, it can be expected that any quake of moderate or even small size will be sufficient to generate a turbidity current. Thus, quakes on continental slopes adjacent to cable routes are likely to be extremely destructive. There is no known method of predicting where earthquakes will occur *outside* the major seismic belts.

Fig. 24 shows the distribution of earthquakes in the North Atlantic. The North Atlantic is the best-monitored ocean because of the extensive network of seismograph stations closely adjacent in North America and Europe. All earthquakes reported for the Atlantic Ocean between 1910 and 1956 have been compiled and plotted together with the best bathy-

metric information. The study resulted in conclusions which are of great geological significance, as well as of interest in cable engineering. It was found that the narrow earthquake belt which runs the length of the ocean accurately follows a median trench or rift in the central highland zone of the Mid-Atlantic Ridge, see Fig. 25. (The Mid-Atlantic Rift
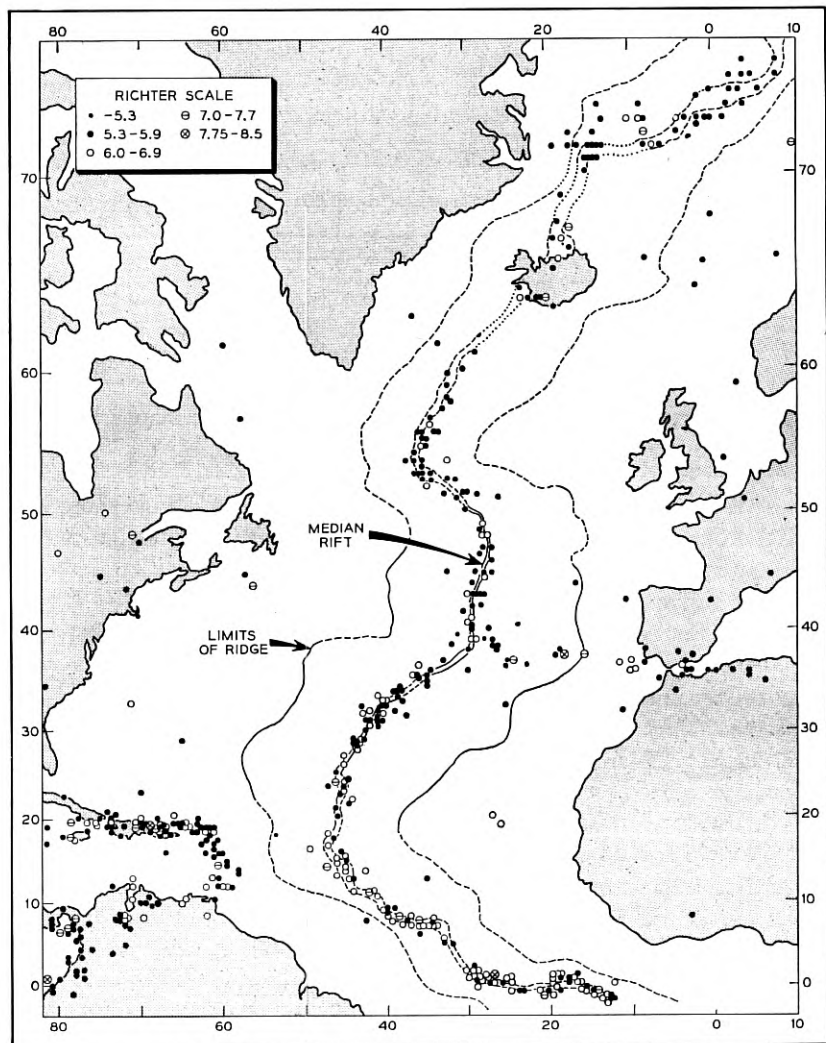

Fig. 24 — Earthquake epicenters in the North Atlantic 1910–1956. Magnitudes according to the Richter scale.

seismic belt is of secondary importance when compared with the intense seismic belt associated with the deep trenches of the Pacific.)

There is a second belt which extends from the Azores to the Iberian Peninsula, and there is a major earthquake belt which follows the West Indies Island Arc along part of the western boundary of the Atlantic. In addition to these belts there are a few scattered earthquakes around the margin of the ocean basin.

The locations of earthquakes in the ocean are in general poorly determined, and an accuracy of $\pm\frac{1}{2}°$ ($\sim$30 miles) is about all that is ever claimed. Within this measurement accuracy, all quakes in the central
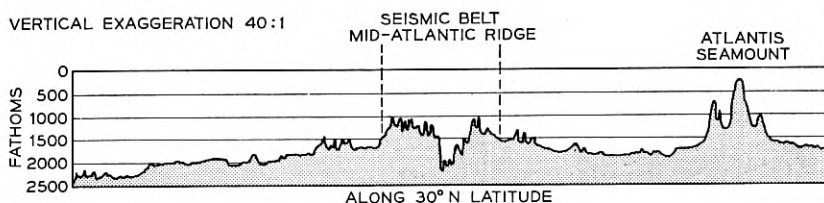

Fig. 25 — Profile of Mid-Atlantic Median Rift showing maximum limits of seismic belt.

part of the Atlantic fall in the Mid-Atlantic rift zone. Thus, there is a strong probability that all quakes on the Mid-Atlantic Ridge fall in this median trench. (Earthquakes of small magnitude are often detected when the signals are not sufficiently clear to allow a position to be determined. There are undoubtedly other quakes that are altogether undetected.) All cables to Europe must cross this rift zone and thus will undoubtedly undergo earthquake shocks from time to time. There is no positive evidence that quakes have broken telegraph cables where they cross the rift. There are, however, several cases where the telegraph cables have parted in or near the rift.

In the western Atlantic there have been recorded only six earthquakes that fall outside the belts described above. Two of these quakes occurred on the Bermuda Rise well away from cable routes. One quake occurred on the continental slope south of Newfoundland (the famous destructive Grand Banks earthquake); a second small shock nearby apparently caused no damage to cables. Two more quakes were centered off the Labrador Coast. Many cases have been recorded along the Pacific coast of Central and South America where the cables failed in deep water following an earthquake.

5.2 *Turbidity Currents — Slumps*

The turbidity current is a flow of sediment-laden water which occurs when an unstable mass of sediment at the top of a relatively steep slope is jarred loose and slides down the slope. As the slide or slump travels down the slope, more and more water becomes mixed in the mass, giving it high fluidity combined with its high density. The currents reach very high velocities, enabling them to spread for vast distances across the abyssal plains. Such slides occur at the edge of continental slopes, in particular, in the vicinity of river mouths, off prominent capes, or near banks. They are triggered by earthquakes, hurricanes, or floods.

Three excellent pieces of evidence support the turbidity-current theory and all have important implications for submarine cables. The turbidity-current hypothesis was first introduced to explain the erosion of submarine canyons in the continental slopes. Supporting evidence was found in submarine cable breakage following the Grand Banks earthquake of 1929[6] and the Orleansville (Algeria) earthquake of 1954.[7] In both cases, submarine cables were broken consecutively in the order of increasing distance *downslope* from the epicenter of the earthquake. All of the cables were broken in at least two widely separated places (100 miles or more apart). The sections between breaks were swept away and/or buried beneath sediment deposited by the current so that repair ships were never able to locate a large proportion of these sections. Fig. 26 shows the area of the Grand Banks turbidity current.

After study of this evidence, Heezen and Ewing concluded that the area covered by the current would show graded sediments as a result of deposition by the turbidity current. This was substantiated by the evidence of cores obtained from the locations shown on Fig. 26.

Cable damage resulting from turbidity currents due to slumps at a river mouth is well illustrated by that off the mouth of the Magdalena River (Columbia, S. A.). On August 30, 1935, the disappearance of 480 meters of the western breakwater and most of the river bar resulted from a slide which produced a 36-foot channel across the bar. The same night, tension breaks occurred in the submarine cable from Barranquilla to Maracaibo, which crosses the submarine canyon 15 miles off the mouth of the Magdalena in a depth of about 700 fathoms. The cable, when brought up for repair, was tightly wrapped with green grass of a type which grows in the marshes near the jetties.

The same pattern has been repeated 15 times since the cable was laid in 1930. The breakage of the cables has occurred most frequently in August and late November to early December; the two periods of the

highest water of the river and of the strongest trade winds — conditions favorable for the triggering of turbidity currents. A chart of the area showing the cable breakage on the steep continental slope is shown in Fig. 27.

Fig. 28 shows areas of the world inaccessible to shallow-water-derived turbidity currents, because of their elevation or because of protective
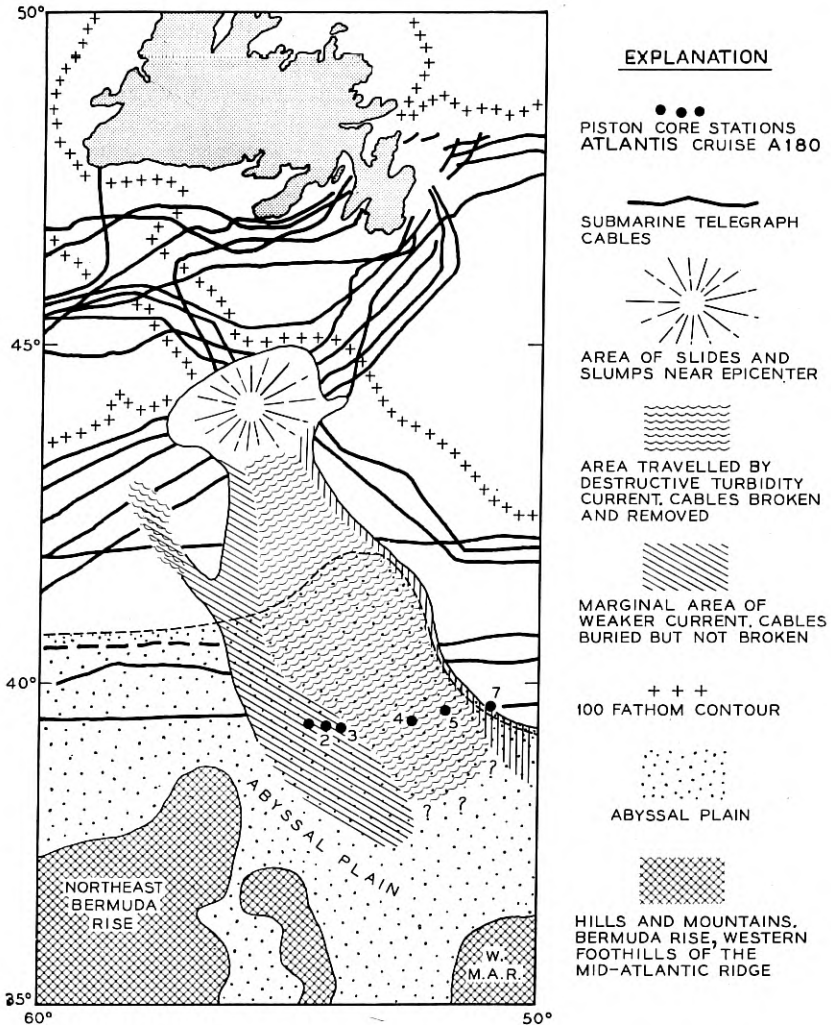

Fig. 26 — The 1929 Grand Banks turbidity current.

barriers. The arrows show some modern turbidity currents which have been documented through the breakage of telegraph cables. This chart is not yet complete and it is expected that many more arrows can be added, each representing one or more currents, and some representing as many as 20 documented cases.

Areas which have experienced turbidity current flows in the past can be determined by a careful study of the nature of the bottom. From a study of sediments and topography of areas along a proposed route it is possible to delimit areas where turbidity current could and could not
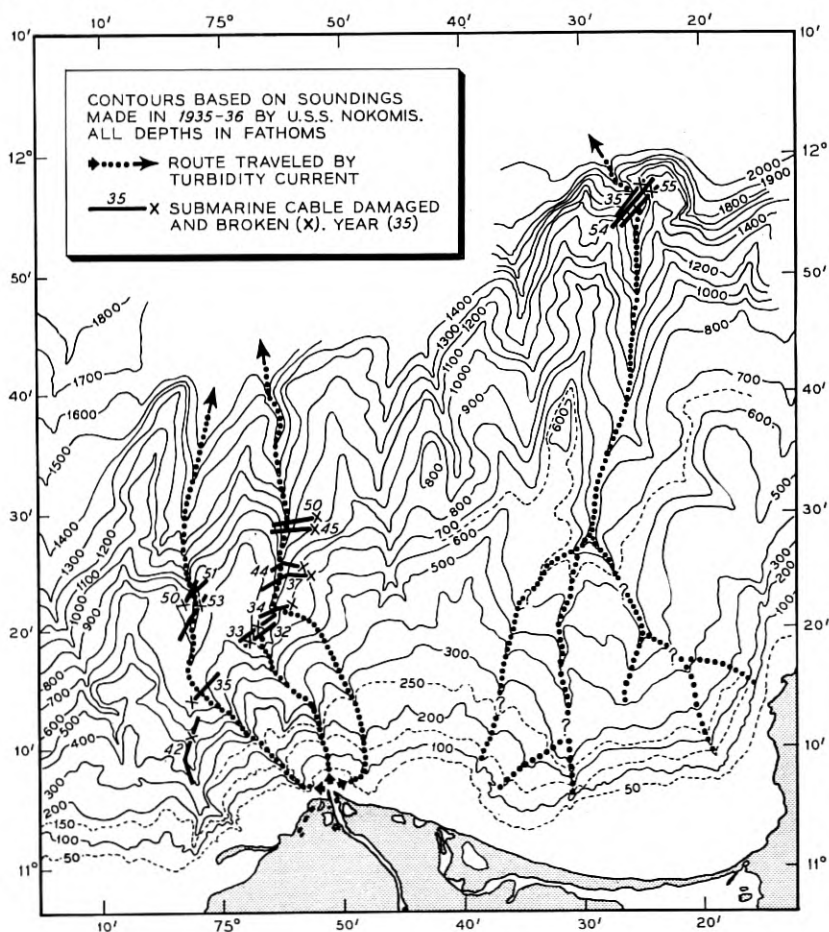

Fig. 27 — Cable breaks in the submarine canyons off the Magdalena River, Colombia, South America.
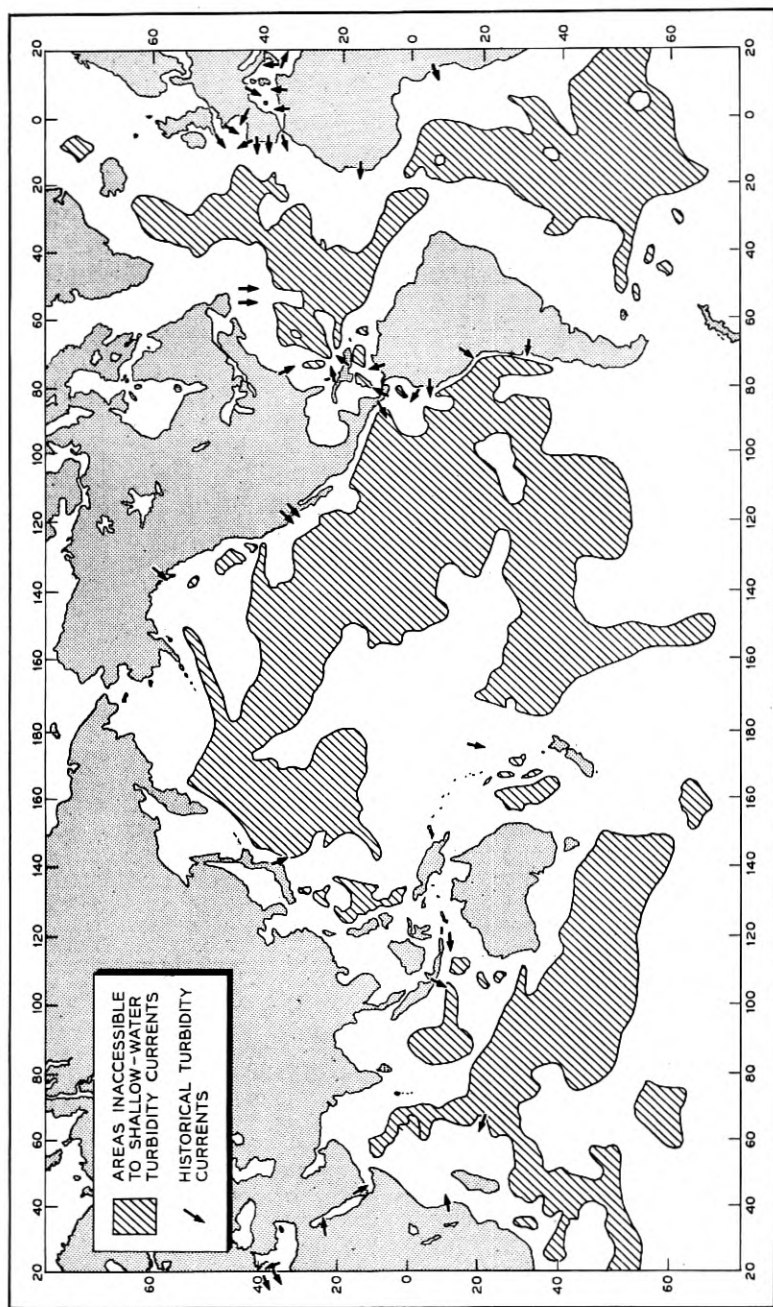
Fig. 28 — Areas of the world inaccessible to turbidity currents from shallow water.

occur, and in some cases to outline areas where they occur at frequent intervals. If, after the completion of such a study, it is decided to take the risk of laying a cable across a dangerous area and at a later date a turbidity current does occur, it will be possible to predict the length of cable to be replaced under various conditions.

VI. CONCLUSIONS

The application of the rapidly developing science of oceanography to the development and engineering of submarine cable systems will permit refinements in design, cable placing techniques, route selection, and repair operations. Existing knowledge, when evaluated and codified, provides many useful data for immediate application. Continuing study of topography, the nature of the bottom, causes of cable failures, and deep sea circulation will permit further advances in the engineering of submarine cable systems. It is to be expected that the value and usefulness of submarine cable oceanographic studies will be substantially extended as geologic and oceanographic researchers broaden the understanding of the natural laws and processes which govern and produce the ocean-bottom environment. Through such knowledge, the data of many fields can be coordinated, permitting better explanation of past events and more accurate prediction of future conditions.

ACKNOWLEDGEMENTS

REFERENCES

1. E. E. Zajac, Dynamics and Kinematics of Laying and Recovery of Submarine Cable, pp. 1129–1208, this issue.
2. L. R. Snoke, Resistance of Organic Materials and Cable Structure to Marine Biological Attack, pp. 1095–1128, this issue.
3. B. Luskin, B. C. Heezen, M. Ewing, and M. Landisman, Precision Measurement of Ocean Depth, Deep-Sea Research, 1, pp. 131–140, April, 1954.
4. D. J. Matthews, *Tables of the Velocity of Sound in Pure Water and Sea Water for Use in Echo Sounding and Sound Ranging*, Admiralty, London, 1939.
5. C. S. Lawton, The Submarine Cable Plow, A.I.E.E. Trans., **58**, p. 685, 1939.
6. B. C. Heezen and M. Ewing, Turbidity Currents and Submarine Slumps, and the 1929 Grand Banks Earthquake, American Journal of Science, **250**, pp. 849–873, Dec., 1952.
7. B. C. Heezen and M. Ewing, Orleansville Earthquake and Turbidity Currents, Bull. Am. Assoc. Petroleum Geologists, **39**, pp. 2505–2514, Dec., 1955.
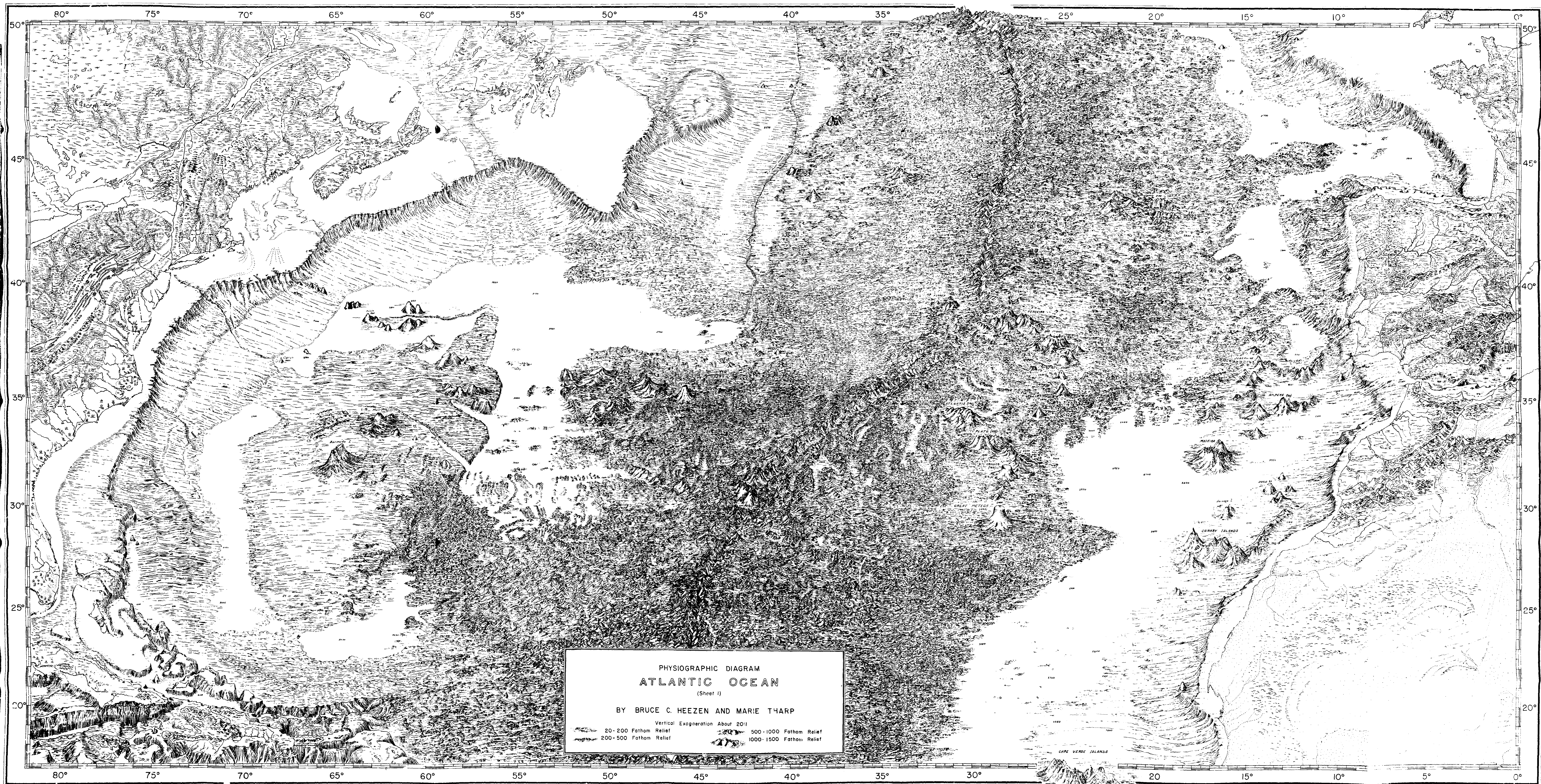
PHYSIOGRAPHIC DIAGRAM

ATLANTIC OCEAN

(Sheet 1)

BY BRUCE C. HEEZEN AND MARIE THARP

Vertical Exaggeration About 20:1

20-200 Fathom Relief
200-500 Fathom Relief
500-1000 Fathom Relief
1000-1500 Fathom Relief

Resistance of Organic Materials and Cable Structures to Marine Biological Attack

By LLOYD R. SNOKE

(Manuscript received June 6, 1957)

The increasing use of submarine telephone cable has resulted in the need for information on the performance of organic materials and cable structures under marine conditions. Recently, Bell Telephone Laboratories initiated a program to acquire fundamental data on the resistance of a wide range of organic materials, as well as immediately applicable engineering information. The present progress report describes the program which includes accelerated, laboratory-microbiological tests, as well as the acquisition of data from actual marine exposures. In biochemical oxygen demand-type tests conducted to date polyethylene was not utilized as a carbon source by marine bacteria. Polyvinyl chloride plastics served as a source of energy for the organisms depending on the way in which the materials were plasticized. Five elastomers were utilized by the bacteria. There has been a steady rise in capacitance values for GRS-insulated conductors exposed in sea water and sediment under laboratory conditions for thirteen months. These increases appear due to biological activity on the insulation. The general performance of materials undergoing marine exposure is reported including reference to penetration of a few synthetic materials by marine borers. Brief mention is made of the examination of submarine cable samples from service.

I. INTRODUCTION

As a result of the increasing use of submarine telephone cable, there is a growing demand for information on the performance of organic materials and cable structures under marine conditions. Particularly important is the need for data on the resistance of materials to attack by marine organisms. Although considerable published information exists on the behavior of natural organic materials such as wood, jute, hemp and the like, there is virtually no data on plastics, elastomers, casting resins or similar materials.

About three and a half years ago, the Laboratories initiated a program to determine the resistance to marine biological attack of materials which might find application in submarine cable. The program has two primary objectives: (1) acquisition of fundamental information regarding the biological resistance of a wide range of selected organic materials, and (2) accumulation of immediately applicable engineering information on materials.

II. OUTLINE OF PROGRAM

It seemed evident that marine borers or microorganisms, particularly bacteria, might be expected to be the major agents of deterioration.

Marine borers are mollusks or crustaceans which bore into a material for food or shelter depending on the particular organism involved. Of the crustaceans, the gribble, *Limnoria,* is the most outstanding. Cellulose material such as wood and cordage form its food supply and natural habitat. There are a few references which suggest that members of the genus *Limnoria* have bored into gutta percha. One by Chilton[1] refers to the activity of *Limnoria* in the splice of a submarine cable in about 60 fathoms off New Zealand. Preece[2] identifies *Limnoria* as the organism responsible for failure of the Holyhead-Dublin cable in 1875. Jona[3] states that he frequently found *Limnoria* in cables in the Adriatic Sea. Menzies[4] points out that no American species is known to occur in depths exceeding 50 feet; however, one species is known to occur off Japan at a depth of 163 fathoms. He suggests that the absence of wood probably limits the distribution of the animals in deep water.

In the bibliography by Clapp and Kenk,[5] there are ten, separate citations to the attack of submarine cables by molluscan borers belonging to the family *Teredinidae.* In most cases, attack was confined to cellulose constituents such as jute and hemp, although in a few instances mention is made of attack on gutta percha insulation. Although the teredine borers, along with *Limnoria,* are considered to be relatively shallow water organisms, Roch,[6] in his paper on Mediterranean teredos, refers to *Teredo utriculus* being obtained from depths as great as 3500 meters. There is one reference[7] to teredo attack of lead-covered submarine cable.

The other important family of boring mollusks is the *Pholadidae.* Members of this family are sometimes referred to as the "burrowing clams" and include rock, shell and wood borers. Some genera, such as *Xylophaga,* are found in water up to 1,000 fathoms or more deep.[4] Bartsch and Rehder[8] report the penetration of the lead sheath of a submarine cable by one of the *Martesia,* another genus of the family *Pholidi-*

dae. Members of the same family were reported by Snoke and Richards[9] to have bored through the lead sheath of a submarine telephone cable.

The bacteria generally are single-celled organisms, a large number of which are heterotrophic, that attack organic matter and use it as a source of carbon or energy. The bacteria play an important part in the biology of the sea, their most important function being to decompose organic material into carbon dioxide, water, ammonia and minerals. The characteristics, distribution and function of the marine bacteria have been described in great detail by ZoBell.[10] Bacteria are found in sea water and sediment from shallow depths to the deepest portions of the sea. During the Danish Galathea Deep-Sea Expedition from 1950 to 1952, bacteria were found in depths as great as 10,280 meters.[11] Many of these bacteria have been found to be barophilic[21], growing exclusively or preferentially at pressures approximating 15,000 psi. ZoBell and Morita[12] have reported experiments performed with these bacteria to determine the effects of high pressure on such factors as viability and enzyme production. Marine bacteria have been found capable of oxidizing rubber products,[13] as well as a wide variety of gaseous, liquid and solid hydrocarbons.[14] Although evidence to date indicates that among the microorganisms, the bacteria are particularly likely agents of deterioration in the ocean, it is possible that the fungi may also be contributors. Barghoorn and Linder[15] report the physiological behavior and growth on various media of seven species of marine fungi isolated from wood continuously submerged in the sea. Deschamps[20] has discussed the role of fungi and bacteria in aiding the attack of wood by marine borers. Also, the occurrence of marine fungi in wood test panels, driftwood and piling in Biscayne Bay has been reported by Myers.[16]

A program designed to provide fundamental and engineering data on the susceptibility of organic materials to marine borers and microorganisms in an environment that covers about 70 per cent of the earth's surface could be almost unlimited. The practical parameters which finally were established were based on a number of considerations. Fundamental data on the basic inertness or relative rates of attack by microorganisms could best be determined under controlled laboratory conditions; however, more than one procedure would be needed to determine performance in the environments of water and sediment. Because of the relatively rapid activity of marine borers under natural conditions, and their critical requirements as far as laboratory culture is concerned, it was decided that any borer tests would be conducted in the field. This meant that the natural exposure tests would serve as correlative tests

for the laboratory microbiological portion of the program, as well as a means of evaluating the relative performance of materials in the physical and chemical conditions of the ocean.

The integrated program, shown in Fig. 1, involves a series of three laboratory tests on the one hand, and actual marine exposure on the other. Eventually, more than fifty different materials including plastics, elastomers, natural and synthetic fibers, as well as sections of cable will be tested. The present paper is in the nature of a progress report in which only a portion of the data to be acquired are presented. The results of the program to date will be examined beginning with the laboratory experiments.

III. LABORATORY TESTS

3.1 *Biochemical Oxygen Demand Type Test*

The BOD (biochemical oxygen demand) type of test as applied in this study is really composed of two separate bioassay procedures. In one case, the oxygen consumed by aerobic bacteria is determined, and in the other a metabolic by-product resulting from anaerobic activity is measured. With a few changes, both methods follow those which have been employed by ZoBell[13] in tests of elastomers and various natural organic materials.

There is one point which should be emphasized regarding both the aerobic and anaerobic procedures used in this accelerated sea water test. It is considered primarily a screening test which provides basic data on
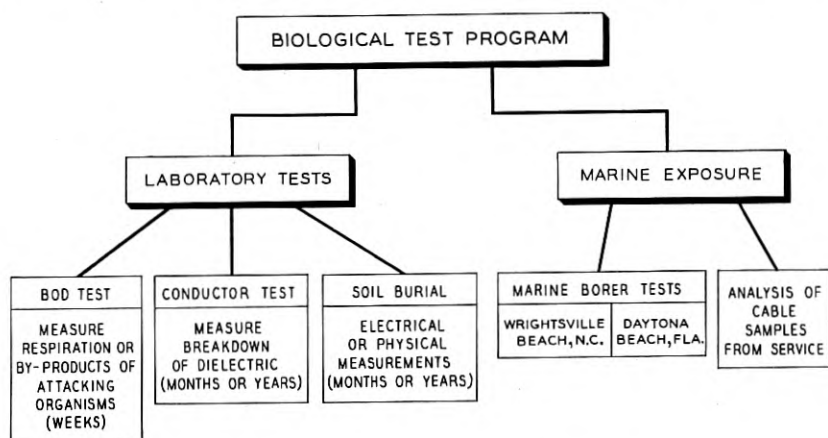

Fig. 1 — Outline of marine biological test program.

the ability of marine bacteria to utilize a compound as a carbon source at the time of test. It will not reflect changes brought about in the material due to prolonged exposure in sea water, or ecological relationships which might make the material more or less susceptible to attack by certain bacteria. The other laboratory tests and natural exposure test will help furnish data on questions involving changes in materials due to long-term marine exposure.

TABLE I — MATERIALS TESTED AGAINST AEROBIC AND
ANAEROBIC MARINE BACTERIA

Designation	Type
Polyethylene[1]	
2.0 melt index[2]	P5310466
0.2 melt index (Source A)	P5304156
0.2 melt index (Source B)	P5312587
0.2 melt index + 5% butyl rubber + antioxidant	P5308396
0.2 melt index + antioxidant	P5308390
0.7 melt index (high density) nat. + antioxidant	P5503135
0.7 melt index (high density) + carbon black and antioxidant	P5503133
Poly(Vinyl Chloride)[3]	
Plasticizer	
Polyester A	BTL 24–54
Di-2-ethylhexyl phthalate (DOP) Shore A 88	BTL 23–54
Tricresyl phosphate (TCP)	BTL 529–53
None (rigid)	P5503087
None[4]	P5502078
None[4]	P5502077
Tri-2-ethylhexyl phosphate	P5502081
Nitrile rubber/polyester C	P5502074
Di-2-ethylhexyl phthalate (DOP) Shore A 62	P5502082
Nitrile rubber	P5502076
Polyester E/DOP (BTL 46–55)	P5503115
None (PVC resin)	P5510645
Casting Resins	
Epoxide (cast), unfilled straight epoxy resin cured with amine hardener	
Styrene polyester, silica-filled	
Elastomers[5]	
GR-S jacket	BTL 54–14
GR-A jacket	BTL 54–18
Butyl jacket	BTL 54–19
Natural rubber jacket	BTL 54–23
Neoprene jacket	BTL 54–164
Jute	

[1] Except where noted polymers are low density grades manufactured by the high pressure process.
[2] ASTM D1238
[3] With the exception of P5510645 all PVC compositions contained typical organo-metallic type stabilizers (such as Ba, Cd, and Pb), fatty acid lubricants in low concentrations, and in some cases small quantities of inorganic fillers.
[4] Semi-flexible PVC copolymer.
[5] These compounds all contain, in addition to the basic elastomers, sulfur, accelerators, waxes, processing oils, and reinforcing quantities of carbon black. (54–164 also contains clay.)
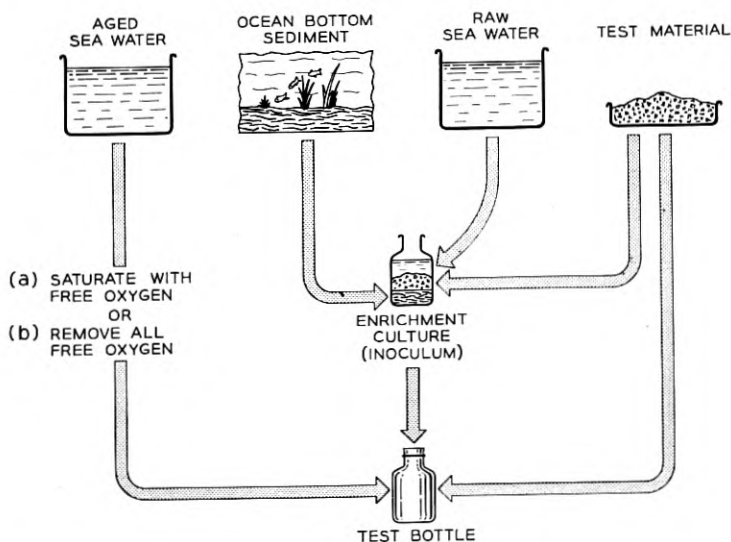
Fig. 2 — Flow chart of biochemical oxygen demand (BOD) type test.

The materials which have been tested thus far by the BOD type procedure include polyethylene, polyvinyl chloride plastics, casting resins, elastomers and jute. The individual materials are listed in Table I. Other plastics and elastomers are still to be tested.

The general features of both the aerobic and anaerobic parts of the test procedure are shown in the flow chart in Fig. 2. Certain features of the test are common to both parts. These features will be described first. The four primary constituents of the test are aged sea water, test material, ocean bottom sediment, and raw (unaltered) sea water. Aged sea water is raw sea water which has been filtered through Millipore filters of 0.5 micron pore size, and then aged in the dark until the biochemical oxygen demand (BOD) is quite low; i.e., until the water contains about 1 ppm of organic matter. This usually requires about eight weeks of aging. In the first tests which were run, materials were finely ground so as to expose a large surface area, and so accelerate attack. However, it soon became apparent in efforts to relate the rate of oxidation to surface area exposed that only crude estimates could be made of the irregular surface areas. Consequently, after the first few tests, thin sheets of material were employed wherever possible so that a measured amount of surface area could be exposed in each case.

The inoculum for the test comes from specially prepared enrichment cultures. Approximately 90 cc of marine sediment is placed in a 250 ml

prescription bottle. About 1 gram of a finely divided test material is also placed in the bottle which is then filled about three-quarters full of raw sea water. To include as heterogeneous a population of marine bacteria as possible, another inoculum is prepared for addition to the enrichment culture. The additional inoculum is made by placing in a vial a small particle of each of seven different sediments furnished by Dr. ZoBell of the Scripps Institute of Oceanography. These sediments are identified in Table II. Following this, one or two drops of liquid are added to the same vial from each of twenty-nine different enrichment cultures which also were provided by Dr. ZoBell. These cultures are identified in Table III. Transfers from eight different cultures of marine sulfate-reducing bacteria are included, and the vial shaken thoroughly. About five drops of pooled inoculum are added to the enrichment culture prepared for each test material. The completed enrichment cultures are incubated at 25° C for a minimum of six weeks prior to use. During the incubation period those bacteria in the culture which are capable of utilizing the test material tend to develop preferentially.

The same enrichment culture is used whether the test procedure is aerobic or anaerobic since both conditions prevail in this type of enrichment culture — aerobic in the water and upper sediment, and anaerobic in the deeper, compacted sediment. From this point on, in describing the method used in the material tests, it is necessary to describe the aerobic and anaerobic procedures separately.

In the aerobic tests, 0.01 per cent ammonium phosphate is added to sufficient sea water (usually about 7 liters) for a given test run. Oxygen is bubbled through the sea water in a carboy for a minimum of sixteen hours at which time the oxygen content of the sea water is about 25 ppm. Since as many as four or more test materials may be included in a test run, the inoculum is prepared by combining in one vial a small amount of liquid from the enrichment culture for each material to be

TABLE II — SOURCES OF SEDIMENTS* USED IN PREPARING
ENRICHMENT CULTURES

Ref. No.	Source
XG 17-4 (surface)...............	Gulf of Mex., Rockport, Texas
5403-1 (surface).................	Gulf of Mex., Miss. Delta
XS-384 (surface)................	Gulf of Mex., Rockport, Texas
5402-7 (0–5 cm).................	Gulf of Mex., Miss. Delta
56:180 (4520 fathoms)...........	Pacific, 7° 22.2′N, 127° 17′W
56:184 (2650 fathoms)...........	Pacific, 19° 02′N, 174° 58′W
56:177 (4550 fathoms)...........	Pacific, 7° 03.8′N, 126° 24.3′W

* Obtained from Dr. C. ZoBell, Scripps Institute of Oceanography.

included in the run. Once in the vial, the inoculum is shaken and added to the aged sea water at the rate of 1 ml per 10 liters of medium. This amount of inoculum was calculated to give the maximum number of bacteria, consistent with a minimum addition of organic matter. The carboy is then placed under slight, positive oxygen pressure.

The test is run in 60 ml glass-stoppered bottles. A small amount of test material is placed in each bottle. At the outset of the experiments, when ground material was used, this amounted to 0.05 gram, or a surface area of 4 to 45 sq cm, depending on the material. Later, when thin sheets of about 4 mils thickness were used, the samples were cut to a size of 2.54 cm square. The samples are placed in the bottles the night before, and enough aged sea water added to permit surface wetting. With many materials this seems to result in less accumulation of air bubbles on the surfaces of the materials during subsequent filling with the medium.

TABLE III — ENRICHMENT CULTURES* USED AS SUPPLEMENTARY SOURCES OF INOCULUM IN PREPARATION OF ENRICHMENT CULTURES FOR CURRENT PROGRAM

Ref. No.	Description
34–134	rubber in distilled water
34–134	anthracene in sea water
34–134	sewage outfall, rubber in sea water
34–134	mixed hydrocarbons in sea water
34–134	garden soil, rubber in sea water
34–132	Athabaska tar sand, hydrocarbon-oxidizing bacteria and sulfate-reducers in sea water
34–134	tricresol in sea water
34–134	mixed hydrocarbons in sea water
25–143	0.10% phenol in sea water
34–134	0.25% phenol in sea water
34–134	cork in sea water
34–134	Shell oil No. 10 in sea water
25–141	lignin in sea water
34–134	sewage outfall, rubber in sea water
34–134	sawdust and mud in sea water
34–134	garden soil, rubber in sea water
34–134	rubber in tap water
34–134	mixed crude oil in sea water
34–134	kerosene in sea water
34–134	paraffin in sea water
34–134	rubber in tap water
–	Athabaska tar sand, mixed crude oil in sea water
–	thiokol in sea water
–	neoprene in sea water
–	cellulose acetate in sea water
–	butadiene (Buna A) in sea water
–	pooled aerobic hydrocarbon-oxidizing bacteria in sea water
–	crude coal tar in sea water
–	shellac in sea water

* Obtained from Dr. C. ZoBell, Scripps Institute of Oceanography.

Of course, air bubbles would be a source of error in later oxygen determinations.

Usually, sufficient test bottles are made up to provide duplicates for analysis after each period of incubation. Oxygen pressure, maintained on the sea water in the carboy, assures no loss of oxygen from the medium and forces it through tubing into the test bottles. Since incubation periods of 0, 1, 2, 4 and 8 weeks are used as a general guide, and two test bottles must be sacrificed for analysis after each interval, ten test bottles are used for each material. One set of ten control bottles containing only inoculated, aged sea water suffices for a test run, as long as the bottles for materials and controls are made up from the same batch of sea water and incubated at the same time. Incubation is carried out in the dark in a constant temperature water bath maintained at 20° ± 0.5°C. Incubation in the water bath minimizes the fluctuation in oxygen content of the sea water which might be encountered as the result of "breathing" of the bottles in atmospheric incubation. After the various incubation periods, the free oxygen content of the sea water in the bottles is determined by a modified Winkler procedure.

In the anaerobic portion of the test, the procedure is essentially the same as for the aerobic part, the only differences being in the preparation and handling of the sea water medium, the incubation times, and the analytical method. Of course, with the anaerobic bacteria it is necessary to remove all free oxygen from the sea water medium if the organisms are to function. Consequently, instead of bubbling oxygen through the medium, the sea water is boiled for ten minutes and placed hot in a

TABLE IV — OXYGEN CONSUMPTION BY MARINE BACTERIA
IN BOD TEST WITH POLYETHYLENE AS THE
ONLY SOURCE OF ORGANIC CARBON

Test Material[2]	O_2 Consumption After Weeks of Incubation			
	1	2	4	8
	ppm	ppm	ppm	ppm
2.0 melt index[3]	2.2	3.7	6.0	10.2
0.2 melt index (Source A)	0.8	1.6	2.4	10.9
0.2 melt index (Source B)	1.4	3.4	5.2	10.8
0.2 melt index + antioxidant	0.9	3.0	6.2	8.5
0.2 melt index + 5% butyl rubber + antiox.	0.2	3.8	5.8	—[1]
0.7 melt index (High Density) + antiox.	0.9	4.3	7.4	9.3
Controls (inoculated sea water)	1.5	5.3	8.3	11.2

[1] Samples accidentally destroyed.
[2] Except where noted polymers are low density grades manufactured by the high pressure process.
[3] ASTM D1238

TABLE V — OXYGEN CONSUMPTION BY MARINE BACTERIA IN BOD TEST WITH POLY(VINYL CHLORIDE) PLASTICS, EPOXIDE CASTING RESIN OR JUTE AS ONLY SOURCES OF ORGANIC CARBON

Test Material	O₂ Consumption After Weeks of Incubation			
	1	2	4	8
	ppm	ppm	ppm	ppm
PVC — no plasticizer (rigid)...............	11.1	12.9	11.6	18.7
PVC — tricresyl phosphate (TCP)..........	9.5	13.2	21.6	22.2
PVC — di-2-ethylhexyl phthalate (DOP) Shore A 88.........................	9.1	13.4	19.7	20.7
PVC — polyester A........................	19.3	22.2	*	*
Epoxide casting resin......................	—	4.1	5.1	4.2
Jute......................................	10.0	15.0	16.5	*
Controls (inoculated sea water)	6.8	6.8	7.7	7.7

* All free O₂ in sea water consumed.

carboy containing 0.01 per cent ammonium phosphate. Nitrogen is introduced into the carboy immediately. When the sea water is cool, inoculum, which is prepared as described for the aerobic procedure, is added and additional nitrogen pressure placed on the carboy for filling the test bottles. Since anaerobic activity is usually slower than aerobic, the time in test is increased. Analysis for hydrogen sulfide in the sea water is carried out at 0, 4, 8, 12 and 16 weeks. Since the sulfate-reducing bacteria are ubiquitous anaerobic marine species, the hydrogen sulfide produced by them in the course of breaking down organic material is used as an indicator of their activity. The sulfide in the sea water is determined volumetrically according to the method described in the Official

TABLE VI — OXYGEN CONSUMPTION BY MARINE BACTERIA IN BOD TEST WITH POLY(VINYL CHLORIDE) PLASTICS AS THE ONLY SOURCE OF ORGANIC CARBON

Plasticizer	O₂ Consumption After Weeks of Incubation			
	1	2	4	8
	ppm	ppm	ppm	ppm
Nitrile rubber/polyester C..................	10.3	12.9	21.4	*
Nitrile rubber.............................	9.2	12.3	18.7	*
None[1]...................................	3.7	4.2	6.5	10.5
None[1]...................................	4.0	5.5	8.4	11.0
Tri-2-ethylhexyl phosphate.................	11.7	14.4	23.1	*
Di-2-ethylhexyl phthalate (DOP) Shore A 62.	6.4	8.4	11.5	*
Polyester E/DOP (BTL 46–55)..............	*			
Controls (inoculated sea water).............	3.5	4.5	7.1	9.7

* All free O₂ in sea water consumed.
[1] Semi-flexible PVC copolymer.

TABLE VII — OXYGEN CONSUMPTION BY MARINE BACTERIA IN BOD
TEST WITH POLYETHYLENE, POLYESTER CASTING RESIN OR POLY-
(VINYL CHLORIDE) RESIN AS ONLY SOURCE OF ORGANIC CARBON

Test Material	O_2 Consumption After Weeks of Incubation			
	1	2	4	8
	ppm	ppm	ppm	ppm
Polyethylene 0.7 melt index (High Dens.) Nat. + antioxidant....................	3.1	3.3	6.1	6.5
Polyethylene 0.7 melt index (High Dens.) Blk.......................	2.9	4.1	7.1	7.0
Styrene polyester, silica-filled..............	5.5	7.0	9.3	12.1
Poly(Vinyl Chloride) resin..................	4.2	4.1	7.3	7.2
Controls (inoculated sea water).............	2.5	3.8	6.7	6.7

and Tentative Methods of Analysis of the Association of Agricultural Chemists.

The results of the aerobic test procedure are presented in Tables IV to VIII inclusive. In these tables the oxygen consumption values obtained with materials which went through the same test run are included in the same table. The materials included in Tables IV and V, with the exception of jute, were exposed in finely ground or shaved form. Since it was not possible to obtain reliable estimates of the surface areas exposed to attack in this case, the oxygen consumption values in these tables are not directly comparable with respect to rate. The data serve the important basic purpose of indicating whether these materials can serve as a source of energy for the bacteria. However, data in Tables VI to VIII inclusive are based on the use of equally thin sheets of material with about 12.9 sq cm of surface area exposed to attack. Two exceptions

TABLE VIII — OXYGEN CONSUMPTION BY MARINE BACTERIA IN BOD
TEST WITH ELASTOMERS AS THE ONLY SOURCE
OF ORGANIC CARBON

Elastomer	O_2 Consumption After Days of Incubation			
	3	7	14	28
	ppm	ppm	ppm	ppm
GR-S jacket (54-14)	15.8	*		
GR-A jacket (54-18)	6.1	10.9	23.5	*
Butyl jacket (54-19)	13.9	*		
Natural rubber jacket (54-23)	14.1	*		
Neoprene jacket (54-164)	1.9	4.1	10.3	*
Controls (inoculated sea water).............	0.0	−0.4	0.0	

* All free O_2 in sea water consumed.

to this are the polyvinyl chloride resin and styrene polyester in Table VII which could not be prepared in sheet form.

Results for polyethylene are described in Tables IV and VII. The oxygen consumption values in these tables are almost identical to the control values obtained using only inoculated sea water. There is no evidence in any of these tests of polyethylene being utilized as a source of carbon by the bacteria. In fact, in Table IV, all of the eight week values for polyethylene are slightly below those for inoculated sea water alone.

The results with the polyvinyl chloride plastics vary according to the manner in which the compounds are plasticized. The data are contained in Tables V, VI and VII. First, as may be noted in Table VII, there is no attack on the polyvinyl chloride resin. This indicates that the susceptibility of these plastics can be attributed to materials added in compounding. Every polyvinyl chloride plastic tested shows some evidence of attack; (distinct oxygen consumption above the control rate), except the semi-flexible copolymers which contain no added external plasticizer. In these compounds, acrylates are employed as copolymers. The most severe attack occurred on the plastic in Table VI which con-
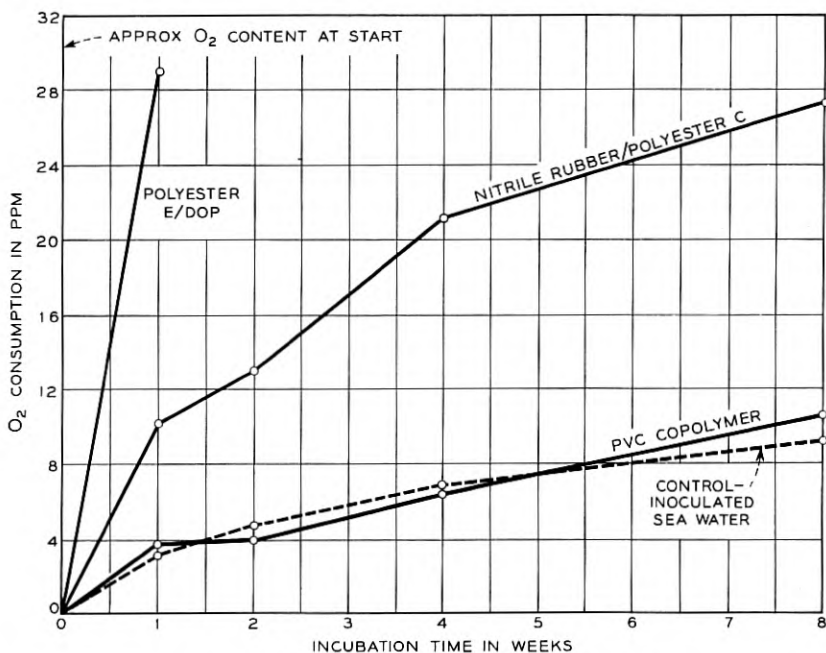
Fig. 3 — Examples of O_2 consumption by marine bacteria in BOD test with Poly(Vinyl Chloride) plastics as carbon source.

tains a combination of polyester E and di-2-ethylhexyl phthalate (DOP), and one in Table V plasticized with polyester A. These polyesters are fatty acid-type compounds. Typical oxygen consumption values for three different polyvinyl chloride plastics, representing different rates of utilization by the bacteria, are plotted in Fig. 3. As noted in Table I, very low concentrations of organo-metallic stabilizers and fatty acid lubricants were in all the compounds tested except the resin alone. However, of the three materials which contained no added external plasticizer only the rigid plastic is utilized. This material contained about 8 to 10 times as much fatty acid lubricant as the other two compounds.

Two casting resins were tested, one an epoxide (Table V), and the other a silica-filled styrene polyester (Table VII). Under the conditions of this test, the epoxide resin is not utilized by the organisms. In the case of the styrene polyester, results are less conclusive. After eight weeks, an oxygen consumption value 5.4 ppm higher than that for the controls suggests the possibility of attack. Additional tests are planned with this material to obtain more data on which to base a final decision.

As might be expected, the jute fibers are quite susceptible to attack; all oxygen was consumed from the test medium between the fourth and eighth week (Table V). The fact that results in the same test run with the polyvinyl chloride compound plasticized with polyester A show that all oxygen was consumed from the test medium in 17 days does not mean that this latter compound is more susceptible to attack than jute. In the jute, bacterial attack is necessarily restricted to a progressive surface attack, but with the polyvinyl chloride compound, leaching of the sus-

TABLE IX — HYDROGEN SULFIDE PRODUCTION BY MARINE BACTERIA IN ANAEROBIC SEA WATER TEST WITH POLYETHYLENE AS THE ONLY SOURCE OF ORGANIC CARBON

Test Material[1]	H_2S Production After Weeks of Incubation			
	4	8	12	16
	ppm	ppm	ppm	ppm
2.0 melt index[2]	0.22	0.32	0.22	—[3]
0.2 melt index (Source A)	0.22	0.29	0.45	—[3]
0.2 melt index (Source B)	0.22	0.32	0.26	0.38
0.2 melt index + antioxidant	0.22	0.64	0.35	0.58
0.2 melt index + 5% butyl rubber + antiox.	0.22	0.32	1.31	0.24
0.7 melt index (High Density) + antiox.	0.22	0.22	0.29	0.45
Controls (inoculated sea water)	0.10	0.64	0.70	0.58

[1] Except where noted polymers are low density grades manufactured by the high pressure process.
[2] ASTM D1238
[3] Insufficient samples

ceptible plasticizer into the sea water medium might greatly accelerate utilization of that material and be reflected in rapid oxygen consumption.

Five different elastomers have been evaluated by the BOD test to date. The results with aerobic bacteria are presented in Table VIII. First, it is apparent that all of the elastomers tested can serve as a source of carbon for the bacteria. As may be noted in the table, GR-S jacket (54–14), butyl jacket (54–19) and natural rubber (54–23) are oxidized at about the same rate—all oxygen being consumed from the test medium between the third and seventh day analyses. GR-A (54–18) and neoprene jacket (53–164) are more resistant than the other three elastomers in the test. During the fourteen-day test period, approximately twice as much oxygen was consumed in the case of the GR-A as with the neoprene.

The results of anaerobic bacterial activity, as reflected by analyses for hydrogen sulfide in the sea water medium, are contained in Tables IX to XII, inclusive. As with the results of the aerobic test, materials in a given test run are included in the same table. No polyethylene is utilized as a source of carbon by the sulfate-reducing bacteria. In no case is the production of hydrogen sulfide, with different polyethylenes

TABLE X — HYDROGEN SULFIDE PRODUCTION BY MARINE BACTERIA IN ANAEROBIC SEA WATER TEST WITH POLY(VINYL CHLORIDE) PLASTICS, EPOXIDE CASTING RESIN, OR JUTE AS ONLY SOURCES OF ORGANIC CARBON

Test Material	H_2S Production After Weeks of Incubation			
	4	8	12	16
	ppm	*ppm*	*ppm*	*ppm*
Poly(Vinyl Chloride) Plastics				
No plasticizer (rigid)	1.90	3.50	4.20	5.60
Tricresyl phosphate (TCP)	0.22	0.22	0.64	0.38
Di-2-ethylhexyl phthalate (DOP) Shore A 88	0.26	0.26	0.26	0.61
Polyester A	2.60	38.40	38.40	47.70
Nitrile rubber/polyester C	1.50	7.00	19.98	18.60
Nitrile rubber	4.10	9.60	12.40	11.50
No plasticizer[1]	0.22	0.22	0.90	0.51
No plasticizer[1]	0.32	0.64	1.89	1.02
Tri-2-ethylhexyl phosphate	0.26	0.96	1.86	0.99
Di-2-ethylhexyl phthalate (DOP) Shore A 62	0.22	0.22	1.09	0.58
Polyester E/DOP (BTL 46-55)	12.20	61.40	94.10	82.90
Epoxide casting resin	0.16	0.64	0.86	0.48
Jute	1.90	13.40	38.60	52.20
Controls (inoculated sea water)	0.10	0.64	0.70	0.58

[1] Semi-flexible PVC copolymer

TABLE XI — HYDROGEN SULFIDE PRODUCTION BY MARINE BACTERIA
IN ANAEROBIC SEA WATER TEST WITH POLYETHYLENE,
POLYESTER CASTING RESIN OR POLY(VINYL CHLORIDE)
RESIN AS ONLY SOURCES OF CARBON

Test Material	H_2S Production After Weeks of Incubation			
	4	8	12	16
	ppm	*ppm*	*ppm*	*ppm*
Polyethylene — 0.7 melt index (High Dens.) Nat. + antioxidant	0.35	0.58	0.90	1.12
Polyethylene — 0.7 melt index (High Dens.) Blk. + antioxidant	0.26	0.48	0.38	0.74
Silica-filled styrene polyester	0.83	0.83	1.02	1.02
Poly(Vinyl Chloride) resin	0.48	0.58	0.58	0.58
Controls (inoculated sea water)	0.45	0.86	0.91	0.91

as the test material (Tables IX and XI), significantly greater than in
the control bottles. In fact, in most cases it is actually less than that for
the controls.

Four polyvinyl chloride plastics appear to have served as a source of
carbon for the anaerobic organisms. In order of decreasing susceptibility
they are the compounds plasticized with (1) polyester E/DOP, (2) poly-
ester A, (3) nitrile rubber/polyester C, and (4) no plasticizer (rigid).
Just as in the case of the aerobic procedure, the plastic plasticized with
polyester E/DOP is used much more rapidly than any of the other
polyvinyl chloride compounds. There is no evidence of attack on poly-
vinyl chloride resin, again indicating that the attack is on the plasticizers,
not the polyvinyl chloride itself. In this regard, it should be pointed out
again that although the polyvinyl chloride compound listed as "no plas-
ticizer (rigid)" in the tables and text does not contain an external plas-

TABLE XII — HYDROGEN SULFIDE PRODUCTION BY MARINE BACTERIA
IN ANAEROBIC SEA WATER TEST WITH ELASTOMERS AS THE
ONLY SOURCES OF ORGANIC CARBON

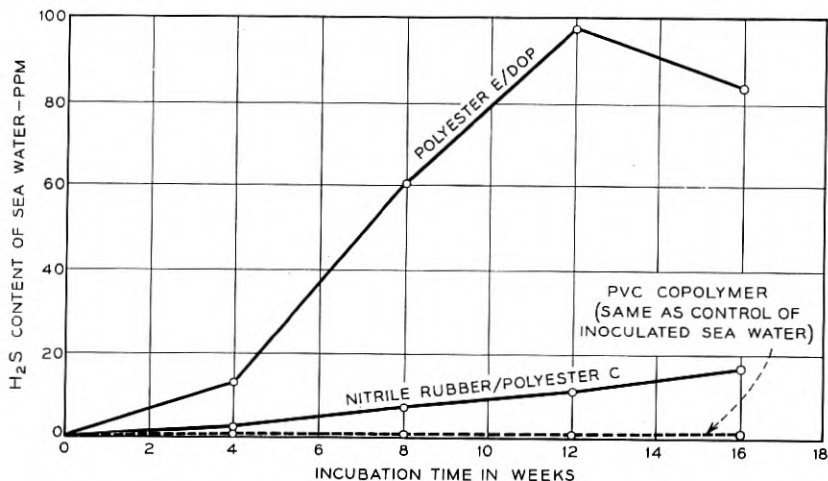| Elastomer	H_2S Production after Weeks of Incubation			
	4	8	12	16
	ppm	*ppm*	*ppm*	*ppm*
GR-S jacket (54-14)	0.66	0.77	0.56	0.75
GR-A jacket (54-18)	0.96	0.95	0.72	0.87
Butyl jacket (54-19)	1.52	6.64	8.03	9.65
Natural rubber jacket (54-23)	1.62	2.48	3.58	3.74
Neoprene jacket (54-164)	1.06	1.20	0.99	0.96
Controls (inoculated sea water)	0.37	0.43	0.43	0.42

Fig. 4 — Examples of H_2S production by marine bacteria in anaerobic sea water test with Poly(Vinyl Chloride) plastics as carbon source.

ticizer, fatty acid lubricant probably serves as a source of nutrient. For comparative purposes, the examples of hydrogen sulfide production plotted in Fig. 4 are for the same plastics included in Fig. 3 which relates to the data from the aerobic procedure.

Jute is attacked by the anaerobic bacteria just as it is utilized by the aerobic organisms. However, neither the epoxide casting resin (Table X) or the polyester casting resin (Table XI) seem to serve as a source of carbon.

The results of the anaerobic test with the elastomers are presented in Table XII. It is interesting to note that early attack occurs on the natural and butyl rubber jackets, but that none of the other elastomers is utilized by the organism. It is somewhat surprising that attack on GR-S did not progress at about the same rate as on natural and butyl rubber.

The data which have been obtained in the aerobic and anaerobic parts of the BOD-type test are summarized in Table XIII. There is one outstanding fact about the data — no material was utilized by the anaerobic bacteria which was not utilized also by the aerobic organisms. Under the conditions of the test, however, materials did serve as a carbon source for aerobic bacteria and not for the anaerobes.

3.2 *Conductor Test*

It is apparent that the BOD test provides considerable fundamental information on the ability of halophilic bacteria to utilize organic ma-

terials as a carbon source in sea water. There is little or no opportunity for ecological factors to come into play, however, particularly with regard to marine sediment. In the conductor test, sea water and marine sediment form a part of the test environment, and the test is run over a much longer period of time, thus encouraging more natural and dynamic organism associations. Likewise, the natural relationship between material and environment is simulated more closely than it is in the more accelerated test. In these respects, the conductor test is intermediate to the BOD-type test and natural marine exposure.

The material to be tested is coated on a conductor to provide about 10 mils of insulation. A standard coil of this insulated conductor is then exposed in a 16-ounce bottle so that half of the coil is in marine sediment, and half is in sea water. The ends of the coil are brought through holes in the bottle cap and attached to terminals in the cap. The general features of the test setup are shown in Fig. 5. The bottle is incubated at 20°C. Capacitance and conductance measurements, taken monthly, indicate any change in the insulation. Some conductors are placed in sterile sea water and sediment to serve as controls. This type of test can be continued for months or years if necessary.

Most of the conductor tests are now being initiated. Two materials, however, GR-S and a rigid polyvinyl chloride, have been under study

TABLE XIII—SUMMARY OF MATERIALS UTILIZED AS SOURCE OF CARBON BY AEROBIC OR ANAEROBIC MARINE BACTERIA IN BOD-TYPE TEST

Utilized as Source of Carbon by	
Aerobic Bacteria	Anaerobic Bacteria
PVC — no plasticizer (rigid)	PVC — no plasticizer (rigid)
PVC — tricresyl phosphate (TCP)	
PVC — di-2-ethylhexyl phthalate (DOP) Shore A88	
PVC — polyester A	PVC — polyester A
PVC — nitrile rubber/polyester C	PVC — nitrile rubber/polyester C
PVC — nitrile rubber	PVC — nitrile rubber
PVC — tri-2-ethylhexyl phosphate	
PVC — di-2-ethylhexyl phthalate (DOP) Shore A 62	
PVC — polyester E/DOP (BTL 46–55)	PVC — polyester E/DOP (BTL 46–55)
Styrene polyester	
GR-S jacket (54-14)	
GR-A jacket (54-18)	
Butyl jacket (54-19)	Butyl jacket (54-19)
Natural rubber jacket (54-23)	Natural rubber jacket (54-23)
Neoprene jacket (54-164)	
Jute	Jute

for several months in a "dry" run to establish the biological procedure, as well as the techniques of measurement which are to be employed. The capacitance and conductance data which have been obtained on these two materials to date are presented in Figs. 6 and 7, respectively. In the case of the test samples, each point represents the average value for four test coils, but for the controls each point represents only one coil.

With the GR-S test samples, there is a sharp rise in the capacitance values between the second and third month, amounting to about 110 $\mu\mu$f. Thereafter, the rise in the curve continues, the slope decreasing somewhat at about the eighth-month point. Over the entire test period, the capacitance ranged from 632 $\mu\mu$f at the start to 850 $\mu\mu$f after 13 months
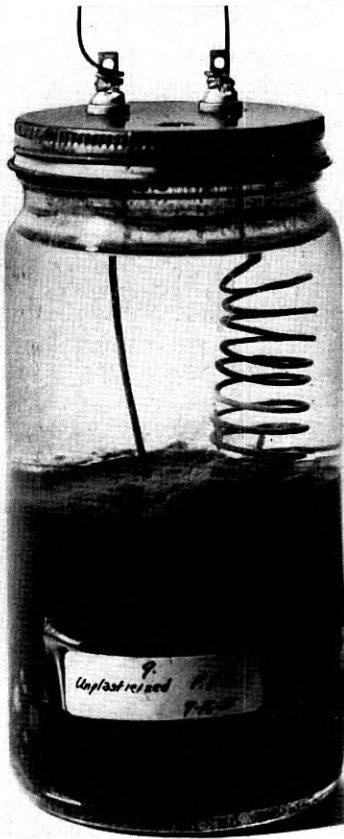
Fig. 5 — General setup of conductor test showing a coil half in sediment and half in sea water.
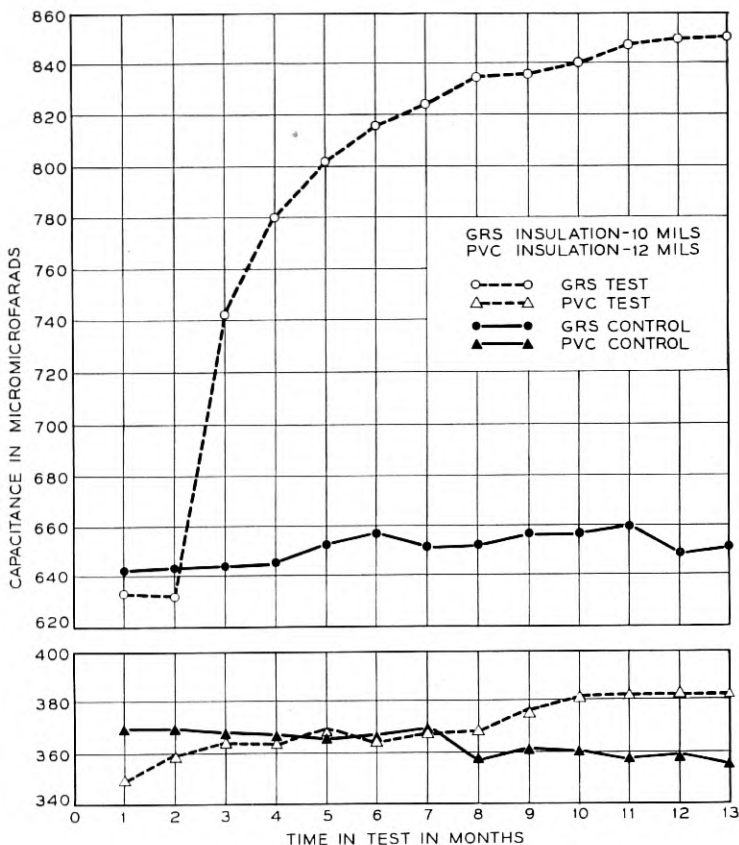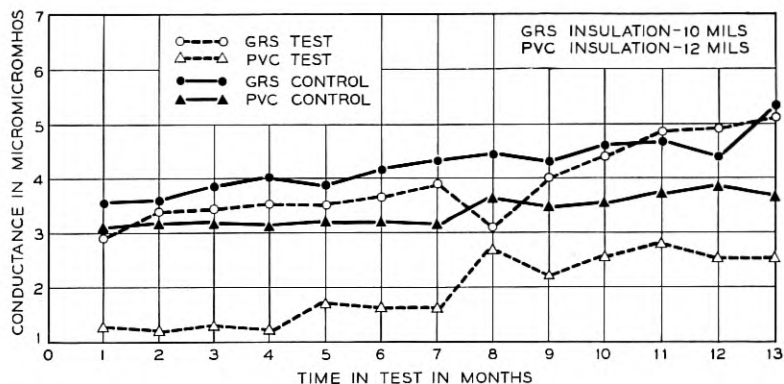
Fig. 6 — Capacitance changes resulting from exposure of GR-S (51-92) and Poly(Vinyl Chloride) (BTL 172-54) insulated conductors in sea water and sediment.

exposure — a total change of 218 $\mu\mu$f. If it is assumed that the insulating materials were removed equally along the length of the coil, it can be computed that this change in capacitance represents a loss of 8.1 mils of insulation. The following formula is used to arrive at this figure:

$$D = d \left(\frac{D_0}{d}\right)^{c_0/c}$$

where D = present diameter in mils,
        D_0 = original diameter in mils,
        d = diameter of wire in mils,
        C_0 = original capacitance in $\mu\mu$f (start of test),
        C = present capacitance in $\mu\mu$f.

In contrast, capacitance values for the controls have remained essentially unchanged.

There has been no substantial increase in the capacitance of the polyvinyl chloride-insulated conductors although there is some evidence of an upward trend in the data for the coils in the biologically active environment. There was a rise in capacitance of about 15 $\mu\mu f$ between the one and three month period, and a similar rise between the eighth and tenth month. Future measurements should indicate whether any biological attack is occurring.

Fig. 7 — Conductance changes resulting from exposure of GR-S (51-92) and Poly(Vinyl Chloride) insulated conductors in sea water and sediment.

As may be noted from the conductance data for both materials in Fig. 7, the patterns of the curves for the test and control samples are essentially the same. In all cases there has been a slight increase in conductance over the 13 month test period. For GR-S it has increased from about 1.5 to 2.0 $\mu\mu$mhos and for the polyvinyl chloride from about 0.75 to 1.5 $\mu\mu$mhos.

In a test of this kind the rise in capacitance, such as that which occurs with the GR-S, without any marked corresponding increase in conductance suggests that the insulation is being modified by the attack, rather than actually removed as assumed previously. It also suggests that the action is most likely due to bacteria rather than fungi which might be expected to penetrate the insulation directly to the conductor and so have a more pronounced effect on conductance. When the test is terminated, it is hoped that these insulated conductors can be run through a capacitance and conductance monitor to locate the specific points of deterioration, and to determine the extent and type of attack.

IV. SOIL BURIAL

Since this phase of the test program is yet to be started no extended coverage is possible in this paper, except to point out the reason for its inclusion. There is some evidence in the results of the marine exposure tests at the Laboratories that the general order of susceptibility of materials to marine microorganisms is the same as it is to terrestrial microorganisms. This observation has also been supported in discussions with some other investigators. The current program at the Laboratories offers an excellent opportunity to compare the performance of a wide range of materials in the two environments. If a correlation pattern can be established, considerably more data in the literature can be brought to bear on the problem. Perhaps at a later date it will be possible to present data comparing material performance in the laboratory soil-burial test and marine-type tests.

V. MARINE EXPOSURE

5.1 *Marine Borer Tests*

The Laboratories, in cooperation with the William F. Clapp Laboratories, Inc., Duxbury, Massachusetts, is conducting the marine borer tests. This phase of the program was initiated in 1954 and involves the natural exposure of specimens at two locations — Wrightsville Beach, North Carolina, and Daytona Beach, Florida. These tests are aimed primarily at obtaining information on marine borer attack; however, the samples are exposed in such a way that information is obtained on microbiological activity as well. In addition, valuable data is obtained on the purely physical and chemical effects of the environment on the materials.

Wrightsville Beach and Daytona Beach were selected as test sites because of the severe and diversified borer activity present in the two areas. At present, more than fifty different materials are exposed at the two locations. Represented are plastics, elastomers and natural organic materials. All of the materials which have been put through the BOD-type test, or are still to be included, are represented in the marine borer portion of the test program. Where possible, test specimens are made in solid rod or tube form about one inch in diameter and three feet long to simulate cable shape. In the case of fibers and tapes, samples are wrapped on $\frac{3}{4}$-inch diameter Lucite rods 3 feet long. These rods are assembled in racks of about 26 rods each. An untreated, southern pine two by four, susceptible to borer attack, is fitted around the samples at midpoint, where it functions as a bait piece to lead the organisms into direct contact with each test rod. Of course, where there is no bait piece
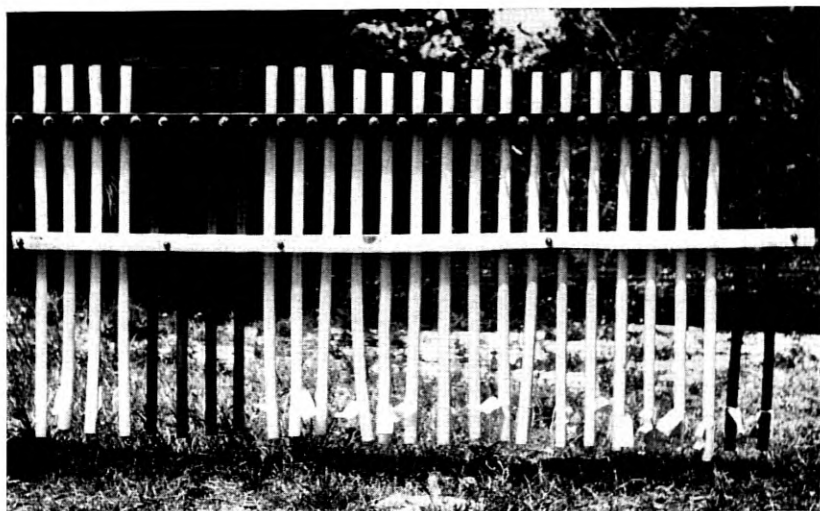
Fig. 8 — A test rack used in marine borer test prior to exposure. Note bait piece of untreated wood fastened across middle of test rods.

it is possible to determine whether the organisms can attack the samples directly from the water. Fig. 8 is a photograph of one of the racks prior to exposure in the sea. The lower 10 inches of the rods are embedded in the bottom sediment where bacterial action is relatively high. Thus, each sample is subjected to water exposure and possible borer attack through the transition zone from water to sediment and into the generally anaerobic conditions of the sediment.

Due to the short time that these tests have been in progress, it is impossible to draw extensive conclusions, particularly with regard to microbiological activity. Long exposure times may bring about physical or chemical changes in a material which may render it more, or less, susceptible to attack. However, until more detailed data are available, some interesting preliminary examples of biological activity can be cited which may be of some interest and serve to illustrate the kind of information which is steadily being acquired.

With but two exceptions, there has been no direct penetration by borers, or microbiological deterioration, of any of the plastics. Polymonochlor-trifluoroethylene in the form of a 0.0035 inch-thick tape wrapped on a $\frac{3}{4}$-inch diameter Lucite rod for exposure, was penetrated at one point by a pholad. This attack occurred after three years of exposure at Daytona Beach. Apparently the mollusk bored through an accumulation of calcareous fouling and then progressed through the plastic into the

Lucite rod. In another instance, after $2\frac{1}{2}$ years of exposure at Wrights-ville Beach, there was penetration of a silicone rubber test rod at a single point by a pholad. In this case, the test sample was a solid rod of the elastomer one inch in diameter. Attack occurred on the cross-sectional face of the mud end of the rod. Penetration was to a depth of about 4 mm, and the dimensions of the hole at the point of entry were 1.5 by 2.0 mm. Although these examples serve to demonstrate the ability of pholads to bore into these materials, it should be emphasized again that attack has been confined to single points and is not general on these materials.

The physical relationship of one material to another can be very important as far as borer attack is concerned. A piece of one of the Lucite rods on which jute roving was wrapped for exposure is shown in Fig. 9. The holes in the rod resulting from penetration by pholads are readily apparent. One of the organisms may be seen protruding from the left-
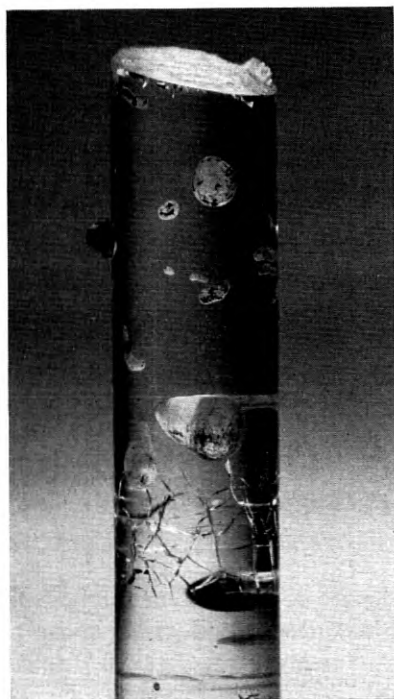
Fig. 9 — Section of Lucite rod showing penetration by pholads. One of the mollusks can be seen protruding from the left-hand side of the rod. Original magnification 2X.
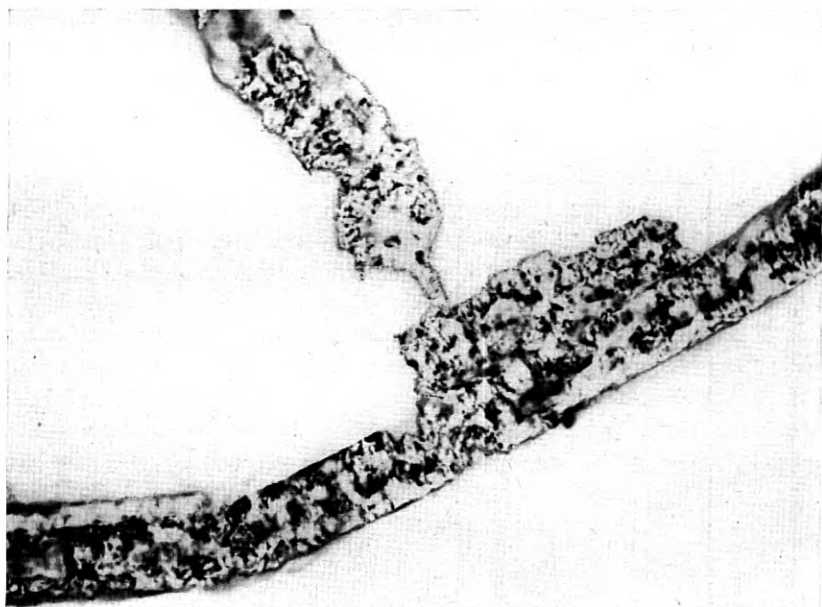
Fig. 10 — Cellulose acetate fiber showing extensive surface erosion after one year of marine exposure. Original magnification 1000X. Photo by F. G. Foster.

hand side of the rod. In this case, the pholads obtained their start in the jute wrapping and then were able to progress into the Lucite. There was no attack evident on portions of the rod which were not wrapped with jute. Also, it is interesting to note that the jute in this particular case was treated with an impregnant consisting of 50 parts asphalt, 50 parts paraffin and 2 parts zinc naphthenate. Although this mixture was not highly effective as a preservative, it did serve to hold the jute in position long enough to enable the borers to become established. There has been no evidence of penetration of Lucite rods on which untreated jute was wrapped. Here, apparently, the jute was destroyed by microbiological attack or other borers such as limnoria before the pholads could become well established.

In this progress report no detailed comparison of the performance of natural fibers, such as jute treated with various preservatives, will be attempted. Results in many cases are still inconclusive. As might be anticipated, however, the jute specimens as a group have suffered much heavier deterioration by borers and microorganisms than the plastics, elastomers and casting resins. Particularly noteworthy is the fact that although there is considerable evidence of bacterial attack upon micro-

scopic examination, there is also much degradation evident by the fungi. Pin holes in the cell walls with associated fungal hyphae are extensive.

Secondary cellulose acetate has been quite susceptible to microbiological deterioration. Yarn has been destroyed in just six months of marine exposure, not by borers, but predominantly by bacteria. Upon microscopic examination, the fibers show severe surface erosion due apparently to bacterial attack. In the marine samples which have been stained and examined, hyphae have been evident in only one isolated instance. The extent of the pitting and surface erosion in one of the marine samples after one year in test can be seen in Fig. 10. This characteristic pattern of erosion is also evident in samples of cellulose acetate yarn from soil burial. Such a sample after 60 days of burial is shown in Fig. 11. Here again attack appears to be predominantly of bacterial origin.

In the marine borer tests, the sample rods become heavily fouled in the water area, as may be noted in Fig. 12. Although these fouling organisms do not use the materials to which they attach as a source of food, it is well known that they can do mechanical damage or chemically influence the environment beneath them. The reader who is particularly interested in the broad subject of fouling and its effect on materials,
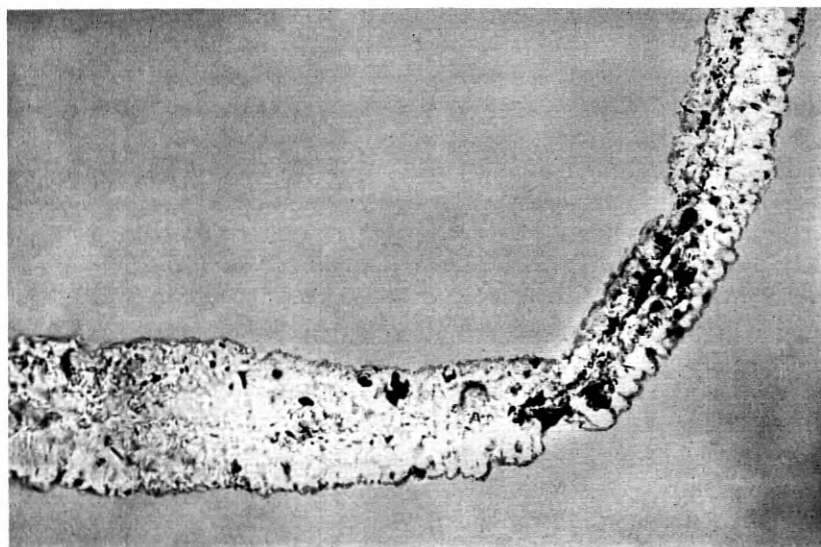
Fig. 11 — Cellulose acetate after 60 days in laboratory soil burial. Note characteristic surface erosion comparable to that shown in Fig. 10 for marine test sample. Original magnification 500X. Photo by F. G. Foster.
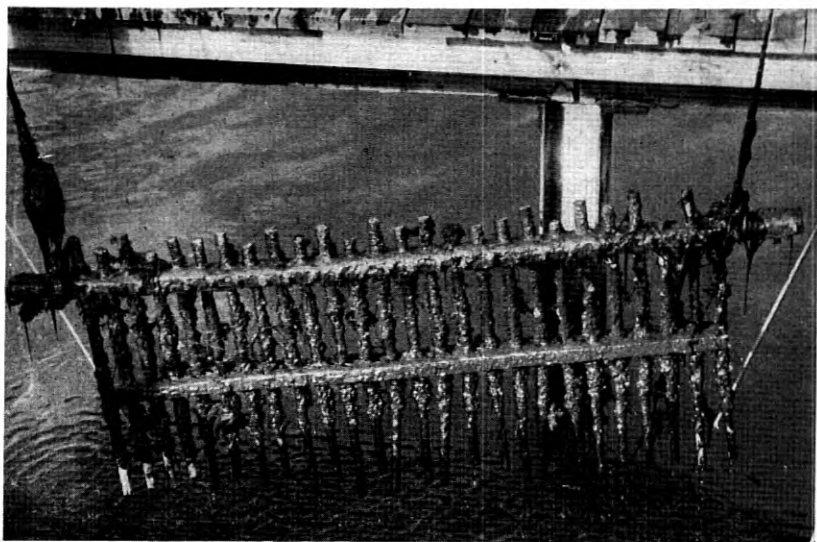
Fig. 12 — Test rack being lifted from water at Wrightsville Beach. Heavy accumulation of fouling on test rods in water-exposed area stops at point where rods entered the sediment.

structures and coatings, is referred to the report of the investigations conducted at the Woods Hole Oceanographic Institution during the years 1940 to 1946.[17] The restricted areas beneath fouling, particularly under the bases of calcareous organisms such as barnacles, provide ideal cells for bacterial activity. Conditions of pH and aeration may be markedly different in these confined areas from those in the surrounding water. Some of the test rods made of polyvinyl chloride plastics containing basic lead stabilizers, illustrate the fact rather dramatically. Anaerobic, sulfate-reducing bacteria are common marine organisms which release hydrogen sulfide in the process of breaking down organic material. Under tightly adhering fouling, aerobic bacteria can utilize the free oxygen much more rapidly than it can be replaced by diffusion from the surrounding water. Once the oxygen has been depleted, the anaerobic organisms begin their activity and cause relatively high concentrations of hydrogen sulfide to be built up. The hydrogen sulfide reacts with the basic lead salts used as stabilizers and produces black lead sulfide. The sharp boundaries of the different environmental conditions existing beneath the base of a barnacle on one of the polyvinyl chloride test rods are illustrated in Fig. 13. Here the pattern of the barnacle base has literally been reproduced by the sulfiding which occurred under it. The black border and black radiating lines correspond to areas of exception-

ally close contact. The radial extent of this sulfiding in the bottom end of the rod which was embedded in the sediment, as compared to the top or water end, is shown in Fig. 14. It must be emphasized that there has been no indication to date of any adverse effect on the physical properties of plastics which have been sulfided in this way.

VI. CABLE SAMPLES FROM SERVICE

The samples of submarine cables which have been examined to the present time represent both telegraph and telephone cables. The samples of telegraph cable have been obtained through the cooperation of the Western Union Telegraph Company. It takes considerable time to assemble a large number of specimens during the course of routine repair operations. As a result, although some 22 different samples, the majority from the North Atlantic, have been examined, it is possible to make only

Fig. 13 — Sulfiding of Poly (Vinyl Chloride) plastic test rod beneath barnacles. The black, circular border and center area represent sulfiding at points of exceptionally close contact. Original magnification 2X. Photo by J. B. DeCoste.
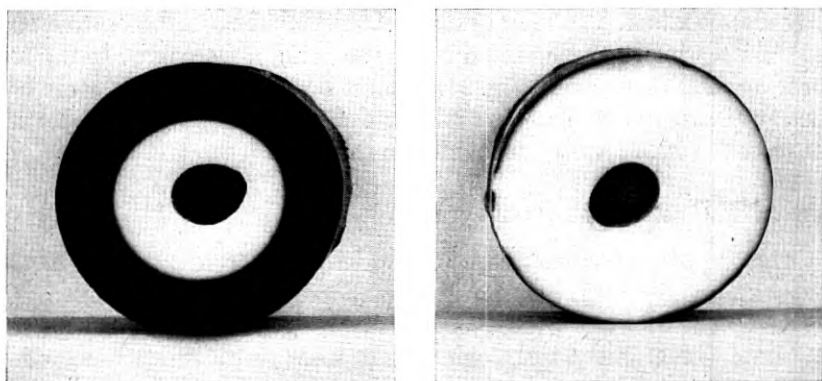
Fig. 14 — Cross-section of Poly(Vinyl Chloride) rod showing sulfiding due to sulfate-reducing marine bacteria. Bottom end was in sediment — top in water. Exposed at Daytona Beach for two years. Original magnification 1.6X.

general observations and broad comparisons. The locations and depths from which the samples were obtained are given in Table XIV. In most cases, a sample 3-feet long is obtained. Twenty-two different pieces of such size represent a rather small sample with respect to the total marine environment. Here again the program assumes more value as additional samples are obtained.

The procedure employed in examining one of these cable sections is about as follows. First, the over-all external condition is observed and recorded. Then, the outer jute covering, armor wires, inner jute bedding, and cloth and metallic tapes, if any, are removed progressively. The armor wires are examined in detail by electrochemists to determine the extent and kind of corrosion. The jute is tested in various ways. If sufficient material is available tensile strength is measured. Microscopic examination of representative fibers is also made. In the case of the inner jute which is not treated with tarry materials, damage counts are run according to the procedure of MacMillan and Basu.[18] According to this method, deoiled and dewaxed fibers are permitted to swell in 10 per cent sodium hydroxide solution. Following this they are treated in a bath of 133 per cent weight to volume, aqueous zinc chloride solution over steam. Undamaged fibers swell as tight helices while damaged fibers swell as bundles of parallel fibrils. The fibers are mounted in zinc chloride solution on a microscope slide and counted to determine the per cent of damaged fibers.

To examine the integrity of the insulation on the conductor, the electrolytic procedure of Blake, Kitchin and Pratt[19] is used. An electrolytic

cell is set up with 20 per cent copper sulfate solution as the electrolyte, and a copper plate as the anode. The cathode is a loop of the insulated conductor from the cable. Any plating out of copper on the cathode indicates a break in the insulation. In this way the integrity of a relatively long length of conductor can be examined critically and simply.

One of the outstanding facts apparent from the examination of cable samples has been the evident importance of the outer jute in limiting the corrosion of armor wires. Galvanized steel armor wires which still retain the protection of flooding compounds, such as asphalt, tar or pitch, together with outer servings of impregnated jute, have shown negligible steel corrosion within 40 years, and in one case for as long as 66 years. On the other hand, most of the corrosion of armor wires which has been observed has occurred in cable from which a major part, or all, of the outer jute has been lost.

TABLE XIV — LOCATIONS AND DEPTHS FROM WHICH SUBMARINE
CABLE SAMPLES HAVE BEEN OBTAINED FOR
LABORATORY EXAMINATION

| BTL No.	Location		Depth
	Latitude	*Longitude*	*Fathoms*
110	approx. 81° 30′ 00″N	24° 30′ 00″W	5 approx.
111	approx. 81° 30′ 00″N	24° 30′ 00″W	5 approx.
112	approx. 81° 30′ 00″N	24° 30′ 00″W	5 approx.
113	approx. 81° 30′ 00″N	24° 30′ 00″W	5 approx.
114	approx. 81° 30′ 00″N	24° 30′ 00″W	5 approx.
135a	23° 45′ 00″N	81° 57′ 30″W	830
136	Several miles south of Long Island, N. Y.		
	Exact location unknown.		90
137	40° 13′ 40″N	71° 07′ 25″W	90
163	48° 36′ 06″N	36° 23′ 36″W	2460
164	51° 53′ 42″N	10° 37′ 18″W	54
165	51° 40′ 42″N	13° 02′ 12″W	630
166	51° 55′ 21″N	11° 58′ 18″W	387
167	47° 52′ 24″N	38° 23′ 12″W	2460
168	47° 22′ 06″N	42° 14′ 12″W	2175
169	36° 41′ 46″N	25° 38′ 09″W	1180
195	45° 28′ 21″N	60° 20′ 24″W	106
196	46° 41′ 36″N	56° 18′ 18″W	37
197	47° 00′ 32″N	56° 51′ 40″W	100
200	44° 25′ 40″N	63° 25′ 15″W	46
212	45° 08′ 38″N	54° 33′ 06″W	82
281	43° 38′ 10″N	55° 07′ 00″W	2090
282	39° 17′ 24″N	70° 12′ 15″W	1450
283	53° 57′ 00″N	165° 50′ 00″W	Unknown
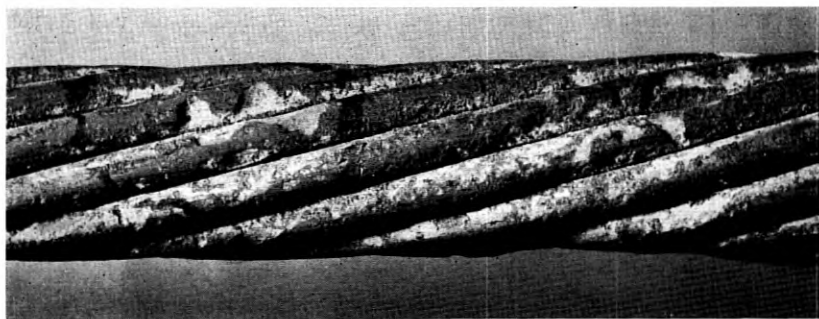
Fig. 15 — Corrosion pockets in galvanized steel armor wires of submarine cable after 12 years of service.

Of special interest is a particular type of corrosion which has occurred in two separate cable samples — one from Alaskan waters, the other from off the southern coast of Newfoundland. In one case the age of the cable was 12 years, and in the other 36 years. The Alaskan sample was located in an area characterized by water velocities of 5 to 9 knots. In both instances, the outer jute and most of the flooding compound was gone. Corrosion, instead of starting and progressing on the outer surface of the wires, had started, and been confined largely to the sides of the wires. Usually there are corresponding areas of corrosion on two adjacent wires to form "corrosion pockets." These pockets are illustrated in Fig. 15. In the case of the 12 year old cable, corrosion caused failure of the armor wires. In the case of the cable which was in service 36 years, failure was reported to have occurred from chaffing on a rocky bottom. Close examination suggests that failure may more reasonably be attributed to severe corrosion of the type just described. The exact cause of the corrosion pattern is still to be determined.

Sufficient samples have not been examined as yet to form a coordinated picture with respect to the inner jute. In the case of cable samples from the North Atlantic, the inner jute bedding was in good condition in cables which had been in service for as long as 30 or 40 years. Samples more than 40 years old showed the effect of deterioration. Although only a limited number of samples have been examined from the Caribbean, most of them from water about 50 feet deep, jute and cotton tape components were in poor condition in certain spots. It was evident that microbiological deterioration of the jute had occurred. In no case has there been any evidence of deterioration of the insulation of the central conductor of any of the cable samples. In the case of the older cable samples the insulation was gutta percha, but in the most recent samples it has been polyethylene.

VII. SUMMARY

A progress report has been presented on the results of a test program designed to determine the relative resistance of materials to marine biological attack. Specific test results have been reported wherever possible, predominantly from the laboratory test procedures. In the case of the natural exposure tests, which are intended to provide correlative data for the laboratory program over longer periods of time, the information which has been assembled thus far is of a more general nature. There follows a summary of the more important information which has been obtained:

1. In the biochemical oxygen demand-type test it has been found that polyethylene is not utilized by the aerobic bacteria or the anaerobic sulfate-reducing bacteria. Polyvinyl chloride plastics are attacked according to the way in which they are plasticized. All of the samples tested which had an added external plasticizer, including the rigid plastic, were attacked to some degree. In the latter case the attack was apparently due to lubricants. The semi-flexible polyvinyl chloride copolymers, and the polyvinyl chloride resin alone, were not utilized by the bacteria. The five elastomers assayed were all attacked by aerobic bacteria, neoprene being the most resistant. The epoxide casting resin did not serve as a source of carbon for the organisms, but further testing is required with a polyester casting resin.

2. Coiled conductors insulated in one case with a rigid polyvinyl chloride, and in the other with GR-S, have been exposed half in sea water and half in marine sediment in the laboratory for thirteen months. Capacitance measurements show that a considerable change has occurred in the GR-S insulation apparently as a result of bacterial attack. Although there has been a slight rise in the capacitance values for the polyvinyl chloride-insulated conductors during the last five months, further observations are necessary before attack can be considered definite.

3. In three years of actual marine exposure of plastics, elastomers and pasting resins, there have been definite penetrations by marine borers of only three materials — a test rod of silicone rubber, a 0.0035-inch film of polymonochlor-trifluoroethylene wrapped on a Lucite rod, and on Lucite rods themselves. The first two cases represent single instances of penetration — both by pholads. The Lucite rods were penetrated at many places by pholads as a result of the organisms getting started in an asphalt-impregnated jute wrapping and then progressing into the Lucite.

Secondary cellulose acetate yarn and tow have been deteriorated badly, apparently by bacteria, in as short a time as six months.

Natural fibers, notably jute, have been degraded extensively by borers and microorganisms. There is considerable evidence of fungus attack.

Under fouling and in the sediment area, rods of polyvinyl chloride plastics containing basic lead stabilizers have been blackened as the result of hydrogen sulfide produced by sulfate-reducing bacteria reacting with the lead salts to give black lead sulfide. This sulfiding has caused no apparent degradation of the physical properties of the plastics.

4. The examination of cable samples from service has indicated that the impregnated outer jute serves an important function in limiting corrosion of armor wires. Generally, when corrosion is present the outer jute has been lost.

Two unusual cases of extensive corrosion have been reported — one in a cable 12 years old, the other in a cable which was in service 36 years. In both cases, corrosion occurred in pockets between adjacent armor wires rather than on the outside surfaces (water side) of the wires.

The performance of the inner jute in samples from service has been generally good for as long as 30 or 40 years in deep water. In samples from relatively shallow water in the Caribbean, inner jute bedding was badly deteriorated in as short a time as five years.

obtaining samples of telegraph cable from service is gratefully acknowledged.

REFERENCES

1. C. Chilton, The Gribble (*Limnoria lignorum*, Rathke) Attacking a Submarine Cable in New Zealand. Annals and Mag. Natural History, Ser. 8, **18**, p. 208, 1916.
2. G. E. Preece, On Ocean Cable Borers, Telegr. Jour. and Electr. Rev., **3**, pp. 296–297, 1875.
3. E. Jona, I cavi sottomarini dall 'Italia alla Libia, Atti della Soc. ital. per il Progr. delle Sci., **6**, pp. 263–292, 1913.
4. R. J. Menzies and Ruth Turner, The Distribution and Importance of Marine Wood Borers in the United States, presented at Second Pacific Area National Meeting, A. S. T. M., Paper **93**, 1956.
5. W. F. Clapp, and R. Kenk, *Marine Borers, A Preliminary Bibliography*, Parts I and II, The Library of Congress, Tech. Inform. Div., Washington, D. C., 1956.
6. F. Roch, Die *Teredinidae* de Mittelmeeres. Thalassia **4**, pp. 1–147, 1940.
7. Notes on Everyday Cable Problems. Distribution of Electricity, **8**, pp. 1896–1898, W. T. Henley's Telegraph Works Co., Ltd., London, November, 1935.
8. P. Bartsch and H. A. Rehder, *The West Atlantic Boring Mollusks of the Genus Martesia*, Smithsonian Inst. Misc. Collections 104, Washington, D. C., **11**, 1945.
9. L. R. Snoke and A. P. Richards, Marine Borer Attack on Lead Cable Sheath, Science, **124**, p. 443, 1956.
10. C. E. ZoBell, *Marine Microbiology*, Chronica Botanica Co., Waltham, Mass., 1946.
11. R. Y. Morita, and C. E. ZoBell, Bacteria in Marine Sediments. Off. of Naval Res., Research Reviews, p. 21, July, 1956.
12. C. E. ZoBell and R. Y. Morita, Effects of High Hydrostatic Pressure on Physiological Activities of Marine Microorganisms, Off. of Naval Res., Contr. N6 onr-275 (18) Project NR 135-020, Semi. Ann. Prog. Rept., July, 1955.
13. C. E. ZoBell and Josephine Beckwith, The Deterioration of Rubber Products by Micro-Organisms, Jour. Amer. Water Works Assoc., **36**, pp. 439–453, 1944.
14. C. E. ZoBell, Action of Microorganisms on Hydrocarbons, Bact. Rev., **10**, Nos. 1–2, March–June, 1946.
15. E. S. Barghoorn and D. H. Linder, Marine Fungi, Their Taxonomy and Biology, Farlowia, **1**, pp. 395–467, Jan., 1944.
16. S. P. Myers, Marine Fungi in Biscayne Bay, Florida. Bull. of Marine Sci. of the Gulf and Caribbean, **2**, pp. 590–601, 1953.
17. *Marine Fouling and Its Prevention*. United States Naval Institute, Annapolis, Md., 1952.
18. W. G. MacMillan and S. N. Basu, Detection and Estimation of Damage in Jute Fibers — Part I: A New Microscopic Test and Implications of Certain Chemical Tests. Jour. Text. Inst., **38**, pp. T350–T369, 1947.
19. J. T. Blake, D. W. Kitchin and O. S. Pratt, The Microbiological Deterioration of Rubber Insulation. Presented at A.I.E.E. General Meeting, New York, Jan., 1953.
20. P. Deschamps, Xylophaga Marins. Protection de Bois Immergés contres les Animaux Perforants. Peint.-Pigm.-Vern., **28**, pp. 607–610, 1952.
21. C. E. ZoBell, Some Effects of High Hydrostatic Pressure on Physiological Activities of Bacteria, Proc. Soc. Amer. Bact., pp. 26–27, 1955.

Dynamics and Kinematics of the Laying and Recovery of Submarine Cable

By E. E. ZAJAC

This paper is an attempt to formulate a comprehensive theory with which the forces and motions of a submarine cable can be determined in typical laying and recovery situations. In addition to the fundamental case of a cable being laid or recovered with a ship sailing on a perfectly calm sea over a horizontal bottom, the effects of ship motion, varying bottom depth, ocean cross currents, and the problem of cable laying control are considered. Most of the results reduce to simple formulas and graphs. Their application is illustrated by examples.

TABLE OF CONTENTS

GLOSSARY OF SYMBOLS

A	Amplitude of harmonic ship motion
c_1, c_2, $\bar{c}_2$	Longitudinal wave velocity; transverse wave velocity in air and water
C_D, C_f	Transverse and tangential drag coefficients
d	Cable diameter, also distance behind the ship at which the cable enters the lower stratum
D_N, D_T	Normal and tangential unit drag forces
e	Sidewise distance from the laid cable to the ship
$\overline{EA}$	Extensile rigidity
h	Ocean depth
$\bar{h} = \dfrac{wh}{\overline{EA}}$	Dimensionless ocean depth
H	Hydrodynamic constant
L	Inclined cable length from surface to bottom, also from ship to surface
N_R	Reynolds number
p, q	Longitudinal and transverse deviational cable displacements
P_0, Q_0	Longitudinal and transverse ship displacements

P_1	Deviation from mean pay-out or haul-in rate
S, X	Arc length and horizontal distance from the touchdown point to the ship
$\bar{S} = \dfrac{S}{h}, \quad \bar{X} = \dfrac{X}{h}$	Dimensionless forms of S and X
t	Time
$\bar{t} = \dfrac{Vt}{h}$	Dimensionless time
T, T_s, T_0	Cable tension at an arbitrary point, at the ship, and at the bottom
$\bar{T} = \dfrac{T}{wh}, \quad \bar{T}_s = \dfrac{T_s}{wh}, \quad \bar{T}_0 = \dfrac{T_0}{wh}$	Dimensionless forms of T, T_s and T_0
T_p, T_q	Cable tension due to longitudinal and transverse ship motion
V, V_c	Ship speed, pay-out or haul-in rate
V_N, V_T	Normal and tangential velocity of the water relative to the cable configuration
V_t	Tangential velocity of the water relative to a cable element
w, w_a	Submerged and in-air unit cable weight
α, α_0	Critical angle, approximate critical angle
α_s	Cable angle at the surface
β	Descent angle, cross current orientation (Section 7.1)
$\gamma = \dfrac{2 - \sin^2 \alpha}{\sin^2 \alpha}$	Constant, also ascent angle
ϵ	Slack
θ	Orientation of a cable element
θ, ψ	Spherical polar coordinates for the three-dimensional model
κ, λ	Constants (see Appendix C)

$$\Lambda = \frac{C_D \rho d V^2}{2} = \frac{\cos \alpha}{\sin^2 \alpha}$$ Constant

μ, ν Constants

ν Kinematic viscosity

ξ, η, ζ Rectangular coordinates for the three-dimensional model

ρ Mass density of water

ρ_c, ρ_w Mass per unit length of cable in air and water

ϕ Deviation from the stationary angle, also angle between ξ axis and $\vec{V}$ (Section 7.1)

I. INTRODUCTION

In the summer of 1857, the first attempted laying of a transatlantic cable ended dismally when, after only a few hundred miles had been laid, the cable broke and fell into the sea. Although fouling of the pay-out gear caused by a negligent workman was the principal suspected reasons for the failure, its occurrence aroused great interest in the detailed dynamics and kinematics of the laying of submarine cable, and leading British scientists such as Kelvin and Airy published analyses of this problem in late 1857 and early 1858.[1, 2, 3, 4, 5]

However, after this initial activity, interest in submarine cable dynamics and kinematics evidently waned for there appear only sporadic subsequent investigations in the literature.[6, 7, 8, 9, 10] Further, the results of the early and subsequent analytical investigations have been, by and large, little utilized in cable laying and recovery practice. One can conjecture several reasons for this. For one, because the early analytical work was done before the advent of modern hydrodynamic theory, it did not rest on a secure base. Thus, as late as 1875, one finds vigorous debate over the nature of the tangential resistance of water to the cable.[9] For another, the results of the analyses could not all be expressed in terms of elementary functions and required the numerical evaluation of some definite integrals. In the 1850's this was a tedious and laborious process. However, these are probably secondary reasons. For, after another failure in the early summer of 1858, a transatlantic cable was successfully laid in August of that year. The mechanical problem of depositing a cable was thus proved surmountable without complicated mathematical analyses, and the marriage of analysis and practice was never fully realized.

However, a present-day submerged-repeater transoceanic cable is a delicate and expensive transmission system. Reducing the amount of cable deposited by as little as one per cent can result in a substantial saving in the first cost of such a system. Its repair is a costly operation requiring the sustenance of an ocean ship and its crew. Therefore, it is important to lay the cable without wasteful excess and with minimum chances for failure after laying. Further, it is important that repair, if necessary, be as efficient as possible. To accomplish these things, an understanding of the dynamics and kinematics of cable laying and recovery is essential.

The purpose of this paper is to provide some of this understanding in as straightforward a way as possible. To this end concepts and results are stressed in the main part of the paper, mathematical details being given in the appendices. Moreover, we hope to show that the results of the analysis can provide a numerical basis for decision making in many of the laying and recovery operations. Most of these results can be expressed in the form of simple formulas and graphs. Several numerical examples are included to illustrate concretely how the results can be applied in practice.

The general plan of the paper is to proceed from simple to more refined models of the laying and recovery processes. Thus, we discuss first what we have called the *two-dimensional stationary model*. This model is appropriate for laying and recovery on or from a perfectly flat bottom while sailing on a perfectly still sea. As a preliminary to this discussion, we consider in some detail the hydrodynamic behavior of typical deep sea submarine cable. We then take up the effects of the ship motions which are induced by wave action and the effects of a bottom of varying depth. These considerations are followed by a short discussion of the problem of controlling the cable pay-out properly during laying and the associated problem of the accuracy of the present taut wire method of determining ship speed. Finally, we consider the *three-dimensional stationary model* and the effects of ocean cross currents.

II. BASIC ASSUMPTIONS

Our analyses, like most analyses of physical problems, are based on idealizations or mathematical models of the actual physical system. The extent of validity of these models must be ultimately determined by experiment and experience. However we shall try to give the reader an idea of when they are clearly applicable and when they are not.

All of the models we consider contain two basic idealizations, namely,

(1) No bending stiffness in cable, i.e., it is a perfectly flexible string,

(2) The average forward speed of the ship is constant.

Bending effects are caused by locally large curvatures, and are significant mainly where the cable leaves the pay-out sheaves and at the ocean bottom. However, for a cable with a steel strength member, bending even to the small radius of the pay-out sheave typically does not materially reduce the tension required to break the cable. Hence, in these cases we can expect an analysis based on the first idealization to give a reasonable idea of when cable rupture will occur. In laying, ship speeds are normally steady and, with the exception of the fluctuations caused by wave action which we consider later in the paper, the second idealization is reasonable also. In recovery, on the other hand, ship speeds are apt not to be steady, and the second idealization is more tenuous. But because of the very slow speeds usually employed, this idealization may in fact be meaningful in recovery as well.

III. TWO-DIMENSIONAL STATIONARY MODEL

3.1 *General*

Assume that the cable ship is sailing at a constant horizontal velocity, that the cable pay-out or haul-in rate is constant, and that the drag of the water on the cable depends only on the relative velocity between the water and the cable. Further, assume that in a frame of reference translating with the ship the cable configuration is time-independent or stationary. This idealized model of the cable laying or recovery process we call the *two-dimensional stationary model*.

This is the model which has been considered in the previous analytical studies.[1-10] As the early investigators quickly pointed out, when the tension at the bottom of the cable is zero, the cable, according to this model, can lie in a straight line from ship to ocean bottom. During laying, when slack is normally paid out, the zero tension condition actually occurs, and hence this case is of considerable practical importance.

The straight line can in fact be shown to be the *only* solution which can satisfy all the observed boundary conditions. This point is discussed in detail in Appendix A. That the straight line is a possible configuration can be seen from Fig. 1. In the vector diagram the velocity of the water with respect to the cable is resolved into a component V_N normal to the cable and a component V_T tangential to it. Associated with V_N and V_T are normal and tangential water resistance or drag forces D_N and D_T. In the straight line configuration, the cable inclination is such that D_N just balances the normal component of the cable weight forces. The situation is thus analogous to that of a chain sliding on an inclined plane, with the forces D_N corresponding to the normal reaction forces of the plane. Summing forces in the normal direction, we get, therefore,

$$w \cos \alpha = D_N, \tag{1}$$

while the summation in the tangential direction gives for T_s, the tension at the ship,

$$T_s = wL \sin \alpha - D_T L. \tag{2}$$

Here w is the weight per unit length of immersed cable, α is the cable's angle of incidence, D_N and D_T are the normal and tangential drag forces per unit length respectively, and L is the inclined length of the cable. For most submarine cable used currently the force $D_T L$ is negligible and we arrive at

$$T_s \approx wL \sin \alpha = wh, \tag{3}$$

where h is the ocean depth at the cable touchdown point. Hence, during slack laying the cable tension at the ship is very nearly equal to the weight in water of a length of cable equal to the ocean depth.
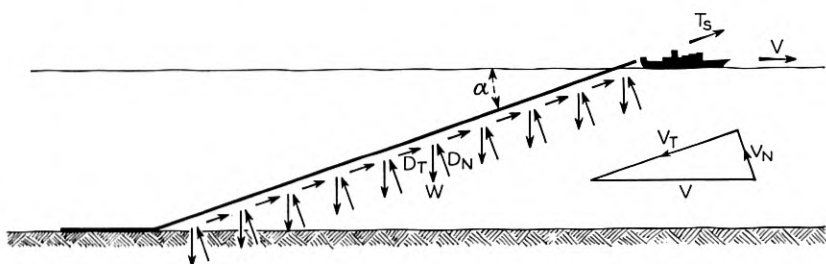

Fig. 1 — Forces acting on a cable in normal laying.

The straight-line solution is the simplest and probably the most important result to be obtained from the stationary two-dimensional model. We shall derive results for other important situations from this model also. As a preliminary, we study first, however, the nature of the normal and tangential drag forces D_N and D_T.

3.2 Normal Drag Force and the Cable Angle α

The resistance at sufficiently slow speeds to the flow of a fluid around an immersed body varies as the square of the fluid velocity. This relationship is usually written as*

$$D_N = C_D \frac{\rho V_N^2 d}{2}, \tag{4}$$

---

* For towed stranded wire experimental verification of this relationship is reported in Reference 11.
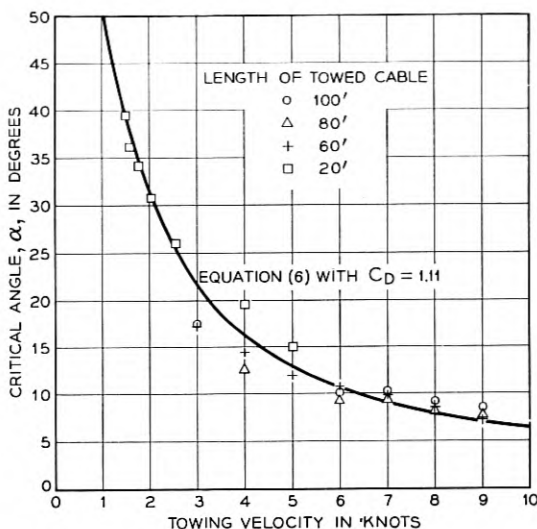
Fig. 2 — Experimental and theoretical variation of critical angle with towing velocity for cable No. 1.

where D_N is the normal drag force per unit length, C_D is the so-called drag coefficient, ρ is the mass density of the fluid, and d is the diameter of the cable. For the straight-line configuration, the vector diagram in Fig. 1 shows that

$$V_N = V \sin \alpha. \tag{5}$$

Substitution of (5) and (4) into (1) yields in turn

$$w \cos \alpha = \frac{C_D \rho V^2 d}{2} \sin^2 \alpha. \tag{6}$$

Equation (6) suggests how the value of the drag coefficient C_D can be obtained experimentally. By towing a length of cable in water at a constant velocity, one can establish the straight-line configuration. The angle α can then be measured as a function of velocity, from which C_D can be computed by (6).

Figs. 2 and 3 show the results of such tests together with plots of (6) for the indicated values of C_D . These results are taken from an analysis by A. G. Norem of experimental data obtained by H. N. Upthegrove, J. J. Gilbert, and P. A. Yeisley. The properties of these cables are listed in Table I.* To eliminate end effects different lengths of cable were towed,

---

* Cable No. 2 is very similar to present type D transatlantic telephone cable. For engineering calculations, type D can be considered the same as cable No. 2.

TABLE I — PROPERTIES OF CABLES No. 1 AND No. 2

Cable	No. 1	No. 2
Diameter (inches)	0.75	1.25
Wt. in water (lbs/ft.)	0.243	0.705
Outer covering	Polyethylene	Tar impregnated jute
Surface condition	Smooth	Rough
EA (twist restrained)	—	4×10^6 lbs
EA (twist unrestrained)	—	1.2×10^6 lbs

as is indicated by the plotted experimental points. It is seen that (6) gives a good fit to the experimental data over the entire velocity range.

If the cable has a smooth exterior, an estimate of the drag coefficient C_D can be computed from published values of resistance to flow about an immersed cylinder. This computation is described in Appendix B, where we have also tabulated computed values of C_D . For the smooth cable No. 1, the value of C_D obtained from Appendix B is 1.00 which is in fair agreement with the experimentally determined value of 1.11.

Although the drag coefficient C_D is a fundamental hydrodynamic parameter, it is not the most convenient description of the effect of the nor-
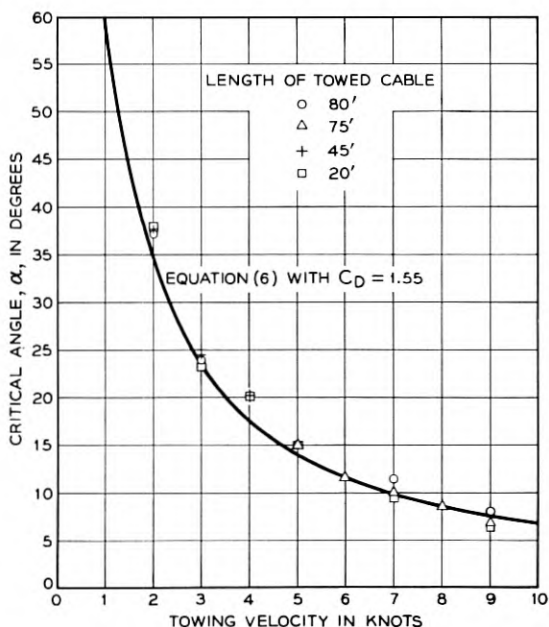

Fig. 3 — Experimental and theoretical variation of critical angle with towing velocity for cable No. 2.

mal component of water velocity. For small values of the incidence angle α

$$\cos \alpha \approx 1,$$

$$\sin \alpha \approx \alpha,$$

and (6) is approximately

$$\alpha_0 V = \left(\frac{2w}{C_D \rho\, d}\right)^{1/2}, \tag{7}$$

where α_0 is the approximate value of α. The quantity $(2w/C_D \rho d)^{\frac{1}{2}}$ is a constant for a given cable. It brings together all the cable parameters which influence the magnitude of the incidence angle α. If the angle α for a given speed is determined accurately, as can be done in a towing test or with a sextant during over-the-stern laying, this quantity is easily computed. Because of its importance, we shall call it the *hydrodynamic constant* of the cable and denote it by H, namely,

$$H = \left(\frac{2w}{C_D \rho\, d}\right)^{1/2}. \tag{8}$$

By virtue of (7) and (8) we may write

$$\alpha_0 V = H. \tag{9}$$

The constant H rather than the drag coefficient C_D will be used from this point on.

When the approximate relationship (9) is not valid, α can be obtained by solving (6). This gives

$$\cos \alpha = \sqrt{1 + \frac{1}{4}\left(\frac{H}{V}\right)^4} - \frac{1}{2}\left(\frac{H}{V}\right)^2, \tag{10}$$

where V is in knots and H in radian-knots. In terms of α_0 we obtain in turn

$$\cos \alpha = \sqrt{1 + \frac{1}{4}\alpha_0^4} - \frac{1}{2}\alpha_0^2. \tag{11}$$

This relationship is shown in Fig. 4, where the incidence angle α is plotted as a function of the approximate incidence angle α_0. It is seen that for $\alpha < 20°$ the difference between α_0 and α is negligible.

Physically α as given by (10) is the angle the cable assumes in the straight-line shape for the velocity V. However, in addition, (10) shows that α can be thought of as a dimensionless parameter which embodies
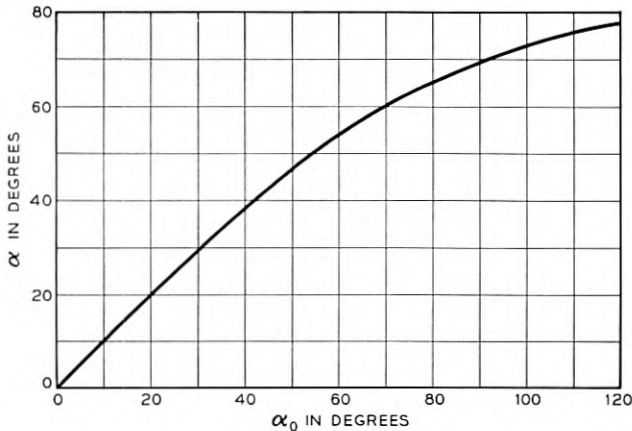
Fig. 4 — Variation of α with α_0.

both the hydrodynamic properties of the cable and the ship speed. Thus, even when the configuration is not a straight line, we shall find it convenient to express results as a function of the single parameter α, rather than as a function of the two parameters H and V. For this reason, following Pode,[11, 12] we call α the *critical angle*.

3.3 *Tangential Drag Force*

Over the range of velocities encountered in laying and recovery the drag coefficient C_D in equation (6) is essentially constant. However, the corresponding coefficient for the skin friction force associated with V_T, the component of flow along the cable, is not constant. For the cable of smooth exterior (cable No. 1), the expression

$$D_T = C_f \tfrac{1}{2} \rho V_t^2 \pi d, \tag{12}$$

with $C_f = 0.055/(N_R)^{0.14}$, was found to give good agreement with the experimental data, as is shown by Fig. 5. Here D_T is the skin friction or tangential drag force per unit length; V_t is the relative velocity of the water with respect to a cable element given for straight-line laying by

$$V_t = V_c - V \cos \alpha, \tag{13}$$

where V_c is the cable pay-out rate; ρ is the mass density of water; and N_R is the Reynolds number defined as $N_R = V_t L/\nu$, where ν is the kinematic viscosity of water. The data of Fig. 5 are for 100 foot lengths of cable towed in fresh water at a temperature of 60°F.

From (12) we find

$$D_T = \frac{0.055}{2} \rho \frac{\nu^{0.14} V_t^{1.86}}{L^{0.14}} \pi d. \tag{14}$$

This expression indicates that D_T for smooth cable depends on the inclined length of the cable as well as the relative tangential velocity V_t. The form of (13) suggests that the flow tangential to a smooth cable is similar to flow past a smooth plate. In such flow a turbulant boundary layer develops which grows in thickness with distance from the leading edge, resulting in a length dependence of the type shown by (14). Since Fig. 5 refers to 100 foot cable lengths, (13) is probably not accurate for the magnitudes of L occurring in deep-sea laying, and should be used only to obtain the order of magnitude of C_f.

Fig. 5 — Experimental values of the tangential drag force for cable No. 1 compared with those obtained by equation (12).

For the cable with conventional jute outer covering, (cable No. 2), it was found that

$$D_T = 0.01 \ V_t^{1.48} \tag{15}$$

fits the experimental data obtained by towing test (Fig. 6). Whereas in (15) the constant 0.055 is dimensionless, the constant 0.01 in this equation has the dimensions necessary to give D_T in units of pounds per foot when V_t is in feet per second. We note that for this cable D_T is independent of the length of the cable.
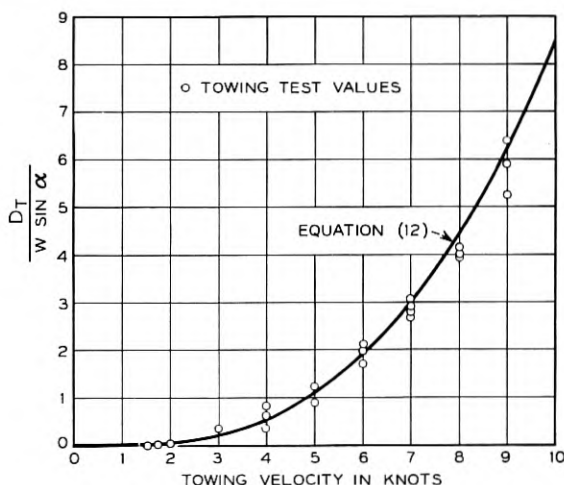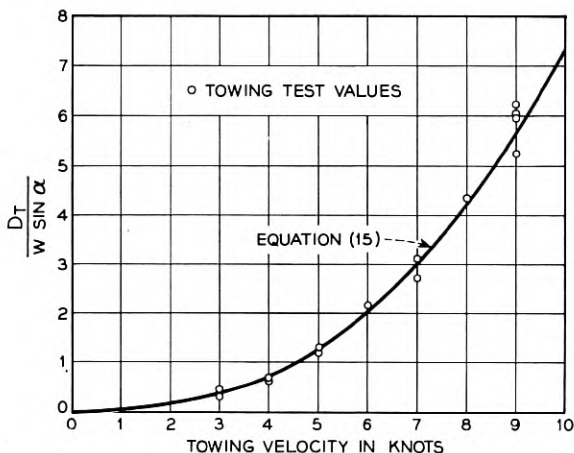
Fig. 6 — Experimental values of the tangential drag force for cable No. 2 compared with those obtained by equation (15).

The ratio of D_T to the tangential component of the cable weight force is given by $D_T/w \sin \alpha$. Equations (14) and (15) indicate that even for small values of α of the order of twelve degrees, $D_T/w \sin \alpha$ is of the order of 6 per cent for relative tangential velocities V_t of 1.0 feet/sec. In many situations V_t will be less than this value, and we can neglect D_T compared to $w \sin \alpha$. As we shall see later, this approximation greatly simplifies the differential equations of the two-dimensional stationary model.

Historically, the question of the variation of D_T with V_t is of some interest. In one of the early papers of 1858 Longridge and Brooks[3] assumed a velocity squared dependence. In 1875, W. Siemens[9] attacked this assumption stating that D_T actually varied linearly with V_t. There ensued a debate in which many bitter words but few experimental data were displayed.[9] In view of our present knowledge that the skin friction force, even in the simplest case of flow past a smooth plate, is the result of complicated boundary layer phenomenon, the existence of this confusion is not surprising.

3.4 *Sinking Velocities and Their Relationship to Drag Forces*

The studies of submarine cable forces in 1857 and 1858 preceded modern fluid mechanics by many years. To characterize the hydrodynamic forces acting on cable the early investigators used *sinking* or *settling* velocities rather than the more recently conceived drag coefficients. The transverse sinking velocity u_s was defined as the terminal velocity attained by a straight, horizontal length of cable sinking in water.

Similarly, the longitudinal sinking velocity v_s was the terminal velocity of a cable length sinking with its axis constrained to be vertical. If for a given cable the drag forces are functions only of velocity, the parameters w, u_s, and v_s, together with the laws of variation of the drag forces with velocity, completely define the hydrodynamic behavior of the cable. Since sinking velocities are still used in submarine cable technology, it is of interest to relate them to the more modern drag coefficient viewpoint.

In the case of transverse or normal flow around the cable, the variation of D_N with the square of the relative transverse velocity gives $(V_N/u_s)^2 = D_N/w$, since at a transverse velocity equal to the sinking velocity the unit transverse drag force is w. Substituting for D_N from (4) we find

$$u_s = \left(\frac{2w}{C_D \rho\, d} \right)^{\frac{1}{2}} = H. \tag{16}$$

Thus, the transverse sinking velocity u_s is identical with the *hydrodynamic consant* H. We can therefore alternatively write the approximate relationship (9) as

$$\alpha_0 V = u_s, \tag{17}$$

where α_0 is in radians and u_s and V are in knots.

For the tangential or skin friction flow along smooth cable, the sinking velocity concept is inadequate because the unit tangential drag force D_T varies with length as well as with the relative tangential velocity V_t. However, for cable with the conventional jute exterior (cable No. 2), we have $(V_t/v_s)^{1.48} = D_T/w$ and from (15) the vertical sinking velocity v_s is $v_s = (46.1w)^{1/1.48}$, where v_s is in knots.

We note in passing that the cable does not, as is sometimes supposed, sink vertically to the bottom at the transverse sinking velocity u_s. Actually, the term "vertical cable sinking rate" is ambiguous. There are in fact two vertical sinking rates which may be important. Although both these rates are normally approximately equal to u_s neither is identical to it.

Relative to the earth, the resultant velocity V_R of a cable element has two components: a horizontal component of the magnitude of the ship velocity, and a component inclined at the angle α of the magnitude of the cable pay-out rate V_c. These are shown in Fig. 7. The component V_{vert} of V_R, given by $V_{\text{vert}} = V_c \sin \alpha$, is the rate at which a cable *element* sinks vertically. For a laying depth h, the time τ it takes for a cable element to sink to bottom is therefore $\tau = h/V_c \sin \alpha$. This time would, for example, tell one how long it takes a lightweight repeater, integral with the cable, to reach the ocean bottom.
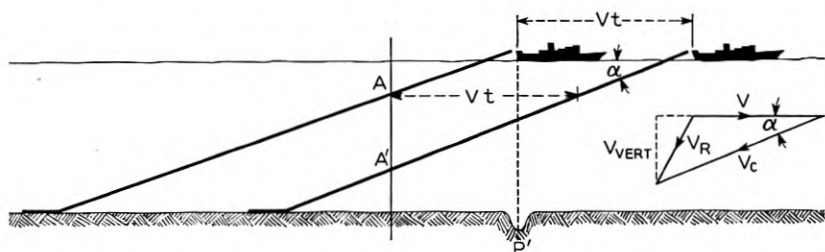
Fig. 7 — Illustration of vertical cable sinking rates.

On the other hand, consider the intersection of the cable *configuration* with a vertical line (Fig. 7). In the time t, as the ship sails a distance Vt, the intersection moves from A to A', a distance $Vt \tan \alpha$. Hence the cable configuration in this sense sinks vertically at the rate $V \tan \alpha$, and the time θ for the configuration to reach bottom in a depth h is $\theta = h/V \tan \alpha$. One may be interested in how long it takes after the ship has passed over an ocean bottom anomaly P' (Fig. 7) for the cable configuration to reach the anomaly. This is just the time θ.

Hence, the vertical sinking rates $V_c \sin \alpha$ and $V \tan \alpha$ can both be of interest. At the usual ship speeds, $\sin \alpha \approx \tan \alpha \approx \alpha \approx u_s/V$. Further V_c normally differs little from V. Hence, both these rates are indeed normally approximately equal to u_s.

3.5 *General Solution of the Stationary Two-Dimensional Model*

Assume that each cable element is traveling along the stationary cable configuration with the constant speed V_c. Starting at the ocean bottom let s be the arc length along the stationary configuration. We define s to be positive in the direction opposite to the direction of travel of the cable elements. So, as Fig. 8 indicates, in laying, positive s is directed from the ocean bottom toward the ship, while in recovery the situation is reversed. We let θ be the angle between the positive s direction and the direction of the ship velocity.
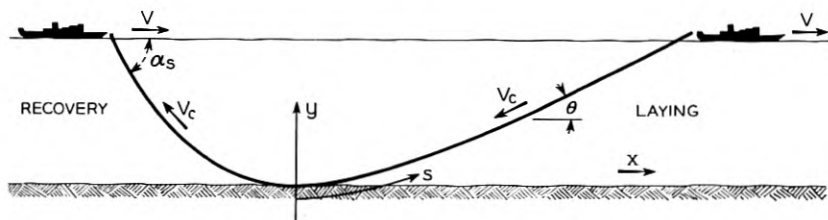

Fig. 8 — Definition of coordinates for the two-dimensional stationary model.

Fig. 9 shows the forces acting on an element of the cable, with tension at the point s being denoted by T. The normal drag force per unit length D_N may, by virtue of (4) and (5), be written in the form

$$D_N = \frac{C_D \rho V^2 \, d}{2} \sin \theta \mid \sin \theta \mid.$$

It is necessary to introduce here $\mid \sin \theta \mid$ in order for D_N to have the proper sign for all θ. We note, however, that if $V_c \geqq V$, we have from (13)

$$V_t = V_c - V \cos \theta \geqq 0.$$

Hence in normal laying and recovery the unit tangential drag force D_T is always in the positive s direction.
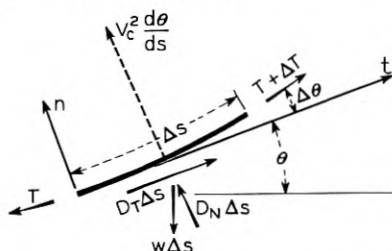

Fig. 9 — Diagram of forces acting on a cable element.

The forces acting on an element produce a centrifugal acceleration $V_c^2 d\theta/ds$. Hence, summing forces along the directions t (tangential) and n (normal), dividing by Δs and sending Δs to zero, we obtain

$$(T - \rho_c V_c{}^2) \frac{d\theta}{ds} + \frac{C_D \rho V^2 \, d}{2} \sin \theta \mid \sin \theta \mid - w \cos \theta = 0, \quad \text{(a)}$$

$$\frac{dT}{ds} + D_T - w \sin \theta = 0, \quad \text{(b)}$$

(18)

where ρ_c is the mass density per unit length of cable.

It is seen at the outset that $\theta = \alpha$ is a solution of (18a). It is in fact the important straight-line solution which has been discussed in Section 3.1.

If $\theta \neq \alpha$ and D_T varies only with V_t we may divide (18b) into (18a) and integrate to obtain the solution for T in the following form:

$$\ln \frac{(T - \rho_c V_c{}^2)}{(T_0 - \rho_c V_c{}^2)} = \int_{\theta_0}^{\theta} \frac{(w \sin \xi - D_T)}{w(\cos \xi - \Lambda \sin \xi \mid \sin \xi \mid)} \, d\xi, \quad \text{(a)}$$

$$\Lambda = \frac{C_D \rho \, d V^2}{2w} = \frac{\cos \alpha}{\sin^2 \alpha}, \quad \text{(b)}$$

(19)

where T_0 is the tension corresponding to the angle θ_0.

At the cable touchdown point on the ocean bottom only two conditions are possible. If the angle θ is not zero or π there, the cable tension T must be zero. Otherwise a finite tension would act on an infinitesimal length of cable, producing an infinite acceleration. Hence, either the tension T must be zero or the angle θ must be zero or π. The first case normally implies a straight-line configuration (see Appendix A), which has already been discussed. In other cases, we define T_0 as the tension at the touchdown point, and we let θ_0 be zero or π, whichever is appropriate.

If x, y are coordinates in the translating (x, y) frame of a point along the cable configuration, then

$$dx = ds \cos \theta,$$

$$dy = ds \sin \theta.$$

Combining these relations with (18a), we have

$$s = \int_{\theta_0}^{\theta} \frac{(T - \rho_c V_c^2)}{w(\cos \xi - \Lambda \sin \xi \mid \sin \xi \mid)} \, d\xi, \qquad \text{(a)}$$

$$x = \int_{\theta_0}^{\theta} \frac{(T - \rho_c V_c^2) \cos \xi}{w(\cos \xi - \Lambda \sin \xi \mid \sin \xi \mid)} \, d\xi, \qquad \text{(b)} \quad \text{(20)}$$

$$y = \int_{\theta_0}^{\theta} \frac{(T - \rho_c V_c^2) \sin \xi}{w(\cos \xi - \Lambda \sin \xi \mid \sin \xi \mid)} \, d\xi. \qquad \text{(c)}$$

Equations (19) and (20) are an integral representation of the complete solution of the basic two-dimensional model. In general, the integrals appearing in these equations cannot be evaluated in terms of elementary functions, and the solution must be obtained by numerical integration. For towing problems where the pay-out velocity is zero, Pode[12] has tabulated these numerical integrations using the approximation that D_T has certain constant values. However, in towing problems the direction of D_T is opposite to what it is in normal laying and recovery problems. Because small magnitudes of D_T were used, these tables nevertheless usually give adequate results in laying and recovery situations as well. At the same time, for submarine cable problems, other approximations allow more convenient ways of evaluating the integrals of (19) and (20).

For example, it is more accurate simply to assume that D_T is zero. As we indicated in Section 3.2, this approximation gives a negligible deviation from the exact solution if the relative tangential velocity V_t is small. Furthermore, in this situation we obtain from (18b)

$$\frac{dT}{ds} = w \sin \theta = w \frac{dy}{ds},$$

and hence the tension at the ship T_s is very nearly

$$T_s = T_0 + wh, \tag{21}$$

where h is the depth at the touchdown point. Thus, if the tangential drag force is negligible, the tension at the ship is essentially the bottom tension plus wh, *regardless* of the nature of the normal drag forces. This is in fact a form of a well-known theorem which, as we shall see in Section 7.1, applies in the three-dimensional case as well.

In the next sections we make further simplifications of the general solution for the specific cases of laying and recovery.

3.6 *Approximate Solution for Cable Laying*

On long cable lays ship speeds are normally of the order of 4–8 knots, with accompanying values of the critical angle α of the order of 10°–30°. For these small values of α, the assumption of zero tangential drag together with some mathematical approximations allow further simplifications of the general solution. These simplifications are derived in detail in Appendix C; here we indicate the results. The angle θ which the configuration makes with horizontal is closely given by

$$\tan\frac{\theta}{2} = \tan\frac{\alpha}{2}\left[\frac{1 - [\overline{T}_0/(\overline{T}_0 + \bar{y})]^\gamma}{1 + [\overline{T}_0/(\overline{T}_0 + \bar{y})]^\gamma \tan^4\frac{\alpha}{2}}\right]^{1/2}, \tag{22}$$

where $\bar{y}$ and $\overline{T}_0$ are dimensionless depth and bottom tension defined by

$$\bar{y} = y/h,$$

$$\overline{T}_0 = T_0/wh.$$

Here we use the cable angle α in the sense of Section 3.2, namely, as a parameter characterizing the hydrodynamic cable properties and the ship speed. The constant γ is in turn defined by

$$\gamma = \frac{(2 - \sin^2\alpha)}{\sin^2\alpha}. \tag{23}$$

For small α, $\tan^4(\alpha/2)$ is negligible and γ is large. Further

$$0 < \frac{\overline{T}_0}{\overline{T}_0 + y} < 1.$$

Hence, the denominator in (22) is very nearly unity and θ approaches the critical angle α at small values of $\bar{y}$, even for relatively large values of $\overline{T}_0$ of the order of three or four. Thus in the laying case, the cable configuration is very close to a straight line except for a short distance at the ocean bottom.

In Appendix C it is further shown that for small α

$$S = L + \kappa T_0/w,$$
$$X = L \cos \alpha + \lambda T_0/w. \tag{24}$$

Here S and X are the distance along the cable and the horizontal distances respectively from the touchdown point to the ship (Fig. 11), L and $L \cos \alpha$ are the corresponding distances for straight-line laying at the same ship speed, and κ and λ are functions of the critical angle α which are plotted in Fig. 10. To illustrate the use of (24) we consider the following.

Example: Cable No. 2 is being laid without slack onto a rough bottom from a ship moving at six knots. If the pay-out rate is decreased so the slack is 1 per cent negative, what is the subsequent rise of the tension with time at the ship?

This is really a transient problem. However, we shall try to get an idea of the average behavior of the cable by assuming it passes through a sequence of stationary configurations. Also, we assume that because of the rough bottom there is no slippage of the cable along the ocean floor.

If δ is the amount of negative slack and V the ship speed, then in a time t an amount $V(1 - \delta)t$ of cable will have been paid out. This amount plus the inclined length L will equal the amount contained in the curve AOC (Fig. 11). We then have

$$L + V(1 - \delta)t = S + Vt - (X - L \cos \alpha). \tag{25}$$

Substituting (24) into this equation and solving for T_0 we find $T_0 = (w/(\lambda - \kappa))\delta Vt$ and that by (21) the tension at the ship is given by
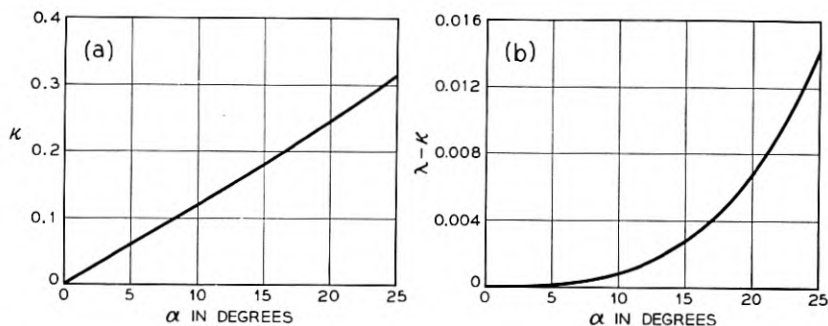
$$T_s = wh + \frac{w}{\lambda - \kappa} \delta Vt.$$

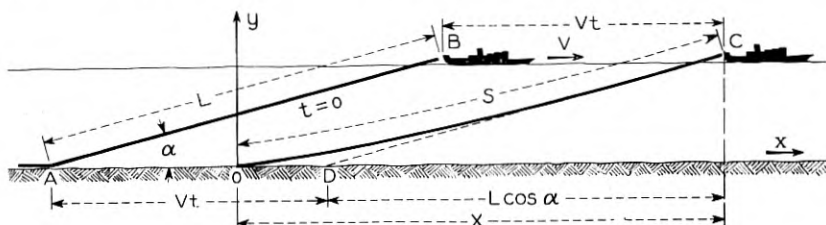Fig. 10 — Variation of κ and λ with the critical angle.

Fig. 11 — Cable geometry at a time t after the onset of negative slack.

For cable No. 2 a ship speed of six knots corresponds to $\alpha = 11.7$ degrees. By Fig. 10, this corresponds to $\lambda - \kappa = 1.4 \times 10^{-3}$. Also $w = 0.705$ lbs/ft by Table I. We get therefore

$$T_s = wh + 3000 \left(\frac{\text{lbs}}{\text{min.}} \right) t.$$

Thus, according to this calculation the tension in this example rises at the extremely rapid rate of 3000 lbs/min. We note also that the rate of tension rise is here independent of the depth h.

In the model which has been postulated, the cable is inextensible; that is, it is assumed not to stretch under load. Because the difference between the lengths of AOC and the sum of the linear segments AD and DC (Fig. 11) is small, one might suspect that the effect of cable extensibility in the present example is important. We can account for this effect in a crude way by assuming that the curve AOC has an additional length corresponding to the stretching caused by the load T_0 acting over the length L. For a cable made of a single material, the stretching would be T_0L/EA, where E is the Young's modulus of the material and A is the cross-sectional area of the cable. In analogy to this we denote the extensile rigidity of the cable by $\overline{EA}$, using the bar to indicate that $\overline{EA}$ is actually a single number obtained directly by measuring the extension of a length of cable loaded in tension. With this notation (25) becomes

$$L + V(1 - \delta)t + \frac{T_0L}{\overline{EA}} = S + Vt - (X - L \cos \alpha),$$

and repeating the previous computation we find

$$T_s = wh + \cfrac{w}{\left[\dfrac{wh}{\overline{EA} \sin \alpha} + \lambda - \kappa \right]} V\delta t.$$

It is to be noted that in this computation, unlike the inextensible case, the rate of tension rise depends on the depth h.

For conventional helically armored cable, one cannot define a single extensile rigidity because of coupling between pulling and twisting. Thus, how such a cable extends under tension depends on how it is restrained from twisting at the ship and at the ocean bottom. Instead of trying to determine these end restraints, we consider the limiting cases of no restraint and complete restraint to twisting. Data supplied by P. Yeisley indicate the values of $\overline{EA}$ for cable No. 2 in these conditions to be those given in Table I (Section 3.2). If we take $h = 6,000$ and $12,000$ feet, we find with these values that

$h = 6000$ feet:

$$T_s = wh + 220 \ (\text{lb/min})t \ \text{(twist unrestrained)},$$
$$= wh + 640 \ (\text{lb/min})t \ \text{(twist restrained)},$$

$h = 12,000$ feet:

$$T_s = wh + 120 \ (\text{lb/min})t \ \text{(twist unrestrained)},$$
$$= wh + 360 \ (\text{lb/min})t \ \text{(twist restrained)}.$$

Comparing with the inextensible computation, we see that the extensibility markedly reduces the rate of tension build-up. Nevertheless, even for the case of no restraint to twisting at a depth of 12,000 feet the rise rate is a relatively high 120 lb/min. Hence, at least over a rough bottom, the tension would quickly indicate the onset of negative slack, although the sensitivity of this indication would decrease with increasing depth.

3.7 *Approximate Solution for Cable Recovery*

Fig. 8 illustrates how cable is in present practice recovered from the ocean bottom. The cable is in front of the ship as it is brought in over the bow, and the ship pulls itself along the cable. In this process the cable tends to guide or lead the ship directly over its resting place on the ocean bottom.

It is clear that during recovery by this procedure the tension at the ocean bottom is not zero and the cable configuration is not a straight line. Furthermore, in this situation the normal component of the water drag force D_N pushes down on the cable instead of buoying it up as in the case of laying. This in turn implies a higher tension at the ship during recovery than during laying.

If the tangential drag is neglected, the tension at the ship T_s during recovery is given in dimensionless form by (see Appendix C)

$$\frac{\overline{T}_s - 1}{\overline{T}_s} = \left[\tan^2 \alpha \ \frac{\cos \alpha + \cos \alpha_s}{1 - \cos \alpha \cos \alpha_s} \right]^{1/\gamma}, \tag{26}$$
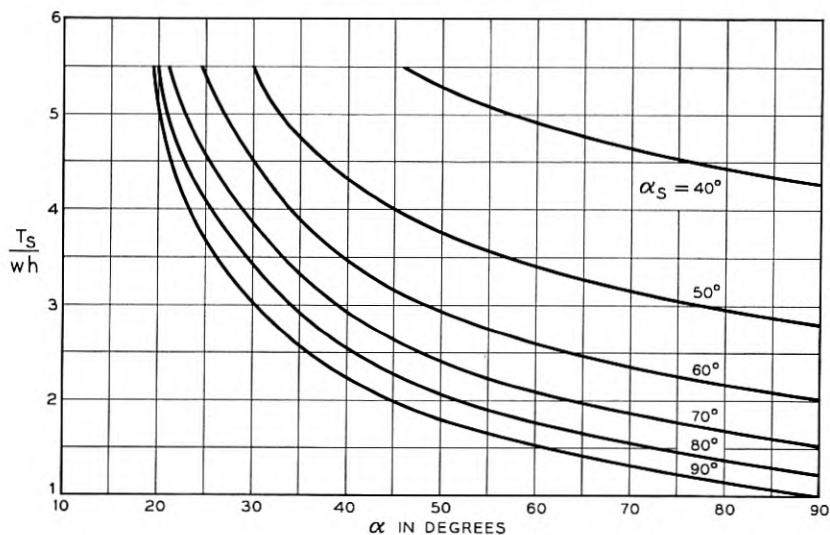
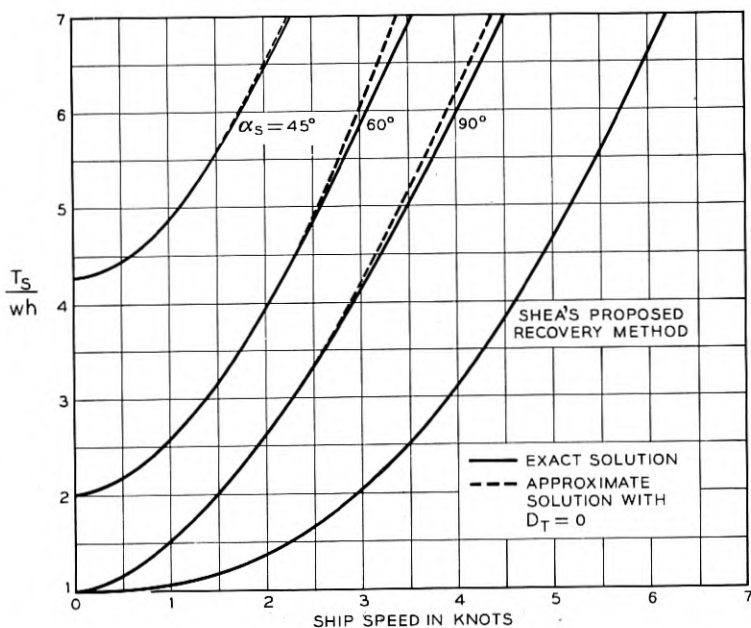Fig. 12 — Variation of the tension factor for recovery with the critical angle α.

Fig. 13 — Variation of exact and approximate tension factors for recovery of cable No. 2.

where $\overline{T}_s$ is the tension factor defined by $\overline{T}_s = T_s/wh$ and γ is given by (23). Equation (26) is plotted in Fig. 12 in the form of $\overline{T}_s$ versus α for various surface incidence angles α_s (Fig. 8). It is seen that the recovery tensions are in fact considerably higher than the laying tension of approximately wh.

To illustrate the smallness of the error of neglecting the tangential drag force in this computation, we have plotted the approximate and exact curves of $\overline{T}_s$ versus ship velocity for cable No. 2 in Fig. 13. The dotted curves have been computed from (26), while the solid curves have been obtained by substituting D_T from (15) into (19) of the general solution and integrating numerically.* (The curve labeled Shea's recovery method is discussed in the next section.)

The distance along the cable S and the horizontal distance X from the touchdown point to the ship cannot be expressed in a simple form as in the case of laying. However, they can be obtained by numerical integration from (20). The results of this computation for $D_T = 0$ are shown in Figs. 14 and 15.

How Figs. 12, 14 and 15 can be used is illustrated in the following example.

---

* The standard form of Simpson's rule was used for all the numerical integrations mentioned in the paper. In each case the interval of integration was chosen fine enough to obtain at least three significant figure accuracy.
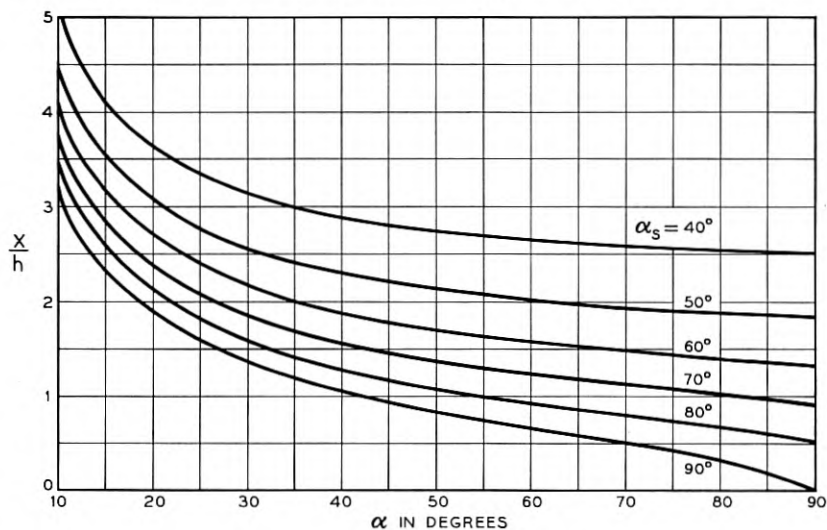

Fig. 14 — Variation of the horizontal distance to the touchdown point during recovery with the critical angle.
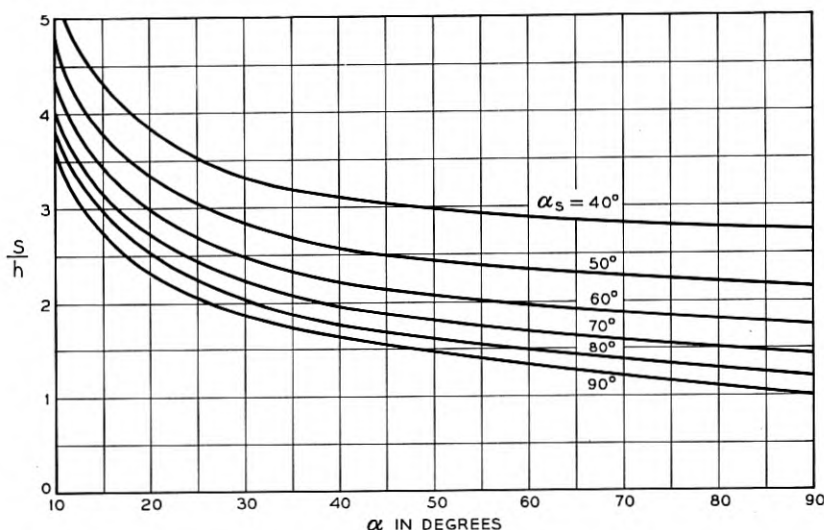
Fig. 15 — Variation of the distance along the cable to the touchdown point during recovery with the critical angle α.

Example: A cable weighing 0.7 lb/ft in sea water and having a hydro-dynamic constant H of 70 degree-knots, is to be picked up from a depth of two thousand fathoms. If the ship speed is one knot what is the cable tension at the ship for surface angles α_s of 40°, 60°, and 90°? How far in front of the ship and how far along the cable will the touchdown point be for these values of α_s ?

As indicated by (9), an H value of 70 degree-knots together with a ship velocity of one knot yields $\alpha_0 = 70$ degrees. Fig. 4 yields in turn $\alpha = 60$ degrees. Entering Fig. 12 with this value of α, we can obtain T_s/wh. In this example the wh tension for a depth of two thousand fathoms is 8,400 lb, and hence the values of T_s/wh and $\overline{T}_s$ are as follows:

α_s	T_s/wh	T_s
40°	4.85	40,700 lbs
60°	2.58	21,700 lbs
90°	1.53	12,900 lbs

From Fig. 14 we get in turn for the horizontal distance from the ship to the touchdown point

α_s	X/h	X
40°	2.65	5300 fathoms
60°	1.56	3120 fathoms
90°	0.66	1320 fathoms

Finally, from Fig. 15 we get for the distance along the cable to the touch-down point

α_s	S/h	S
40°	2.88	5760 fathoms
60°	1.95	3900 fathoms
90°	1.33	2660 fathoms

3.8 *Shea's Alternative Recovery Procedure*

The high tensions which result in the usual recovery operation require slow ship speeds of the order of one knot or less if the cable is not to be broken. One wonders if it is possible to mitigate these tensions and thus speed the recovery process. J. F. Shea discovered that this can theoretically be done by allowing α_s to exceed 90°, thus establishing the straightline configuration (Fig. 16). As in laying, the normal drag forces in this scheme support the cable, rather than push down on it as in conventional recovery. However, in contrast to the laying situation we have $V_t = V_c + V \cos \alpha$. Thus V_t is the sum of V_c and $V \cos \alpha$ instead of their difference and D_T is not necessarily negligible. Furthermore, the direction of D_T is now such as to increase rather than decrease the tension over the wh value. Hence, instead of (2), a summation of forces along the cable yields $T_s = wh + D_T L$, and the tension at the ship can be considerably higher than wh. A curve of T_s as a function of ship speed for cable No. 2 is shown in Fig. 13 with the label "Shea's recovery method". This has been computed for the case of haul-in speed equal to ship speed by means of the above equation and (15). It is seen that the tensions computed for this method of recovery, at least for the cable No. 2, are nevertheless considerably smaller than those which occur in the usual recovery procedure. It would seem that the straight-line recovery technique could fruitfully bear further examination, especially for application to the recovery of long stretches of cable.
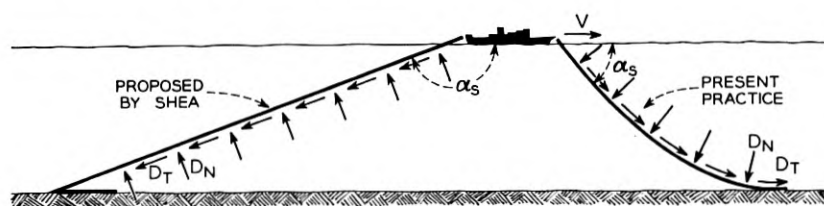

Fig. 16 — The present and Shea recovery methods.

IV. EFFECTS OF SHIP MOTIONS

4.1 *Tensions Caused by Ship Motions*

In the basic stationary model a perfectly calm sea is postulated. However, in reality, wave action gives rise to a random motion of the ship which in turn induces variations in cable tensions around those corresponding to the basic model.

To analyze this effect, we assume that the mean forward velocity of the ship and the mean pay-out or haul-in rate are constant and that the mean tension at the ship and the mean direction of the cable as it enters water are those given by the stationary model. In a reference frame moving with the mean velocity, we resolve the ship displacement into a longitudinal component P_0 (Fig. 17) along the mean or stationary direction and a transverse component Q_0 perpendicular to the stationary direction.
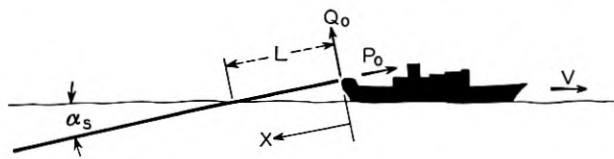
Fig. 17 — Longitudinal and transverse components P_0 and Q_0 of the ship displacement.

Intuitively, one might expect the tensions caused by the transverse displacement Q_0 to be negligible compared to those caused by the longitudinal displacement P_0. An analysis we have carried through in fact yields this conclusion. Because of its complexity and length, this analysis and the model upon which it is based are given in Appendix D. The results for the case of harmonic variation of Q_0 with time indicate, at least for cable No. 2, that the tension associated with the transverse component Q_0 is indeed negligible for all except ship motions so extreme as to rarely occur.

In addition, this analysis indicates that for the transverse disturbance Q_0, the amplitude of the responding transverse cable motion decreases exponentially after the cable enters the water because of the damping action of the water drag forces. The "half-life" distance for cable No. 2, that is, the distance along the cable at which the amplitude of a harmonic transverse motion is damped to one-half its surface value, is plotted in Fig. 18 as a function of the period of the motion for various depths h and ship velocities V. The striking feature of these figures is the rapidity of this damping. The analysis thus shows for cable No. 2 that the effect of a transverse disturbance penetrates only a short distance into the water.
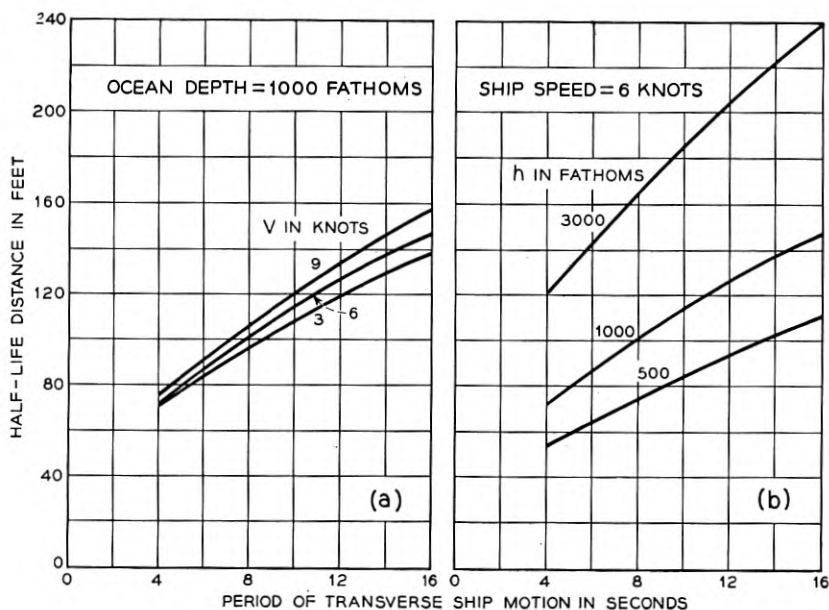
Fig. 18 — Variation of half-life distance of cable No. 2 with the period of ship motion.

As far as cable tensions are concerned, the important ship displacement then is the longitudinal component P_0, directed along the stationary direction of the cable. The analysis of Appendix D leads to the basic one-dimensional wave equation

$$\frac{\partial^2 p}{\partial x^2} - \frac{1}{c_1^2} \frac{\partial^2 p}{\partial t^2} = 0 \qquad (27)$$

for the description of the longitudinal motion. In this equation p is the deviation in longitudinal displacement from the mean pay-out or haul-in displacement, and the remaining symbols are defined as (Fig. 17)

x = distance from the mean ship position along the stationary cable configuration,

t = time,

$c_1^2 = \overline{EA}/\rho_c$.

The additional tension T_p due to ship motion is in turn given by

$$T_p = \overline{EA} \frac{\partial p}{\partial x} . \qquad (28)$$

As in the example of Section 3.6, we have again assumed that by using

in (28) the limiting values of $\overline{EA}$ obtained by complete restraint to twisting and no restraint to twisting during pulling, one can obtain bounds on the actual displacements and tensions.

The solution of (27) under arbitrary boundary conditions can be obtained from standard textbooks. Probably it is most representative to assume the cable is semi-infinite. That is, although damping of the cable is normally so small that we neglect it in (27), we may assume, because of the cable's great length, that the damping is sufficient to cause complete decay of a disturbance initiated at the ship, and that such a disturbance is not reflected from the ocean bottom. Under this condition the additional tension T_p is given by

$$T_p = -\sqrt{\overline{EA\rho_c}}\,\frac{dP}{dt}, \tag{29}$$

where $P = P_0 + P_1$ with dP_1/dt being in turn the increment in pay-out rate or decrement in haul-in rate from the mean. For cable No. 2, Table I (Section 3.2) indicates that

$$\sqrt{\overline{EA\rho_c}} = 220 \text{ lb/ft/sec (twist unrestrained)},$$

$$= 400 \text{ lb/ft/sec (twist restrained)}.$$

Two examples will make clear the application of (29).

Example 1: Steady-State Laying or Recovery in a Regular Seaway.

Assume that in a frame of reference traveling at the mean horizontal ship velocity ship surging (to and fro forward motion) is zero and the combined heave and pitch motion is normal to the ocean surface and is given by

$$W = A \sin 2\pi \frac{t}{\tau}.$$

If the period τ is 6 seconds and the amplitude A is 15 feet find for cable No. 2,

a) $(T_p)_{max}$ for laying at a constant pay-out rate and at a ship speed of 6 knots,

b) $(T_p)_{max}$ for recovery at a constant haul-in rate and with a surface incidence angle of 60°.

In both cases (a) and (b), the deviation P_1 in pay-out or haul-in rate is zero, hence $P = P_0 = W \sin \alpha_s$, and $(dP/dt)_{max} = (2\pi/\tau) A \sin \alpha_s$. Since

cable No. 2 has a hydrodynamic constant H of 70 degree-knots, we have in case (a)

$$\alpha_s = 11.7 \text{ degrees and } \left(\frac{dP}{dt}\right)_{\max} = 2.12 \text{ ft/sec.}$$

From (29) we get therefore

$$(T_p)_{\max} = 466 \text{ lbs (twist unrestrained)},$$
$$= 848 \text{ lbs (twist restrained)}.$$

In case (b) we have $\alpha_s = 60°$, $(dP/dt)_{\max} = 13.6$ ft/sec, and hence

$$(T_p)_{\max} = 2{,}990 \text{ lbs (twist unrestrained)},$$
$$= 5{,}430 \text{ lbs (twist restrained)}.$$

During recovery by conventional methods the surface incidence angle α_s is in general much larger than that which occurs during laying. The above example points up that one can expect correspondingly larger ship motion tensions during recovery than during laying in the same sort of seas. Since the stationary tensions are also much larger during recovery, recovery is the condition for which the strength of the cable should be designed.

In this example we have considered a regular seaway, something which does not exist in nature. Recent work in the application of the theory of stochastic processes to the study of ocean waves and ship dynamics promises to develop into a realistic description of the behavior of ships at sea.[13] When such a description becomes available, we shall be able to obtain a better estimate of the magnitudes of ship motion tensions.

As far as data presently available are concerned, the maximum storm condition vertical velocity at the bow or stern recorded by the *U.S.S. San Francisco* during her research voyage of 1934 was 22 feet/sec.[14] Since this ship was roughly the size of a cable ship such as the *H.M.S. Monarch*, this figure might indicate the order of the maximum velocities to be expected in cable practice. In terms of our example, for six knot laying this vertical velocity would imply

$$T_p = 980 \text{ lbs (twist unrestrained)},$$
$$= 1{,}780 \text{ lbs (twist restrained)}.$$

For recovery at a surface incidence angle of 60°, it would imply in turn

$$T_p = 4{,}200 \text{ lb (twist unrestrained)},$$
$$= 7{,}600 \text{ lb (twist restrained)}.$$

However, it is to be cautioned that these numbers are merely indicative and might differ considerably from those which occur on a particular cable ship.

Example 2: Brake Seizure

While laying cable No. 2 at six knots in a perfectly calm sea, a sudden seizure of the brake occurs. What is the resulting initial rise in tension? Because of the calm sea we have $P_0 = 0$. Therefore

$$\frac{dP}{dt} = P_1 = -V \cos \alpha_s .$$

With the value of $V = 6$ knots and a corresponding α_s of $11.7°$ (see Example 1) we have $dP/dt = 9.9$ ft/sec and hence from (29)

$$T_p = 2180 \text{ lbs (twist unrestrained)},$$

$$= 3970 \text{ lbs (twist restrained)}.$$

These values of T_p pertain only to the transient values occurring while the tension wave is being transmitted to the ocean bottom. If the seizure in this case occurred at a depth of three thousand fathoms, the time of transit to the ocean bottom would be only of the order of nine seconds. After reaching bottom our initial assumption of no reflection from the bottom would be violated and (29) would no longer hold. In reality the cable tension would continually increase at the ship and reversing ship engines or some other action would be required to avoid rupture of the cable.

V. DEVIATIONS FROM A HORIZONTAL BOTTOM

5.1 *Kinematics of Laying Over a Bottom of Varying Depth*

Ocean bottom topography is not everywhere flat and horizontal as postulated in the basic model. In the Mid-Atlantic ridge, for example, there exist bottom slopes of thirty or forty degrees. In other places submarine canyons with almost vertical sides have been found. Furthermore, where the bottom is steepest it is most likely to be rocky and craggy since erosion tends to smooth out a sandy or muddy bottom. Therefore, it is important to know how the cable should be paid out to cover a bottom of varying depth. To help determine this, we extend here the stationary model to the case of a non-horizontal bottom.

In Section 3.1 we indicated that if the cable tension at the touchdown point is zero the configuration according to the basic model is a straight line, regardless of how the cable is paid out. If the cable is paid out with

slack with respect to the bottom, the zero touchdown tension condition is fulfilled. Hence, under the proper slack pay-out, the cable geometry and, as we shall see, the cable kinematics are particularly simple.

Essentially, we must consider two deviations from the horizontal bottom, namely, downhill or descent laying and uphill or ascent laying. We consider these situations in turn, confining ourselves to bottoms of constant slope since any bottom contour can be approximated by straight-line segments.

To cover a descending bottom, the cable pay-out rate must exceed the ship speed, Fig. 19(a). To cover an ascending bottom, the angle of incidence α of the cable, which as we have seen in Sections 3.1 and 3.2 depends only on the ship speed, must exceed the ascent angle γ, Fig. 19(b). Otherwise, the situation shown in Fig. 19(c) develops. Hence the critical parameters are pay-out speed and ship speed.
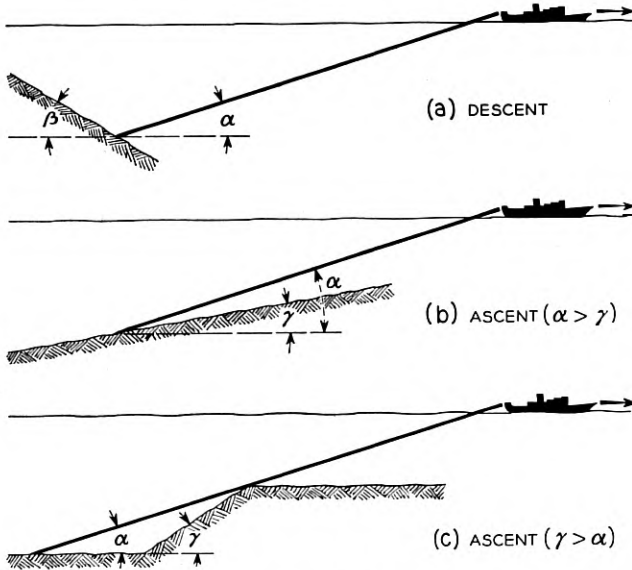
Fig. 19 — Cable geometry during straight-line descent and ascent laying.

During descent laying we see from Fig. 20 that in a time t an amount of cable equal to $a + b$ must be paid out. Hence the required pay-out rate V_c is $(a + b)/t$. But by straightforward trigonometry

$$V_c = \frac{a + b}{t} = \frac{\sin \alpha + \sin \beta}{\sin (\alpha + \beta)} V, \qquad (30)$$

where β is the angle of descent and α is the straight-line incidence angle.
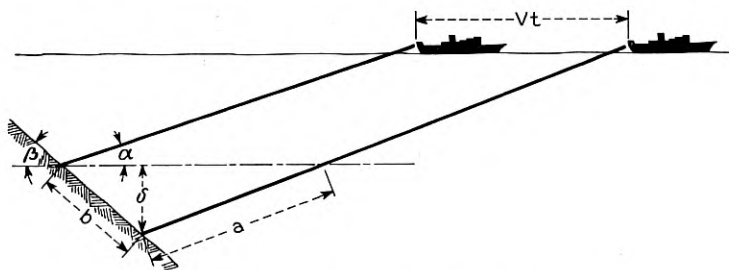
Fig. 20 — Kinematics of straight-line descent laying.

In accordance with usual terminology we define the *slack* ϵ as

$$\epsilon = (V_c - V)/V. \tag{31}$$

We shall think of the slack as being composed of two parts: a *fill f*, which is the amount of slack required for the cable to cover the bottom, and an *excess*, equal to $\epsilon - f$, which will normally be laid to provide a margin of safety. Substituting V_c from (31) into (30) we get the expression for the fill f. The result can be transformed to the form

$$\tan\frac{\alpha}{2}\tan\frac{\beta}{2} = \frac{f}{2+f}. \tag{32}$$

The quantities α, β and f are normally all small quantities and we may make the approximations

$$\tan\frac{\alpha}{2} \approx \frac{\alpha}{2},$$

$$\tan\frac{\beta}{2} \approx \frac{\beta}{2},$$

$$\frac{f}{2+f} \approx \frac{f}{2}.$$

For α, $\beta < 30°$ and $f < 0.06$, the error in each of these approximations is less than 3 per cent. Hence, with good accuracy we write (32) as

$$f = \frac{\alpha\beta}{2}, \tag{33}$$

where α and β are expressed in radians. Further, we have from (9) that α in radians is very nearly $\alpha = H/V$, where H is in radian knots. Substituting this expression into (33), we get for the fill

$$f = \frac{H\beta}{2V} . \qquad (34)$$

Finally, using this expression for f in (31), we arrive at*

$$V_c - V = \frac{H\beta}{2}. \qquad (35)$$

Thus, the *increment* in required pay-out rate is essentially a function only of the descent angle β and is *independent* of ship speed.

In the case of an ascending bottom for which $\alpha > \gamma$, Fig. 19(b), positive bottom slack may be obtained with a pay-out of less than the ship speed. The allowable decrement in pay-out rate is given by

$$V - V_c = \frac{H\gamma}{2}, \qquad (36)$$

that is, the same as the required increment for ascent laying. Likewise, the fill f in this case is simply $f = -(H\gamma/2V)$.

The only way to avoid the situation shown in Fig. 19(c) where $\alpha < \gamma$ is to sail slowly enough to maintain an incidence angle α greater than the angle of rise γ. By (9), we have for most laying speeds $\alpha V \approx H$. With good accuracy the condition $\alpha > \gamma$ thus implies

$$V < \frac{H}{\gamma}. \qquad (37)$$

Therefore, for a given rise γ the limiting ship speed is simply H/γ.

5.2 *Time-Wise Variation of the Mean Tension in Laying Over a Bottom of Varying Depth*

In the cases where the cable is paid out with excess onto a bottom of constant slope, the variation of the mean tension at the ship with time is easily computed. During descent laying the increase in depth δ after a time t is by elementary trigonometry (Fig. 20)

$$\delta = \frac{\sin \alpha \sin \beta}{\sin (\alpha + \beta)} Vt.$$

Hence, the rate of rise of the mean shipboard tension is

$$\frac{dT}{dt} = \frac{w\delta}{t} = \frac{\sin \alpha \sin \beta}{\sin (\alpha + \beta)} wV . \qquad (38)$$

Similarly, during an ascent lay for which the bottom is less steeply

---

* Note that in (33), (34) and (35), H may be replaced by the numerically identical transverse settling velocity u_s (see Section 3.4).

inclined than the cable ($\alpha > \gamma$), the rate of decrease in shipboard tension is

$$\frac{dT}{dt} = -\frac{\sin \alpha \sin \gamma}{\sin (\alpha - \gamma)} wV.$$

Like negative slack laying on a flat bottom, the variation of tension with time depends greatly on the frictional characteristics of the bottom in cases other than the above. We therefore limit ourselves to situations where the cable does not move with respect to the ocean floor. This case might be approximated by rough bottoms, where the cable might wedge itself between rocks.

A nomograph giving a rough estimate of the rise of mean tension with time when a cable becomes completely suspended is worked out in Appendix E. In deriving this nomograph it is assumed that the cable takes on a sequence of stationary configurations. This assumption is probably reasonable if the time span of the tension rise is large compared to the time of passage of a tension wave from the ship to ocean floor and return, which as mentioned in Section 4.1 is of the order of 18 seconds. However, because of this assumption and others mentioned in Appendix E, we regard the tension variation computed by the nomograph only as a crude approximation.

Fig. 21 shows the mean ship-board tension versus time computed by means of the nomograph for various slacks ϵ, where ϵ is defined by (31). The values which were used for the other parameters entering the calculation were

$$\frac{wh}{EA} = 3.1 \times 10^{-3},$$

$$\alpha = 12°.$$

Also shown on this curve is the tension rise computed for the case of laying down a vertical slope without excess. The rise for this case is given by (38) with $\beta = 90°$. It is seen that as the slack ϵ is increased the curves for a complete suspension approach the $\beta = 90°$ curve. Indeed, it can be shown that under the assumptions made in computing Fig. 21 the $\beta = 90°$ curve gives a lower bound on the tension rise with time in the case of a complete suspension. A tension rise rate greater than the $\beta = 90°$ rate is thus an indication of unsatisfactory covering of the bottom.

In the case of too rapid a ship speed resulting in $\alpha < \gamma$ (Fig. 19c) restraint of movement of the cable along a rough bottom would cause the tension on the high side of the crest to be zero. There would thus be a sudden drop in tension corresponding to the sudden decrease in depth at the touchdown point after the cable was laid over the crest of the hill.
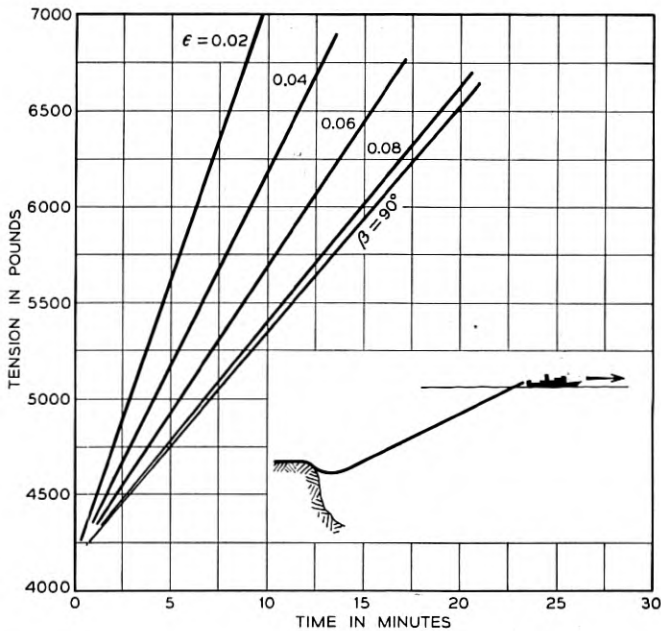
Fig. 21 — Variation of tension with time when cable No. 2 is completely suspended.

On the other hand, in the case of a frictionless bottom, the removal of the supporting water drag forces would cause the cable to seek a catenary equilibrium position on the low side of the crest. But in doing this, the cable would drag itself over the crest, with an accompanying *increase* in shipboard tension.

Thus for the case of a bottom rise steeper than the cable inclination $(\alpha < \gamma)$ either an increase or a decrease of tension with time is possible, depending on the nature of the bottom.

5.3 *Residual Suspensions*

If the cable is not paid out rapidly enough, or if the ship speed is excessive, the cable will be left with residual suspensions after it has been laid. To get an idea of the possible magnitudes of the tensions accompanying these suspensions, we consider here some numerical examples pertaining to cable No. 2. As before, we assume for definiteness the extreme case of a bottom rough enough to prevent movement of the cable.

In Fig. 22 is shown the profile of a 35 fathom (210 feet) increase in depth with a maximum slope of 45°. This profile was obtained from

fathometer records of the Mid-Atlantic Ridge provided by Professor Bruce C. Heezen of the Lamont Geological Observatory. Laying down this slope at a ship speed of six knots requires a slack of 8.5 per cent (see Section 5.1). If the slack were only 5 per cent, the successive cable configurations as calculated by the methods of Appendix E would be those shown in Fig. 22(a).* The cable would touch bottom after 2.6 minutes,
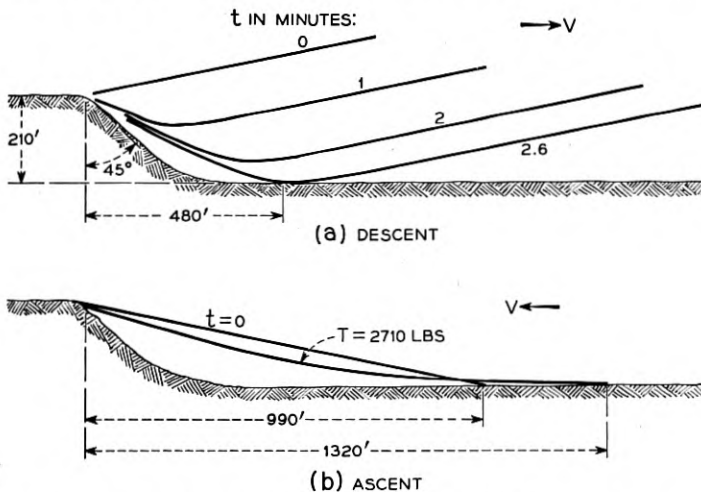
Fig. 22 — Successive cable configurations during a 35-fathom descent and ascent lay of cable No. 2 at a 6,000-ft depth with an assumed 5 per cent slack and 6-knot ship speed.

leaving a residual suspension with a half-span of 480 feet and a tension of 525 lbs. The mean tension at the ship would correspondingly increase by 525 lbs during the 2.6 minute time interval. In even moderately rough seas, this tension change could be obscured by the ship motion tensions.

Consider this profile next to represent an ascending lay under a ship speed of six knots. Fig. 22(b) shows the initial $(t = 0)$ and residual cable configuration. Because of the small incidence angle of the initial straight-line shape, the residual half-span of the catenary is a quarter of a mile (1320 feet) long, and the accompanying residual tension is 2,710 lbs, or roughly that which normally occurs in laying at a depth of $\frac{3}{4}$ of a nautical mile. At the ship, there would be a decrease in the mean tension of 130 lbs. corresponding to the 35 fathom decrease in depth. Again, a tension change of this magnitude would be difficult to discern because of ship motion tensions.

---

* We have further taken the ratio $wh\,/\overline{EA}$ to be 3.1×10^{-3} in this computation. However, the results are very insensitive to change in the $wh\,/\overline{EA}$ ratio.

If the above 35 fathom change occurred at a depth of say three thous-
and fathoms, a very sensitive fathometer would be required to detect it.
Thus, although complete restraint of cable movement along the bottom
is an extreme and unlikely condition, the above examples indicate that
long residual suspensions can occur with essentially no manifestation at
the ship, especially in deep water.

VI. CABLE LAYING CONTROL

6.1 *General*

We have seen that the mean cable tension at the ship reflects the
amount of slack which is being paid out and how the cable is covering
the bottom. However, in most cases this reflection is not sensitive. For
example, the tangential drag force D_T varies with V_t, the longitudinal
velocity of the cable relative to the water. In theory, as (2) shows, one
can therefore determine the amount of slack being paid out from ship-
board tension measurements. For cable No. 2, we have plotted in Fig.
23 the variation of the mean tension at the ship as a function of slack for
a ship speed of six knots and a depth of two thousand fathoms. At three
per cent slack the tension is 8,240 pounds, while at six per cent slack it
is 8,020 pounds, a difference of only 220 pounds. This amount of tension
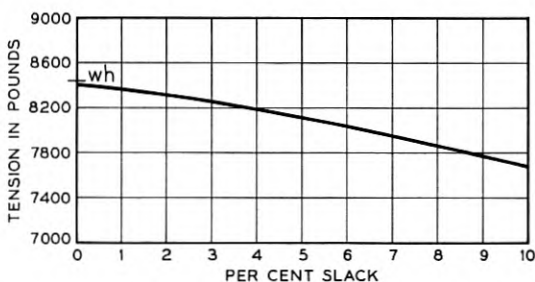
Fig. 23 — Variation of shipboard tension with per cent slack for laying cable
No. 2 at a ship speed of 6-knots in a depth of two thousand fathoms.

could be easily obscured by the effect of ship motion. Thus, to measure
slack accurately by relating it to cable tensions one would have to know
the depth and cable parameters very precisely and, in addition, would
need a very efficient filter to separate out the "noise" tension caused by
ship motion.

Similarly, it has been shown that residual suspensions can occur with
essentially no reflection in the tension readings at the ship. Hence, al-
though tension readings can give a valuable check on how the cable is

covering the bottom, it would seem difficult for them to provide exact enough data for the control of cable laying.

At the same time we have seen that if the bottom contour is known in advance, then for a given ship speed one can compute the required cable pay-out rate. Also with foreknowledge of the bottom, one can anticipate steep bottom ascents and decrease the ship speed accordingly. Such a purely kinematic attack on the cable laying problem would seem more fruitful than an attack which depends on measurements of shipboard cable tensions.

Possibly the simplest way of measuring the bottom contour is by means of a fathometer located at the ship. Since the cable ship is normally far forward of the touchdown point of the cable, one could in theory obtain in this manner the required advance knowledge of the contour. In present practice, a taut piano wire is used to obtain the ground speed of the ship. We examine briefly the accuracy of this method in the next section.

6.2 *Accuracy of the Piano Wire Technique*

The taut wire is laid simultaneously with the cable, but under a constant mean shipboard tension. If the bottom is perfectly horizontal, the speed of the wire coincides with the ground speed of the ship. However, when the bottom depth is variable and the wire is laid up and down hill, the wire's pay-out speed deviates from the ship speed. By (31), it is seen that the error in the ship speed which is indicated by the wire is just equal to the slack ϵ with which the wire is paid out. This slack, which may be positive or negative, can in turn be estimated by the methods of the previous sections.

Consider the beginning (denoted by (1) in Fig. 24) and end (denoted by (2) in Fig. 24) of a downhill lay of the piano wire. As before we neglect the tangential drag force. Then, the condition that the tension at the ship remains constant gives, by (21),

$$(T_0)_1 + wh_1 = (T_0)_2 + wh_2 , \qquad (39)$$

where the subscripts 1 and 2 refer to the configurations at the beginning and end of the downhill lay. If $\bar{\epsilon}$ is the average slack or error of the piano wire during the descent, then $(1 + \bar{\epsilon})V$ is its average pay-out rate, and we have by Fig. 24,

$$S_1 + (1 + \bar{\epsilon})Vt = \frac{h_2 - h_1}{\sin \beta} + S_2 , \qquad (40)$$

where S_1 and S_2 are lengths along the cable from the touchdown point to the ship. Also, from Fig. 24

$$X_1 + Vt = (h_2 - h_1)/\tan \beta + X_2. \tag{41}$$
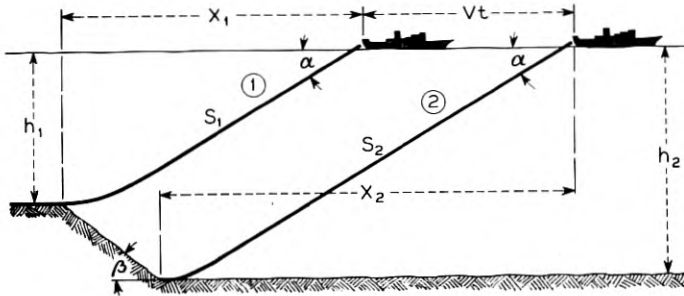
Fig. 24 — Piano wire configurations at the beginning and end of a descent lay.

Equations (39), (40), and (41), together with the general equations (Section 3.6)

$$S = \frac{h}{\sin \alpha} + \kappa \frac{T_0}{w},$$

$$X = \frac{h}{\tan \alpha} + \lambda \frac{T_0}{w}, \tag{24}$$

allow one readily to solve for the average error $\bar{\epsilon}$ in the piano wire indication of ship ground speed. The result is

$$\bar{\epsilon} = \frac{\sin \alpha + \sin \beta - \kappa \sin \alpha \sin \beta}{\sin (\alpha + \beta) - \lambda \sin \alpha \sin \beta} - 1. \tag{42}$$

For the small values of α and β which normally occur during the laying of the piano wire, the terms $\lambda \sin \alpha \sin \beta$ and $\kappa \sin \alpha \sin \beta$ are negligible. Hence, the average error $\bar{\epsilon}$ is thus very nearly

$$\bar{\epsilon} = \frac{\sin \alpha + \sin \beta}{\sin (\alpha + \beta)} - 1, \tag{43}$$

which, as (30) indicates, coincides with the amount of fill which would be required to lay downhill with the straight-line or zero touchdown tension configuration. Equation (43) is in turn closely approximated by (Section 5.1)

$$\bar{\epsilon} = \frac{\alpha \beta}{2} = \frac{H \beta}{2V}. \tag{44}$$

Similarly, for ascent laying of the wire on a bottom which rises less steeply than the inclination of the wire (19b), we get

$$\bar{\epsilon} = \frac{\sin \alpha - \sin \gamma + \kappa \sin \alpha \sin \gamma}{\sin (\alpha - \gamma) + \lambda \sin \alpha \sin \gamma} - 1, \tag{45}$$

which is very nearly

$$\bar{\epsilon} = \frac{-\alpha\gamma}{2} = -\frac{H\gamma}{2V}. \tag{46}$$

Thus, in both the above cases, the error in the piano wire technique can be closely obtained by assuming that the configuration of the wire is a straight line during ascent and descent laying. This is not surprising since, as we saw in Section 3.6, the deviation from the straight-line configuration during piano wire laying is normally small.

Because of its smooth exterior, the normal or transverse drag coefficient of the piano wire probably can be obtained from published curves for flow past a smooth right circular cylinder as shown in Appendix B. For typical 12 gauge (0.0290 inch diameter) piano wire, these curves yield a value of C_D of 1.45 and an H value of 25.0 degree-knots. However, these values of C_D and H must be considered tentative until confirmed experimentally.

Knowing the wire's H value, we can compute the error of the ground speed caused by descent and ascent laying of the piano wire by means of (44) and (46). The result of this computation for $H = 25.0$ degree-knots is shown in Fig. 25.

When the ascent angle of the bottom exceeds the incidence angle of the wire, suspensions result and the error cannot be computed without
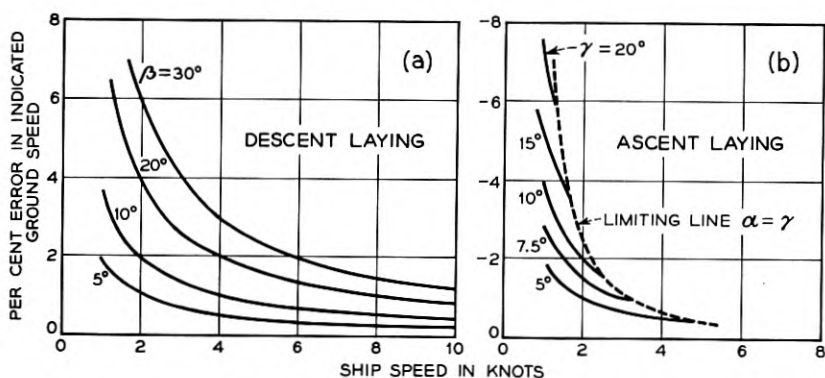

Fig. 25 — Error during descent and ascent laying of 12-gauge piano wire.

knowledge of the frictional properties of the bottom. For an H value of 25.0 degree-knots, (37) indicates that suspensions will occur for ship speeds V greater than $V = 25.0/\gamma$, where V is in knots and the ascent angle γ is in degrees. Hence, for a typical laying speed of 6 knots, ascent angles greater than 4.2 degrees will cause suspensions of the piano wire. These magnitudes indicate that suspensions of the piano wire probably actually develop in practice.

It is seen from Fig. 25 that for the usual small ascent or descent angles, the piano-wire technique is quite accurate, while for large bottom slopes it can be considerably in error. Again, however, if the bottom contour is known in advance, these errors can be estimated in the cases plotted in Fig. 25 and therefore can be corrected for. In this manner, the piano wire could be improved to give accurate ground speeds in all two-dimensional situations, with the exception of the case of a suspension caused by a too steeply ascending bottom. Such suspensions can be avoided only by maintaining a sufficiently slow ship speed. However, as seen by the small computed H value of 25.0 degree-knots, the ship speeds required to avoid piano wire suspensions on uneven bottoms are probably prohibitively slow. Hence, for steeply ascending bottoms it is likely that some other means of determining the ship ground speed is necessary.

VII. THREE-DIMENSIONAL STATIONARY MODEL

7.1 *General*

Thus far we have assumed that the cable lies entirely in the plane formed by the ship's velocity vector and the gravity vector. Because of the symmetry of the cable cross-section, this assumption seems reasonable.* However in certain cases, as for example in the presence of ocean cross-currents, the assumption of a planar configuration is clearly untenable. We consider therefore the case where the cable configuration is not necessarily planar but is still time independent with respect to a reference frame translating with the constant velocity of the ship. In analogy with previous terminology, we call this the three-dimensional stationary model.

Assume there is a constant velocity ocean current in each of a finite number of layers. Let the vector $\vec{V}_w$ denote the ocean-current velocity in a reference layer. In the stationary situation the velocity of the cable

---

* Because of asymmetries caused by the helical armor wire or because of minor out-of-roundness, it is conceivable that a sidewise drag force might develop which would cause the cable to move out of the ship's velocity-gravity plane. For a report of experimental observations of such yawing in wire stranded cables, see Reference 11.

configuration is everywhere the velocity of the ship, which we denote by the vector $\vec{V}$. Hence the velocity $\vec{V}'$ of the water with respect to the cable configuration in the reference layer is

$$\vec{V}' = \vec{V}_w + (-\vec{V}) = \vec{V}_w - \vec{V}.$$

Further, in this layer we choose a set of coordinate axes ξ, η, ζ translating at the velocity $\vec{V}$ as follows: The ξ axis has the direction of $-\vec{V}'$, while η is measured vertically upward, and ζ is perpendicular to η and ξ so that the axes ξ, η, ζ form a right-handed system. A plan view of this configuration is shown in Fig. 26. We have denoted the angle between $\vec{V}$ and $\vec{V}_w$ by β, while the angle between the ξ axis and $\vec{V}$ is denoted by φ. (The distances d and e refer to a subsequent section.) To describe the cable configuration with respect to the ξ, η, ζ axes, we use the spherical polar coordinates θ and ψ shown in Fig. 27. (The $\vec{t}, \vec{u}, \vec{v}$ vectors are discussed in Appendix F.)
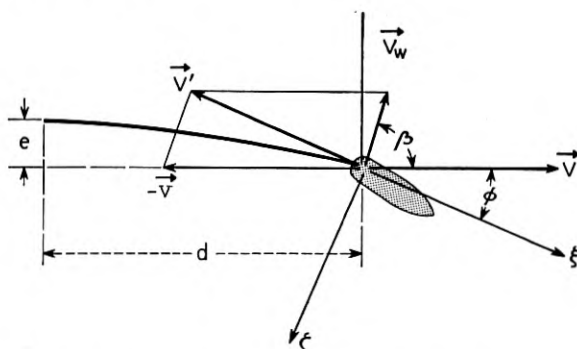
Fig. 26 — Plan view of the coordinate system for the three-dimensional stationary model.

As in the two-dimensional case, we resolve the velocity of the water with respect to a cable element in the reference layer into a component V_N normal to the cable and a component V_t tangential to the cable, and associate with V_N and V_t the drag forces D_N and D_T. The resulting differential equations, which are derived in detail in Appendix F, are the following:

$$(T - \rho_c V_c^2)\, \frac{d\theta}{ds}$$

$$+ w\Lambda'(\cos^2\psi \sin^2\theta + \sin^2\psi)^{1/2} \cos\psi \sin\theta - w\cos\theta = 0, \quad \text{(a)}$$

$$(T - \rho_c V_c^2) \cos \theta \, \frac{d\psi}{ds} \qquad\qquad (47)$$

$$+ w\Lambda'(\cos^2 \psi \sin^2 \theta + \sin^2 \psi)^{1/2} \sin \psi = 0, \quad \text{(b)}$$

$$\frac{dT}{ds} + D_T - w \sin \theta = 0, \qquad \text{(c)}$$

where $\Lambda' = C_D \rho d V'^2/2$, and V' is the magnitude of $\vec{V}'$.

In addition, connecting the coordinates $\xi(s)$, $\eta(s)$, and $\zeta(s)$ of a point s along the cable with the angles θ and ψ we have the geometric relationships

$$\frac{d\xi(s)}{ds} = \cos \theta \cos \psi, \qquad \text{(a)}$$

$$\frac{d\eta(s)}{ds} = \sin \theta, \qquad\qquad \text{(b)} \qquad (48)$$

$$\frac{d\zeta(s)}{ds} = -\cos \theta \sin \psi. \quad \text{(c)}$$

Two important general results follow from (47) and (48). For one, if the tangential drag force D_T is negligibly small, (48b) substituted into equation (47c) yields upon integration

$$T = T_0 + w\eta, \qquad (49)$$

where T_0 is the tension at $\eta = 0$. Hence, if η is measured from the ocean

Fig. 27 — Definition of the spherical polar coordinates θ and ψ and the unit vectors $\vec{t}$, $\vec{u}$, and $\vec{v}$.
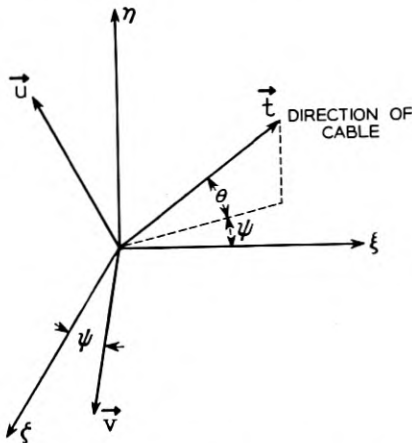
surface, and if at the bottom ($\eta = -h$) the tension is zero, the tension at the ship is essentially *wh*, *regardless* of the nature of the normal drag forces. Since in most laying situations for present cables, the tangential drag force can be reasonably neglected, this fact provides a convenient over-all check on the laying process. That is, if the cable is being laid with excess, the tension at the ship for *any* stationary cable configuration, *planar* or *non-planar*, should be essentially *wh*. Any marked increase of tension over the *wh* value necessarily means the bottom tension is non-zero and insufficient cable is being paid out.

The second important result is derived in Appendix F. This result is that if the bottom ocean layer in our model is devoid of cross currents, and if the bottom tension is zero, then, for the boundary conditions which are normally observed, the cable configuration in the bottom layer is a straight line. Further, this straight line is in the plane formed by the ship's velocity vector $\vec{V}$ and the gravity vector. Hence, for example, in laying with excess in a sea which contains surface currents, the cable configuration in the lower, current-free portion will be a straight line in a vertical plane parallel to the resultant velocity of the ship. The laid cable will be parallel to the ship's path, but displaced a certain distance from it. Thus, because the lower portion is a straight line, our previous results about the kinematics of straight-line laying still apply. Only they now are pertinent to the displaced bottom contour rather than to the contour which lies directly beneath the ship.

7.2 *Perturbation Solution for a Uniform Cross-Current*

Cross-currents are commonly confined to a region near the ocean surface. It is of interest therefore to determine for such surface currents the distance e (Fig. 26) which the laid cable will be displaced from the path of the ship. In Appendix F we consider the problem for a cross-current of uniform but comparatively small velocity. In addition, we determine the distance d (Fig. 26) back of the ship at which the cable leaves the upper, cross-current stratum and assumes the straight-line configuration it has in the lower stratum. Let us assume for the sake of reference that the resultant ship velocity V is due east, and that the cross-current V_w is inclined at an angle β to the north (Fig. 26). The resultant velocity V' of the water with respect to the cable in the surface stratum has the magnitude therefore of

$$V' = [(V - V_w \cos \beta)^2 + (V_w \sin \beta)^2]^{\frac{1}{2}}, \tag{50}$$

and is inclined at the angle φ from due west, where

$$\tan \varphi = \frac{V_w \sin \beta}{V - V_w \cos \beta}. \tag{51}$$

Associated with V' we have a critical angle α' which is given approximately by H/V' or exactly by (10) or (11).

In terms of φ, α', and α the analysis of Appendix F yields the following values of d and e.

$$d = h'\left(\mathrm{ctn}\alpha' - \frac{\Delta\alpha}{2\cos^2\alpha'}\frac{h-h'}{h'}\left[1-\left(1-\frac{h'}{h}\right)^{2\mathrm{ctn}^2\alpha'}\right]\right) \quad \text{(a)}$$

$$e = h'\varphi\,\mathrm{ctn}\alpha'\left(1-\frac{h-h'}{h'}\tan^2\alpha'\left[1-\left(1-\frac{h'}{h}\right)^{\mathrm{ctn}^2\alpha'}\right]\right), \quad \text{(b)} \tag{52}$$

where $\Delta\alpha = \alpha - \alpha'$ is the difference of lower and upper stratum critical angles, h' is the depth of the upper, cross-current stratum and h is the total depth.* Curves from which d and e may be evaluated are given in Figs. 28 and 29 in dimensionless form. To illustrate their application we consider the following.
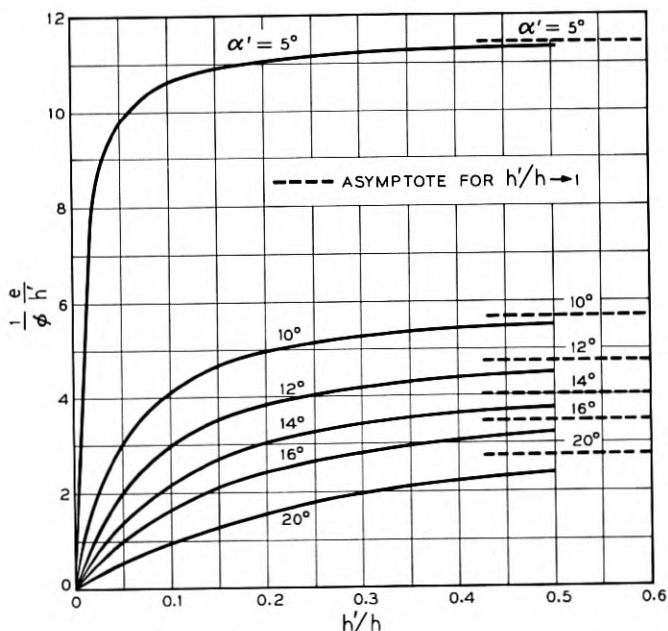
Fig. 28 — Distance the laid cable is offset from the ship's path.

* In Appendix F the equation of the space curve formed by the cable in the upper stratum is also given.
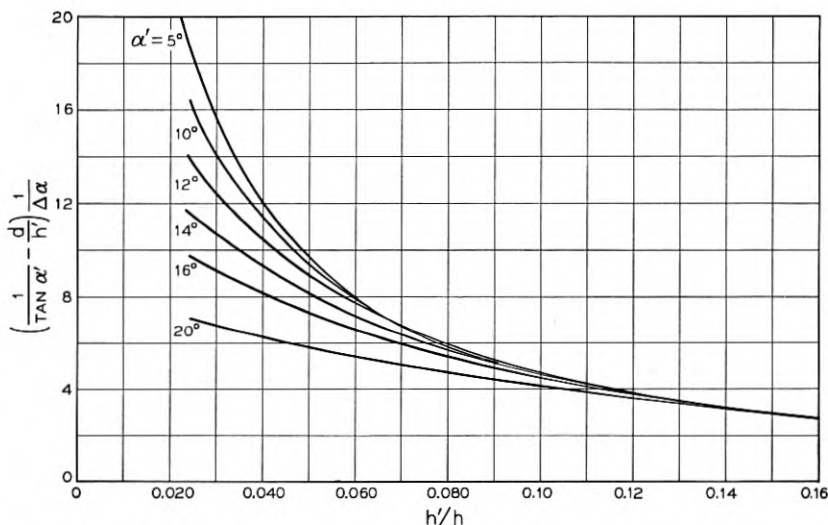
Fig. 29 — Distance behind the ship at which the cable enters the lower stratum.

Example: A ship is laying cable No. 2 at a depth of 6,000 ft at a resultant ground speed of 6 knots due east. There is a one knot cross-current 600 feet deep running 30° east of north. Find e and d.

Here $\beta = 60°$ and we obtain from (50) by a simple computation $V' = 5.57$ knots. Also since for cable No. 2 $H = 70$ degree-knots,

$$h'/h = 600/6000 = 0.1,$$

$$\alpha' = 70/5.57 = 12.3 \text{ degrees.}$$

By interpolation, we find from Figs. 28 and 29

$$\frac{1}{\varphi}\frac{e}{h'} = 2.7,$$

$$\left(\frac{1}{\tan \alpha'} - \frac{d}{h'}\right)\frac{1}{\Delta\alpha} = 4.7.$$

Equation (51) yields in turn $\varphi = 0.156$ radians, and $\Delta\alpha$ is given by

$$\Delta\alpha = \frac{70}{V} - \frac{70}{V'} = -0.6 \text{ degrees} = -0.010 \text{ radians.}$$

Hence, we have

$$e = 3.6 \, h'\varphi = 2.7 \times 600 \times 0.156 = 253 \text{ ft,}$$

$$d = h'\left[\frac{1}{\tan \alpha'} - 4.7\Delta\alpha\right] = 6000 \, [4.59 + 4.7 \times 0.010] = 2800 \text{ ft.}$$

APPENDIX A

Discussion of the Two-Dimensional Stationary Configuration for Zero Bottom Tension

We assume again that the tangential drag D_T depends only on the relative tangential velocity V_T, and we consider in a T, θ plane the solution trajectories of equations (18). These trajectories satisfy the equation

$$\frac{dT}{d\theta} = \frac{(\sin\theta - D_T/w)}{\cos\theta - \Lambda\sin\theta \mid \sin\theta \mid} (T - \rho_c V_c^2), \qquad (53)$$

and are periodic in θ with a period of 2π. In Fig. 30 we have plotted the solution trajectories qualitatively for $(\alpha - \pi) \leqq \theta \leqq (\alpha + \pi)$. It is seen that the trajectories are either the vertical straight lines $\theta = \alpha$, $\theta = \alpha \pm \pi$ or they lie completely within one of four regions, labelled I, II, III, or IV, which are bounded by these vertical lines and the horizontal line $T = \rho_c V_c^2$. The trajectory $\theta = \alpha$ corresponds to the straight-line laying configuration, while the trajectories $\theta = \alpha \pm \pi$ correspond to Shea's straight-line recovery method.

Examine now the trajectories in Regions II and III at a point of which $T = 0$. As J. F. Shea has pointed out, these trajectories all lie below the line $T = \rho_c V_c^2$. On the other hand, the trajectory $\theta = \alpha$ con-
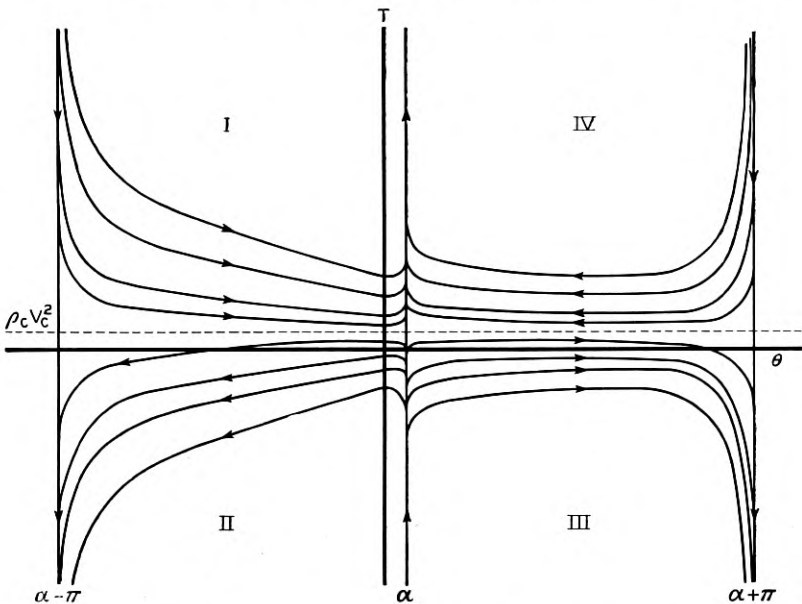

Fig. 30 — Qualitative representation of the solution trajectories of the two-dimensional stationary model.

tains all values of T. Hence, according to the stationary model, the only cable configuration for laying which has the value $T = 0$ and values of $T \geqq \rho_c V_c^2$ is the straight line inclined at the critical angle α. The magnitude of $\rho_c V_c^2$ is small. For example, for cable No. 2 paid out at six knots $\rho_c V_c^2$ is roughly six pounds, and for conditions approximating stationary laying the observed tensions at the ship are in practice always many times the $\rho_c V_c^2$ value. For such magnitudes of shipboard tensions and a zero bottom tension, the two-dimensional stationary model thus yields the straight line as the only possible cable configuration.

However, the empirical fact that $T > \rho_c V_c^2$ does not guarantee that the shipboard tension must be greater than $\rho_c V_c^2$. We might somehow contrive to lay at a zero bottom tension with $T < \rho_c V_c^2$ and with the cable in one of the non-straight line configurations of Regions II or III.

Consider the cable configuration lying in Region II. From Fig. 7 it can be seen that the vertical velocity of a cable element is given by

$$\frac{dy}{dt} = -V_{\text{vert}} = -V_c \sin \theta,$$

where y is measured upward. Hence, of the possible trajectories for which the bottom tension is zero only those for which the bottom cable angle θ_0 is between zero and π correspond to cable laying. For region II, therefore we need consider only the trajectories in the range $0 \leqq \theta_0 < \alpha$ at $T_0 = 0$. From (20c) the maximum value of y_m for these trajectories is given by

$$y_m = \frac{\rho_c V_c^2}{w} \int_0^{\theta_0} \left\{ \frac{\sin \xi}{(\cos \xi - \Lambda \sin^2 \xi)} \right. \tag{54}$$
$$\left. \times \exp\left[-\int_\xi^{\theta_0} \frac{w \sin \eta - D_T(\eta)}{w (\cos \eta - \Lambda \sin^2 \eta)} \, d\eta \right] \right\} d\xi.$$

Let $(D_T)_m$ be the maximum value of D_T, $0 \leqq \eta < \alpha$. With D_T set equal to $(D_T)_m$, the right-hand side of (54) gives an upper bound on y_m. This substitution further allows one to evaluate the right-hand side of this equation in terms of standard integrals. The result yields the following upper bound on y_m:

$$y_m < 2.1 \frac{\rho_c V_c^2}{w} \frac{1}{1 - r},$$

where

$$r = \frac{(D_T)_m}{w \sin \alpha}.$$

In general, this upper bound will be much less than the laying depth. For example, for cable No. 2 being laid with 6 per cent slack at 6 knots $y_m < 12.5$ feet. That is, the cable configurations corresponding to Region II do not reach the ocean surface. Hence these solutions of the stationary model do not in general satisfy all the required boundary conditions and can be discarded.

Similarly, in Region III, the laying trajectories for which $T_0 = 0$ are in the range $\alpha < \theta_0 \leqq \pi$. Consider those for which $\theta_0 < \pi/2$. We get for these trajectories

$$
y_{\pi/2} = \frac{\rho_c V_c^2}{w} \int_{\theta_0}^{\pi/2} \left\{ \frac{\sin \xi}{(\Lambda \sin^2 \xi - \cos \xi)} \right.
$$
$$
\left. \times \exp \left[- \int_{\theta_0}^{\xi} \frac{w \sin \eta - D_T(\eta)}{w (\Lambda \sin^2 \eta - \cos \eta)} \, d\eta \right] \right\} d\xi, \tag{55}
$$

where $y_{\pi/2}$ is the value of y at $\theta = \pi/2$. Let m be the minimum value of $\sin \eta - (D_T(\eta)/w)$ in the range $\alpha < \eta \leqq \pi/2$. If, as in the usual case, m is positive, we can obtain an upper bound on $y_{\pi/2}$ by replacing $\sin \eta - (D_T(\eta)/w)$ by m in the right-hand side of (55). By this means we find that

$$
y_{\pi/2} < \frac{\rho_c V_c^2}{w} \frac{2(1 + \cos^2 \alpha)}{m \tan \alpha/2}.
$$

For cable No. 2 being laid with 6 per cent slack at 6 knots this relation yields $y_{\pi/2} < 1,100$ feet. So in the usual laying depths, which are many times greater than $y_{\pi/2}$, the configurations in Region III for which $T_0 = 0$ correspond to a value of θ at the surface greater than $\pi/2$, or to cable being paid out *in front* of the ship during laying. It is doubtful whether such configurations would be stable and, at any rate, doubtful whether cable would ever be laid in such a manner. Hence, we conclude that these $T_0 = 0$ solutions of Regions II and III will in general be mathematical curiosities, and that the only realistic laying solution of the stationary model for which the bottom tension is zero is the straight line $\theta \equiv \alpha$.

APPENDIX B

Computation of the Transverse Drag Coefficient and the Hydrodynamic Constant of a Smooth Cable from Published Data

From (6) of Section 3.2 we obtain the relationship

$$\frac{V \sin \alpha}{\sqrt{\cos \alpha}} = \left(\frac{2w}{C_D \rho d}\right)^{1/2} = H, \tag{56}$$

where H is the hydrodynamic constant. Also, we define the Reynolds number for flow normal to the cable in the usual way;

$$N_R = \frac{dV \sin \alpha}{\nu}, \tag{57}$$

ν being the kinematic viscosity of water. For smooth cable we now assume that the drag coefficient C_D depends on N_R in the same way as for flow around a smooth cylinder of infinite length. Experimental data for this relationship, namely,

$$C_D = C_D(N_R) \tag{58}$$

are available in the literature and have been collated by Eisner.[15]

For a given velocity V, (56) through (58) represent three equations for the unknowns α, C_D, and N_R. In general, the solution of these equations depends on V, thus contradicting the assumption made in Section 3.2 that C_D, and therefore H, are constants independent of V. However, for sufficiently large V we can expect the resulting α to be small so that $\sqrt{\cos}\, \alpha \approx 1$. In this case (56) and (57) combine to give

$$C_D = \frac{2wd}{\rho \nu^2} \frac{1}{N_R^2}, \tag{59}$$

which together with (58) yields two equations for C_D and N_R that are indeed independent of V. In laying, V will normally be large enough for this approximation to hold.

Equations (58) and (59) are in turn easily solved graphically by finding the intersection on log-log paper of the curves, C_D versus N_R, that these equations represent. Since ρ and ν are properties only of the water, we see that C_D is a function only of the product wd of the unit weight of the cable times its diameter. In Fig. 31 we have plotted the resulting values of C_D for wd ranging from 10^{-7} to 10 pounds. For this computation we have assumed sea water at 32°F with an assumed density of 1.994 slugs per cubic foot and a kinematic viscosity of 2.006×10^{-5} ft^2/sec.

For other than large values of V, (56) through (58) can be readily solved if one interchanges the roles of α and V, that is, if one considers α as given and V as unknown. Equations (56) and (57) can again be combined in this case to give

$$C_D = \frac{2wd \cos \alpha}{\rho v^2} \frac{1}{N_R{}^2},$$ (60)

and with $wd \cos \alpha$ a known number, (60) and (58) can be solved for C_D and N_R as before. Thus, one can obtain C_D from Figure 31 by merely reading $wd \cos \alpha$ rather than wd on the abscissa. Knowing C_D one can solve for V from (56).
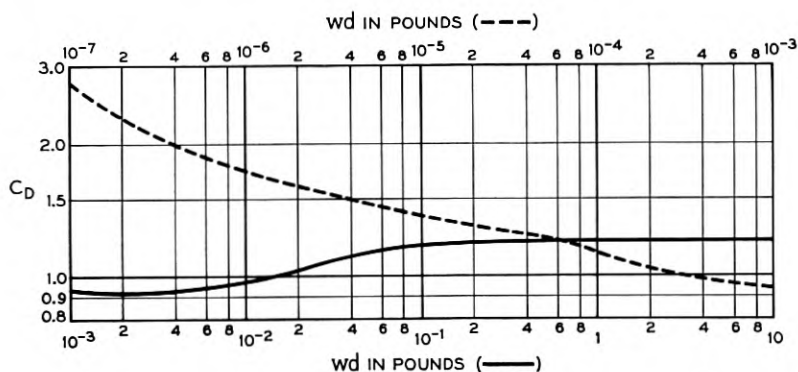
Fig. 31 — Variation of C_D with wd for cables of smooth exterior.

The results of such a computation are shown in Table II for cable No. 1. For $V > 1.5$ knots the experimentally determined H is 64.0 degree-knots. The corresponding computed values of H, ranging from 67.4 to 70.0 degree-knots, compare favorably with this experimental value. Over the entire range of V, from 0.25 to 10.00 knots, the variation in H is about 4 per cent. This small variation makes the assumption of Section 3.2 that H is a constant for all V appear reasonable, especially since we can only hope to use this computation in a preliminary design before the hydrodynamic properties of a cable are established by experiment.

TABLE II — COMPUTED VALUES OF N_R, C_D, AND H FOR CABLE NO. 1

V (knots)	N_R	C_D	H (deg.-knots)
0.25	1.25×10^3	0.935	67.5
0.50	2.50	0.922	70.0
1.50	5.20	0.965	67.8
3.00	5.80	0.985	67.5
10.00	6.05	1.000	67.4

In Table III we have indicated computed high-velocity H values as a function of the unit weight w and the diameter d of a cable. Table IV shows the computed high-velocity C_D and H for various gauge piano wire. The American Steel and Wire gauge scale is used in this tabulation.

TABLE III — COMPUTED VALUES OF THE HYDRODYNAMIC CONSTANT H IN DEGREE-KNOTS FOR SMOOTH CABLE

Submerged Weight in lb/ft	Diameter in Inches									
	0.5	0.75	1.00	1.25	1.50	1.75	2.0	2.5	3.0	4.0
0.1	54.5	44.2	37.9	33.7	30.6	28.1	26.2	23.2	21.0	17.9
0.2	75.9	61.1	52.3	46.4	41.9	38.5	35.8	31.6	28.5	24.4
0.3	91.7	73.6	62.9	55.6	50.2	46.1	42.8	38.0	34.4	29.7
0.4	104.7	83.9	71.5	63.1	57.1	52.5	48.9	43.5	39.6	34.3
0.5	115.9	92.6	78.9	69.8	63.3	58.3	54.4	48.5	44.3	38.3
0.6	125.8	100.4	85.6	75.9	68.9	63.6	59.5	53.2	48.5	42.0
0.7		107.6	91.9	81.6	74.2	68.7	64.2	57.4	52.4	45.3
0.8		114.2	97.8	87.0	79.3	73.4	68.6	61.3	55.9	48.4
0.9		120.6	103.4	92.1	84.1	77.8	72.7	65.0	59.3	51.3
1.0		126.5	108.7	97.1	88.6	82.0	76.6	68.5	62.5	54.1
2.0			153.3	137.0	125.0	115.7	108.2	96.7	88.2	76.3
3.0				167.6	152.9	141.5	132.3	118.2	107.9	93.3

TABLE IV — COMPUTED C_D AND H VALUES OF PIANO WIRE

Gauge (Am. Steel & Wire)	Dia. (inches)	C_D	H (deg-knots)
0	0.009	2.49	10.7
5	0.014	1.91	15.2
10	0.024	1.56	22.1
15	0.035	1.39	28.2
20	0.045	1.31	33.0
25	0.059	1.24	38.7
30	0.080	1.14	47.2
35	0.106	1.02	57.1
40	0.138	0.970	67.1

APPENDIX C

Some Approximate Solutions for Laying and Recovery

c.1 *Laying*

We assume that the tangential drag and the centrifugal forces are negligible. Then, since for laying $0 \leqq \theta \leqq \pi$, (18a) by virtue of (21) becomes

$$\left(\frac{T_0}{w} + y\right)\frac{d\theta}{ds} + \Lambda \sin^2 \theta - \cos \theta = 0. \tag{61}$$

Let the origin of an x, y coordinate system be at the cable touchdown point (Fig. 8). Further, let x be the x coordinate of a point along the cable configuration and s the corresponding distance along the cable from the origin. If we define

$$\Delta = s - x, \tag{62}$$

then

$$\frac{d\Delta}{dy} = \frac{ds}{dy} - \frac{dx}{dy} = \tan \frac{\theta}{2}, \tag{63}$$

and

$$\frac{dy}{ds} = \sin \theta. \tag{64}$$

By means of (63) and (64), (61) transforms to

$$(\overline{T}_0 + \bar{y}) \frac{d\bar{\Delta}}{d\bar{y}} \frac{d^2\bar{\Delta}}{d\bar{y}^2} + \frac{1}{4} \frac{(d\bar{\Delta})^4}{(d\bar{y})} + \Lambda \frac{(d\bar{\Delta})^2}{(d\bar{y})} - \frac{1}{4} = 0, \tag{65}$$

where we have in addition introduced the non-dimensional variables

$$\overline{T}_0 = T_0/wh,$$

$$\bar{\Delta} = \Delta/h,$$

$$\bar{y} = y/h.$$

Here h is the ocean depth at the touchdown point. Using the condition that $\theta = 0$ at $y = 0$, which implies $d\Delta/dy = 0$ at $y = 0$, we get upon integrating (65)

$$\frac{d\bar{\Delta}}{d\bar{y}} = \tan \frac{\alpha}{2} \left(\frac{1 - [\overline{T}_0/(\overline{T}_0 + \bar{y})]^\gamma}{1 + [\overline{T}_0/(\overline{T}_0 + \bar{y})]^\gamma \tan^4 \frac{\alpha}{2}} \right)^{1/2}, \tag{66}$$

where

$$\gamma = \frac{2 - \sin^2 \alpha}{\sin^2 \alpha}. \tag{67}$$

The usual range of the critical angle α is between 10 and 30 degrees. Also

$$0 \leqq \frac{\overline{T}_0}{\overline{T}_0 + \bar{y}} \leqq 1.$$

Therefore, we approximate the denominator of equation (67) by unity.

With the boundary condition that $\Delta = s - x = 0$ at $y = 0$, we thus obtain

$$\bar{\Delta}(1) = \bar{S} - \bar{X} = \tan \frac{\alpha}{2} \int_0^1 (1 - [\bar{T}_0/(\bar{T}_0 + \xi)]^\gamma)^{\frac{1}{2}} \, d\xi, \qquad (68)$$

where $\bar{S}$ and $\bar{X}$ are the dimensionless values of s and x at the ship.

Next we let

$$\omega = s + x, \qquad \bar{\omega} = \omega/h.$$

Then we have

$$\frac{d\bar{\omega}}{d\bar{y}} = 1 \bigg/ \frac{d\bar{\Delta}}{d\bar{y}},$$

and, as can be seen from (66) through (68),

$$\bar{\omega}(1) = \bar{S} + \bar{X} = \text{ctn} \frac{\alpha}{2} \int_0^1 (1 - [\bar{T}_0/(T_0 + \xi)]^\gamma)^{-\frac{1}{2}} \, d\xi. \qquad (69)$$

For convenience we define u and R by

$$u = \frac{\bar{T}_0}{\bar{T}_0 + \xi},$$

$$R = \frac{\bar{T}_0}{1 + \bar{T}_0}.$$

In terms of u and R (68) and (69) become

$$\bar{\Delta}(1) = \bar{T}_0 \tan \frac{\alpha}{2} \int_R^1 \frac{(1 - u^\gamma)^{\frac{1}{2}}}{u^2} \, du, \qquad (70)$$

$$\bar{\omega}(1) = \bar{T}_0 \, \text{ctn} \frac{\alpha}{2} \int_R^1 \frac{du}{u^2 (1 - u^\gamma)^{\frac{1}{2}}}. \qquad (71)$$

Further, integration by parts gives

$$\int_R^1 \frac{(1 - u^\gamma)^{\frac{1}{2}}}{u^2} \, du = \frac{(1 - R^\gamma)^{\frac{1}{2}}}{R} + \frac{\gamma}{2} \int_R^1 \frac{(1 - u^\gamma)^{\frac{1}{2}}}{u^2} \, du - \frac{\gamma}{2} \int_R^1 \frac{du}{u^2(1 - u^\gamma)^{\frac{1}{2}}}.$$

Combining the above three equations and making the approximation $(1 - R^\gamma)^{\frac{1}{2}} \approx 1$, we find

$$\left(1 - \frac{\gamma}{2}\right) \bar{\Delta}(1) + \frac{\gamma}{2} \tan^2 \frac{\alpha}{2} \, \bar{\omega}(1) = (1 + \bar{T}_0) \tan \frac{\alpha}{2}. \qquad (72)$$

Thus $\bar{\Delta}(1)$ and $\bar{\omega}(1)$ are related, and we need evaluate only one of the quantities numerically by means of equation (70) or (71) in order to compute both $\bar{\Delta}(1)$ and $\bar{\omega}(1)$, and hence $\bar{S}$ and $\bar{X}$.

The singularity at $u = 1$ makes the numerical evaluation of the integral in (71) cumbersome. Therefore we consider the evaluation of $\bar{\Delta}(1)$. But for convenience of numerical calculation we write (70) as

$$\bar{\Delta}(1) = -\overline{T}_0 \tan \frac{\alpha}{2} \int_R^1 (1 - u^\gamma)^{\frac{1}{2}} \, d\left(\frac{1 - u}{u}\right),$$

and integrate by parts to get

$$\bar{\Delta}(1) = \tan \frac{\alpha}{2} \left((1 - R^\gamma)^{\frac{1}{2}} - \frac{\gamma}{2} \overline{T}_0 \int_R^1 \frac{1 - u}{u^2} \frac{u^\gamma}{(1 - u^\gamma)^{\frac{1}{2}}} \, du\right).$$

We note again that $(1 - R^\gamma)^{\frac{1}{2}} \approx 1$. Further, essentially all of contribution to the integral in this equation occurs near $u = 1$ because of the large value of γ. On the other hand, the values of $\overline{T}_0$ which are of interest will normally be smaller than unity. Hence R, the lower limit, will normally be less than one-half, and thus will be outside of the region of significant contribution to the integral. Therefore, we can take the integral to be a constant for a given α. Denoting this integral by n and combining these considerations we obtain

$$\bar{\Delta}(1) = \tan \frac{\alpha}{2} - \frac{\gamma}{2} n \tan \frac{\alpha}{2} \overline{T}_0. \tag{73}$$

Finally solving for $\bar{S}$ and $\bar{X}$ from (68) and (69), we find

$$\bar{S} = \frac{1}{\sin \alpha} + \kappa \overline{T}_0,$$

$$\bar{X} = \frac{1}{\tan \alpha} + \lambda \overline{T}_0,$$

which are a dimensionless form of (24). For brevity we have written

$$\kappa = \frac{1}{2} \left(\frac{2}{\lambda} \left[1 - \frac{\gamma}{2} \left(\frac{\gamma}{2} - 1\right) n\right] \text{ctn} \frac{\alpha}{2} - \frac{\gamma}{2} n \tan \frac{\alpha}{2}\right),$$

$$\lambda = \frac{1}{2} \left(\frac{2}{\gamma} \left[1 - \frac{\gamma}{2} \left(\frac{\gamma}{2} - 1\right) n\right] \text{ctn} \frac{\alpha}{2} + \frac{\gamma}{2} n \tan \frac{\alpha}{2}\right).$$

Since the integral n and the constant γ depend only on α, the constants κ and λ are also functions of α only. We have evaluated n by numerical integration and have plotted the resulting values of κ and $\lambda - \kappa$ in Fig. 10.

c.2 *Recovery*

In the conventional recovery situation we have as boundary conditions

$$\theta = 0 \qquad \text{at} \quad y = 0,$$
$$\theta = -\alpha_s \quad \text{at} \quad y = h, \tag{74}$$

where α_s is the incidence angle of the cable at the ship (Fig. 8). With these boundary conditions, the development leading to (66) yields (26) for the relationship between shipboard tension $\overline{T}_s$ and the incidence angle α_s.

To evaluate S and X, the values of s and x at the ship, we use (19), (20a) and (20b). Again we simplify by assuming $D_T = \rho_c V_c^2 = 0$. Further, since for recovery $-\pi \leqq \theta \leqq 0$, we may write $|\sin \xi| = -\sin \xi$. This gives

$$\overline{S} = T_0 \int_0^{-\alpha_s} \left[\frac{1}{\cos \xi + \Lambda \sin^2 \xi} \exp \int_0^{\xi} \frac{\sin \eta}{\cos \eta + \Lambda \sin^2 \eta} \, d\eta \right] d\xi,$$

$$\overline{X} = T_0 \int_0^{-\alpha_s} \left[\frac{\cos \xi}{\cos \xi + \Lambda \sin^2 \xi} \exp \int_0^{\xi} \frac{\sin \eta}{\cos \eta + \Lambda \sin^2 \eta} \, d\eta \right] d\xi. \tag{75}$$

The dimensionless bottom tension $\overline{T}_0$ is computed from (26). The integrals appearing in (75) have been evaluated numerically. The results are shown in Figs. 14 and 15.

APPENDIX D

Analysis of the Effect of Ship Motion

D.1 *Formulation of the Differential Equations*

To analyze the effect of ship motion on cable tensions, we use the model shown in Fig. 32. We assume the cable is a perfectly flexible and elastic string whose motion is planar. The distance L along the cable from the ship to the point of entry into the water is taken as constant, and the longitudinal damping as negligible.
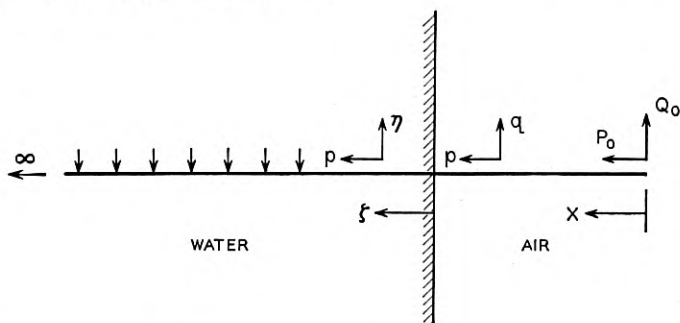
Fig. 32 — Model used for the analysis of ship motion tensions.

Unlike the solution of the basic stationary model, the complete solution of this model is not simple. To make the problem tractable, we shall make further simplifying assumptions. Although these assumptions may seem reasonable, they must be ultimately justified by comparison of experience with predicted results.

Force diagrams of a differential element of cable are shown in Figs. 33(a) and (b) for the two regions, air and water respectively. The notation is

p = longitudinal displacement of a point of the cable,

q = transverse displacement of a point of the cable (in air),

η = transverse displacement of a point of the cable (in water),

θ = the stationary angle, i.e. the angle the cable configuration makes with the ship velocity in the absence of ship motion,

φ = deviation from the stationary angle – positive in the clockwise direction,

s = distance along the stretched cable,

x = distance along the unstretched cable (in air),

ζ = distance along the unstretched cable (in water),

w_a = weight per unit length of cable in air.

Fig. 33 — Diagram of forces acting on a cable element in air and in water.

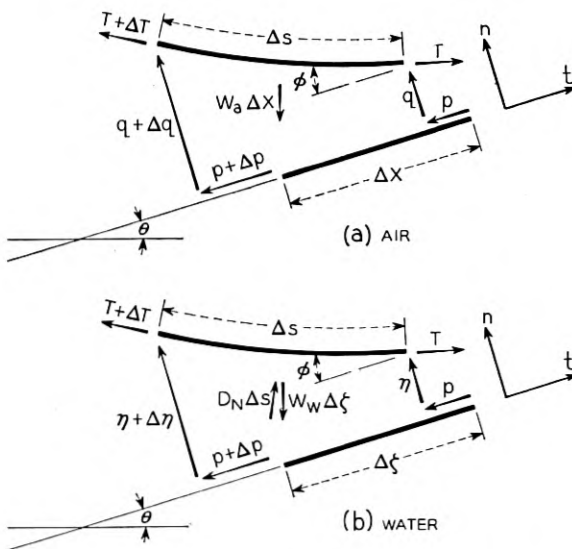Summing forces along the directions t (tangential) and n (normal) shown in Fig. 33, dividing by Δx (air) or $\Delta \zeta$ (water) and letting $\Delta x \to 0$ and $\Delta \zeta \to 0$, we obtain the following equations of equilibrium*

Air:

$$T\varphi_x - w_a \cos (\theta - \varphi) = \rho_c(q_{tt} \cos \varphi - p_{tt} \sin \varphi),$$

$$T_x + w_a \sin (\theta - \varphi) = \rho_c(q_{tt} \sin \varphi + p_{tt} \cos \varphi),$$

(76)

Water:

$$T\varphi_\zeta + D_N s_\zeta - w \cos (\theta - \varphi) = \rho_w(q_{tt} \cos \varphi - p_{tt} \sin \varphi),$$

$$T_\zeta + w \sin (\theta - \varphi) = \rho_c(q_{tt} \sin \varphi + q_{tt} \cos \varphi).$$

(77)

Here, ρ_c denotes the mass per unit length of the cable in air. As is known from hydrodynamic theory, in order to accelerate a body through a fluid, one must change not only the momentum of the body but that of some of the surrounding fluid as well. Thus the body has a virtual or apparent mass in addition to its intrinsic mass. In the first (77), the equation of equilibrium in the normal direction in water, we accordingly use ρ_w, given by

$$\rho_w = \rho_c + \frac{\pi}{4} d^2 \rho$$

as the intrinsic plus virtual mass per unit length of cable moving through water. The quantities d and ρ are the outer diameter of the cable and mass density of the water, respectively, and the quantity $(\pi/4)d^2\rho$ is the virtual mass of a unit length circular cylinder moving transversely through water.

We take for the normal drag force per unit length

$$D_N = \frac{C_D \rho d}{2} V_N \mid V_N \mid.$$

(78)

Here V_N is the normal component of velocity of the water relative to the cable, i.e.,

$$V_N = V \sin (\theta - \varphi) + u_t \sin \varphi - \eta_t \cos \varphi,$$

(79)

and $C_D \rho d/2$ is a constant.

The quantities s and φ are given by the following geometric relations which can be obtained from Fig. 33:

---

* We use the subscript notation for differentiation throughout this section, e.g., $\varphi_x = \partial \varphi/\partial x$.

$$s_\zeta = [(1 + p_\zeta)^2 + \eta_\zeta^2]^{\frac{1}{2}}, \tag{80}$$

$$\tan \varphi = \eta_\zeta / (1 + \eta_\zeta), \tag{81}$$

with similar expressions obtaining for the cable in air.

The tension T in turn is given by the Hooke's Law or stress-strain relation

$$
\begin{aligned}
T &= \overline{EA}\{[(1 + p_x)^2 + q_x^2]^{\frac{1}{2}} - 1\}, \quad \text{(air)} \\
T &= \overline{EA}\{[(1 + p_\zeta)^2 + \eta_\zeta^2]^{\frac{1}{2}} - 1\}. \quad \text{(water)}
\end{aligned}
\tag{82}
$$

As we indicated in Section 4.1, we shall assume that the extensile rigidities $\overline{EA}$ corresponding to complete restraint and no restraint to twisting will give the limiting values of the ship motion tension.

Equations (76) through (82) form a complete system in terms of the independent variables x or ζ and t. Formulating boundary conditions in terms of the coordinate x (or ζ) is awkward. This coordinate is measured along the unstretched cable so that a disturbance applied at the ship is applied at different x's as the cable is paid out. At the same time, if the velocity of the pay-out is small compared to the significant wave velocity of the cable then we can plausibly neglect the paying out effect. As will be shown subsequently, in the problem at hand there are two significant wave velocities, roughly corresponding to transverse and longitudinal motion. The first of these is of the order of 200 ft/sec, while the second is of the order of 5,000–10,000 ft/sec. On the other hand, the pay-out velocity is of the order of 10 ft/sec. Hence, we take the pay-out velocity to be zero. This allows us to use (76) through (82) without further transformations and to identify x and ζ as coordinates fixed in the translating reference frame.

D.2 *Perturbation Equations*

We assume that the motion is a small perturbation about the undisturbed configuration of our model. To determine which terms of the differential equations are important in this case, we adopt the following procedure. Let

$$M = \max[(P_0 + P_1)^2 + Q_0^2]^{\frac{1}{2}},$$

where P_0 and Q_0 are displacements of the cable at the ship, and P_1 is the variation of the pay-out displacement from the mean. The quantity $e = M/L$ will normally be less than unity, and for no ship motion will be

zero. We write

$$P_0 + P_1 = af(t),$$

$$Q_0 = bg(t),$$

where $f(t)$, $g(t)$ are some bounded functions of time and a and b are constants. We assume that for given $f(t)$ and $g(t)$, T, p, and q vary analytically with e, namely

$$
\begin{aligned}
T &= T_0 + eT_1 + e^2T_2 + \cdots, \\
q &= eq_1 + e^2q_2 + \cdots, \\
p &= p_0 + ep_1 + e^2p_2 + \cdots,
\end{aligned}
\qquad (83)
$$

with counterparts for the submerged cable. The stationary transverse deflection is further assumed zero, and therefore the series for q contains no q_0 term. Substituting, for example, (83) into (82) for air and equating like powers of e, we find

$$
\begin{aligned}
T_0 &= \overline{EA}\,p_{0x}, & \text{(a)} \\
T_1 &= \overline{EA}\,p_{1x}, & \text{(b)} \\
T_2 &= \overline{EA}\left[p_{2x} + \frac{q_{1x}^2}{1 + p_{0x}} \right]. & \text{(c)}
\end{aligned}
\qquad (84)
$$

Equation (84a) of this sequence shows that only longitudinal displacements are associated with stationary tensions, while (84b) indicates that for small ship motions cable tensions are independent of the transverse component of ship motion. To compute the effect of transverse motion, (84c) shows that terms of the order e^2 in p and e in q must be considered. We assume further that $1 + p_{0x} \approx 1$, since p_{0x} is the order of magnitude of a strain.

Equations (83) and (84) substituted into (76) yield with this approximation

$$
\begin{aligned}
w_a \cos \alpha &= 0, & \text{(a)} \\
\overline{EA}\,p_{0xx} - \rho_a\,p_{0tt} + w_a \sin \alpha &= 0, & \text{(b)}
\end{aligned}
\qquad (85)
$$

$$
\begin{aligned}
q_{1xx} - \frac{1}{c_2^2}\, q_{1tt} &= 0, & \text{(a)} \\[2mm]
p_{1xx} - \frac{1}{c_1^2}\, p_{1tt} &= 0, & \text{(b)} \\[2mm]
p_{2xx} - \frac{1}{c_1^2}\, p_{2tt} &= \frac{1}{c_1^2}\, q_{1tt}q_{1xx} - q_{1x}q_{1xx}, & \text{(c)}
\end{aligned}
\qquad (86)
$$

where

$$c_1^2 = \overline{EA}/\rho_a ,$$

$$c_2^2 = T_0/\rho_a .$$

For non-zero w_a and $\alpha \neq \pi/2$, (85a) cannot be satisfied. This is a consequence of the assumption of $q_0 = 0$. With $p_{0tt} = 0$, equation (b) implies in turn that $T_0 = $ constant, which agrees with our model. For the submerged part of the cable, the equations do not yield a constant T_0 and thus contradict the assumed model. However, on the assumption that the transverse motion is confined to a region near the surface, we consider T_0 to be constant in the submerged part of the cable as well. We thus arrive at

$$\eta_{1\zeta\zeta} - \delta\eta_{1\zeta} - \gamma\eta_{1t} - \frac{1}{\bar{c}_2^2}\,\eta_{1tt} = 0 \qquad\qquad \text{(a)}$$

$$p_{1\zeta\zeta} - \frac{1}{c_1^2}\,p_{1tt} = 0, \qquad\qquad \text{(b)} \quad \text{(87)}$$

$$p_{2\zeta\zeta} - \frac{1}{c_1^2}\,p_{2tt} = \frac{1}{c_1^2}\,\eta_{1tt}\eta_{1\zeta} - \eta_{1\zeta}\eta_{1\zeta\zeta}, \quad \text{(c)}$$

where

$$\bar{c}_2^2 = T_0/\rho_w ,$$

$$\delta = \frac{C_D\rho\,dV^2}{T_0}\cos\alpha\,\sin\alpha,$$

$$\gamma = \frac{C_D\rho\,dV^2}{T_0}\sin\alpha,$$

as the differential equations governing the motion of the submerged cable. The constant c_1 is the velocity of propagation of a longitudinal wave in the cable, while the constants c_2 and $\bar{c}_2$ represent the propagation velocities of a transverse wave in air and water respectively.

D.3 *Solution of the Perturbation Equations*

We write

$$p(0, t) = P_0(t) + P_1(t),$$

$$q(0, t) = Q_0(t),$$

and take as boundary conditions

$$p_1(0, t) = \frac{P_0(t) + P_1(t)}{e}, \quad \text{(a)}$$

$$p_2(0, t) = 0, \quad \text{(b)} \qquad (88)$$

$$q_1(0, t) = Q_0/e. \quad \text{(c)}$$

That is, we apportion all of the longitudinal boundary motion to p_1, and all of the transverse boundary motion to q_1. Equations [(84b), (86b) and (87b)] then give the complete tension due to the longitudinal component of ship motion to first order. As mentioned in the text, this tension is easily obtained from standard references, and is also the greater part of the ship motion tension.

To determine the tensions due to transverse ship motion, we solve (86c) and (87c) for boundary conditions (88b) and (88c). In addition, we have the transition conditions

$$q_1(L, t) = \eta_1(0, t), \quad \text{(a)}$$

$$q_{1x}(L, t) = \eta_{1\zeta}(0, t), \quad \text{(b)} \quad (89)$$

$$p_2(x = L, t) = p_2(\zeta = 0, t), \quad \text{(c)}$$

$$p_{2x}(L, t) = p_{2\zeta}(0, t), \quad \text{(d)}$$

which follow if we assume that at the point of entry into the water the cable is continuous and the tensions are finite and continuous.

We consider only the problem of the tensions associated with a harmonic steady-state transverse disturbance. Equations (86a) and (87a) show the transverse response to this disturbance to be independent of the longitudinal motion to first order. The first-order transverse motion in turn can be thought of as a forcing action on the second order longitudinal motion, as (86c) and (87c) indicate. This suggests the program we follow to compute tensions. Namely, we first determine the first-order steady-state transverse response, then the second-order steady-state longitudinal response which is excited by the first-order transverse oscillation, and finally, by (84c) the resulting tension caused by transverse motion.

D.4 *Transverse Response*

At the ship we assume a harmonic forcing function

$$Q_0(t) = A \cos \omega t, \qquad (90)$$

and we introduce complex exponential representation

$$q_1 = \mathrm{Re}\ Q_1(x)\ e^{i\omega t},$$

$$\eta_1 = \mathrm{Re}\ H_1(\zeta)\ e^{i\omega t},$$

where the factor $e^{i\omega t}$ will be henceforth suppressed.

The solution of (86a) and (87a) for the steady state may then be written

$$Q_1(x) = B_1 \exp \frac{i\omega x}{c_2} + B_2 \exp \left(- \frac{i\omega x}{c_2}\right),$$

$$H_1(\zeta) = F_1 \exp (q_1\zeta) + F_2 \exp (q_2\zeta),$$

where the B's and F's are complex constants and q_1 and q_2 are the roots of the quadratic

$$q^2 - \delta q - i\omega\gamma + \frac{\omega^2}{\bar{c}_2^2} = 0.$$

Throwing away the root of this equation which corresponds to the incoming wave in water, we get

$$H_1(\zeta) = F \exp (q_1\zeta).$$

where q_1 is the root corresponding to the outgoing wave. The three complex constants B_1, B_2, and F can now be determined from (89a), (89b) and (90)

$$B_1 + B_2 = A/e,$$

$$B_1 \exp \frac{i\omega L}{c_2} + B_2 \exp \left(- \frac{i\omega L}{c_2}\right) - F = 0, \tag{91}$$

$$\frac{i\omega}{c_2} \left[B_1 \exp \frac{i\omega L}{c_2} - B_2 \exp \left(- \frac{i\omega L}{c_2}\right) \right] - q_1 F = 0.$$

We note that B_1, B_2 and F are proportional to the amplitude A of the forcing motion.

D.5 *Second-Order Longitudinal Response*

From the preceding results, the right-hand sides of the equations of longitudinal motion (86c) and (87c) can be computed. This computation for (86c) results in

$$\frac{1}{c_1^2} v_{1tt}v_{1x} - v_{1xx}v_{1x} = \frac{1}{2}\left(\frac{c_2^2}{c_1^2} - 1\right)\left(\frac{\omega}{c_2}\right)^3$$

$$\times \left[\left(r_1 \sin \frac{2\omega x}{c_2} + r_2 \cos \frac{2\omega x}{c_2}\right) \cos 2\omega t\right.$$

$$+ \left(r_3 \cos \frac{2\omega x}{c_2} - r_4 \sin \frac{2\omega x}{c_2}\right) \sin 2\omega t$$

$$\left. + r_5 \sin \frac{2\omega x}{c_2} + r_2 \cos \frac{2\omega x}{c_2}\right], \tag{92}$$

where the r's, which are proportional to the square of the amplitude A, are

$$r_1 = \text{Re } (B_1^2 + B_2^2),$$

$$r_2 = \text{Im } (B_1^2 - B_2^2),$$

$$r_3 = \text{Re } (B_1^2 - B_2^2),$$

$$r_4 = \text{Im } (B_1^2 + B_2^2),$$

$$r_5 = 2\text{Re } B_1 \bar{B}_2,$$

$$r_6 = r_5 + \frac{e^2 r_2^2}{A^2}.$$

[The quantity r_6 will be used subsequently.] Similarly, for the right-hand side of (87c) we get

$$\eta_{1\zeta}\left(\frac{1}{c_1^2} \eta_{1tt} - \eta_{1\zeta\zeta}\right) = e^{-2\rho\zeta}[(a_1 \cos 2\sigma\zeta + a_2 \sin 2\sigma\zeta) \cos 2\omega t \tag{93}$$

$$+ (a_1 \sin 2\sigma\zeta - a_2 \cos 2\sigma\zeta) \sin 2\omega t + a_3],$$

where

$$q_1 = -(\rho + i\sigma),$$

$$a_1 = \frac{|F|^2}{2} |q_1| \left[\left(\frac{\omega}{c_1}\right)^2 \cos (2f + g) + |q_1|^2 \cos (2f + 3g)\right],$$

$$a_2 = \frac{|F|^2}{2} |q_1| \left[\left(\frac{\omega}{c_1}\right)^2 \sin (2f + g) + |q_1|^2 \sin (2f + 3g)\right],$$

$$a_3 = |F| \left[\left(\frac{\omega}{c_1}\right)^2 + |q_1|^2\right] \rho,$$

and

$$f = \arg F, \qquad 0 \leqq f \leqq 2\pi,$$

$$g = \arg(-q_1), \qquad 0 \leqq g \leqq \frac{\pi}{2}.$$

It is seen that expression (92) and (93) have terms of the form

$$F(x)\begin{cases} \sin 2\omega t \\ \cos 2\omega t \end{cases} \qquad (94)$$

in addition to functions of x (or ζ) alone. In accordance with the idea that the first order transverse motion is a forcing action on the second order longitudinal motion, we take as solutions of (86c) and (87c) functions of the form

$$G(x)\begin{cases} \sin 2\omega t \\ \cos 2\omega t \end{cases}$$

to correspond to terms of the type given by (94) and functions of x (or ζ) alone to correspond to forcing terms which are independent of time. This again gives linear differential equations which can be readily solved. For example, corresponding to the first term in (92) multiplying $\cos 2\omega t$ we have the assumed solution

$$G(x) \cos 2\omega t,$$

and the differential equation

$$\frac{d^2 G}{dx^2} + \frac{4\omega^2}{c_1^2} G = \frac{1}{2}\left[\left(\frac{c_2}{c_1}\right)^2 - 1\right]\left(\frac{\omega}{c_2}\right)^3\left[r_1 \sin \frac{2\omega x}{c_2} + r_2 \cos \frac{2\omega x}{c_2}\right].$$

This has the solution

$$G = \left[A_1 \cos \frac{\omega x}{c_1} + A_2 \sin \frac{\omega x}{c_1} + \frac{\omega}{8c_2}\left(r_1 \sin \frac{2\omega x}{c_2} + r_2 \cos \frac{2\omega x}{c_2}\right)\right],$$

where A_1 and A_2 are undetermined constants.

In this manner, the solution for the longitudinal motion can be obtained in terms of a set of constants. These in turn can be evaluated by means of the boundary and transition conditions on p_2. This evaluation, although straightforward, is very tedious. We shall omit the details of it here. The final result is

Air:

$$e^2 T_2 = \frac{e^2 \omega^2 \overline{EA}}{4 c_1 c_2} \left\{ \left[r_2 \sin \frac{2\omega x}{c_1} + \left(r_3 + \frac{c_1}{c_2} r_4 \sin \frac{2\omega L}{c_1} \right. \right. \right.$$

$$\left. \left. - \frac{c_1}{c_2} r_6 \cos \frac{2\omega L}{c_1} \right) \cos \frac{2\omega x}{c_1} + \frac{c_1}{c_2} r_6 \right] \cos 2\omega t + \left[r_3 \sin \frac{2\omega L}{c_1} \right.$$

$$\left. - \left(r_2 + \frac{c_1}{c_2} r_4 \cos \frac{2\omega L}{c_1} + \frac{c_1}{c_2} r_6 \sin \frac{2\omega L}{c_1} \right) \cos \frac{2\omega x}{c_1} + \frac{c_1}{c_2} r_4 \right] \sin 2\omega t$$

$$\left. + \frac{c_2}{c_1} \left[r_5 \left(\cos \frac{2\omega x}{c_2} - \cos \frac{2\omega L}{c_2} \right) - r_2 \left(\sin \frac{2\omega x}{c_2} - \sin \frac{2\omega L}{c_2} \right) - \frac{|F|^2}{4} \right] \right\},$$

Water:

$$e^2 T_2 = \frac{e^2 \omega^2 \overline{EA}}{4 c_1 c_2} \left\{ \left[- r_2 \cos \frac{2\omega L}{c_1} + r_3 \sin \frac{2\omega L}{c_1} \right. \right.$$

$$\left. + \frac{c_1}{c_2} \sin \frac{2\omega L}{c_1} \left(r_4 \sin \frac{2\omega L}{c_1} - r_6 \cos \frac{2\omega L}{c_1} \right) \right] \sin 2\omega \left(t - \frac{\zeta}{c_1} \right)$$

$$+ \left[r_2 \sin \frac{2\omega L}{c_1} + r_3 \cos \frac{2\omega L}{c_1} + \frac{c_1}{c_2} \sin \frac{2\omega L}{c_1} \left(r_6 \sin \frac{2\omega L}{c_1} \right. \right.$$

$$\left. \left. + r_4 \cos \frac{2\omega L}{c_1} \right) \right] \cos 2\omega \left(t - \frac{\zeta}{c_1} \right) - |F|^2 \frac{c_2}{c_1} e^{-2\rho\zeta} \right\}.$$

D.6 *Numerical Results*

Since the r's are each proportional to the square of the amplitude A, the above results indicate that the transverse motion tension varies as A squared also. It is additionally a function of the frequency of ship motion ω, the forward mean ship velocity V, and the stationary tension T_0. The computation of the transverse ship motion tension for the laying situation was carried out for cable No. 2. The results are shown in Fig. 34. Here we have denoted the transverse motion tension by T_q and have plotted T_q/A^2 against the period of ship motion τ. Rather than the stationary tension T_0, we have used the depth h, which during laying is directly related to T_0 by $h = T_0/w$. Fig. 34(a) is a plot of T_q/A^2 versus the period $\tau = 2\pi/\omega$ for $h = \frac{1}{2}$, 2 and 3 nautical miles and for $V = 6$ knots. Figure 34(b) is a plot of T_q/A^2 versus τ for $V = 3$, 6, and 9 knots and $h = $ one nautical mile.

For representative laying, for example at 6 knots with a ship period of 6 seconds into a depth of one nautical mile, Fig. 34 gives

$$T_q/A^2 = 0.50 \text{ lb/ft}^2 \text{ (twist unrestrained)},$$

$$T_q/A^2 = 0.93 \text{ lb/ft}^2 \text{ (twist restrained)}.$$

For an extreme value of $A = 20$ feet, we get therefore that T_q is between 200 and 370 pounds.

Additionally, by means of the above analysis, one can compute the rate of damping of a transverse disturbance after it enters the water. The results of this computation are shown in Fig. 18 and are discussed in Section 4.1.
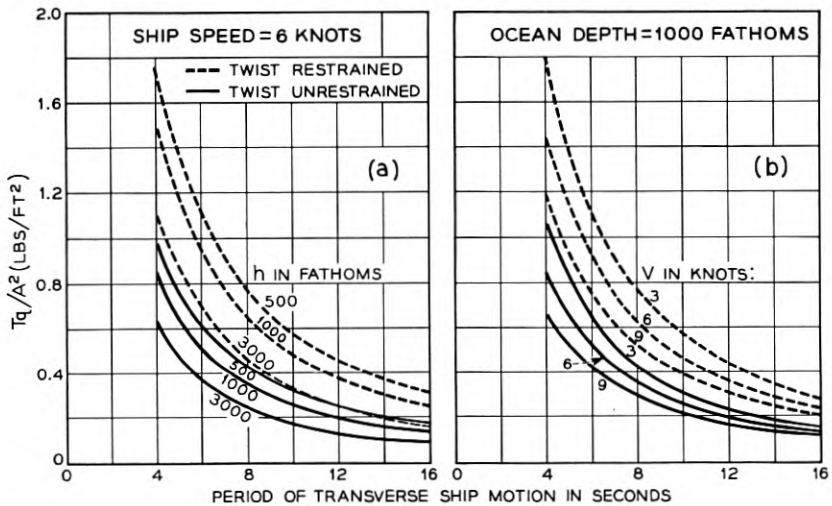
Fig. 34 — Variation of the transverse ship motion tension of cable No. 2 with the period of ship motion.

APPENDIX E

Tension Rise with Time for Suspended Cable

E.1 *Formulation of the Solution of the Problem*

Let O be the lowest point of the cable at time t after the suspension has begun (Fig. 35). We make the following definitions:

$$h = \text{depth at onset of the suspension,}$$

$$S_1 = \text{cable length from } A \text{ to } 0,$$

$$S_2 = \text{cable length from ship at } B \text{ to } 0,$$

$$X_1 = \text{horizontal distance from } A \text{ to } 0,$$

X_2 = horizontal distance from B to 0,

δ = vertical distance from A to 0,

T_0 = cable tension at 0.

If the cable is being paid out with a slack ϵ, then conservation of the total cable length gives the equation

$$S_1 + S_2 = \frac{h}{\sin \alpha} + (1 + \epsilon)Vt + \text{cable stretching.} \qquad (95)$$
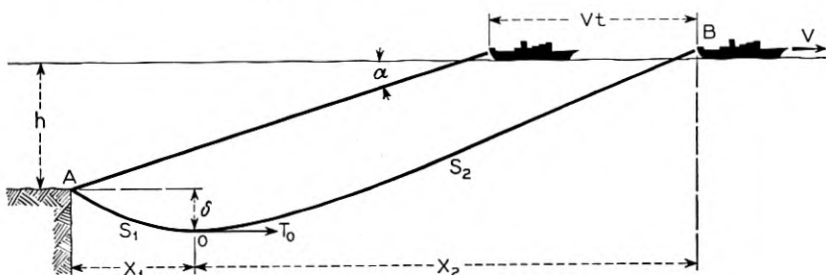
Fig. 35 — Coordinates for the analysis of tension rise when a cable is completely suspended.

It is assumed that there is no cable pulled from the bottom. The cable stretching we evaluate as in the example of Section 3.6, viz.,

$$\text{cable stretching} = (S_1 + S_2) \frac{T_0}{EA}.$$

This makes (95) read

$$S_1 + S_2 = \frac{h}{\sin \alpha} + (1 + \epsilon)Vt + (S_1 + S_2) \frac{T_0}{EA}. \qquad (96)$$

To obtain further relations for the unknowns appearing in (96), we assume that from the ship to point 0 the cable configuration is a stationary one governed by the equations developed in Section 3.6, while from points 0 to A we assume that the cable configuration is a static catenary. These assumptions yield the following relations:

$$S_1 = \frac{T_0}{w} \sinh \sigma, \qquad (a)$$

$$S_2 = \frac{h + \delta}{\sin \alpha} + \kappa \frac{T_0}{w}, \qquad (b)$$

$$X_2 = \frac{h + \delta}{\tan \alpha} + \lambda \frac{T_0}{w}, \qquad \text{(c)}$$

$$\delta = \frac{T_0}{w} (\cosh \sigma - 1), \qquad \text{(d)} \quad (97)$$

$$X_2 + X_1 = \frac{h}{\tan \alpha} + Vt, \qquad \text{(e)}$$

$$\sigma = \frac{wX_1}{T_0}, \qquad \text{(f)}$$

$$T_s = T_0 + w(h + \delta). \qquad \text{(g)}$$

Here κ and λ are constants, defined and plotted in Section 3.6, which depend only on α, the critical angle corresponding to V. Equations (96) and (97) form a complete set of equations in the unknowns X_1, X_2, S_1, S_2, T_0, T_s, δ, and σ. They can be reduced to a set which contain only the unknowns σ and T_s:

$$\varphi_1(\sigma) \sin \alpha - \epsilon \varphi_2(\sigma) \sin \alpha - \bar{h}\left(1 + \frac{\varphi_3(\sigma)}{\varphi_2(\sigma)} \bar{t} \sin \alpha\right) = 0, \quad \text{(a)}$$

$$\bar{T}_s = 1 + \frac{\bar{t} \cosh \sigma}{\varphi_2(\sigma)}, \qquad \text{(b)} \quad (98)$$

where

$$\bar{h} = wh/EA,$$

$$\bar{t} = Vt/h,$$

$$\bar{T}_s = T_s/wh,$$

and

$$\varphi_1 = \sinh \sigma - \sigma + (\cosh \sigma - 1) \tan \frac{\alpha}{2} - (\lambda - \kappa),$$

$$\varphi_2 = \frac{\cosh \sigma - 1}{\tan \alpha} + \lambda + \sigma,$$

$$\varphi_3 = \frac{\cosh \sigma - 1}{\sin \alpha} + \sinh \sigma.$$

A graphical iteration method will be used to solve (98). First we solve

$$\varphi_1(\sigma) \sin \alpha - \epsilon \varphi_2(\sigma) \sin \alpha - \bar{h} = 0 \qquad (99)$$

for σ by means of a nomograph to be described later. Next the quantities

$$\frac{\cosh \sigma}{\varphi_2(\sigma)}, \qquad \frac{\varphi_3(\sigma)}{\varphi_2(\sigma)} \sin \alpha,$$

are plotted as functions of σ for various α. These plots can then be used as follows to solve (98) for a given $\bar{t}$. Solve (99) to obtain σ_0. From the plot of $\varphi_3(\sigma)/\varphi_2(\sigma) \sin \alpha$ compute

$$\bar{h}_1{}^* = \bar{h}\left(1 + \frac{\varphi_3(\sigma_0)}{\varphi_2(\sigma_0)} \bar{t} \sin \alpha\right).$$

Using the value $\bar{h}_1{}^*$ for $\bar{h}$, compute σ_1 from (99). With this value of σ_1, compute $h_2{}^*$ from

$$\bar{h}_2{}^* = \bar{h}\left(1 + \frac{\varphi_3(\sigma_1)}{\varphi_2(\sigma_1)} \bar{t} \sin \alpha\right),$$

etc. In this way a convergent sequence $\sigma_0, \sigma_1, \cdots, \sigma_n$ is generated. Finally, from the plot of $\cosh \sigma/\varphi_2(\sigma)$ obtain $\bar{T}_s$.

The above iteration procedure sounds tedious. Actually, in most cases the iteration is not necessary because σ remains essentially independent of time. Thus, the solution of (99) by means of the accompanying nomograph will usually give the complete solution of the problem.

E.2 *Nomograph (Alignment Chart) for the Solution of Equation* (99)

The relations

$$x_1 = 0, \qquad x_2 = d, \qquad x_3 = \frac{10\varphi_2(\sigma)\, d \sin \alpha}{1 + 10\varphi_2(\sigma) \sin \alpha},$$

$$y_1 = \bar{h}, \qquad y_2 = \frac{\epsilon}{10}, \qquad y_3 = \frac{\varphi_1(\sigma) \sin \alpha}{1 + 10\varphi_2(\sigma) \sin \alpha}, \tag{100}$$

where d is an arbitrary constant define parametrically three curves

$$y_i = y_i(x_i), \qquad i = 1, 2, 3,$$

which we imagine plotted on a cartesian (x, y) coordinate system. A set of values $\bar{h}$, ϵ, and σ determine three points (x_i, y_i) $(i = 1, 2, 3)$ which lie on these curves. If these points lie on a straight line, it can be shown that they satisfy (99).

On the left-hand sides of Fig. 36 we have plotted the curves given by (100) for various values of the critical angle α. The values of the parameters $\bar{h} = wh/\overline{EA}$ and ϵ, which describe the curves $y_1 = y_1(x_1)$ and $y_2 = y_2(x_2)$ respectively, are plotted on the indicated scales. Rather than indicate the values of σ along the curve $y_3 = y_3(x_2)$ we have for con-
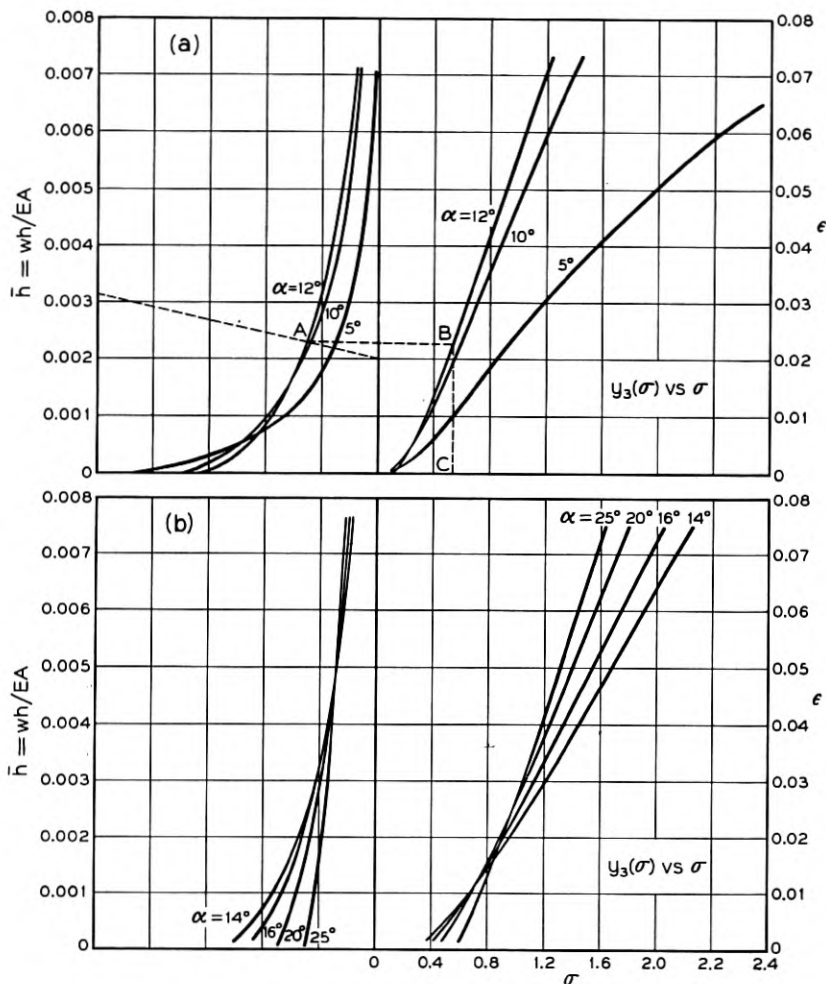
Fig. 36 — Nomograph for the solution of equation (99).

venience made an auxiliary plot on the right-hand sides of Fig. 36 of $y_3(\sigma)$ versus σ, but with numerical values of the ordinate omitted.

In addition, we have plotted in Figs. 37 and 38 the functions $1/\varphi_2$ (cosh σ) and (φ_3/φ_2) sin α for various α.

E.3 *Numerical Example*

To illustrate the method of obtaining the tension rise with time described above, we consider a numerical example for cable No. 2. The
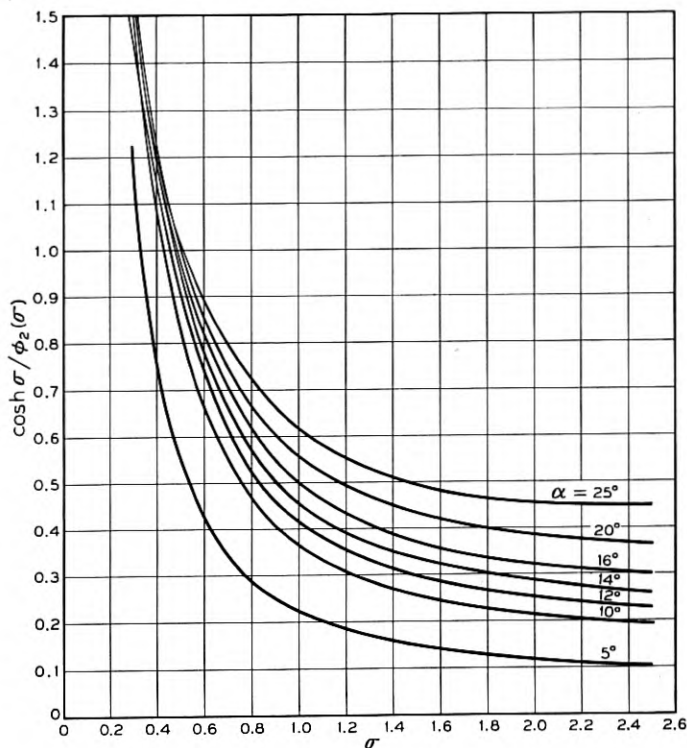
Fig. 37 — Variation of $\dfrac{\cosh \sigma}{\phi_2(\sigma)}$ with σ.

values we assume for the parameters which enter the calculation are the following:

$$\epsilon = 0.02,$$

$$V = 6 \text{ knots, } (\alpha \approx 12°),$$

$$h = 6{,}000 \text{ ft,}$$

$$\overline{EA} = 1.2 \times 10^6 \text{ lbs,}$$

$$\bar{h} = 3.1 \times 10^{-3}.$$

To solve (99), we connect on Fig. 36 the points $\epsilon = 0.02$ and $\bar{h} = wh/\overline{EA} = 0.0031$ with a straight edge and note the intersection with the intermediate $y_3 = y_3(x_3)$ curve for $\alpha = 12°$ (point A). We then locate the point on the y_3 versus σ curve having the same ordinate (point B).

Finally, we obtain the root of (99), $\sigma = 0.555$ by reading off the corresponding abscissa (point C). This value of σ now serves as the starting point in the iteration procedure by which we find the tension corresponding to a given t.

For example, for $\bar{t} = 1.0$ ($t = 600$ seconds) we have the following sequence of values

σ	$(\varphi_3 \sin \alpha)/\varphi_1$	$\bar{h}^* = \bar{h}\,[1 + (\varphi_3 \sin \alpha)\,\bar{t}/\varphi_2]$
$\sigma_0 = 0.555$	0.212	0.00379
$\sigma_1 = 0.580$	0.213	0.00380
$\sigma_2 = 0.580$		

with σ converging to the value 0.580. For $\sigma = 0.580$, Fig. 37 gives

$$\cosh \sigma/\varphi_2 = 0.800.$$

Hence, by (98b) for $\bar{t} = 1.0$

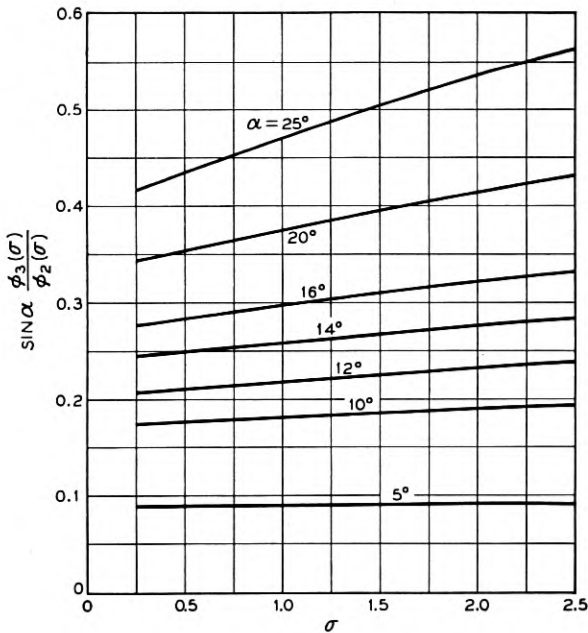$$\overline{T}_s = 1.80,$$

and $T_s = 1.80$ wh or 7,600 pounds.

Fig. 38 — Variation of $\sin \alpha \dfrac{\phi_3(\sigma)}{\phi_2(\sigma)}$ with σ.

APPENDIX F

The Three-Dimensional Stationary Model

F.1 *Derivation of the Differential Equations*

Let $\vec{i}, \vec{j}, \vec{k}$ be unit vectors along the ξ, η, ζ axes (Fig. 26) and $\vec{t}$ a unit vector along the tangent to the cable configuration in the direction of positive s. As in the two-dimensional model, we take this to be opposite to the direction of travel of the cable elements along the configuration. With respect to the cable configuration the resultant velocity vector of the water is in the $-\vec{i}$ direction. We resolve this velocity into directions normal and tangential to the cable in the plane formed by $\vec{i}$ and $\vec{t}$. The unit vector in the normal direction we denote by $\vec{n}$, namely,

$$n = \frac{-i + (i \cdot \vec{t})\vec{t}}{|-\vec{i} + (\vec{i} \cdot \vec{t})\vec{t}|}. \tag{101}$$

In analogy to the two-dimensional model we assume the normal and tangential drag forces depend only on the corresponding water velocity components. Thus, we take

$$D_N = \frac{C_D \rho d}{2} (\vec{i} \cdot \vec{n} V)^2. \tag{102}$$

Equilibrium of the forces acting on a cable element yields the equation

$$T \frac{d\vec{t}}{ds} + \vec{t} \frac{dT}{ds} + \vec{t} D_T + \vec{n} D_N - \vec{j} w = \rho_c \vec{a}. \tag{103}$$

The vector a denotes the acceleration of an element of the cable as it moves at the constant pay-out velocity V_c along the cable configuration. It is easily shown that

$$\vec{a} = V_c^2 \frac{d\vec{t}}{ds}. \tag{104}$$

For convenience we introduce a second reference triad of orthogonal unit vectors $\vec{t}, \vec{u},$ and $\vec{v}$ as follows. The $\vec{v}$ vector is taken in the (ξ, ζ) plane normal to $\vec{t}$; the $\vec{u}$ vector is chosen equal to the vector product $\vec{v} \times \vec{t}$. The angles ψ and θ shown in Fig. 27 describe the orientation of the $(\vec{t}, \vec{u}, \vec{v})$ triad. In terms of these angles, we read from Fig. 27 the following table of direction cosines

	$\vec{i}$	$\vec{j}$	$\vec{k}$
$\vec{t}$	$\cos\theta \cos\psi$	$\sin\theta$	$-\cos\theta \sin\psi$
$\vec{u}$	$-\sin\theta \cos\psi$	$\cos\theta$	$\sin\theta \sin\psi$
$\vec{v}$	$\sin\psi$	0	$\cos\psi$

In the $(\vec{t}, \vec{u}, \vec{v})$ system the vector $\vec{n}$ becomes for example

$$\vec{n} = \frac{\vec{u} \sin \theta \cos \psi - \vec{v} \sin \psi}{[\sin^2 \theta \cos^2 \psi + \sin^2 \psi]^{\frac{1}{2}}}.$$

Imagine the origin of the $(\vec{t}, \vec{u}, \vec{v})$ triad to traverse the cable at unit velocity. The triad during this traverse rotates like a rigid body with respect to the fixed (ξ, η, ζ) frame. The rotation, which we denote by $\vec{\Omega}$, is seen from Fig. 27 to be

$$\vec{\Omega} = \vec{j}\,\dot{\psi} + \vec{v}\,\dot{\theta} = \vec{u} \cos \theta\,\dot{\psi} + \vec{v}\,\dot{\theta} + \vec{t} \sin \theta\,\dot{\psi}.$$

Here the dot denotes differentiation with respect to time, or since $ds/dt = 1$ it may be interpreted as differentiation with respect to distance along the cable. The vector $\vec{t}$ is a fixed vector of constant magnitude in the rotating $(\vec{t}, \vec{u}, \vec{v})$ triad, hence

$$\frac{d\vec{t}}{ds} = \vec{\Omega} \times \vec{t} = \vec{u}\dot{\theta} - \vec{v} \cos \theta\,\dot{\psi}. \tag{105}$$

From (101), (102), (104), and (105) we obtain for (103)

$$(T - \rho_c V_c^2)(\vec{u}\dot{\theta} - \vec{v} \cos \theta\,\dot{\psi}) + \vec{t}\left(\frac{dT}{ds} + D_{\mathrm{T}}\right)$$

$$+ \frac{C_{\mathrm{D}}\rho d V^2}{2}(\sin^2 \theta \cos^2 \psi + \sin^2 \psi)^{\frac{1}{2}}(\vec{u} \sin \theta \cos \psi - \vec{v} \sin \psi) \tag{106}$$

$$- w(\vec{u} \cos \theta + \vec{t} \sin \theta) = 0,$$

which gives the three scalar equations, (47).

Further, let $\vec{r}(s)$ be the cable configuration, i.e.,

$$\vec{r}(s) = \vec{i}\,\xi(s) + \vec{j}\,\eta(s) + \vec{k}\,\zeta(s),$$

where $\xi(s)$, $\eta(s)$, and $\zeta(s)$ are the ξ, η, ζ coordinates of a point s of the cable. Then

$$\vec{t} = \vec{i}\,\frac{d\xi(s)}{ds} + \vec{j}\,\frac{d\eta(s)}{ds} + \vec{k}\,\frac{d\zeta(s)}{ds}.$$

Forming the scalar product of $\vec{t}$ with $\vec{i}, \vec{j}, \vec{k}$ respectively, we get (48) of Section 7.1.

In a θ, ψ, T space the solution trajectories of (47) are given by the solutions of

$$(T - \rho_c V_c^2)\frac{d\theta}{dT} = \frac{\Lambda(\cos^2 \psi \sin^2 \theta + \sin^2 \psi)^{\frac{1}{2}} \cos \psi \sin \theta - \cos \theta}{D_T/w - \sin \theta},$$

$$(T - \rho_c V_c^2)\frac{d\psi}{dT} = \frac{\Lambda(\cos^2 \psi \sin^2 \theta + \sin^2 \psi)^{\frac{1}{2}} \sin \psi}{\cos \theta(D_T/w - \sin \theta)}.$$

We see that the trajectories are periodic in both θ and ψ with a period of 2π, and only a single region, say

$$0 \leqq \theta \leqq 2\pi,$$

$$0 \leqq \psi \leqq 2\pi,$$

need be considered. It is apparent that the straight lines

(1) $\psi \equiv 0,$ $\quad \theta \equiv \alpha;$ $\qquad$ (2) $\psi \equiv 0,$ $\quad 0 \equiv \alpha + \pi;$

(3) $\psi \equiv \pi,$ $\quad \theta \equiv 2\pi - \alpha;$ $\qquad$ (4) $\psi \equiv \pi,$ $\quad \theta \equiv \pi - \alpha;$

are solution trajectories which contain all values of T. Along other solution trajectories in this region one easily verifies that

$$T = \frac{\rho_c V_c^2}{w}$$

$$\times \left(1 - \exp \int_{\theta_0}^{\theta} \frac{\left(\dfrac{D_T}{w} - \sin \theta \right) d\theta}{\Lambda [\cos^2 \psi(\theta) \sin^2 \theta + \sin^2 \psi(\theta)]^{\frac{1}{2}} \cos \psi(\theta) \sin \theta - \cos \theta} \right),$$

where $\psi = \psi(\theta)$ is obtained from the solution of

$$\frac{d\psi}{d\theta} = \frac{[\cos \theta - \Lambda(\cos^2 \psi \sin^2 \theta + \sin^2 \psi)^{\frac{1}{2}} \cos \psi \sin \theta] \cos \theta}{\Lambda(\cos^2 \psi \sin^2 \theta + \sin^2 \psi)^{\frac{1}{2}} \sin \psi}.$$

From the definitions of ψ and θ, it follows that the lines (3) and (4) are physically identical with lines (1) and (2), and represent straight-line laying and recovery respectively. Likewise, the expression for T shows that any non-straight line trajectory with zero bottom tension is bounded by $\rho_c V_c^2/w$. Hence, as in the case of the two-dimensional model, we conclude that if the tension is somewhere greater than $\rho_c V_c^2/w$ and the bottom tension is zero, the only possible stationary configuration is the straight line lying in the plane of the resultant ship velocity and gravity vectors, and making the critical angle α with the horizontal.

F.2 *Perturbation Solution for a Uniform Cross Current*

At the outset we assume the tangential drag force to be zero. This gives by (49)

$$T = w(h + \eta), \tag{107}$$

where h is the total ocean depth. Furthermore, we take $\rho_c V_c^2$ to be zero.

If the angle φ (Fig. 26) is small compared to unity, we assume that θ and ψ will vary only slightly from the values they would have if the

upper, cross-current stratum extended all the way to the ocean bottom. That is, we take θ and ψ to be of the form

$$\theta = \alpha' + \bar{\theta},$$
$$\psi = \tilde{\psi}, \tag{108}$$

where α' is the stationary incidence angle corresponding to the velocity V', and $\bar{\theta}$ and $\tilde{\psi}$ are assumed small compared to unity.

Substituting (48b), (107), and (108) into (47a, b) and retaining only linear terms in θ, ψ and their derivatives, we get the linear first order equations

$$(h + \eta)\frac{d\bar{\theta}}{d\eta} + (2\text{ctn}^2\alpha' + 1)\bar{\theta} = 0, \qquad \text{(a)}$$
$$(h + \eta)\frac{d\tilde{\psi}}{d\eta} + \text{csc}^2\alpha'\tilde{\psi} = 0. \qquad \text{(b)} \tag{109}$$

Because in the lower stratum the cable is a straight line parallel to the path of the ship, we have as boundary conditions:

$$\eta = -h', \begin{cases} \bar{\theta} = \alpha - \alpha', \\ \tilde{\psi} = \varphi, \end{cases} \tag{110}$$

where h' is the depth of the upper, cross-current stratum and α is the stationary incidence angle corresponding to the velocity V.

The solution of (109) for the boundary conditions (110) is

$$\bar{\theta} = \left(\frac{h - h'}{h + \eta}\right)^{\mu} \Delta\alpha,$$
$$\tilde{\psi} = \left(\frac{h - h'}{h + \eta}\right)^{\nu} \varphi, \tag{111}$$

where

$$\mu = (2\,\text{ctn}^2\alpha' + 1),$$
$$\nu = \text{csc}^2\alpha', \tag{112}$$
$$\Delta\alpha = \alpha - \alpha'.$$

Equation (48) for the space-coordinates ξ, η, and ζ of the cable in turn can be written to terms of first order in the form

$$\frac{d\xi}{d\eta} = \text{ctn}\alpha' - \bar{\theta}\text{csc}^2\alpha',$$
$$\frac{d\zeta}{d\eta} = -\tilde{\psi}\text{ctn}\alpha'. \tag{113}$$

Substituting (111) into (113) and integrating under the condition that at $\eta = 0$, $\xi = 0$ and $\zeta = 0$, we find

$$\xi = \eta \operatorname{ctn}\alpha' + \frac{(h - h')\Delta\alpha}{(\mu - 1)} \csc^2\alpha' \left[\frac{1}{(h + \eta)^{\mu-1}} - \frac{1}{h^{\mu-1}}\right],$$

$$\zeta = \operatorname{ctn}\alpha' \frac{(h - h')}{(\nu - 1)} \varphi \left[\frac{1}{(h + \eta)^{\nu-1}} - \frac{1}{h^{\nu-1}}\right]. \tag{114}$$

These equations describe the space curve formed by the cable in the cross-current stratum.

To determine the distances d and e (Fig. 32), we transform (114) for the cable configuration to coordinates ξ' and ζ' oriented along the ship's path and normal to it respectively by means of

$$\xi' = \xi \cos\varphi - \zeta \sin\varphi,$$

$$\zeta' = \xi \sin\varphi + \zeta \cos\varphi.$$

The result to terms of the first order is

$$\xi' = \eta \operatorname{ctn}\alpha' + \frac{(h - h')\Delta\alpha}{(\mu - 1)} \csc^2\alpha' \left[\frac{1}{(h + \eta)^{\mu-1}} - \frac{1}{h^{\mu-1}}\right],$$

$$\zeta' = \varphi \left(\eta \operatorname{ctn}\alpha' + \frac{\operatorname{ctn}\alpha'(h - h')}{(\nu - 1)} \left[\frac{1}{(h + \eta)^{\nu-1}} - \frac{1}{h^{\nu-1}}\right]\right).$$

Letting $\eta = -h'$ and denoting the corresponding values of ξ' and ζ' by $-d$ and $-e$ respectively, we obtain (52).

REFERENCES

1. W. H. Thomson (Lord Kelvin), On Machinery for Laying Submarine Telegraph Cables, The Engineer, **4**, pp. 185–186, Sept. 11, 1857.

2. W. H. Thomson, Machinery for Laying Submarine Cables, The Engineer, **4,** p. 280, Oct. 16, 1857.

3. J. A. Longridge and C. E. Brooks, On Submerging Telegraph Cables, Proceedings of the Institution of Civil Engineers, pp. 269–314, Feb. 16, 1858.

4. G. B. Airy, On the Mechanical Conditions of the Deposit of a Submarine Cable, Philosophical Magazine, **16,** pp. 1–18, July, 1858.

5. W. Gravatt, On the Atlantic Cable, Philosophical Magazine, **16,** pp. 34–37, July, 1858.

6. W. S. B. Woolhouse, On the Deposit of Submarine Cables, Philosophical Magazine, **19,** pp. 345–364, May, 1860.

7. W. H. Thomson, On the Forces Concerned in the Laying and Lifting of Deep Sea Cables, *Mathematical and Physical Papers,* Vol. 2, Cambridge Univ. Press, Cambridge, 1884, pp. 153–167.

8. E. J. Routh, *Dynamics of a System of Rigid Bodies,* Vol. 2, Macmillan Co., London, 1905, pp. 401–403.

9. W. Siemens, Contributions to the Theory of Submerging and Testing Submarine Telegraphs, Journal of the Society of Telegraph Engineers, **5,** pp. 42–66, Feb. 1875. Reprinted in *Scientific and Technical Papers of Werner von Siemens,* John Murray, London, Vol. I, 1892, pp. 237–263. Also see discussions of Siemens paper in the J. of the Soc. of Telegraph Eng., **5,** by Willoughby Smith, pp. 67–76; F. C. Webb, pp. 92–97; W. Siemens, pp. 100–102; W. H. Preece, pp. 102–106; J. A. Longridge, pp. 107–112; F. C. Webb, pp. 113–115; and W. Siemens, pp. 122–126.

10. I. Brunelli, Note sur la théorie mécanique de l'immersion des câble sous-marins, Journal Télégraphique, **36,** pp. 4–6, 25–29, and 49–53, 1912.

11. L. Pode, An Experimental Investigation of the Hydrodynamic Forces on Stranded Cables, Report **713,** David W. Taylor Model Basin, Navy Department, May 1950.

12. L. Pode, Tables for Computing the Equilibrium Configuration of a Flexible Cable in a Uniform Stream, Report **687,** David W. Taylor Model Basin, Navy Department, March 1951.

13. J. W. Johnson (editor), *Proceedings of the First Conference on Ships and Waves at Hoboken, New Jersey, Oct. 1954.* Published by the Council on Wave Research and the Society of Naval Architects and Marine Engineers, 1955.

14. F. Horn, High Sea Test Trip Oscillation and Acceleration Measurements, Translation No. **26,** U. S. Experimental Model Basin, Navy Yard, Washington, D. C., March 1936.

15. F. Eisner, Das Widerstands Problem, *Third International Congress of Applied Mechanics,* Stockholm, 1930.

Theory of Curved Circular Waveguide Containing an Inhomogeneous Dielectric

By SAMUEL P. MORGAN

Generalized telegraphist's equations are derived, following Schelkunoff, for all modes in a curved circular waveguide containing an inhomogeneous dielectric. Particular attention is paid to the coupling between the TE_{01} mode and other modes in the curved guide. The results are applied to the problem of preventing the mode conversion from TE_{01} to TM_{11} which normally occurs in a curved round waveguide, by partially filling the cross section of the curved guide with a suitably shaped dielectric, such as polystyrene foam. Design equations are given for various compensators, and criteria are set up for keeping the power levels of all spurious modes low in a compensated bend. Dielectric losses, which may be important at millimeter wavelengths, are briefly treated. The potentialities of different compensator designs are illustrated by numerical examples.

INTRODUCTION

It has been recognized for several years that a major problem in the transmission of circular electric waves through multimode round waveguides is the question of negotiating bends. Theoretical studies[1, 2, 3] have shown that a gentle bend couples the TE_{01} mode to the TE_{11}, TE_{12}, TE_{13}, $\cdots$ modes and to the TM_{11} mode. The TM_{11} mode presents the most serious problem, since it has the same phase velocity as TE_{01} in a perfectly conducting straight guide. It follows that power introduced in the TE_{01} mode at the beginning of a gradual bend will be essentially completely transferred to the TM_{11} mode at odd multiples of a certain critical bending angle ϑ_c. The angle ϑ_c is proportional to the ratio of wavelength to guide radius but independent of bending radius; in other words, power transfer cannot be avoided merely by using a sufficiently gentle bend.

S. E. Miller[4] has discussed a number of methods for transmitting the circular electric wave around bends with small net power loss to TM_{11}. These methods are of two general types.

In the first type the TE_{01} mode, which is not itself a normal mode of the curved guide, is deliberately converted to a combination of TE_{01} and TM_{11} which is a normal mode, or to a particular polarization of TM_{11} which is another normal mode of the curved guide. After traversing the bend the energy is reconverted to TE_{01}. A disadvantage of the normal-mode approach is that the mode conversions necessary at the ends of the bend are frequency sensitive, so that bandwidths appear to be limited to the order of 10 per cent.

A second approach to the bend problem is to break up, by some modification of the guide, the degeneracy which exists between the propagation constants of the TE_{01} and TM_{11} modes in a perfectly conducting straight pipe. The two modes are still coupled by the curvature of the guide, but as Miller has shown, the maximum power transfer will be small if there is sufficient difference between the phase constants or between the attenuation constants of the coupled modes. A difference in phase constants may be provided, for example, by circular corrugations in the waveguide wall, or perhaps most easily by applying a thin layer of dielectric to the inner surface of the guide.[5] Differential attenuation may be introduced into the TM_{11} mode by a number of methods, in particular by making the guide out of spaced copper rings or a closely-wound wire helix surrounded by a lossy sheath.[6] Unfortunately, the larger the guide diameter in wavelengths the more difficult it is to get the separation of propagation constants necessary to negotiate a bend of given radius satisfactorily.

Still another solution of the bend problem is to decouple the TE_{01} and TM_{11} modes in a curved guide by partially filling the cross section of the curved guide with dielectric material. The dielectric must be arranged to produce coupling between the TE_{01} and TM_{11} modes which is equal and opposite to the coupling produced by the curvature of the guide. This condition may be satisfied in a great variety of ways; but it is not the only requirement for a good bend compensator. Practical restrictions are that the power levels of all other modes which are coupled to TE_{01} by the dielectric-compensated bend must be kept low, and of course dielectric losses in the compensator must not be excessive.

Part I of this paper treats the general problem of a curved circular waveguide containing an inhomogeneous dielectric. A convenient formulation of the problem is provided by S. A. Schelkunoff's generalized telegraphist's equations for waveguides.[7] The field at any cross section of the dielectric-compensated curved circular guide is represented as a superposition of the fields of the normal modes of an air-filled straight circular guide. A current amplitude and a voltage amplitude are asso-

ciated with each normal mode, and the currents and voltages satisfy an infinite set of generalized telegraphist's equations. The coupling terms in these equations depend upon the curvature of the guide axis and upon the variation of dielectric permittivity over the cross section. In the present application, the distribution of dielectric is taken to be independent of distance along the bend.*

The generalized telegraphist's equations for all modes in a curved circular waveguide containing an inhomogeneous dielectric are set up in Section 1.1. As a special case one has the equations for an air-filled curved guide, or for a straight guide with an inhomogeneous dielectric. In Section 1.2 we transform from current and voltage amplitudes to the amplitudes of forward and backward traveling waves on a system of coupled transmission lines and in Section 1.3 we work out in some detail the coupling coefficients which involve the TE_{01} mode. An approximate formula for dielectric loss in a compensated bend, which is valid at least in the important practical case when the relative permittivity of the dielectric differs but little from unity, is given in Section 1.4.

Part II applies the foregoing theory to the design of bend compensators for the TE_{01} mode. In a well-designed compensator the amplitudes of the backward (reflected) waves are very low, so we shall neglect reflections. The amplitudes of the spurious forward waves should also be low compared to TE_{01}, so that we may consider them one at a time. We assume that the TE_{01} mode crosstalks independently into each spurious mode, and represent the interaction between modes by a pair of linear, first-order, differential equations in the wave amplitudes. Miller's treatment[8] of these equations is reviewed in Section 2.1, and applied in Section 2.2 to TE_{01}–TM_{11} coupling in plain and compensated bends. Some results of the Jouguet-Rice theory[1, 2] for plain bends are confirmed by coupled-line theory. The condition for decoupling TE_{01} and TM_{11} in a compensated bend is written down, and the consequences of imperfect decoupling are discussed.

Three different compensator designs are described in Section 2.3, and evaluated with regard to mode conversions and approximate dielectric losses. In the first case, which may be called the "geometrical optics" solution, the permittivity is supposed to vary continuously in such a way that a bundle of parallel rays entering the bend would be bent into coaxial circular arcs all of the same optical length. This is not a perfect solution of the problem if the wavelength is finite, but it is of some

---

* We shall not consider the effects of random inhomogeneities, such as bubbles in polystyrene foam, although these might conceivably add to the mode conversion if their dimensions were comparable to the operating wavelength.

theoretical interest nevertheless. In the second case, a dielectric sector of constant permittivity is attached to the inner surface of the bend nearest the center of curvature; the angle of the sector is determined to satisfy the decoupling condition. Such a sector may be an effective compensator if the guide is small enough to propagate only 40 to 50 modes at the operating frequency, as, for example, a $\frac{7}{8}$-inch guide at a wavelength of 5.4 mm. Finally, we consider a compensator made of three dielectric sectors, whose angles and spacings are chosen to decouple the modes (TE$_{21}$ and TE$_{31}$) with phase velocities closest to TE$_{01}$. The three-sector compensator may be necessary if the guide is large enough to propagate 200 to 300 modes, say a 2-inch guide at 5.4 mm.

In Section 2.4 we investigate the effect of increasing the attenuation of the spurious modes generated by the compensated bend. The conclusion is that it is not feasible to add enough loss to the worst spurious modes to reduce appreciably the power which they abstract from TE$_{01}$.

As a sample of numerical results, it appears possible to negotiate a 90° bend of radius 20 inches in the $\frac{7}{8}$-inch guide at 5.4 mm with an insertion loss of about 0.3 db. This assumes a single-sector polyfoam compensator with a relative permittivity of 1.036 and a loss tangent of 5×10^{-5} (polyfoam with approximately these constants is currently available). About 0.2 db of the quoted loss is due to mode conversions and 0.1 db to dielectric dissipation. For a 2-inch guide with a three-sector polyfoam compensator, a bending radius of about 12 feet appears feasible. The total loss in a 90° bend should be about 0.35 db, with approximately 0.1 db going into mode conversion and about 0.25 db into dielectric dissipation. The dielectric loss is proportional, of course, to the total bend angle, and for a 180° bend would be double the above figures.
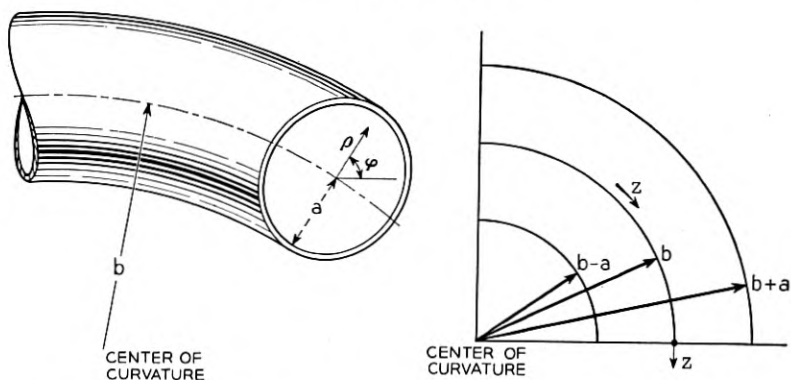

Fig. 1 — Coordinates used in circular bend in circular waveguide.

The appendix contains brief descriptions of three dielectric compensators which can be inserted in a straight section of guide adjacent to a bend. The first two are transducers which convert TE_{01} to a normal mode of the curved guide; they are subject to bandwidth limitations as mentioned by Miller.[9] The third type merely takes the output mixture of TE_{01} and TM_{11} from a plain bend with a pure TE_{01} input, and reconverts it all to TE_{01} ; it is essentially a broadband device. The spurious modes generated by a bend plus compensator have not been calculated, but it is very unlikely that a smaller bending radius will be permitted when the compensator is outside the bend than when it is inside.

I. THEORY

1.1 *Generalized Telegraphist's Equations*

To describe electromagnetic fields in a curved circular waveguide one is naturally led to use "bent cylindrical coordinates" (ρ, φ, z),[1, 2, 3] in which the longitudinal coordinate z is distance measured along the curved axis of the guide, while ρ and φ are polar coordinates in a plane normal to the axis of the guide, with origin at the guide axis. The lines $\varphi = 0$ and $\varphi = \pi$ lie in the plane of the bend. The radius of the guide is denoted by a and the radius of the bend (i.e., the radius of curvature of the guide axis) is denoted by b. The coordinate system is shown in Fig. 1.

For the moment regarding (ρ, φ, z) as general orthogonal curvilinear coordinates (u, v, w), we let

$$u = \rho, \qquad v = \varphi, \qquad w = z. \tag{1}$$

The element of length in this system is

$$ds^2 = e_1^2 du^2 + e_2^2 dv^2 + e_3^2 dw^2, \tag{2}$$

where

$$e_1 = 1, \qquad e_2 = \rho, \qquad e_3 = 1 + \xi, \tag{3}$$

and

$$\xi = (\rho/b) \cos \varphi. \tag{4}$$

Maxwell's equations for a field with time dependence $e^{i\omega t}$ may be

written in the form:[10]

$$\frac{1}{e_2 e_3}\left[\frac{\partial}{\partial v}(e_3 E_w) - \frac{\partial}{\partial w}(e_2 E_v)\right] = -i\omega\mu H_u,$$

$$\frac{1}{e_3 e_1}\left[\frac{\partial}{\partial w}(e_1 E_u) - \frac{\partial}{\partial u}(e_3 E_w)\right] = -i\omega\mu H_v,$$

$$\frac{1}{e_1 e_2}\left[\frac{\partial}{\partial u}(e_2 E_v) - \frac{\partial}{\partial v}(e_1 E_u)\right] = -i\omega\mu H_w,$$

$$\frac{1}{e_2 e_3}\left[\frac{\partial}{\partial v}(e_3 H_w) - \frac{\partial}{\partial w}(e_2 H_v)\right] = i\omega\epsilon E_u,$$ (5)

$$\frac{1}{e_3 e_1}\left[\frac{\partial}{\partial w}(e_1 H_u) - \frac{\partial}{\partial u}(e_3 H_w)\right] = i\omega\epsilon E_v,$$

$$\frac{1}{e_1 e_2}\left[\frac{\partial}{\partial u}(e_2 H_v) - \frac{\partial}{\partial v}(e_1 H_u)\right] = i\omega\epsilon E_w.$$

In these equations the permeability μ and the permittivity ϵ may be functions of position. If there is dissipation in the medium, either ϵ or μ or both may be complex.

To convert Maxwell's equations into generalized telegraphist's equations, we introduce the field distributions characteristic of the normal modes of a straight, cylindrical guide filled with a homogeneous dielectric. The derivation follows very closely that given by Schelkunoff[11] for an inhomogeneously-filled straight guide. Each mode is described by a transverse field distribution pattern $T(u, v)$, where $T(u, v)$ satisfies

$$\nabla^2 T = \frac{1}{e_1 e_2}\left[\frac{\partial}{\partial u}\left(\frac{e_2}{e_1}\frac{\partial T}{\partial u}\right) + \frac{\partial}{\partial v}\left(\frac{e_1}{e_2}\frac{\partial T}{\partial v}\right)\right] = -\chi^2 T,$$ (6)

and χ is a separation constant which takes on discrete values for the various TE and TM modes. We shall denote the function corresponding to the nth TE mode by $T_{[n]}(u, v)$, and the separation constant by $\chi_{[n]}$, with the subscript in *brackets*. The normal derivative of $T_{[n]}$ vanishes on the perfectly conducting waveguide boundary. Similarly the function corresponding to the nth TM mode is denoted by $T_{(n)}(u, v)$, and the separation constant by $\chi_{(n)}$, with the subscript in *parentheses*. The function $T_{(n)}$ vanishes on the boundary of the waveguide. For the present the

modes may be assumed to be numbered in order of increasing cutoff frequency; later when we have occasion to refer to specific modes we shall replace the subscript n by the customary double subscript notation for TE and TM modes in a circular guide.

The T-functions are assumed to be so normalized that

$$\int_S (\text{grad } T) \cdot (\text{grad } T) \, dS \equiv \int_S (\text{flux } T) \cdot (\text{flux } T) \, dS$$

$$\equiv \chi^2 \int_S T^2 \, dS = 1, \tag{7}$$

where S is the cross section of the guide. The gradient and flux of a scalar point-function W are transverse vectors with the following components:

$$\text{grad}_u \, W = \frac{\partial W}{e_1 \partial u}, \qquad \text{grad}_v \, W = \frac{\partial W}{e_2 \partial v},$$

$$\text{flux}_u \, W = \frac{\partial W}{e_2 \partial v}, \qquad \text{flux}_v \, W = -\frac{\partial W}{e_1 \partial u}. \tag{8}$$

Various orthogonality relationships exist among the T-functions corresponding to different modes of the guide, and among their gradients and fluxes. These relationships have been listed by Schelkunoff.[12]

The transverse components of the fields in the curved guide may be derived from potential and stream functions, U and Ψ for TE waves and V and Π for TM waves. Thus

$$E_t = -\text{grad } V - \text{flux } \Psi,$$

$$H_t = \text{flux } \Pi - \text{grad } U. \tag{9}$$

We now assume series expansions for the potential and stream functions in terms of the functions $T(u, v)$, with coefficients depending on w. Let

$$V = -\sum_n V_{(n)}(w) \, T_{(n)}(u, v), \qquad \Pi = -\sum_n I_{(n)}(w) \, T_{(n)}(u, v),$$

$$\Psi = -\sum_n V_{[n]}(w) \, T_{[n]}(u, v), \qquad U = -\sum_n I_{[n]}(w) \, T_{[n]}(u, v). \tag{10}$$

The I's and V's have the dimensions and properties of transmission-line currents and voltages. If we substitute (10) into (9) and expand in

components by (8), we obtain:

$$
E_u = \sum_n \left[V_{(n)} \frac{\partial T_{(n)}}{e_1 \partial u} + V_{[n]} \frac{\partial T_{[n]}}{e_2 \partial v} \right],
$$

$$
E_v = \sum_n \left[V_{(n)} \frac{\partial T_{(n)}}{e_2 \partial v} - V_{[n]} \frac{\partial T_{[n]}}{e_1 \partial u} \right],
$$

$$
H_u = \sum_n \left[-I_{(n)} \frac{\partial T_{(n)}}{e_2 \partial v} + I_{[n]} \frac{\partial T_{[n]}}{e_1 \partial u} \right],
$$

$$
H_v = \sum_n \left[I_{(n)} \frac{\partial T_{(n)}}{e_1 \partial u} + I_{[n]} \frac{\partial T_{[n]}}{e_2 \partial v} \right].
$$

$$(11)$$

For the longitudinal field components it is convenient to expand the combinations $e_3 E_w$ and $e_3 H_w$ in the following series:

$$
e_3 E_w = \sum_n \chi_{(n)} V_{w,(n)}(w) T_{(n)}(u, v),
$$

$$
e_3 H_w = \sum_n \chi_{[n]} I_{w,[n]}(w) T_{[n]}(u, v).
$$

$$(12)$$

It should be noted that the boundary conditions in the curved circular guide are

$$
E_v = E_w = 0 \tag{13}
$$

at the boundary of the guide, and that these conditions are satisfied by the individual terms of the series for E_v and E_w, on account of the boundary conditions already imposed on $T_{(n)}$ and $T_{[n]}$. Hence we do not have the problem of nonuniform convergence which sometimes arises in treating waveguides of varying cross section by the present method.

The procedure for transforming Maxwell's equations into generalized telegraphist's equations is now straightforward, if a trifle tedious. One substitutes the series (11) and (12) into equations (5), and integrates certain combinations of the latter equations over the cross section of the guide, taking account of the orthogonality properties of the T-functions. For example, subtracting $\partial T_{(m)}/e_2 \partial v$ times the first of equations (5) from $\partial T_{(m)}/e_1 \partial u$ times the second equation, and integrating over the cross section, yields

$$
\frac{dV_{(m)}}{dw} - \chi_{(m)} V_{w,(m)}
$$

$$
= -i\omega \sum_n \left[I_{(n)} \int_S \mu e_3 \, (\mathrm{grad}\ T_{(n)}) \cdot (\mathrm{grad}\ T_{(m)}) \, dS \right.
$$

$$
\left. + I_{[n]} \int_S \mu e, \, (\mathrm{grad}\ T_{(m)}) \cdot (\mathrm{flux}\ T_{[n]}) \, dS \right].
$$

$$(14)$$

Adding $\partial T_{[m]}/e_1 \partial u$ times the first equation to $\partial T_{[m]}/e_2 \partial v$ times the second

and integrating gives

$$\frac{dV_{[m]}}{dw} = -i\omega \sum_n \left[I_{(n)} \int_S \mu e_3 \,(\text{grad } T_{(n)}) \cdot (\text{flux } T_{[m]}) \, dS \right.$$
$$\left. + I_{[n]} \int_S \mu e_3 \,(\text{grad } T_{[m]}) \cdot (\text{grad } T_{[n]}) \, dS \right]. \tag{15}$$

Similarly, from the fourth and fifth equations we get

$$\frac{dI_{(m)}}{dw} = -i\omega \sum_n \left[V_{(n)} \int_S \epsilon e_3 \,(\text{grad } T_{(m)}) \cdot (\text{grad } T_{(n)}) \, dS \right.$$
$$\left. + V_{[n]} \int_S \epsilon e_3 \,(\text{grad } T_{(m)}) \cdot (\text{flux } T_{[n]}) \, dS \right], \tag{16}$$

$$\frac{dI_{[m]}}{dw} - \chi_{[m]} I_{w,[m]}$$

$$= -i\omega \sum_n \left[V_{(n)} \int_S \epsilon e_3 \,(\text{grad } T_{(n)}) \cdot (\text{flux } T_{[m]}) \, dS \right. \tag{17}$$

$$\left. - V_{[n]} \int_S \epsilon e_3 \,(\text{grad } T_{[m]}) \cdot (\text{grad } T_{[n]}) \, dS \right].$$

From the third of equations (5) using the fact that the T-functions satisfy (6), then multiplying through by $T_{[m]}$ and integrating over the cross section, we get,

$$V_{[m]} = -i\omega \sum_n I_{w,[n]} \chi_{[n]} \int_S \frac{\mu T_{[n]} T_{[m]}}{e_3} \, dS. \tag{18}$$

Similarly, from the sixth equation,

$$I_{(m)} = -i\omega \sum_n V_{w,(n)} \chi_{(n)} \int_S \frac{\epsilon T_{(n)} T_{(m)}}{e_3} \, dS. \tag{19}$$

These equations may be written in the form

$$V_{[m]} = -\sum_n \frac{Z_{w,[m][n]} I_{w,[n]}}{\chi_{[m]}},$$
$$I_{(m)} = -\sum_n \frac{Y_{w,(m)(n)} V_{w,(n)}}{\chi_{(m)}}, \tag{20}$$

where we define

$$Z_{w,[m][n]} = i\omega \chi_{[m]} \chi_{[n]} \int_S \frac{\mu T_{[m]} T_{[n]}}{e_3} \, dS,$$
$$Y_{w,(m)(n)} = i\omega \chi_{(m)} \chi_{(n)} \int_S \frac{\epsilon T_{(m)} T_{(n)}}{e_3} \, dS. \tag{21}$$

Solving (20) for $I_{w,[m]}$ and $V_{w,(m)}$ in terms of $V_{[n]}$ and $I_{(n)}$ respectively, we may write

$$I_{w,[m]} = -\sum_n \frac{Y_{w,[m][n]}}{\chi_{[m]}} V_{[n]},$$

$$V_{w,(m)} = -\sum_n \frac{Z_{w,(m)(n)}}{\chi_{(m)}} I_{(n)},$$

(22)

where $Y_{w,[m][n]}$ and $Z_{w,(m)(n)}$ may be defined as the ratios of certain determinants involving $Z_{w,[m][n]}$ and $Y_{w,(m)(n)}$ respectively.*

We are now able to eliminate $V_{w,(m)}$ and $I_{w,[m]}$ from (14) and (17), and to write down the generalized telegraphist's equations for the curved circular waveguide filled with an inhomogeneous dielectric in the following form:

$$\frac{dV_{(m)}}{dw} = -\sum_n [Z_{(m)(n)}I_{(n)} + Z_{(m)[n]}I_{[n]}],$$

$$\frac{dV_{[m]}}{dw} = -\sum_n [Z_{[m](n)}I_{(n)} + Z_{[m][n]}I_{[n]}],$$

$$\frac{dI_{(m)}}{dw} = -\sum_n [Y_{(m)(n)}V_{(n)} + Y_{(m)[n]}V_{[n]}],$$

$$\frac{dI_{[m]}}{dw} = -\sum_n [Y_{[m](n)}V_{(n)} + Y_{[m][n]}V_{[n]}].$$

(23)

The impedance and admittance coefficients are defined by:

$$Z_{(m)(n)} = i\omega \int_S \mu e_3 \, (\text{grad } T_{(m)}) \cdot (\text{grad } T_{(n)}) \, dS + Z_{w,(m)(n)},$$

$$Z_{(m)[n]} = i\omega \int_S \mu e_3 \, (\text{grad } T_{(m)}) \cdot (\text{flux } T_{[n]}) \, dS,$$

$$Z_{[m](n)} = i\omega \int_S \mu e_3 \, (\text{flux } T_{[m]}) \cdot (\text{grad } T_{(n)}) \, dS,$$

$$Z_{[m][n]} = i\omega \int_S \mu e_3 \, (\text{grad } T_{[m]}) \cdot (\text{grad } T_{[n]}) \, dS,$$

$$Y_{(m)(n)} = i\omega \int_S \epsilon e_3 \, (\text{grad } T_{(m)}) \cdot (\text{grad } T_{(n)}) \, dS,$$

(24)

* If (20) are actually regarded as infinite sets of equations, one has to pay some attention to defining the meaning of the statement that their solutions are given by (22). In practice we shall deal with a finite number of modes, and shall by-pass all questions about infinite processes.

$$Y_{(m)[n]} = i\omega \int_S \epsilon e_3 \,(\mathrm{grad}\ T_{(m)}) \cdot (\mathrm{flux}\ T_{[n]})\ dS,$$

$$Y_{[m](n)} = i\omega \int_S \epsilon e_3 \,(\mathrm{flux}\ T_{[m]}) \cdot (\mathrm{grad}\ T_{(n)})\ dS,$$

$$Y_{[m][n]} = i\omega \int_S \epsilon e_3 \,(\mathrm{grad}\ T_{[m]}) \cdot (\mathrm{grad}\ T_{[n]})\ dS + Y_{w,[m][n]}.$$

It may be noted that if the guide were straight, so that $e_3 = 1$, and if μ and ϵ were constant over the cross section, the Y's and Z's would all be zero except for those having equal subscripts. If the curvature of the guide is gentle, and if μ and ϵ do not vary much over the cross section (or if they vary extensively only in a small part of the cross section), then the Y's and Z's with unequal subscripts will be small, and we can obtain approximate solutions of (23) based upon the smallness of the coupling.

We shall now compute first-order approximations to the impedance and admittance coefficients under the following assumptions:

$$\mu = \mu_0 ,$$
$$\epsilon = \epsilon_0 (1 + \delta), \tag{25}$$

where μ_0 and ϵ_0 are constants (usually but not necessarily the permeability and permittivity of free space), and δ is a dimensionless function of position. No mathematical difficulties would follow from assuming μ as well as ϵ to be variable, but since the case of varying permeability is not of such immediate practical interest we shall omit this slight additional complication. In order that the coupling per unit length due to curvature and to inhomogeneity of the dielectric be small, we further assume that

$$|\xi| \leqq a/b \ll 1,$$
$$\frac{1}{S} \int_S |\delta|\ dS \ll 1, \tag{26}$$

where, as usual, S is the cross-sectional area of the guide.

From (21), first-order approximations to $Z_{w,[m][n]}$ and $Y_{w,(m)(n)}$ are

$$Z_{w,[m][n]} = i\omega\mu_0[\delta_{mn} - \xi_{[m][n]}],$$
$$Y_{w,(m)(n)} = i\omega\epsilon_0[\delta_{mn} + \delta_{(m)(n)} - \xi_{(m)(n)}], \tag{27}$$

where

$$\xi_{[m][n]} = \chi_{[m]}\chi_{[n]} \int_S \xi T_{[m]} T_{[n]} \, dS,$$

$$\xi_{(m)(n)} = \chi_{(m)}\chi_{(n)} \int_S \xi T_{(m)} T_{(n)} \, dS, \tag{28}$$

$$\delta_{(m)(n)} = \chi_{(m)}\chi_{(n)} \int_S \delta T_{(m)} T_{(n)} \, dS.$$

The quantity δ_{mn} is the Kronecker delta, and is not to be confused with $\delta_{(m)(n)}$, which is defined by the last of equations (28). Note that $\xi_{[m][n]}$ and $\xi_{(m)(n)}$ are zero unless the angular indices of the two modes involved differ by exactly unity.

It is not difficult to obtain approximate solutions of (20) in the forms (22), since the off-diagonal elements of the coefficient matrices of (20) are small compared to the diagonal elements. Using the expression derived by Rice[13] for the inverse of an almost-diagonal matrix (we shall not attempt to prove this result for infinite matrices), we find the first-order approximations

$$Y_{w,[m][n]} = \frac{\chi_{[m]}\chi_{[n]}}{i\omega\mu_0} [\delta_{mn} + \xi_{[m][n]}],$$

$$Z_{w,(m)(n)} = \frac{\chi_{(m)}\chi_{(n)}}{i\omega\epsilon_0} [\delta_{mn} + \xi_{(m)(n)} - \delta_{(m)(n)}]. \tag{29}$$

Approximate expressions for the impedance and admittance coefficients appearing in the generalized telegraphist's equations (23) are:

$$Z_{(m)(n)} = i\omega\mu_0[\delta_{mn} + \Xi_{(m)(n)}] + Z_{w,(m)(n)},$$

$$Z_{(m)[n]} = i\omega\mu_0\Xi_{(m)[n]},$$

$$Z_{[m](n)} = i\omega\mu_0\Xi_{[m](n)},$$

$$Z_{[m][n]} = i\omega\mu_0[\delta_{mn} + \Xi_{[m][n]}], \tag{30}$$

$$Y_{(m)(n)} = i\omega\epsilon_0[\delta_{mn} + \Xi_{(m)(n)} + \Delta_{(m)(n)}],$$

$$Y_{(m)[n]} = i\omega\epsilon_0[\Xi_{(m)[n]} + \Delta_{(m)[n]}],$$

$$Y_{[m](n)} = i\omega\epsilon_0[\Xi_{[m](n)} + \Delta_{[m](n)}],$$

$$Y_{[m][n]} = i\omega\epsilon_0[\delta_{mn} + \Xi_{[m][n]} + \Delta_{[m][n]}] + Y_{w,[m][n]}.$$

where

$$\Xi_{(m)(n)} = \int_S \xi \,(\text{grad } T_{(m)}) \cdot (\text{grad } T_{(n)}) \, dS,$$

$$\Xi_{(m)[n]} = \int_S \xi \,(\text{grad } T_{(m)}) \cdot (\text{flux } T_{[n]}) \, dS,$$

$$\Xi_{[m](n)} = \int_S \xi \,(\text{flux } T_{[m]}) \cdot (\text{grad } T_{(n)}) \, dS, \tag{31}$$

$$\Xi_{[m][n]} = \int_S \xi \,(\text{grad } T_{[m]}) \cdot (\text{grad } T_{[n]}) \, dS,$$

and

$$\Delta_{(m)(n)} = \int_S \delta \,(\text{grad } T_{(m)}) \cdot (\text{grad } T_{(n)}) \, dS,$$

$$\Delta_{(m)[n]} = \int_S \delta \,(\text{grad } T_{(m)}) \cdot (\text{flux } T_{[n]}) \, dS,$$

$$\Delta_{[m](n)} = \int_S \delta \,(\text{flux } T_{[m]}) \cdot (\text{grad } T_{(n)}) \, dS, \tag{32}$$

$$\Delta_{[m][n]} = \int_S \delta \,(\text{grad } T_{[m]}) \cdot (\text{grad } T_{[n]}) \, dS.$$

The Ξ's are zero unless the angular indices of the two modes involved differ by exactly unity.

1.2 *Representation in Terms of Coupled Traveling Waves*

From now on we shall assume that the distribution of dielectric over the cross section of the curved guide is independent of distance along the guide, so that the impedance and admittance coefficients are constants independent of z. (We shall henceforth designate the coordinates by (ρ, φ, z), instead of the (u, v, w) of the preceding section.) The generalized telegraphist's equations now represent an infinite set of coupled, uniform transmission lines, and their solution would be equivalent to the solution of an infinite system of linear algebraic equations and the corresponding characteristic equation.

For our purposes it is convenient to write the transmission-line equations not in terms of currents and voltages, but in terms of the amplitudes of forward and backward traveling waves, assumed to exist in a straight guide filled with a homogeneous medium. Thus let a and b be the amplitudes of the forward and backward waves of a typical mode at

a certain point. In what follows the wave amplitudes a and b will always carry mode subscripts, so they need never be confused with guide radius and radius of curvature. The mode current and voltage are related to the wave amplitudes by

$$V = K^{\frac{1}{2}}(a + b),$$
$$I = K^{-\frac{1}{2}}(a - b),$$

(33)

where K is the wave impedance. We have

$$K_{(n)} = h_{(n)}/\omega\epsilon_0,$$
$$K_{[n]} = \omega\mu_0/h_{[n]},$$

(34)

for TM and TE waves respectively, where $h_{(n)}$ and $h_{[n]}$ represent the unperturbed phase constants,

$$h_{(n)} = (\beta^2 - \chi_{(n)}^2)^{\frac{1}{2}},$$
$$h_{[n]} = (\beta^2 - \chi_{[n]}^2)^{\frac{1}{2}},$$

(35)

and

$$\beta^2 = \omega^2\mu_0\epsilon_0.$$

(36)

For a cutoff mode, h is negative imaginary; but we shall deal only with propagating modes in the present analysis.

If we represent the currents and voltages in the generalized telegraphist's equations (23) in terms of the traveling-wave amplitudes, and then perform some obvious additions and subtractions, we obtain the following equations for coupled traveling waves:

$$\frac{da_{(m)}}{dz} = -i \sum_n [\kappa^+_{(m)(n)}a_{(n)} + \kappa^-_{(m)(n)}b_{(n)} + \kappa^+_{(m)[n]}a_{[n]} + \kappa^-_{(m)[n]}b_{[n]}],$$

$$\frac{db_{(m)}}{dz} = +i \sum_n [\kappa^-_{(m)(n)}a_{(n)} + \kappa^+_{(m)(n)}b_{(n)} + \kappa^-_{(m)[n]}a_{[n]} + \kappa^+_{(m)[n]}b_{[n]}],$$

$$\frac{da_{[m]}}{dz} = -i \sum_n [\kappa^+_{[m](n)}a_{(n)} + \kappa^-_{[m](n)}b_{(n)} + \kappa^+_{[m][n]}a_{[n]} + \kappa^-_{[m][n]}b_{[n]}],$$

$$\frac{db_{[m]}}{dz} = +i \sum_n [\kappa^-_{[m](n)}a_{(n)} + \kappa^+_{[m](n)}b_{(n)} + \kappa^-_{[m][n]}a_{[n]} + \kappa^+_{[m][n]}b_{[n]}].$$

(37)

The κ's are coupling coefficients defined in terms of the impedance and admittance coefficients by

$$i\kappa^\pm_{(m)(n)} = \tfrac{1}{2}[(K_{(m)}K_{(n)})^{\frac{1}{2}} Y_{(m)(n)} \pm (K_{(m)}K_{(n)})^{-\frac{1}{2}} Z_{(m)(n)}],$$

$$i\kappa^\pm_{(m)[n]} = \tfrac{1}{2}[(K_{(m)}K_{[n]})^{\frac{1}{2}} Y_{(m)[n]} \pm (K_{(m)}K_{[n]})^{-\frac{1}{2}} Z_{(m)[n]}],$$

$$i\kappa^\pm_{[m](n)} = \tfrac{1}{2}[(K_{[m]}K_{(n)})^{\frac{1}{2}} Y_{[m](n)} \pm (K_{[m]}K_{(n)})^{-\frac{1}{2}} Z_{[m](n)}],$$

$$i\kappa^\pm_{[m][n]} = \tfrac{1}{2}[(K_{[m]}K_{[n]})^{\frac{1}{2}} Y_{[m][n]} \pm (K_{[m]}K_{[n]})^{-\frac{1}{2}} Z_{[m][n]}].$$

(38)

In these definitions the plus signs are taken together, likewise the minus signs. The factors of i are introduced in order that the κ's may be real for propagating modes in a lossless guide.

For the small-coupling case discussed at the end of the preceding section, it is convenient to separate a typical coupling coefficient into two parts; thus,

$$\kappa = c + d. \tag{39}$$

Here c is the coupling coefficient due to curvature and is zero unless the angular indices of the two modes involved differ by unity. The coupling coefficient d is due to the dielectric. All d's vanish if the dielectric is homogeneous; otherwise particular symmetries may cause certain classes of d's to be zero. The c's and d's may be expressed in terms of integrals written down in the preceding section if we substitute for the Y's and Z's in (38) their definitions according to (30).

The κ^+'s which have equal subscripts $(n)(n)$ or $[n][n]$ may be regarded as phase constants (of particular TM or TE modes) which have been modified by the presence of the dielectric. For the modified phase constants we introduce the symbols $\beta_{(n)}$ and $\beta_{[n]}$; thus,

$$\begin{aligned}
\beta_{(n)} &\equiv \kappa^+_{(n)(n)} = h_{(n)} + \frac{\chi_{(n)}{}^2 \delta_{(n)(n)} + h_{(n)}{}^2 \Delta_{(n)(n)}}{2 h_{(n)}} , \\
\beta_{[n]} &\equiv \kappa^+_{[n][n]} = h_{[n]} + \frac{\beta^2 \Delta_{[n][n]}}{2 h_{[n]}} .
\end{aligned} \tag{40}$$

The general expressions for the coupling coefficients between any two different modes are as follows:

$$\begin{aligned}
c^{\pm}_{(m)(n)} &= \frac{1}{2}\left[\sqrt{h_{(m)} h_{(n)}} \; \Xi_{(m)(n)} \pm \frac{\beta^2 \Xi_{(m)(n)} - \chi_{(m)} \chi_{(n)} \xi_{(m)(n)}}{\sqrt{h_{(m)} h_{(n)}}} \right], \\
d^{\pm}_{(m)(n)} &= \frac{1}{2}\left[\sqrt{h_{(m)} h_{(n)}} \; \Delta_{(m)(n)} \pm \frac{\chi_{(m)} \chi_{(n)} \delta_{(m)(n)}}{\sqrt{h_{(m)} h_{(n)}}} \right], \\
c^{\pm}_{(m)[n]} &= \tfrac{1}{2} \beta \Xi_{(m)[n]} \left[\sqrt{h_{(m)}/h_{[n]}} \pm \sqrt{h_{[n]}/h_{(m)}} \right], \\
d^{\pm}_{(m)[n]} &= \tfrac{1}{2} \beta \Delta_{(m)[n]} \sqrt{h_{(m)}/h_{[n]}}, \\
c^{\pm}_{[m](n)} &= \tfrac{1}{2} \beta \Xi_{[m](n)} \left[\sqrt{h_{(n)}/h_{[m]}} \pm \sqrt{h_{[m]}/h_{(n)}} \right], \\
d^{\pm}_{[m](n)} &= \tfrac{1}{2} \beta \Delta_{[m](n)} \sqrt{h_{(n)}/h_{[m]}} , \\
c^{\pm}_{[m][n]} &= \frac{1}{2}\left[\frac{\beta^2 \Xi_{[m][n]} - \chi_{[m]} \chi_{[n]} \xi_{[m][n]}}{\sqrt{h_{[m]} h_{[n]}}} \pm \Xi_{[m][n]} \sqrt{h_{[m]} h_{[n]}} \right], \\
d^{\pm}_{[m][n]} &= \frac{\beta^2 \Delta_{[m][n]}}{2 \sqrt{h_{[m]} h_{[n]}}},
\end{aligned} \tag{41}$$

where the symbols with double subscripts are defined by (28), (31), and (32).

1.3 *Coupling Coefficients Involving the* TE$_{01}$ *Mode*

In Part II we shall consider a well-compensated bend in which the total power in all spurious modes is everywhere low compared to the power level of TE$_{01}$. (This is somewhat more restrictive than merely assuming that the power in any one spurious mode is everywhere small compared to the power in TE$_{01}$.) To first order, therefore, we may compute the power abstracted from TE$_{01}$ by mode conversion by assuming that the TE$_{01}$ mode crosstalks into each spurious mode independently. For this calculation we need the values of the forward coupling coefficients between TE$_{01}$ and all other modes. The crosstalk into backward modes will be negligible in all practical cases.

We shall use the customary double-subscript notation for the various modes in a round guide, but shall continue to denote TM waves with parentheses and TE waves with brackets. *We assume that the distribution of dielectric is symmetric with respect to the plane of the bend,* so that TE$_{01}$ is coupled to a definite polarization of each spurious mode. The normalized T-functions are then:

$$
\begin{aligned}
T_{(nm)} &= \sqrt{\frac{\epsilon_n}{\pi}} \frac{J_n(\chi_{(nm)}\rho) \sin n\varphi}{k_{(nm)} J_{n-1}(k_{(nm)})}, \\
T_{[nm]} &= \sqrt{\frac{\epsilon_n}{\pi}} \frac{J_n(\chi_{[nm]}\rho) \cos n\varphi}{(k_{[nm]}^2 - n^2)^{\frac{1}{2}} J_n(k_{[nm]})},
\end{aligned}
\tag{42}
$$

where

$$
\begin{aligned}
k_{(nm)} &= \chi_{(nm)}a, \qquad J_n(k_{(nm)}) = 0, \\
k_{[nm]} &= \chi_{[nm]}a, \qquad J_n{}'(k_{[nm]}) = 0,
\end{aligned}
\tag{43}
$$

and

$$
\epsilon_n = \begin{cases} 1, & n = 0, \\ 2, & n \neq 0. \end{cases}
\tag{44}
$$

1.3.1 *Coupling Coefficients due to Curvature*

We know that to first order the curvature of the guide can couple the TE$_{01}$ mode only to modes of angular index unity. Let us calculate the

coupling between TE_{01} and TM_{1m}. Referring to (31), we have

$$\Xi_{(1m)[01]} = \Xi_{[01](1m)}$$

$$= \int_S \xi(\text{grad } T_{(1m)}) \cdot (\text{flux } T_{[01]}) \, dS$$

$$= \int_0^{2\pi} \int_0^a \frac{\sqrt{2} J_1(\chi_{[01]}\rho) J_1(\chi_{(1m)}\rho) \cos^2 \varphi}{\pi ab k_{(1m)} J_0(k_{[01]}) J_0(k_{(1m)})} \rho \, d\rho \, d\varphi \tag{45}$$

$$= \begin{cases} a/\sqrt{2}\, k_{[01]}b & \text{if } m = 1, \\ 0 & \text{if } m \neq 1. \end{cases}$$

Hence the only transverse magnetic mode coupled to TE_{01} by the bend is TM_{11}, and from (41) the forward coupling coefficient is:

$$c^+_{(11)[01]} = c^+_{[01](11)} = \beta a/\sqrt{2}\, k_{[01]}b = 0.18454\beta a/b. \tag{46}$$

To obtain the coupling between TE_{01} and TE_{1m}, we must evaluate two integrals. From (28), the first is

$$\xi_{[01][1m]} = \xi_{[1m][01]}$$

$$= \chi_{[01]}\chi_{[1m]} \int_S \xi T_{[01]} T_{[1m]} \, dS$$

$$= \int_0^{2\pi} \int_0^a \frac{\sqrt{2}\chi_{[1m]}\rho^2 J_0(\chi_{[01]}\rho) J_1(\chi_{[1m]}\rho) \cos^2 \varphi}{\pi ab(k_{[1m]}^2 - 1)^{\frac{1}{2}} J_0(k_{[01]}) J_1(k_{[1m]})} \, d\rho \, d\varphi \tag{47}$$

$$= \frac{\sqrt{2}a}{b} \frac{k_{[1m]}(k_{[01]}^2 + k_{[1m]}^2)}{(k_{[1m]}^2 - 1)^{\frac{1}{2}}(k_{[01]}^2 - k_{[1m]}^2)^2},$$

and from (31), the second is

$$\Xi_{[01][1m]} = \Xi_{[1m][01]}$$

$$= \int_S \xi(\text{grad } T_{[01]}) \cdot (\text{grad } T_{[1m]}) \, dS$$

$$= -\int_0^{2\pi} \int_0^a \frac{\sqrt{2}\chi_{[1m]}\rho^2 J_1(\chi_{[01]}\rho) J_1'(\chi_{[1m]}\rho) \cos^2 \varphi}{\pi ab(k_{[1m]}^2 - 1)^{\frac{1}{2}} J_0(k_{[01]}) J_1(k_{[1m]})} \, d\rho \, d\varphi \tag{48}$$

$$= \frac{2\sqrt{2}a}{b} \frac{k_{[01]}k_{[1m]}^2}{(k_{[1m]}^2 - 1)^{\frac{1}{2}}(k_{[01]}^2 - k_{[1m]}^2)^2}.$$

A short table of numerical values of the above two integrals follows:

m	$\xi_{[01][1m]}$	$\Xi_{[01][1m]}$
1	0.23871 a/b	0.18638 a/b
2	0.32865 a/b	0.31150 a/b
3	0.03682 a/b	0.02751 a/b

Putting these values into the expression (41) for the forward coupling coefficient, we obtain:

$$c_{[01][11]}^{+} = \left[\frac{0.09319(\beta a)^2 - 0.84204}{\sqrt{h_{[01]}a h_{[11]}a}} + 0.09319\sqrt{h_{[01]}a h_{[11]}a}\right]\frac{1}{b},$$

$$c_{[01][12]}^{+} = \left[\frac{0.15575(\beta a)^2 - 3.35688}{\sqrt{h_{[01]}a h_{[12]}a}} + 0.15575\sqrt{h_{[01]}a h_{[12]}a}\right]\frac{1}{b}, \quad (49)$$

$$c_{[01][13]}^{+} = \left[\frac{0.01376(\beta a)^2 - 0.60216}{\sqrt{h_{[01]}a h_{[13]}a}} + 0.01376\sqrt{h_{[01]}a h_{[13]}a}\right]\frac{1}{b}.$$

1.3.2 Coupling Coefficients due to Dielectric

Depending upon the distribution of the dielectric material over the cross section of the guide, the TE_{01} mode may be coupled to any mode except those of the TM_{0m} family. The dielectric coupling coefficients, as given by equations (41), are

$$d_{[01](nm)}^{+} = d_{(nm)[01]}^{+} = \tfrac{1}{2}\beta\Delta_{[01](nm)}\sqrt{h_{(nm)}/h_{[01]}},$$

$$d_{[01][nm]}^{+} = d_{[nm][01]}^{+} = \frac{\beta^2\Delta_{[01][nm]}}{2\sqrt{h_{[01]}h_{[nm]}}}. \quad (50)$$

The Δ's are obtained from equations (32); thus,

$$\Delta_{[01](nm)} = \int_S \delta(\text{grad } T_{(nm)})\cdot(\text{flux } T_{[01]}) \, dS$$

$$= \int_0^{2\pi}\int_0^a \frac{\delta(\rho,\varphi)n\sqrt{\epsilon_n}J_n(\chi_{(nm)}\rho)J_1(\chi_{[01]}\rho)\cos n\varphi}{\pi a k_{(nm)}J_{n-1}(k_{(nm)})J_0(k_{[01]})} \, d\rho \, d\varphi,$$

$$\Delta_{[01][nm]} = \int_S \delta(\text{grad } T_{[nm]})\cdot(\text{grad } T_{[01]}) \, dS \qquad (51)$$

$$= -\int_0^{2\pi}\int_0^a \frac{\delta(\rho,\varphi)\sqrt{\epsilon_n}\chi_{[nm]}J_n{}'(\chi_{[nm]}\rho)J_1(\chi_{[01]}\rho)\cos n\varphi}{\pi a(k_{[nm]}^2 - n^2)^{\frac{1}{2}}J_n(k_{[nm]})J_0(k_{[01]})} \, \rho \, d\rho \, d\varphi.$$

1.4 Dielectric Losses

To take account of dielectric dissipation we may introduce a complex permittivity,

$$\epsilon = \epsilon' - i\epsilon'' = \epsilon'(1 - i\tan\varphi), \qquad (52)$$

where φ is the loss angle of the dielectric and is not, of course, to be confused with the coordinate φ. If we let

$$\epsilon' = \epsilon_0(1 + \delta'), \qquad (53)$$

where δ' is real, then (52) may be written

$$\epsilon = \epsilon_0[1 + \delta' - i(1 + \delta') \tan \varphi] = \epsilon_0(1 + \delta), \tag{54}$$

where

$$\delta = \delta' - i(1 + \delta') \tan \varphi. \tag{55}$$

No changes in the formal analysis result from the fact that δ now has a complex value.

If the compensator is designed (assuming a lossless dielectric) so that the total power coupled from TE_{01} into all spurious modes is small at all points, it is reasonable to assume that the principal effect of dielectric loss on the TE_{01} mode will be seen in the modified phase constant $\beta_{[01]}$ of this mode in the presence of the compensator. If the compensator is made by filling a certain part S_1 of the guide cross section with a medium of constant (complex) permittivity, and the rest of the cross section with air, then from (32) and (40) the modified phase constant of the TE_{01} mode is

$$\beta_{[01]} = h_{[01]} + \frac{\beta^2 \delta}{2h_{[01]}} \int_{S_1} (\text{grad } T_{[01]})^2 \, dS, \tag{56}$$

where δ is given by (55). Since δ is complex, the attenuation constant is

$$\alpha_{[01]} = -\text{Im } \beta_{[01]} = \frac{\beta^2(1 + \delta') \tan \varphi}{2h_{[01]}} \int_{S_1} (\text{grad } T_{[01]})^2 \, dS, \tag{57}$$

where the integration may be carried out as soon as the area S_1 is specified.

The approximation (57) for the attenuation constant due to dielectric losses has a simple physical interpretation. It corresponds to the power which would be dissipated in a medium of conductivity $\omega\epsilon''$ if the electric field existing in the medium were the same as the field of the TE_{01} mode in a straight, empty guide. This is probably a very good approximation if δ' is small, as it will be for the foam dielectrics from which compensators are most likely to be made.

It is doubtful that (57) furnishes a good approximation to the dielectric loss when the permittivity of the compensator is high (δ not small compared to unity). If the permittivity is high the cross section of the dielectric member will be small, but the field perturbation may be large in the immediate neighborhood of the dielectric. The series which represent the fields in terms of the normal modes of the empty guide may converge slowly; in other words, when using the telegraphist's equations one must consider the coupling between TE_{01} and a large number of

other modes, none of which appears by itself to be very strongly coupled to TE$_{01}$.

Of course if we had a single normal mode of the *compensated* guide, with a field pattern independent of distance along the guide, it might well be possible to calculate the field distribution and the dielectric losses approximately, without reference to the telegraphist's equations and regardless of the permittivity of the dielectric. However, we do not have a single normal mode of the compensated guide, but rather a mixture of modes. The field pattern varies along the guide as the modes phase in and out; and it is not easy to conclude from this picture what the actual dielectric losses will be.

Finally it should be remembered that we have said nothing about the possible effect of a dielectric compensator on eddy current losses in the waveguide walls. If one attempted to use a compensator of small physical size and correspondingly high permittivity, the resulting perturbation of the electric field might very well increase the eddy current losses in the wall adjacent to the compensator. On the other hand, the increase would probably be negligible for a compensator made out of a foam dielectric.

II. APPLICATION

2.1 *Properties of Uniformly Coupled Transmission Lines*

We shall now apply the preceding theory to the calculation of TE$_{01}$ mode coupling in gentle bends. To describe propagation in a curved waveguide in terms of the modes of a straight guide requires, in general, the solution of the infinite set of equations (37); but we can give an adequate approximate treatment by considering just two modes at a time, one mode of each pair always being TE$_{01}$. Furthermore we need consider only the forward waves, since the relative power coupled from the forward waves into the backward waves is quite small.

The differential equations representing the forward waves on two uniformly coupled transmission lines are:

$$\frac{da_0}{dz} + \gamma_0 a_0 + i\kappa a_1 = 0,$$

$$i\kappa a_0 + \frac{da_1}{dz} + \gamma_1 a_1 = 0. \tag{58}$$

In these equations $a_0(z)$ and $a_1(z)$ are the amplitudes of the forward traveling waves, normalized so that $|a_0|^2$ and $|a_1|^2$ represent power flow directly. We may think of the subscript 0 as always referring to the TE$_{01}$

mode. The complex constants γ_0 and γ_1 may be regarded as (modified) propagation constants; note that because of the coupling they are not necessarily equal to the propagation constants of the uncoupled modes. The coupling coefficient is denoted by κ; it will be real if the coupling mechanism is lossless, but is not required to be so in the general mathematical solution.

We are interested in the case in which line 0 contains unit power at $z = 0$, and line 1 contains no power. Subject to the initial conditions

$$a_0(0) = 1, \qquad a_1(0) = 0, \tag{59}$$

the solution of (58) is

$$a_0(z) = \left[\frac{1}{2} + \frac{(\gamma_0 - \gamma_1)}{2r} \right] e^{m_2 z} + \left[\frac{1}{2} - \frac{(\gamma_0 - \gamma_1)}{2r} \right] e^{m_1 z},$$

$$a_1(z) = \frac{i\kappa}{r} [e^{m_2 z} - e^{m_1 z}], \tag{60}$$

where

$$r = \sqrt{(\gamma_0 - \gamma_1)^2 - 4\kappa^2}, \tag{61}$$

and

$$m_1 = \tfrac{1}{2}[-(\gamma_0 + \gamma_1) + r],$$

$$m_2 = \tfrac{1}{2}[-(\gamma_0 + \gamma_1) - r]. \tag{62}$$

For the case of two propagating modes without loss, κ is real and we may write

$$\gamma_0 = i\beta_0, \qquad \gamma_1 = i\beta_1, \tag{63}$$

so that

$$r = i\sqrt{(\beta_0 - \beta_1)^2 + 4\kappa^2}. \tag{64}$$

A straightforward calculation now gives the power in each line at any point:

$$P_0 = |a_0(z)|^2 = 1 - \frac{4\kappa^2}{(\beta_0 - \beta_1)^2 + 4\kappa^2} \sin^2 \tfrac{1}{2}[(\beta_0 - \beta_1)^2 + 4\kappa^2]^{\frac{1}{2}} z,$$

$$P_1 = |a_1(z)|^2 = \frac{4\kappa^2}{(\beta_0 - \beta_1)^2 + 4\kappa^2} \sin^2 \tfrac{1}{2}[(\beta_0 - \beta_1)^2 + 4\kappa^2]^{\frac{1}{2}} z. \tag{65}$$

Hence the maximum power transferred from line 0 to line 1 is

$$(P_1)_{\max} = \frac{4\kappa^2}{(\beta_0 - \beta_1)^2 + 4\kappa^2} = \frac{[2\kappa/(\beta_0 - \beta_1)]^2}{1 + [2\kappa/(\beta_0 - \beta_1)]^2}, \tag{66}$$

and the points of maximum power transfer are

$$z = \frac{(2n + 1)\pi}{\sqrt{(\beta_0 - \beta_1)^2 + 4\kappa^2}}, \tag{67}$$

where n is any integer.

As is well known, complete power transfer from line 0 to line 1 is possible if and only if the (modified) phase constants β_0 and β_1 are equal. In general the maximum power transferred to line 1 depends on the ratio of the coupling coefficient to the difference in phase constants, and if this ratio is small, then

$$(P_1)_{max} \approx 4\kappa^2/(\beta_0 - \beta_1)^2. \tag{68}$$

If the difference in phase constants is not large enough to prevent undesirable power loss from line 0, an alternative possibility, as Miller[8] has shown, is to increase the attenuation constant of line 1 while leaving the attenuation constant of line 0 as nearly unchanged as possible. We can get an idea of the required attenuation difference from the following approximate treatment.

Let

$$\begin{aligned} \gamma_0 &= \alpha_0 + i\beta_0 , \\ \gamma_1 &= \alpha_1 + i\beta_1 , \end{aligned} \tag{69}$$

and assume that

$$| 2\kappa/(\gamma_0 - \gamma_1) |^2 \ll 1. \tag{70}$$

Then

$$r \approx \gamma_0 - \gamma_1 - \frac{2\kappa^2}{(\gamma_0 - \gamma_1)}, \tag{71}$$

and

$$\begin{aligned} m_1 &\approx -\gamma_1 - \frac{\kappa^2}{\gamma_0 - \gamma_1}, \\ m_2 &\approx -\gamma_0 + \frac{\kappa^2}{\gamma_0 - \gamma_1}. \end{aligned} \tag{72}$$

We are interested in the power in line 0. From the first of equations (60), we have

$$a_0(z) \approx \left[1 + \frac{\kappa^2}{(\gamma_0 - \gamma_1)^2} \right] e^{m_2 z} - \frac{\kappa^2}{(\gamma_0 - \gamma_1)^2} e^{m_1 z}. \tag{73}$$

Let us consider the case in which line 1 has a much higher attenuation constant than line 0; that is,

$$\alpha_1 \gg \alpha_0 . \tag{74}$$

The second term on the right side of (73) is provided with a small coefficient, and also its exponential factor decays much faster than the exponential in the first term. The second term, therefore, rapidly becomes negligible as z increases, and we may write,

$$a_0(z) \approx \left[1 + \frac{\kappa^2}{(\gamma_0 - \gamma_1)^2} \right] e^{\kappa^2 z/(\gamma_0 - \gamma_1)} e^{-\gamma_0 z}. \tag{75}$$

If the attenuation constant of line 0 is not modified* by the presence of the coupled lossy line 1, then in the absence of line 1 the amplitude of $a_0(z)$ would be $e^{-\alpha_0 z}$, and the factor by which the amplitude is reduced owing to the presence of line 1 is

$$\left| 1 + \frac{\kappa^2}{(\gamma_0 - \gamma_1)^2} \right| \, | e^{\kappa^2 z/(\gamma_0 - \gamma_1)} | . \tag{76}$$

The first factor on the right is very nearly unity, but not less than unity if κ is real (lossless coupling mechanism) and

$$(\alpha_1 - \alpha_0)^2 \geqq (\beta_1 - \beta_0)^2. \tag{77}$$

Hence the factor by which the amplitude is multiplied is not less than

$$\left| \exp \frac{\kappa^2 z}{\gamma_0 - \gamma_1} \right| = \exp \frac{(\alpha_0 - \alpha_1)\kappa^2 z}{(\alpha_0 - \alpha_1)^2 + (\beta_0 - \beta_1)^2}, \tag{78}$$

assuming that κ is real. If the amplitude of the wave on line 0 is not to be down by more than N nepers, after a distance z, from what it would have been in the absence of the coupled line, it suffices to have

$$\frac{(\alpha_1 - \alpha_0)\kappa^2 z}{(\alpha_1 - \alpha_0)^2 + (\beta_1 - \beta_0)^2} = N, \tag{79}$$

or

$$\alpha_1 - \alpha_0 = \tfrac{1}{2}[(\kappa^2 z/N) + \sqrt{(\kappa^2 z/N)^2 - 4(\beta_1 - \beta_0)^2}]. \tag{80}$$

2.2 TE_{01}–TM_{11} *Coupling in Plain and Compensated Bends*

In Jouguet's[1] and Rice's[2] analysis of propagation in a curved waveguide, the curvature is treated as a perturbation and the field com-

---

* The value of α_0 may very well be modified by the coupling; but if it is this can easily be taken into account when computing the over-all change in $| a_0(z) |$ due to the presence of line 1.

ponents are developed in powers of the small parameter a/b, but the field perturbations are not expressed in terms of the modes of the straight waveguide. We shall now consider propagation in plain and compensated bends from the coupled-mode viewpoint.

Denote the coefficient of coupling between the TE_{01} mode and the TM_{nm} mode or the TE_{nm} mode by

$$\kappa_{(nm)} = c_{(nm)} + d_{(nm)},$$
$$\kappa_{[nm]} = c_{[nm]} + d_{[nm]},$$

(81)

respectively, where as usual we indicate TM modes by enclosing the subscripts in *parentheses* and TE modes by enclosing the subscripts in *brackets*. In Part I the coupling coefficients are written with two pairs of subscripts, since in general they may refer to any two modes, but here one pair of subscripts would always be [01] and will be omitted. The coefficient c represents that part of the coupling (if any) which is due to the curvature of the guide, and d represents the coupling (if any) which is due to the inhomogeneity of the dielectric. We assume that the dielectric loading, if present, is symmetric with respect to the plane of the bend, so that coupling to only one polarization of each mode need be considered.

The phase constants of the TM_{nm} and TE_{nm} modes in a straight, empty guide are, respectively,

$$h_{(nm)} = \sqrt{\beta^2 - \chi_{(nm)}^2}, \qquad h_{[nm]} = \sqrt{\beta^2 - \chi_{[nm]}^2},$$

(82)

where

$$\chi_{(nm)} = k_{(nm)}/a, \qquad \chi_{[nm]} = k_{[nm]}/a,$$

(83)

and

$$J_n(k_{(nm)}) = 0, \qquad J_n'(k_{[nm]}) = 0.$$

(84)

Also

$$\beta = 2\pi/\lambda,$$

(85)

where λ is the free-space wavelength.

As noted in the preceding section, the presence of coupling may cause the modified phase constants $\beta_{(nm)}$ and $\beta_{[nm]}$ of the coupled modes to differ slightly from the unperturbed phase constants $h_{(nm)}$ and $h_{[nm]}$. In a plain bend (curvature coupling only), the β's are equal to the h's, and in most cases the effect of a small amount of dielectric coupling on the phase constants may be neglected. Exact values of $\beta_{[nm]}$ and $\beta_{(nm)}$ may be obtained if necessary from (40).

The coupling coefficient between the TE_{01} and TM_{11} modes in a plain bend is given by equation (46) as

$$c_{(11)} = \beta a / \sqrt{2} k_{[01]} b = 0.18454\ \beta a/b = 1.1595 a/\lambda b. \tag{86}$$

The (smallest) critical distance for maximum power transfer is given by (67) with $\beta_0 = \beta_1$, namely

$$z_{c_0} = \frac{\pi}{2 c_{(11)}} = \frac{k_{[01]} b \lambda}{2 \sqrt{2} a} = \frac{1.3547 b \lambda}{a}, \tag{87}$$

and the critical angle ϑ_{c_0} is

$$\vartheta_{c_0} = z_{c_0}/b = 1.3547\ \lambda/a \text{ radians} = 77.62\ \lambda/a \text{ degrees.} \tag{88}$$

This expression agrees, as it must, with that obtained by Jouguet and Rice. (We write ϑ_{c_0} for the uncompensated bend in order to reserve ϑ_c for a bend with dielectric loading.)

It should be pointed out that $c_{(11)}$ is not necessarily the largest of the coupling coefficients due to curvature. In a guide sufficiently far above cutoff, it appears from (49) that $c_{[11]}$ is approximately equal to $c_{(11)}$, and $c_{[12]}$ is one and two-thirds times as large as $c_{(11)}$. If two transmission lines are coupled over a distance z which is small compared to the distance required for maximum power transfer, then by (65) the relative power transferred to line 1 is

$$P_1(z) \approx \kappa^2 z^2, \tag{89}$$

which is proportional to the square of the coupling coefficient. It follows that for a sufficiently small bending angle the largest amount of power will go into the mode which has the largest coupling coefficient to TE_{01} (in the above example, TE_{12}). Each coupling coefficient, however, is proportional to $1/b$, and can be made as small as desired by increasing the radius of curvature of the bend. Since the phase constants are unaltered to first approximation by the curvature, the maximum power transferred tends to zero with $1/b^2$ for every mode whose unperturbed phase constant differs from $h_{[01]}$. The only mode with finite power transfer for a finite bending angle with an arbitrarily large bending radius is TM_{11}, since $h_{(11)} = h_{[01]}$. For the present we shall assume a bending radius so large that power transfer to modes other than TM_{11} is negligible. Complete power transfer from TE_{01} to TM_{11} will then take place in a plain bend at odd multiples of the critical bending angle ϑ_{c_0}.

We now consider a dielectric-loaded bend in which the permittivity ϵ is a function of the transverse coordinates (ρ, φ), but does not vary

from one cross section to another. The permeability μ is assumed to be constant. Thus we shall write, as in (25),

$$\mu = \mu_0 ,$$
$$\epsilon = \epsilon_0[1 + \delta(\rho, \varphi)], \tag{90}$$

and assume that

$$\frac{1}{S} \int_S |\delta| \, dS \ll 1, \tag{91}$$

where S is the cross-sectional area of the guide. The inequality (91) implies either that ϵ does not vary much over the cross section, or that it varies extensively over only a small part of the cross section. The first alternative corresponds to a dielectric whose relative permittivity differs but little from unity, and is the most likely case in practice. If, on the other hand, δ is large in a small region (a thin sliver of high-permittivity material), the dielectric coupling coefficients will not diminish very rapidly with increasing mode number. The TE_{01} mode will be appreciably coupled to a large number of modes, and it may not be safe to assume that the total power converted into spurious modes is small just because the conversion into any given mode is small. We shall not try to decide here what maximum value of $|\delta|$ is practicable.

If the distribution of dielectric is symmetric with respect to the plane of the bend, the dielectric couples the TE_{01} mode to a definite polarization of each spurious mode, and in particular to the same polarization of the TM_{11} mode that is coupled by curvature alone.* The dielectric coupling coefficient between TE_{01} and TM_{11} is, from (50) and (51),

$$d_{(11)} = \frac{\beta}{\sqrt{2}\pi a k_{[01]} J_0^{\,2}(k_{[01]})} \int_S \delta(\rho, \varphi) J_1^{\,2}(\chi_{[01]}\rho) \frac{\cos\varphi}{\rho} \, dS. \tag{92}$$

It is obvious that the *decoupling condition*, namely:

$$\kappa_{(11)} \equiv c_{(11)} + d_{(11)} = 0, \tag{93}$$

may be satisfied by an infinite number of different distributions of permittivity. Ingenuity is required, however, to find a configuration which is easy to fabricate and which does not couple the TE_{01} mode too strongly to any other mode in the guide. The spurious mode problem is quite serious when the diameter of the guide (in wavelengths) is so large that

---

* A dielectric insert which is not symmetric with respect to the plane of the bend will couple TE_{01} to the other polarization of TM_{11}, with potentially complete power transfer to this mode on account of the equality of phase velocities. A small accidental lack of symmetry should not lead to serious mode conversion in a bend of moderate angle.

many modes have phase velocities close to TE_{01}. In the next section we shall compute the coupling to various modes for a number of cases.

Mention may be made here of the effect of imperfect decoupling. If we could satisfy the decoupling condition (93) exactly, then to first order there would be no transfer of power from TE_{01} to TM_{11} in a bend of any angle. In practice we cannot expect to satisfy (93) exactly, on account of uncertainties in the permittivity and dimensions of the compensator. If the coupling coefficients are constant along the bend, the effect of reducing $\kappa_{(11)}$ by making $d_{(11)}$ nearly equal and opposite to $c_{(11)}$ is to increase the distance required for maximum power transfer to TM_{11} to take place. In the simple case where $\beta_{(11)} = \beta_{[01]}$, as, for example, when the compensator is made of a bent half-cylinder of dielectric, the critical angle for a fixed bend radius is inversely proportional to $\kappa_{(11)}$. The critical angle ϑ_c for an imperfectly compensated bend, in terms of the critical angle ϑ_{c_0} for an uncompensated bend, is

$$\vartheta_c = \left| \frac{c_{(11)}}{c_{(11)} + d_{(11)}} \right| \vartheta_{c_0} . \tag{94}$$

If $d_{(11)}$ can be made equal and opposite to $c_{(11)}$ within 1 per cent, say, then $\vartheta_c = 100 \, \vartheta_{c_0}$. The power transferred in a bend of angle ϑ is simply proportional to $\sin^2 (\vartheta/\vartheta_c)$.

2.3 Various Compensator Designs

From now on we shall consider a compensated bend in which the TE_{01} and TM_{11} modes are completely decoupled, and we shall investigate the coupling between TE_{01} and spurious modes. (By "spurious mode" we mean any mode of the straight round guide except TE_{01} or TM_{11}.) We shall assume that the power in all spurious modes is everywhere low compared to the power level of TE_{01}. To first order, therefore, we may compute the power abstracted from TE_{01} by mode conversion by assuming that the TE_{01} mode crosstalks into each spurious mode independently. In practice the crosstalk is greatest into modes whose phase velocities are nearest to the phase velocity of TE_{01}; and it seems more than adequate, at least for foam dielectric compensators, to consider about a dozen modes.

From (68), the maximum relative power (assumed small) which crosstalks from TE_{01} into a given spurious mode is

$$(P_1)_{\max} \approx [2\kappa/(\beta_0 - \beta_1)]^2, \tag{95}$$

where κ is the total coupling coefficient. For all spurious modes we assume that the difference in phase constants is not much changed by

the dielectric loading; this assumption obviates the somewhat laborious calculation of β_1 for each spurious mode from (40). Thus,

$$\beta_0 - \beta_1 \approx h_0 - h_1, \tag{96}$$

and a good estimate of the maximum power which crosstalks into any spurious mode is

$$(P_1)_{\max} \approx [2(c + d)/(h_0 - h_1)]^2. \tag{97}$$

If the form and dimensions of a bend compensator are fixed, and the TE_{01}—TM_{11} decoupling condition is assumed to be met by adjusting the permittivity, it turns out that the maximum power which crosstalks into a given mode is proportional to $(a/b)^2$. It is thus easy to calculate the bending radius which makes $(P_1)_{\max}$ for any given mode equal to a (small) preassigned value. The total power abstracted from the TE_{01} mode by mode conversion will be a complicated, fluctuating function of distance along the bend, or of frequency at a fixed distance, because of the different critical distances for maximum power transfer into the different spurious modes, but we can get an idea of the minimum tolerable bending radius by considering just the crosstalk into the one or two most troublesome modes.

It seems likely that with present-day dielectrics at millimeter wavelengths, dielectric losses in a compensated bend will be comparable to mode conversion losses. For this reason an estimate of dielectric losses is given in connection with each type of compensator design discussed below.

2.3.1 *The Geometrical Optics Solution*

An obvious way to design a bend compensator on paper is to load the bend with a medium of continuously varying permittivity for which*

$$\delta = -2(\rho/b) \cos \varphi. \tag{98}$$

This may be called the geometrical optics solution of the bend problem, since to first order it equalizes the optical length of all circular paths which are coaxial with the curved center line of the waveguide. Physically the required variation of permittivity is rather simple; the permittivity at each point depends only on the distance of the point from a line through the center of curvature perpendicular to the plane of the bend. An attempt to indicate this variation by shading has been made

---

* In order that the relative permittivity of the medium be nowhere less than unity, the constant ϵ_0 in the expression $\epsilon = \epsilon_0(1 + \delta)$ must be greater than the permittivity of free space; but this does not affect the analysis in any way.
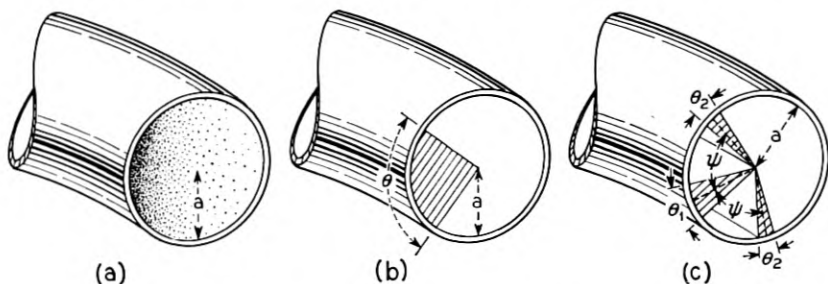
Fig. 2 — Various bend compensators.

in Fig. 2(a). One could approximate the continuous variation with a laminated structure consisting of a number of layers of different permittivities, the permittivity varying slightly from one layer to the next.

Although the geometrical optics approach provides a very good theoretical solution to the bend problem, it does not lead to a perfect compensator. It is shown at the end of this section that a perfect compensator, in the sense of one which does not couple TE_{01} to any other mode at any frequency, does not exist. The geometrical optics compensator couples the same modes to TE_{01} that are coupled by the curvature of the bend itself, namely TM_{11} and the TE_{1m} family; but the coupling coefficients of the various modes are not in exactly the same ratios. Thus if δ is given by (98), the net coupling between TE_{01} and TM_{11} in the compensated bend is zero, but there will be a small residual coupling between TE_{01} and each of the TE_{1m} modes.

The curvature coupling coefficients are given by (49). Table I contains numerical values which have been worked out for $\beta a = 12.930$ and $\beta a = 29.554$, corresponding respectively to guide diameters of $\frac{7}{8}$ inch and 2 inches at an operating wavelength of 5.4 mm.

Dielectric coupling coefficients can be worked out without much dif-

TABLE I — COUPLING COEFFICIENTS AND POWER TRANSFER
IN GEOMETRICAL OPTICS COMPENSATOR

Mode	$\beta a = 12.930$			$\beta a = 29.554$		
	c	d	$2\frac{(c+d)}{(h_0 - h_1)}$	c	d	$2\frac{(c+d)}{(h_0 - h_1)}$
TM_{11}	$2.386/b$	$-2.386/b$	—	$5.454/b$	$-5.454/b$	—
TE_{11}	$2.344/b$	$-2.479/b$	$0.600a/b$	$5.480/b$	$-5.537/b$	$0.597a/b$
TE_{12}	$3.759/b$	$-4.318/b$	$-1.962a/b$	$9.092/b$	$-9.322/b$	$-1.954a/b$
TE_{13}	$0.306/b$	$-0.420/b$	$-0.087a/b$	$0.793/b$	$-0.834/b$	$-0.083a/b$

ficulty from (50), (51), and (98). The first few coefficients are:

$$d_{(11)} = -0.18454\beta a/b,$$

$$d_{[11]} = -\frac{0.18638(\beta a)^2/b}{\sqrt{h_{[01]}ah_{[11]}a}},$$

$$d_{[12]} = -\frac{0.31150(\beta a)^2/b}{\sqrt{h_{[01]}ah_{[12]}a}}, \tag{99}$$

$$d_{[13]} = -\frac{0.02751(\beta a)^2/b}{\sqrt{h_{[01]}ah_{[13]}a}}.$$

Some numerical values are recorded in Table I.

The phase constant of any mode in the compensated bend is equal to the phase constant of the same mode in a guide filled with material of constant permittivity ϵ_0. We may therefore set $\beta_{[01]} - \beta_{[1m]}$ equal to $h_{[01]} - h_{[1m]}$. Strictly speaking, λ is then the wavelength of a free wave in a medium of permittivity ϵ_0; but ϵ_0 differs little from the permittivity of vacuum if the compensator is made from a foam dielectric. The ratio of total coupling coefficient to difference in phase constants, namely $2(c + d)/(h_0 - h_1)$, which determines the maximum power transfer by (97), is given in Table I for the $\frac{7}{8}$-inch and 2-inch guides at $\lambda = 5.4$ mm.

For large βa the leading terms in $c_{[1m]}$ and $d_{[1m]}$, which are proportional to βa, cancel each other, and $c_{[1m]} + d_{[1m]}$ decreases like $1/\beta a$. The difference in phase constants, $h_{[01]} - h_{[1m]}$, is also proportional to $1/\beta a$ for large βa. Hence the ratio of coupling coefficient to difference in phase constants approaches a finite limit as βa approaches infinity; to three decimal places the limiting values are the same as those given in Table I for $\beta a = 29.554$.

If we choose a sufficiently large value of a/b, the maximum power transferred to a given mode may be made to approach any preassigned small value as λ/a approaches zero. *This is a special property of the geometrical optics compensator.* For other compensator designs $c + d$ will be of the order of βa while $h_0 - h_1$ will be of the order of $1/\beta a$, so that $2(c + d)/(h_0 - h_1)$ will tend to infinity like $(\beta a)^2$. Hence in the short-wavelength limit the bend output will be a jumble of modes all at comparable power levels. Practically, one must expect the same end result with a geometrical optics compensator, because of the impossibility of meeting exact mathematical specifications; but a carefully-designed geometrical optics compensator should work satisfactorily up to a considerably higher frequency than any other type.

To get an idea of tolerable bending radii with a geometrical optics compensator, we shall calculate the radius at which the maximum mode conversion loss from TE_{01} into TE_{12} (the worst spurious mode) is 0.1 db. Setting $P_1 = 0.02276$, we find from (68) that the minimum bending radius for a $\frac{7}{8}$-inch guide is 5.69 inches, and for a 2-inch guide, 12.95 inches, both at a wavelength of 5.4 mm. It is worth noting that if $| d_{[12]} |$ is increased by 5 per cent of its theoretical value, the minimum bending radius becomes 7.89 inches for the $\frac{7}{8}$-inch guide and 39.2 inches for the 2-inch guide. (This assumes that the TM_{11} mode is still properly de-coupled and that TE_{12} is still the worst spurious mode.)

Dielectric losses are likely to be a serious problem in a geometrical optics compensator, inasmuch as the whole volume of the bent guide has to be filled with dielectric. Relatively large values of δ are required to negotiate bends as sharp as those just discussed. For example, if $b = 13a$, in a practical case δ might range from 0.058 at the inner surface of the bend to 0.250 at the center of the guide to 0.442 at the outer surface (referred to ϵ_0 as the permittivity of free space). The loss tangent of present-day dielectrics in this range is approximately 2×10^{-4}. A large (i.e., far above cutoff) waveguide filled with a dielectric of relative permittivity 1.25 and loss tangent 2×10^{-4} will show a dielectric loss of about 1.13 db/meter or 0.34 db/ft at 5.4 mm. The dielectric loss in a $90°$ bend with a bending radius of 1 foot would be about 0.54 db, and for other bends the loss would be directly proportional to the length of the bend, and to the loss tangent if different from 2×10^{-4}. It is true that loss tangents as low as 5×10^{-5} may be obtained with lower values of permittivity, say $\delta = 0.033$; but with such a small δ the bend radius must be proportionately larger, and the total dielectric losses in a bend of given angle would be larger than with a higher permittivity material.

We proceed now to demonstrate the assertion made earlier that a perfect bend compensator does not exist. More precisely, we shall show that it is impossible to compensate the bend with an isotropic medium whose permittivity and permeability are everywhere finite, but otherwise arbitrary, in such a way that there is no conversion from TE_{01} to any other mode at any point at any frequency.

If there is no mode conversion at any point of the bend then the fields at all points must be those of the TE_{01} mode, referred to the bent cylindrical coordinate system described at the beginning of Section 1.1. In other words, we have prescribed the electromagnetic field and are asking whether it is possible to choose the permeability and permittivity so that the given field will satisfy Maxwell's equations. Usually the

answer to this question will be "No." The Maxwell equations,

$$\vec{\nabla} \times \vec{E} = -i\omega\mu\vec{H},$$
$$\vec{\nabla} \times \vec{H} = i\omega\epsilon\vec{E}, \tag{100}$$

are equivalent to six scalar equations, and if the components of E and $\vec{H}$ are prescribed, one cannot in general satisfy all these equations by merely adjusting the two scalar functions μ and ϵ.

It is particularly easy to see the difficulty for the TE_{01} mode in a curved guide. Recall that the TE_{01} mode fields are independent of the coordinate φ, and that the only non-vanishing field components are $E_\varphi(\rho, z)$, $H_\rho(\rho, z)$, and $H_z(\rho, z)$. The fourth of equations (5) is:

$$\frac{1}{\rho[1 + (\rho/b) \cos \varphi]} \left[\frac{\partial}{\partial \varphi} ([1 + (\rho/b) \cos \varphi]H_z) - \frac{\partial}{\partial z} (\rho H_\varphi) \right] \tag{101}$$
$$= i\omega\epsilon E_\rho .$$

Since $E_\rho = 0$, the right side of the equation is zero for any finite value of ϵ at any finite frequency, and the whole equation reduces to

$$- \frac{H_z \sin \varphi}{b + \rho \cos \varphi} = 0, \tag{102}$$

which can be true for all values of ρ and φ only if the radius of curvature of the bend is infinite. Hence a perfect compensator cannot be designed with *any* value of ϵ.

The practical importance of this result does not appear to be great, since theoretically the geometrical optics solution would provide an extraordinarily good compensator. Until one has a dielectric whose permittivity is continuously variable and precisely controllable, and whose loss tangent is very low, even this solution is of only academic interest.

2.3.2 The Single-Sector Compensator

In practice the simplest way to compensate a bend is to fill part of the cross section of the guide with homogeneous dielectric material of relative permittivity $(1 + \delta)$, and leave the remainder empty. In many cases a suitable shape for the cross section of the dielectric is a sector of a circle, inserted on the side of the guide nearest the center of curvature of the bend, and symmetrically placed with respect to the plane of the bend. Such a sector, of total angle θ, is shown in Fig. 2(b). We shall now discuss the properties of a single-sector compensator.

For future reference, the modified phase constants of the TE_{01} and TM_{11} modes may be calculated from (40) as:

$$\beta_{(11)} = h_{(11)} + \frac{\delta}{4\pi h_{(11)}} \left[(\theta - 0.29646 \sin \theta)\beta^2 \right.$$
$$\left. - (0.70354 \sin \theta)\chi_{(11)}^2 \right], \qquad (103)$$

$$\beta_{[01]} = h_{[01]} + \frac{\beta^2 \delta \theta}{4\pi h_{[01]}}.$$

The dielectric coupling coefficients for the single-sector compensator are given by (50) and (51), provided that some of the Bessel functions are integrated by Simpson's rule. In particular, the dielectric coupling coefficient between TE_{01} and TM_{11} is

$$d_{(11)} = -0.12066 \, \beta\delta \sin \theta/2. \qquad (104)$$

Substituting (86) and (104) into (93), we obtain *the decoupling condition for a single-sector compensator*, namely

$$\delta = \frac{1.5295}{\sin \theta/2} \frac{a}{b}. \qquad (105)$$

No circular magnetic modes (TM_{0m}) and no higher circular electric modes (TE_{02}, TE_{03}, etc.) are coupled to TE_{01} by the single-sector compensator. We also observe that the coupling coefficients of the TE_{1m} and TM_{1m} modes do not depend upon the sector angle θ so long as δ and θ are related by (105). This is because these modes have the same angular dependence as the TM_{11} mode, which we are trying to compensate.

The most troublesome spurious modes are those whose phase velocities are closest to TE_{01}, namely TE_{21} and TE_{31}. The coupling coefficients and power transfer ratios for these two modes in $\frac{7}{8}$-inch and 2-inch guide are given in Table II. Either of these modes could be decoupled by proper choice of the sector angle, provided we had a uniform, low-dissipation dielectric with the required value of δ, but it is impossible to decouple both modes at once with a single sector. As a compromise, we might adopt the sector angle which equalizes the maximum power transferred to TE_{21} and TE_{31} (the distances for maximum power transfer are of course not the same for the two modes). This angle is approximately 144°.

Suppose we wish to employ a 144° sector in a $\frac{7}{8}$-inch guide at 5.4 mm. If the criterion is that TE_{01} is to lose a maximum of 0.1 db each to TE_{21} and TE_{31}, so that the total mode conversion losses are of the order of 0.2

TABLE II — COUPLING COEFFICIENTS AND POWER TRANSFER TO TE_{21} AND TE_{31} MODES DUE TO SINGLE-SECTOR COMPENSATOR

Mode	$\beta a = 12.930$		$\beta a = 29.554$	
	d	$2d/(h_0 - h_1)$	d	$2d/(h_0 - h_1)$
TE_{21}	$\dfrac{1.1152}{b}\dfrac{\sin\theta}{\sin\theta/2}$	$-10.38\dfrac{a}{b}\dfrac{\sin\theta}{\sin\theta/2}$	$\dfrac{2.4727}{b}\dfrac{\sin\theta}{\sin\theta/2}$	$-54.23\dfrac{a}{b}\dfrac{\sin\theta}{\sin\theta/2}$
TE_{31}	$-\dfrac{0.6579}{b}\dfrac{\sin 3\theta/2}{\sin\theta/2}$	$-10.89\dfrac{a}{b}\dfrac{\sin 3\theta/2}{\sin\theta/2}$	$-\dfrac{1.4426}{b}\dfrac{\sin 3\theta/2}{\sin\theta/2}$	$-56.91\dfrac{a}{b}\dfrac{\sin 3\theta/2}{\sin\theta/2}$

db, then the bending radius can be 19.5 inches. The corresponding value of δ is 0.036.

If we try to use a 144° sector in a 2-inch guide at 5.4 mm, with the same mode conversion criterion as before, the bending radius must be so large that no currently available dielectric has a small enough value of δ to satisfy the decoupling condition. We are therefore forced to use a smaller sector angle. With a sector of small angle, TE_{31} is the worst spurious mode. It turns out that if $\delta = 0.033$ and if TE_{01} is not to lose more than 0.1 db by conversion into TE_{31}, the minimum bending radius is 1131 inches or 94.3 feet, and the corresponding sector angle is 4.70°.

An approximate formula for the attenuation constant due to dielectric losses in a single-sector compensator is given by (57), provided that δ is small. The result is

$$\alpha_d = \frac{\beta^2(1 + \delta)\tan\varphi}{2h_{[01]}}\frac{\theta°}{360} \text{ nepers/meter,} \qquad (106)$$

where $\tan\varphi$ is the loss tangent of the dielectric, and $\theta°$ is the sector angle in degrees. As numerical examples, we find that the dielectric loss at 5.4 mm in a $\frac{7}{8}$-inch guide compensated with a 144° sector having $\delta = 0.036$, $\tan\varphi = 5 \times 10^{-5}$, amounts to 0.085 db in a 90° bend of radius 19.5 inches. In a 2-inch guide compensated with a 4.70° sector ($\delta = 0.033$, $\tan\varphi = 5 \times 10^{-5}$), the dielectric loss is 0.155 db in a 90° bend of radius 94.3 feet.

2.3.3 The Three-Sector Compensator

Although the single-sector compensator should work well in a guide which will propagate only 40 to 50 modes, it does not look so promising for a 200- to 300-mode guide, chiefly because of the unavoidable crosstalk into TE_{21} and/or TE_{31}. We are therefore led to consider the design of a

three-sector compensator which will not couple either TE$_{21}$ or TE$_{31}$ to TE$_{01}$.

A three-sector compensator is shown schematically in Fig. 2(c). The angle of the center sector is called θ_1 and the angle of each outer sector θ_2 . Each outer sector makes an angle ψ, measured between center planes, with the center sector.

The condition for decoupling TE$_{01}$ from TM$_{11}$ with the three-sector compensator is

$$\delta = \frac{1.5295}{(2 \cos \psi \sin \theta_2/2 + \sin \theta_1/2)} \frac{a}{b} . \tag{107}$$

If δ and a/b are given, two additional conditions may be imposed upon θ_1 , θ_2 , and ψ. The conditions are taken to be:

$$2 \cos 2\psi \sin \theta_2 + \sin \theta_1 = 0,$$
$$2 \cos 3\psi \sin 3\theta_2/2 + \sin 3\theta_1/2 = 0. \tag{108}$$

If equations (108) are satisfied, the compensator does not couple TE$_{01}$ to any modes of the TE$_{2m}$, TE$_{3m}$, TM$_{2m}$, or TM$_{3m}$ families.

To design a three-sector compensator with given values of a/b and δ, one can solve (107) and (108) numerically for θ_1 , θ_2 , and ψ. However, if θ_1 is small ($\leq 20°$, for example), a simpler design procedure may be used. The following equations are approximately true:

$$\theta_1 = \frac{126.8a}{b\delta} \text{ degees},$$
$$\theta_2 = 0.618\theta_1 , \tag{109}$$
$$\psi = 72°.$$

It should perhaps be pointed out that the precision of θ_1 , θ_2 , and ψ individually is not critical, since there is no necessity for the coupling to TE$_{21}$ and TE$_{31}$ to be exactly zero, so long as it is reasonably small. One should, however, strive to make the TE$_{01}$–TM$_{11}$ coupling as nearly zero as possible, and it is therefore important to satisfy (107) with the greatest possible precision.

Expressions for the dielectric coupling coefficients due to the three-sector compensator may be obtained from those for the single-sector compensator if we merely replace $\sin n\theta/2$, wherever it occurs, by $\sin n\theta_1/2 + 2 \cos n\psi \sin n\theta_2/2$, where n is the angular mode index, as usual. If θ_1 , θ_2 , and ψ satisfy (108), then the coupling to TE$_{2m}$, TE$_{3m}$, TM$_{2m}$, and TM$_{3m}$ is zero, and the mode having the largest value of $2(c + d)/(h_0 - h_1)$ is TE$_{12}$. As noted earlier, since the fields of TM$_{11}$

TABLE III — COUPLING COEFFICIENT AND POWER TRANSFER
TO TE_{12} MODE DUE TO THREE-SECTOR COMPENSATOR

Mode	$\beta a = 12.930$			$\beta a = 29.554$		
	c	d	$2 \frac{(c+d)}{(h_0 - h_1)}$	c	d	$2 \frac{(c+d)}{(h_0 - h_1)}$
TE_{12}	$3.7591/b$	$-3.0334/b$	$2.549a/b$	$9.0919/b$	$-6.5491/b$	$21.59a/b$

and TE_{12} have the same angular dependence, the coupling to TE_{12} is
independent of the number and arrangement of sectors used in the com-
pensator so, long as the decoupling condition for TM_{11} is satisfied. Nu-
merical values are given in Table III.

The formula analogous to (106) for the attenuation constant due to
dielectric loss in a three-sector compensator is

$$\alpha_d = \frac{\beta^2 (1 + \delta) \tan \varphi}{2 h_{[01]}} \frac{(\theta_1° + 2\theta_2°)}{360°} \text{ nepers/meter.} \qquad (110)$$

As a numerical example, let us design a three-sector compensator for
a $\frac{7}{8}$-inch guide at 5.4 mm. Under the requirement that the TE_{01} loss due
to conversion into TE_{12} must not be greater than 0.1 db, the minimum
bending radius is 7.39 inches. If the angles are *

$$\theta_1 = 60°,$$

$$\theta_2 = 30°,$$

$$\psi = 75°,$$

the value of δ should be 0.143, which is not difficult to obtain with foam
dielectrics. Assuming a loss tangent of 2×10^{-4} we find that dielectric
losses in a 90° bend are about 0.12 db.

As a second example, for a 2-inch guide at 5.4 mm with the same mode
conversion criterion, one needs a bending radius of 143.1 inches or 11.92
feet. With $\delta = 0.033$, the compensator angles are

$$\theta_1 = 27.6°,$$

$$\theta_2 = 16.4°,$$

$$\psi = 72.5°;$$

---

* It is not practicable to use larger angles, because if $\theta_1 > 60°$ portions of the
outer sectors counteract the effect of the rest of the compensator on TM_{11}, and
dielectric losses make the design inefficient.

and if $\tan \varphi = 5 \times 10^{-5}$, the dielectric loss in a 90° bend is about 0.25 db.

2.4 *Can Dissipation Be Used to Discourage Spurious Modes?*

It was shown in Section 2.1 that the effect of markedly increasing the attenuation constant of one of two coupled transmission lines is to reduce the over-all attenuation of a wave introduced on the other line. One might wonder whether it would be practicable to decrease the permissible radius of a compensated bend by introducing loss into the spurious modes. The answer is "No", at least for guides large enough to propagate 200 to 300 modes at the operating wavelength. One simply cannot get the required magnitude of loss into the spurious modes without simultaneously introducing intolerable loss into TE_{01}. A numerical example will make this clear.

We found in Section 2.3.3 that with a three-sector compensator in 2-inch guide at 5.4 mm it would be possible to negotiate a bend of radius about 12 feet with a maximum loss of 0.1 db by mode conversion to TE_{12} (the worst spurious mode). Let us now ask what the attenuation constant of TE_{12} would have to be if we wished to transmit around a bend of radius 6 feet with a three-sector compensator, and have the mode conversion loss suffered by TE_{01} not greater than 0.1 db in a 90° bend. Preparing to substitute into (80) of Section 2.1, we have the following values:

$$b = 72 \text{ inches},$$

$$\kappa_{[12]} = c_{[12]} + d_{[12]} = 2.54/b = 0.0353 \text{ in}^{-1},$$

$$z = \pi b/2 = 113.1 \text{ inches},$$

$$\beta_0 - \beta_1 \approx h_0 - h_1 = 0.236 \text{ radians/inch},$$

$$N = 0.1 \text{ db} = 0.0115 \text{ nepers}.$$

From (80) we get

$$\alpha_{[12]} - \alpha_{[01]} = 12.2 \text{ nepers/inch} \approx 4200 \text{ db/meter}.$$

Since the maximum TE_{12} attenuation which can be achieved in a 2-inch guide by a mode filter which transmits TE_{01} freely is of the order of 10 db/meter,* the value of $\alpha_{[12]}$ called for by the above calculation is obviously out of the question.

---

* This estimate is based on calculations described in Reference 6 for modes in a helix surrounded by a lossy sheath; but it is doubtful that much greater loss could be produced by other types of filter, such as resistance card "killers".

It should be noted that a moderate amount of loss in the spurious modes may be worse than none, so far as the effect on TE_{01} is concerned. Miller[14] has shown that the total power dissipated in the system goes through a maximum when $(\alpha_1 - \alpha_0)/\kappa \approx 2$. It appears that $\alpha_1 - \alpha_0$ must exceed κ by a couple of orders of magnitude before the loss in the driven line (i.e., TE_{01}) becomes really small, if we are counting on dissipation to counteract the coupling to spurious modes.

Since by use of the compensator we are attempting to make the $TE_{01} - TM_{11}$ coupling coefficient zero, we may expect that this coefficient, if not exactly zero, will at least be small compared to the coupling coefficients of spurious modes such as TE_{12}. Because $\kappa_{(11)}$ is very small, it may be that a practicable amount of loss in the TM_{11} mode would improve the performance of the bend. But in view of the preceding paragraph we must be careful, when introducing loss into TM_{11}, not to introduce the wrong amount of loss into some spurious mode which has a larger coupling coefficient to TE_{01}.

ACKNOWLEDGMENTS

APPENDIX

Compensation of a Gradual Bend by a Dielectric Insert in the Adjacent Straight Pipe

We shall discuss briefly three different ways of transmitting the TE_{01} mode around a plain (i.e., air-filled) bend with the aid of dielectric mode transducers inserted into the straight sections of guide on one or both sides of the bend. The first two methods involve converting the TE_{01} mode to a normal mode of the bend and reconverting to TE_{01} on the other side.[9] In the third method, the input to the bend is pure TE_{01}, and the output mixture of TE_{01} and TM_{11}, whatever it may be, is reconverted to TE_{01} by a dielectric transducer.

A.1 *The TM_{11}' Normal Mode Solution*

One of the normal modes of the bend is a pure TM_{11} mode (TM_{11}') which is polarized at right angles to the TM_{11} mode (TM_{11}'') that the bend couples to TE_{01}. Clearly if one has a transducer in a straight guide which converts TE_{01} entirely to TM_{11}, it is a mere matter of rotating the

transducer about the guide axis to insure that the polarization which enters the bend is TM_{11}'. We shall design such a transducer using a dielectric sector in a straight pipe.

From Section 2.1, for complete power transfer from TE_{01} to TM_{11} we must have

$$\beta_{[01]} - \beta_{(11)} = 0; \tag{111}$$

the transfer then takes place in a distance

$$l = \pi/2 \mid \kappa_{(11)} \mid . \tag{112}$$

The modified phase constants $\beta_{[01]}$ and $\beta_{(11)}$ for a single dielectric sector of angle θ are given by (103) of Section 2.3.2. Substituting these values into (111), we find that the only condition under which it is satisfied is

$$\sin \theta = 0,$$
$$\theta = 180°. \tag{113}$$

The transducer must therefore be a half cylinder. From (104) we have

$$\kappa_{(11)} = d_{(11)} = -0.12066 \, \beta\delta, \tag{114}$$

and so (112) gives for the length of the transducer,

$$l = 2.072 \, \lambda/\delta. \tag{115}$$

The $TE_{01} - TM_{11}'$ transducer should be placed on either side of the diametral plane of the straight guide which lies in the plane of the bend. An exactly similar transducer on the other side of the bend will reconvert TM_{11}' into TE_{01} . Since TE_{01} and TM_{11} have the same velocity in a straight guide, the transducer can be made of a number of sections with arbitrary spacing and of total length l; but in practice one will not wish to have too long a run of TM_{11} in the empty guide because of the higher heat losses of this mode.

A.2 *The* $TE_{01} \pm TM_{11}''$ *Normal Mode Solution*

If we write the coupled wave equations for TE_{01} and TM_{11}'' in a plain bend in the form

$$\frac{da_0}{dz} + iha_0 + ica_1 = 0,$$
$$ica_0 + \frac{da_1}{dz} + iha_1 = 0, \tag{116}$$

where

$$h = h_{[01]} = h_{(11)},$$

$$c = c_{(11)},$$

(117)

it is evident that we can add and subtract to get the equivalent pair of equations:

$$\frac{d(a_0 + a_1)}{dz} + i(h + c)(a_0 + a_1) = 0,$$

$$\frac{d(a_0 - a_1)}{dz} + i(h - c)(a_0 - a_1) = 0.$$

(118)

Hence the normal modes of the curved guide are the combinations $a_0 \pm a_1$, or $\mathrm{TE}_{01} \pm \mathrm{TM}''$.

In order to launch only the normal mode $\mathrm{TE}_{01} + \mathrm{TM}_{11}''$ at the input of the bend, the amplitude of the other mode must be zero, or $a_0 = a_1$. Similarly, to launch only the mode $\mathrm{TE}_{01} - \mathrm{TM}_{11}''$, the condition is $a_0 = -a_1$. Hence the output of the normal mode transducer of length l, say, must be

$$a_0(l) = \pm a_1(l).$$

(119)

We return to the solution of the coupled line equations in Section 2.1 and write

$$\kappa = d_{(11)} = d,$$

$$\gamma_0 = i\beta_{[01]} = i\beta_0,$$

$$\gamma_1 = i\beta_{(11)} = i\beta_1,$$

$$r = is = i\sqrt{(\beta_0 - \beta_1)^2 + 4d^2}.$$

(120)

Then equations (60) of Section 2.1 become:

$$a_0(l) = \left[\cos \tfrac{1}{2}sl - i \frac{(\beta_0 - \beta_1)}{s} \sin \tfrac{1}{2}sl \right] e^{-\frac{1}{2}i(\beta_0 + \beta_1)l},$$

$$a_1(l) = -i \frac{2d}{s} \sin \tfrac{1}{2}sl \; e^{-\frac{1}{2}i(\beta_0 + \beta_1)l}.$$

(121)

Substituting into (119) and equating real and imaginary parts gives:

$$l = \pi/s,$$

(122)

$$|\beta_0 - \beta_1| = |2d|.$$

(123)

In view of (103) and (104) of Section 2.3.2, (123) is equivalent to

$$\cos \theta/2 = \frac{\pm\sqrt{1 - \nu^2}}{0.4640\nu^2 + 0.1955},$$ (124)

and (122) becomes

$$l = \frac{1.465\lambda}{\delta \, | \sin \theta/2 |},$$ (125)

where

$$\nu = \lambda/\lambda_c = 3.8317 \, \lambda/2\pi a$$ (126)

is the cutoff ratio for TE_{01} and TM_{11} waves in a straight, empty guide.

A TE_{01} to $TE_{01} \pm TM_{11}''$ mode transducer may thus consist of a dielectric sector, attached to the surface of the straight guide on the side nearest the center of curvature of the bend, if the angle of the sector satisfies (124) and the length satisfies (125). However, the condition (124) can be satisfied by a real angle only if

$$0.8483 \leqq \lambda/\lambda_c \leqq 1;$$ (127)

that is, only if the guide is very near cutoff; and the value of θ which satisfies (124) varies rapidly with λ over the above range. This form of normal mode transducer is therefore too narrow band to be of much practical interest.

A.3 *A Broadband Compensator*

We shall now show how to design a dielectric compensator, in a straight section of guide, which takes the mixture of TE_{01} and TM_{11}'' put out by an adjacent bend and reconverts it to pure TE_{01}, independent of frequency.

First let us write the solution of (116) for a plain bend in terms of arbitrary initial values $a_0(0)$ and $a_1(0)$. We have

$$\begin{aligned}
a_0(z) + a_1(z) &= [a_0(0) + a_1(0)]e^{-ihz-icz}, \\
a_0(z) - a_1(z) &= [a_0(0) - a_1(0)]e^{-ihz+icz},
\end{aligned}$$ (128)

and hence

$$\begin{aligned}
a_0(z) &= [a_0(0) \cos cz - ia_1(0) \sin cz]e^{-ihz}, \\
a_1(z) &= [-ia_0(0) \sin cz + a_1(0) \cos cz]e^{-ihz}.
\end{aligned}$$ (129)

The bend may be compensated with a dielectric-loaded straight guide,

provided that* $\beta_0 = \beta_1$ in the straight guide (this may be arranged, for example, by using a half-cylinder of dielectric), and provided that the length of the compensator and the coupling coefficient d are properly chosen. The amplitudes of the two modes in the straight guide, in terms of arbitrary initial values $a_0(0)$ and $a_1(0)$, are

$$a_0(z) = [a_0(0) \cos dz - ia_1(0) \sin dz]e^{-i\beta_0 z},$$
$$a_1(z) = [-ia_0(0) \sin dz + a_1(0) \cos dz]e^{-i\beta_0 z}. \tag{130}$$

Now suppose that the length of the bend is l_1 and the length of the compensator l_2, and take the origin of z at the input to the bend. A pure TE_{01} input is represented by

$$a_0(0) = 1,$$
$$a_1(0) = 0, \tag{131}$$

and so, applying (129) and (130) in succession,

$$a_0(l_1) = \cos cl_1 \, e^{-ihl_1},$$
$$a_1(l_1) = -i \sin cl_1 \, e^{-ihl_1}, \tag{132}$$

$$a_0(l_1 + l_2) = \cos (cl_1 + dl_2)e^{-i(hl_1+\beta_0 l_2)},$$
$$a_1(l_1 + l_2) = -i \sin (cl_1 + dl_2)e^{-i(hl_1+\beta_0 l_2)}. \tag{133}$$

The condition that all the power be in TE_{01} at the output of the compensator at every frequency is

$$cl_1 + dl_2 = 0, \tag{134}$$

or

$$dl_2 = -0.18454 \, \beta a l_1/b, \tag{135}$$

on referring to equation (86) of Section 2.2 for the value of c.

A convenient form of compensator would be a half cylinder of dielectric whose diametral plane is perpendicular to the plane of the bend. The coupling coefficient of the half cylinder is given by (104), and the condition for complete compensation becomes

$$l_2\delta = 1.5295 \, l_1a/b. \tag{136}$$

The most easily adjustable parameter is probably the length l_2 of the compensator.

---

* The necessity for $\beta_0 = \beta_1$ is apparent if we consider that under certain conditions the bend may put out a pure TM_{11}'' mode, and complete reconversion is possible only if the compensator has $\beta_0 = \beta_1$.

We have analyzed the compensator as if it were all on one side of the bend; but it may evidently be divided into sections of total length l_2 which are distributed arbitrarily on both sides of the bend. An obvious configuration would be to put a section of length $l_2/2$ on each side of the bend immediately adjacent to it.

Limitations on the usefulness of this kind of compensator will be dielectric losses and mode conversions. The former can presumably be reduced as the dissipation of available dielectrics is reduced. Mode conversions could be calculated by the general methods of Part I, but one would have to work out the values of the coupling coefficients between TM_{11} and all other modes, which has not yet been done. In any case it is likely that the minimum tolerable bending radius would be no less than for the within-the-bend compensators discussed earlier in this paper.

REFERENCES

1. M. Jouguet, Cables & Transmission, **1,** pp. 133–153, 1947.
2. S. O. Rice, unpublished memorandum.
3. W. J. Albersheim, B. S. T. J., **28,** pp. 1–32, January, 1949.
4. S. E. Miller, Proc. I. R. E., **40,** pp. 1104–1113, September, 1952.
5. H. G. Unger, pp. 1253–1278, this issue.
6. S. A. Morgan and J. A. Young, B. S. T. J., **35,** pp. 1347–1384, November, 1956.
7. S. A. Schelkunoff, B. S. T. J., **31,** pp. 784–801, July, 1952.
8. S. E. Miller, B. S. T. J., **33,** pp. 661–719, May, 1954; especially pp. 677–692.
9. Reference 4, p. 1110.
10. S. A. Schelkunoff, *Electromagnetic Waves*, D. Van Nostrand Co., Inc., New York, 1943, pp. 12, 94.
11. Reference 7, pp. 786–791.
12. Reference 7, pp. 787–788.
13. S. O. Rice, B. S. T. J., **27,** pp. 305–349, April, 1948; especially p. 348.
14. Reference 8, pp. 692–693, Figs. 31 and 32.

Circular Electric Wave Transmission in a Dielectric-Coated Waveguide

By H. G. UNGER

(Manuscript received January 9, 1957)

The mode conversion from the TE_{01} wave to the TM_{11} wave which normally occurs in a curved round waveguide may be reduced by applying a uniform dielectric coat a few mils thick to the inner wall of the waveguide. Such a dielectric coat changes the phase constant of the TM_{11} wave without affecting appreciably the phase and attenuation constants of the TE_{01} wave. Thus, relatively sharp bends can be negotiated to change the direction of the line or deviations from straightness can be tolerated. For each of these two cases a different optimum thickness of the dielectric coat keeps the TE_{01} loss at a minimum. At 5.4-mm wavelength a bending radius of 8 ft in a $\frac{7}{8}$-inch pipe or 50 ft in a 2-inch pipe can be introduced with 0.2 db mode conversion loss. Deviations from straightness corresponding to an average bending radius of 300 ft can be tolerated in a 2-inch pipe at 5.4-mm wavelength with an increase in TE_{01} attenuation of 5 per cent. Serpentine bends caused by equally spaced supports of the pipe may, however, increase the mode conversion and cause appreciable loss at certain discrete frequencies. Compared with the plain waveguide the dielectric-coated guide behaves more critically in such serpentine bends. The mode conversion from TE_{01} to the TE_{02}, TE_{03}, $\cdots$ waves at transitions from a plain waveguide to the dielectric-coated guide is usually very small.

I. INTRODUCTION

In a curved section of cylindrical waveguide the circular electric wave couples to the TE_{11}, TE_{12}, TE_{13} $\cdots$ modes and to the TM_{11} mode.[1] The coupling to the TM_{11} mode presents the most serious problem since the TE_{01} and TM_{11} modes are degenerate, in that they have equal phase velocities in a perfectly conducting straight guide. In a bend all TE_{01} power introduced at the beginning will be converted to the TM_{11} power at odd multiples of a certain critical bending angle. One can reduce this complete power transfer by removing the degeneracy between TE_{01} and

TM_{11} modes. The finite conductivity of the walls introduces a slight difference in the propagation constants and in a 2-inch pipe at 5.4 mm wavelength a bending radius of a few miles can be tolerated with about double the attenuation constant of the TE_{01} wave. To get more difference in the phase constants of the TM_{11} and TE_{01} modes, one might consider a dielectric layer next to the wall of the waveguide. Since the electric field intensity of the TE_{01} mode goes to zero at the wall but the electric field intensity of the TM_{11} mode has a large value there, one might expect a larger effect of the dielectric layer on the propagation characteristics of the TM_{11} wave than on the TE_{01} wave.

In doing this, however, one has to be aware of the influence the dielectric layer will have on the propagation characteristics of the TE_{1m} modes which also couple to the TE_{01} wave in curved sections. The TE_{12} wave couples most strongly to the TE_{01} wave and of the TE_{1m} family it is the next above the TE_{01} wave in phase velocity. With the dielectric layer one has to expect this difference in phase velocity to be decreased and consequently the mode conversion to the TE_{12} wave to be increased.

In the next section we will solve the characteristic equation of the cylindrical waveguide with a dielectric layer for the normal modes and arrive at approximate formulas for the phase constants. We will also compute the increase in attenuation of the normal modes as caused by the dielectric losses in the layer. The change in wall current losses as caused by the dielectric layer is of importance here only for the TE_{01} wave and we will calculate it only for this wave.

In order to know what bending radii can be tolerated with a dielectric coat, we have to evaluate the coupled wave theory[2] for small differences in propagation constants between the coupled waves. This will be done in Section III. Especially we will consider serpentine bends which occur in any practical line with discrete supports. In that situation, at certain critical frequencies, when the supporting distance is a multiple of the beat wavelength between TE_{01} and a particular coupled wave, we will have to expect serious effects on the propagation constant of the TE_{01} wave.

In Section IV we will combine the results of Sections II and III and establish formulas and curves for designing circular electric waveguides with a dielectric coat. We will distinguish there between two different applications. The first case is to negotiate uniform bends of as small a radius as possible and the second is to tolerate large bending radii which may occur in a normally straight line.

At transitions from plain waveguide to the dielectric-coated guide, power of an incident TE_{01} wave will be partly converted into higher

TE_{om} waves. In Section V we shall calculate the power level in the TE_{om} waves resulting from this conversion.

II. THE NORMAL MODES OF THE DIELECTRIC-COATED WAVEGUIDE

The waveguide structure under consideration is shown in Fig. 1. To find the various normal modes existing in this structure, Maxwell's equations have to be solved in circular cylindrical coordinates in the air-filled region 1 and dielectric-filled region 2. The boundary conditions are: equal tangential components of the electric and magnetic field intensities at the boundary $(r = b)$ between regions 1 and 2 and, assuming infinite conductivity of the walls, zero tangential component of the electric field at the walls $(r = a)$. Upon introducing the general solutions into these boundary conditions, we get a homogeneous system of four linear equations in the amplitude factors. Non-trivial solutions of this system require the coefficient determinant to be zero. This condition is called the characteristic equation. Solutions of the characteristic equation represent the propagation constants of the various modes. These calculations have been carried out elsewhere,[3, 4] and the characteristic equation arrived at there has the following form:

$$
n^2 \left[\frac{1}{x_1^2} - \frac{1}{x_2^2} \right]^2 - \rho^2 \frac{x_2^2 - x_1^2}{x_2^2 - \epsilon x_1^2} \left[\frac{1}{x_1} \frac{J_n'(\rho x_1)}{J_n(\rho x_1)} + \frac{\epsilon}{\rho x_2^2} \frac{W_n(x_2, \rho x_2)}{U_n(x_2, \rho x_2)} \right]
$$

$$
\cdot \left[\frac{1}{x_1} \frac{J_n'(\rho x_1)}{J_n(\rho x_1)} + \frac{1}{\rho x_2^2} \frac{V_n(x_2, \rho x_2)}{Z_n(x_2, \rho x_2)} \right] = 0.
\tag{1}
$$
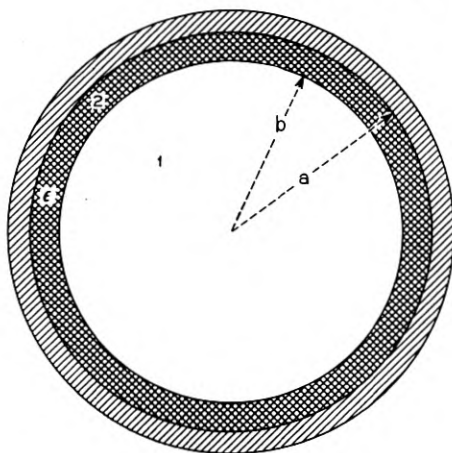

FIG. 1 — The dielectric-coated waveguide; $\rho = b/a$, $\delta = 1 - \rho = (a - b)/a$.

Here we have used the following definitions:

$$
\begin{aligned}
U_n(x, \rho x) &= J_n(\rho x)N_n(x) - N_n(\rho x)J_n(x), \\
V_n(x, \rho x) &= \rho x^2[J_n{'}(\rho x)N_n{'}(x) - N_n{'}(\rho x)J_n{'}(x)], \\
W_n(x, \rho x) &= \rho x[J_n(x)N_n{'}(\rho x) - J_n{'}(\rho x)N_n(x)], \\
Z_n(x, \rho x) &= x[J_n{'}(x)N_n(\rho x) - J_n(\rho x)N_n{'}(x)].
\end{aligned}
\tag{2}
$$

J_n and N_n are cylinder functions of the first and second kind, respectively, and the prime marks differentiation with respect to the argument. The other symbols are:

$$
\begin{aligned}
\rho &= b/a \text{ ratio of radii}, \\
x_1 &= \xi_1 a, \\
x_2 &= \xi_2 a.
\end{aligned}
\tag{3}
$$

The relative dielectric constant of region 2 is indicated by ϵ which is assumed to be complex to take dielectric losses into account. The radial propagation constants ξ_1 and ξ_2 are related to the axial propagation constant γ and the free-space propagation constant $k = 2\pi/\lambda$ by

$$
\begin{aligned}
\xi_1^2 &= k^2 + \gamma^2, \\
\xi_2^2 &= \epsilon k^2 + \gamma^2.
\end{aligned}
\tag{4}
$$

The circumferential order of the solution is indicated by n.

For $n = 0$, equation (1) splits into the two equations

$$
\frac{1}{x_1}\frac{J_0{'}(\rho x_1)}{J_0(\rho x_1)} + \frac{\epsilon}{\rho x_2^2}\frac{W_0(x_2, \rho x_2)}{U_0(x_2, \rho x_2)} = 0,
\tag{5}
$$

and

$$
\frac{1}{x_1}\frac{J_0{'}(\rho x_1)}{J_0(\rho x_1)} + \frac{1}{\rho x_2^2}\frac{V_0(x_2, \rho x_2)}{Z_0(x_2, \rho x_2)} = 0
\tag{6}
$$

representing the TM_{om} and TE_{om} waves, respectively.

Except for $n = 0$ the solutions of (1) and the modes in the waveguide do not have transverse character as in the case of a uniformly filled waveguide. They are hybrid modes. However, it is reasonable to label them as TE_{nm} or TM_{nm}, according to the limit which they approach as the dielectric layer becomes very thin.[5]

Modes in the dielectric-coated guide with a very thin coat may be treated as perturbed TE_{nm} or TM_{nm} modes of the ideal circular waveguide. The perturbation terms are found by expanding (1) for small

values of $\delta = 1 - \rho$. This is done in Appendix 1. The perturbation of the propagation constants for the various normal modes is:

$$\mathrm{TM}_{nm} \quad \frac{\Delta\gamma}{\gamma_{nm}} = \frac{\epsilon - 1}{\epsilon}\,\delta, \tag{7}$$

$$\mathrm{TE}_{\substack{nm \\ n \neq 0}} \quad \frac{\Delta\gamma}{\gamma_{nm}} = \frac{n^2}{p_{nm}^2 - n^2}\,\frac{\epsilon - 1}{\epsilon(1 - \nu_{nm}^2)}\,\delta, \tag{8}$$

$$\mathrm{TE}_{om} \quad \frac{\Delta\gamma}{\gamma_{om}} = \frac{\epsilon - 1}{1 - \nu_{om}^2}\,\frac{p_{om}^2}{3}\,\delta^3. \tag{9}$$

In these equations p_{nm} is the mth root of $J_n(x) = 0$ for TM_{nm} waves and the mth root of $J_n'(x) = 0$ for TE_{nm} waves. Furthermore, $\nu_{nm} = \lambda/\lambda_{cnm}$ where $\lambda_{cnm} = 2\pi a/p_{nm}$.

We note that the change in propagation constant is of first order in δ for the TM_{nm} and TE_{nm} waves with $n \neq 0$, but of third order in δ for TE_{om} waves.

With $\epsilon = \epsilon' - j\epsilon''$ the perturbation of the propagation constant splits into phase perturbation $\Delta\beta$ and dielectric attenuation α_D. For a low loss dielectric we may assume $\epsilon'' \ll \epsilon'$ and get:

$$\mathrm{TM}_{nm} \quad \frac{\Delta\beta}{\beta_{nm}} = \frac{\epsilon' - 1}{\epsilon'}\,\delta,$$

$$\mathrm{TE}_{\substack{nm \\ n \neq 0}} \quad \frac{\Delta\beta}{\beta_{nm}} = \frac{n^2}{p_{nm}^2 - n^2}\,\frac{\epsilon' - 1}{\epsilon'(1 - \nu_{nm}^2)}\,\delta,$$

$$\mathrm{TE}_{om} \quad \frac{\Delta\beta}{\beta_{om}} = \frac{p_{om}^2}{3}\,\frac{\epsilon' - 1}{1 - \nu_{om}^2}\,\delta^3,$$

$$\mathrm{TM}_{nm} \quad \frac{\alpha_D}{\beta_{nm}} = \frac{\epsilon''}{\epsilon'^2}\,\delta, \tag{10}$$

$$\mathrm{TE}_{\substack{nm \\ n \neq 0}} \quad \frac{\alpha_D}{\beta_{nm}} = \frac{n^2}{p_{nm}^2 - n^2}\,\frac{\epsilon''}{\epsilon'^2(1 - \nu_{nm}^2)}\,\delta,$$

$$\mathrm{TE}_{om} \quad \frac{\alpha_D}{\beta_{nm}} = \frac{p_{om}^2}{3}\,\frac{\epsilon''}{1 - \nu_{om}^2}\,\delta^3.$$

Unfortunately the range in which (7), $\cdots$ (10) are good approximations is rather limited. Actually

$$\frac{1 - \nu_{nm}^2}{\nu_{nm}} \cdot \frac{2\pi a}{\lambda} \cdot \frac{\Delta\beta}{\beta_{nm}}$$

has to be small compared to unity, at least not larger than 0.1. In the

case of the TM_{11} wave in a 2-inch pipe at $\lambda = 5.4$ mm this limit is reached with $\Delta\beta/\beta_{11} = 0.45 \times 10^{-3}$ or $\delta = 0.75 \times 10^{-3}$ with $\epsilon = 2.5$.

To evaluate (1) beyond this limit we may use the approximations:

$$\frac{1}{\rho x} \frac{W_n(x, \rho x)}{U_n(x, \rho x)} = \cot (1 - \rho)x = \cot \delta x,$$

$$\frac{1}{\rho x} \frac{V_n(x, \rho x)}{Z_n(x, \rho x)} = -\tan (1 - \rho) = -\tan \delta x. \tag{11}$$

The approximations (11) require $x \gg n$, and $\delta x < \pi/2$, as shown in Appendix I. These requirements are usually satisfied for the lower order modes in a multimode waveguide with a thin dielectric layer.

Equation (1) has been evaluated for the TM_{11} mode using the approximations (11) and a method which is described in Appendix I. The results are shown in Fig. 2 for $\epsilon = 2.5$ and several values of a/λ.

In introducing a dielectric coat we have to be aware of the change in attenuation constant the TE_{01} mode will suffer. Not only the loss factor of the dielectric material will cause additional losses, but the concentration of more field energy into the dielectric will increase the wall currents and so the wall current losses.

To calculate the wall current attenuation of the TE_{01} mode in the round waveguide with the dielectric layer, we proceed in the usual
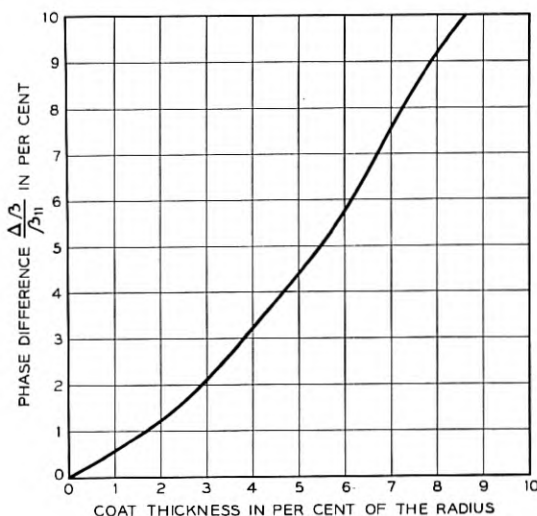

Fig. 2(a) — Change in phase constant of the TM_{11} wave in the dielectric-coated waveguide. $\epsilon = 2.5$; $a/\lambda = 1.03$.
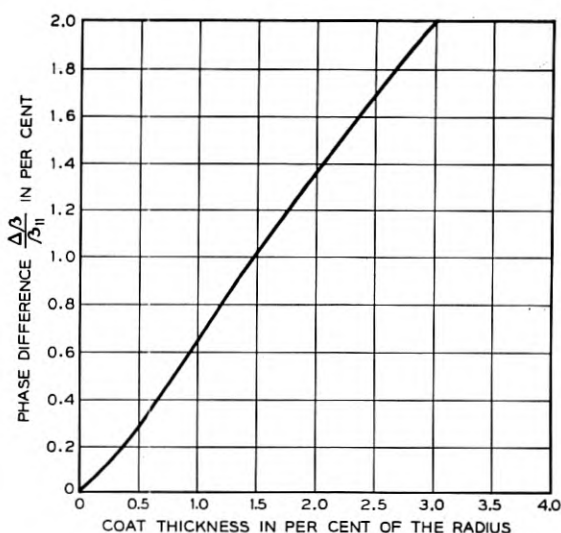
Fig. 2(b) — Change in phase constant of the TM_{11} wave in the dielectric-coated waveguide. $\epsilon = 2.5$; $a/\lambda = 2.06$.
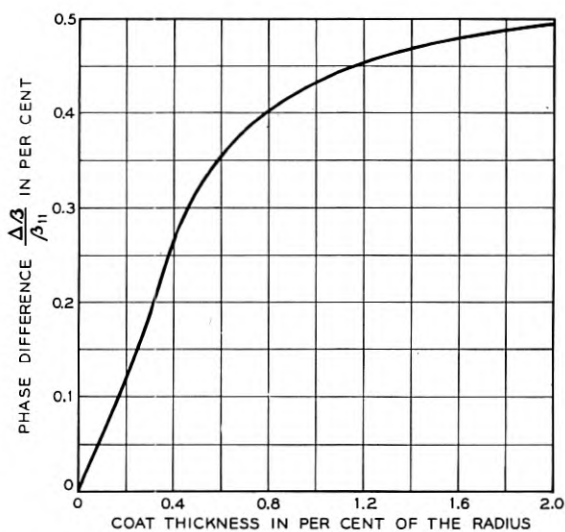

Fig. 2(c) — Change in phase constant of the TM_{11} wave in the dielectric-coated waveguide. $\epsilon = 2.5$; $a/\lambda = 4.70$.

manner. Assuming the conductivity to be high though finite and the loss factor of the dielectric material to be small, we take the field pattern and wall currents of the lossless case and calculate the total transmitted power P and the power P_M absorbed per unit length of the waveguide by the metal walls of finite conductivity. The wall current attenuation α_M is then given by

$$\alpha_M = \frac{1}{2} \frac{P_M}{P}. \tag{12}$$

The result of this calculation as carried through in Appendix II is:

$$\frac{\alpha_M}{\alpha_{om}} = \frac{x_2^2}{p_{om}^2} \sqrt{\frac{x_2^2 - x_1^2}{x_2^2 - \epsilon x_1^2}} \left\{ 1 + \frac{\pi^2}{2} \rho x_2 \left[\frac{x_2^2}{x_1^2} - 1 \right] \right.$$
$$\left. \cdot \left[U_1(x_2, \rho x_2) - \frac{\rho x_2}{2} R_1(x_2, \rho x_2) \right] R_1(x_2, \rho x_2) \right\}^{-1}. \tag{13}$$

In this expression α_M is related to the TE_{om} attenuation constant α_{om} of the plain waveguide.

For $1 - \rho = \delta \ll 1$ we introduce the series expansions of the functions $U_1(x_2, \rho x_2)$ and $R_1(x_2, \rho x_2)$,

$$\frac{\Delta \alpha_M}{\alpha_{om}} = (\epsilon - 1) \frac{p_{om}^2}{\nu_{om}^2} \delta^2. \tag{14}$$

Here $\Delta \alpha_M$ is defined as the change in wall current attenuation compared to the attenuation in the plain waveguide.

III. PROPERTIES OF COUPLED TRANSMISSION LINES

Wave propagation in gentle bends of a round waveguide can be described in terms of normal modes of the straight guide.[1] The bend causes coupling between the normal modes. The TE_{01} wave couples to the TM_{11} wave and to the TE_{1n} waves and the propagation in the bend is described by an infinite set of simultaneous linear differential equations. An adequate approximate treatment is to consider only coupling between TE_{01} and one of the spurious modes at a time. Furthermore, only the forward waves need to be considered, since the relative power coupled from the forward waves into the backward waves is quite small. Thus, the infinite set of equations reduces to the well known coupled line equations:[2]

$$\frac{dE_1}{dz} + \gamma_1 E_1 - jc E_2 = 0,$$
$$\frac{dE_2}{dz} + \gamma_2 E_2 - jc E_1 = 0, \tag{15}$$

in which

$E_{1,2}(z)$ = wave amplitudes in mode 1 (here always TE_{01}) and mode 2 (TM_{11} or one of the TE_{1n}), respectively;

$\gamma_{1,2}$ = propagation constant of mode 1 and 2, respectively (the small perturbation of $\gamma_{1,2}$ caused by the coupling may be neglected here); and

c = coupling coefficient between modes 1 and 2.

Subject to the initial conditions:

$$E_1(0) = 1, \qquad E_2(0) = 0,$$

the solution of (15) is:

$$E_1 = \frac{1}{2}\left[1 + \frac{\Delta\gamma}{\sqrt{\Delta\gamma^2 - 4c^2}}\right]e^{-\Gamma_1 z} + \frac{1}{2}\left[1 - \frac{\Delta\gamma}{\sqrt{\Delta\gamma^2 - 4c^2}}\right]e^{-\Gamma_2 z},$$

$$E_2 = \frac{jc}{\sqrt{\Delta\gamma^2 - 4c^2}}[e^{-\Gamma_2 z} - e^{-\Gamma_1 z}], \tag{16}$$

where $\Delta\gamma = \gamma_1 - \gamma_2$ and $\Gamma_{1,2} = \frac{1}{2}[\gamma_1 + \gamma_2 \pm \sqrt{\Delta\gamma^2 - 4c^2}]$. Γ_1 and Γ_2 are the propagation constants of the two coupled line normal modes. Both coupled line normal modes are excited by the initial conditions. For $|c/\Delta\gamma| \ll 1$, equations (16) can be simplified:

$$E_1 = \left[1 - 2\frac{c^2}{\Delta\gamma^2}\sinh\frac{1}{2}\Delta\gamma z\, e^{\frac{1}{2}\Delta\gamma z}\right]e^{-(\gamma_1 - (c^2/\Delta\gamma))z},$$

$$E_2 = j\frac{2c}{\Delta\gamma}\sinh\frac{1}{2}\Delta\gamma z\, e^{-\frac{1}{2}(\gamma_1+\gamma_2)z}. \tag{17}$$

We are concerned with a difference in phase constant which is much larger than the difference in attenuation constant. Consequently in $\Delta\gamma = j\Delta\beta + \Delta\alpha$ we have $|\Delta\beta| \gg |\Delta\alpha|$ and we may write:

$$E_1 = \left[1 + j\frac{2c^2}{\Delta\beta^2}\sin\frac{1}{2}\Delta\beta z\, e^{j\frac{1}{2}\Delta\beta z}\right]$$

$$\cdot \exp\left[-j\left(\beta_1 + \frac{c^2}{\Delta\beta^2}\Delta\beta\right)z - \left(\alpha_1 - \frac{c^2}{\Delta\beta^2}\Delta\alpha\right)z\right],$$

$$E_2 = j\frac{2c}{\Delta\beta}\cdot\sin\frac{1}{2}\Delta\beta z\,\exp\left[-j\frac{1}{2}(\beta_1 + \beta_2)z - \frac{1}{2}(\alpha_1 + \alpha_2)z\right]. \tag{18}$$

We note that the amplitude E_1, apart from suffering an attenuation, varies in an oscillatory manner, the maximum being $E_1 = 1$ and the minimum $E_1 = 1 - 2(c^2/\Delta\beta^2)$. Accordingly, the maximum mode conversion loss is given by:

$$20 \log_{10} \frac{E_{1\max}}{E_{1\min}} = 17.35 \frac{c^2}{\Delta\beta^2}. \tag{19}$$

The attenuation constant of E_1 is modified by the presence of the coupled wave. Compared to the uncoupled attenuation constant it has been changed by

$$\frac{\Delta\alpha_c}{\alpha_1} = \frac{c^2}{\Delta\beta^2}\left(\frac{\alpha_2}{\alpha_1} - 1\right). \tag{20}$$

The amplitude E_2 varies sinusoidally. From our point of view it is an unwanted mode. The power level compared to the E_1 power is

$$20 \log_{10} \frac{E_{2\max}}{E_1} = 20 \log_{10} \frac{2c}{\Delta\beta}. \tag{21}$$

So far we have considered only a constant value of the coupling coefficient, c, corresponding to a uniform bend. The attenuation in such a uniform bend is increased according to (20), and the worst condition we can encounter at the end of the bend is a mode conversion loss (19) and a spurious mode level (21).

A practical case of changing curvature and consequently changing coupling coefficient is the serpentine bend. A waveguide with equally spaced supports deforms into serpentine bends under its own weight. The curve between two particular supports is well known from the theory of elasticity. An analysis of circular electric wave transmission through serpentine bends[6] shows that mode conversion becomes seriously high at certain critical frequencies when the supporting distance is a multiple of the beat wavelength between the TE_{01} and a particular coupled mode. The beat wavelength is here defined as

$$\lambda_b = \frac{2\pi}{\Delta\beta}. \tag{22}$$

In serpentine bends formed by elastic curves, mode conversion at the critical frequencies causes an increase in TE_{01} attenuation[6]

$$\frac{\Delta\alpha_s}{\alpha_{01}} = -\left[\frac{w}{EI}\frac{c_0}{\Delta\beta^2\alpha_{01}}\right]^2\frac{\alpha_{01}}{\Delta\alpha}, \tag{23}$$

and a spurious mode level in the particular coupled mode[6]

$$\left|\frac{E_2}{E_1}\right| = \frac{w}{EI}\frac{c_0}{\Delta\beta^2\alpha_{01}}\left|\frac{\alpha_{01}}{\Delta\alpha}\right|, \tag{24}$$

where w = weight per unit length of the pipe,
       E = modulus of elasticity,
       I = moment of inertia,

and c_0 is the factor in the bend coupling coefficient $c = c_0/R$ determined by waveguide dimensions, frequency and the particular mode. R is the bend radius.

Equations (23) and (24) hold only as long as

$$4\Delta\alpha_s \ll |\Delta\alpha| \qquad (25)$$

is satisfied. The rate of conversion loss has to be small compared to the difference between the rates of decay for the unwanted mode and TE_{01} amplitudes. If (25) is not satisfied a cyclical power transfer between TE_{01} and the particular coupled mode occurs, and the TE_{01} transmission is seriously distorted.

Another case of changing curvature of the waveguide is random deviation from straightness, which must be tolerated in any practical line. Such deviations from straightness change the curvature only very gradually, and since there is no coupled wave in the dielectric coated guide, which has the same phase constant as the TE_{01} wave, the curvature may be assumed to vary only slowly compared to the difference in phase constants. Under this condition[7] the normal mode of the straight waveguide, which here is the TE_{01} mode, will be transformed along the gradually changing curvature into the normal mode of the curved waveguide, which is a certain combination of TE_{01} and the coupled modes. This normal mode will always be maintained and no spurious modes will be excited.

The change in transmission loss is therefore given alone by the difference between the attenuation constants of the TE_{01} wave and the normal mode of the curved waveguide. The propagation constants of the normal modes of the coupled lines are Γ_1 and Γ_2 as given by (16). Only the mode with Γ_1 will be excited here and consequently the attenuation difference is given by (20).

IV. CIRCULAR ELECTRIC WAVE TRANSMISSION THROUGH CURVED SECTIONS
    OF THE DIELECTRIC-COATED GUIDE

In curved sections of the plain waveguide the wave solution has been described in terms of the normal modes of the straight waveguide. In this presentation it has been found that the TE_{01} wave couples to the TM_{11} and TE_{1n} waves in gentle bends. Likewise, the wave solution in curved sections of the dielectric-coated guide can be described in terms of the normal waves of the straight dielectric-coated guide. In a waveguide with a thin dielectric coat the normal waves may be considered as perturbed normal modes of the plain waveguide. Consequently the bend solution of the plain waveguide may be taken as the first order approximation

for the bend solution of the dielectric-coated guide. In this first order approximation the TE_{01} wave of the dielectric-coated guide couples to the TM_{11} and TE_{1n} waves of the dielectric-coated guide and the coupling coefficients are the same as in the bend-solution of the plain waveguide:[1]

$$TE_{01} \rightleftarrows TM_{11} \qquad c = 0.18454 \frac{\beta a}{R},$$

$$TE_{01} \rightleftarrows TE_{11}$$

$$c = \left[\frac{0.09319(\beta a)^2 - 0.84204}{\sqrt{\beta_{01} a \beta_{11} a}} + 0.09319 \sqrt{\beta_{01} a \beta_{11} a} \right] \frac{1}{R},$$

$$TE_{01} \rightleftarrows TE_{12} \tag{26}$$

$$c = \left[\frac{0.15575(\beta a)^2 - 3.35688}{\sqrt{\beta_{01} a \beta_{12} a}} + 0.15575 \sqrt{\beta_{01} a \beta_{11} a} \right] \frac{1}{R},$$

$$TE_{01} \rightleftarrows TE_{13}$$

$$c = \left[\frac{0.01376(\beta a)^2 - 0.60216}{\sqrt{\beta_{01} a \beta_{13} a}} + 0.01376 \sqrt{\beta_{01} a \beta_{13} a} \right] \frac{1}{R},$$

β = free-space phase constant.

With the coupling coefficients (26) and the propagation constants as given by (10) and (14) the coupled line equations can be used to compute the TE_{01} transmission through curved sections. Since the absolute value of $c/\Delta\gamma$ is usually small compared to unity, the mode conversion loss is given by (19), the increase in TE_{01} attenuation by (20), and the spurious mode level by (21).

The curves in Figs. 3, 4 and 5 have been calculated for the 2-inch pipe at a wavelength of 5.4 mm. They take into account the effects of the three most seriously coupled modes, TM_{11}, TE_{11}, and TE_{12}.

In very gentle bends of a guide with a very thin coat, coupling effects to the TE_{1m} modes are small and only TM_{11} coupling influences the TE_{01} transmission. The increase in TE_{01} attenuation in such bends is obtained by substituting the expression (10) for the TM_{11} phase difference in (20).

$$\frac{\Delta\alpha_c}{\alpha_{01}} = \frac{0.034}{\nu_{01}^2} \frac{\epsilon'^2}{(\epsilon' - 1)^2} \frac{1}{\delta^2} \frac{a^2}{R^2}. \tag{27}$$

Note that (27) requires $|c/\Delta\gamma| \ll 1$ and consequently $(1/\delta)(a/R) \ll 1$. In Fig. 4, as well as in (27), losses in the dielectric coat have been neglected. Equations (10) show that the dielectric losses are small compared to the wall current losses for a low loss dielectric coat.
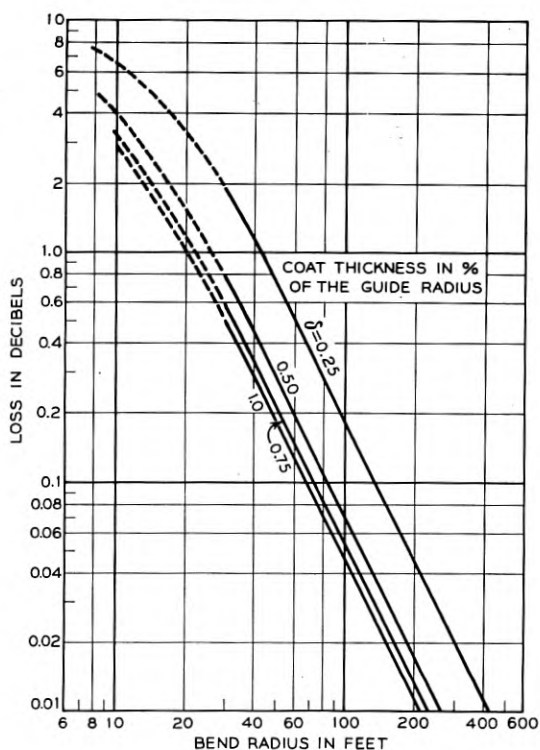
Fig. 3 — Maximum conversion loss of the TE_{01} wave in a uniform bend of the dielectric-coated waveguide. $2a = 2$ inches; $\lambda = 5.4$ mm; $\epsilon = 2.5$.

There are two different applications of the dielectric-coated guide, which require different designs:

1. Intentional bends

These are relatively short sections and the increase in TE_{01} attenuation is usually small compared to the bend loss. Also, a high spurious mode level can be tolerated, because with a mode filter at the end of the bend we can always control the spurious mode level. Consequently, the only limit set for this type of bend is the mode conversion loss of the TE_{01} wave. There is conversion loss mainly to TE_{11}, TE_{12} and TM_{11}. Increasing the phase difference of the TM_{11} wave by making the dielectric coat thicker decreases the phase-difference between TE_{01} and TE_{12} and increases the phase-difference between TE_{01} and TE_{11}. Apparently we get
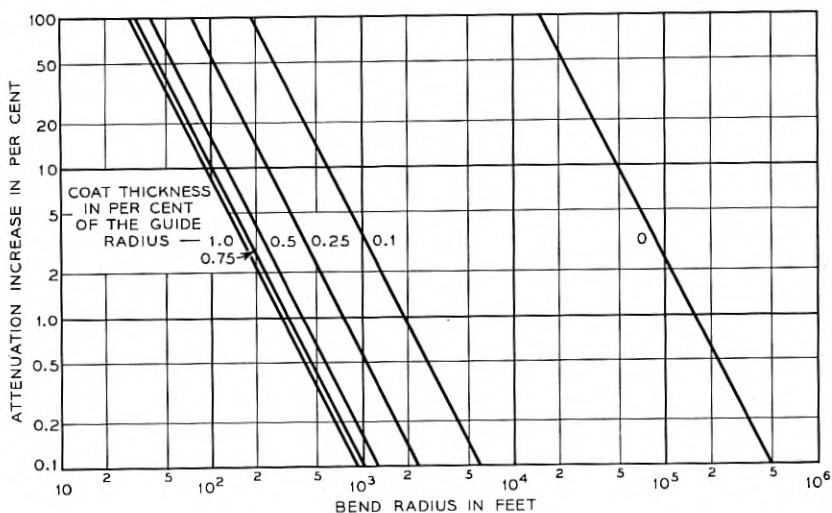
Fig. 4 — Increase in TE_{01} attenuation of a dielectric-coated guide in a uniform bend. $2a = 2$ inches; $\epsilon = 2.5$; $\lambda = 5.4$ mm.

very near to an optimum design with a dielectric coat for which:

$$\left(\frac{\Delta\beta}{c}\right)_{TM_{11}} = \left(\frac{\Delta\beta}{c}\right)_{TE_{12}}. \tag{28}$$

For this condition conversion losses to TM_{11} and TE_{12} are equal, while the conversion loss to TE_{11} is small.

To find values which satisfy (28) we will generally have to solve (1) because the TM_{11} phase difference required by (28) is too large to be calculated with the first order approximation. At a wavelength of $\lambda = 5.4$ mm and a dielectric constant $\epsilon = 2.5$ the optimum thickness of the coat according to (28) is $\delta = 1.25$ per cent in the 2-inch pipe. In Fig. 6 the mode conversion loss in a dielectric-coated guide of this design is plotted versus bending radius.

2. Random deviations from straightness

As mentioned before, random deviations from straightness change the curvature only gradually and only one normal mode propagates. Mode conversion loss and spurious mode level are very low. The normal mode attenuation depends on the curvature. The increase in normal mode attenuation as caused by curvature is obtained by adding the attenuation terms (20) of the various straight guide modes which are contained
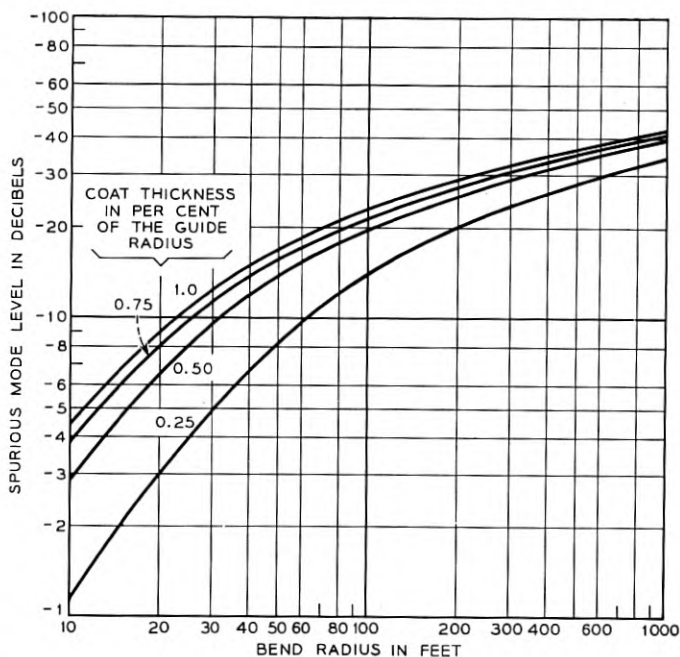
Fig. 5 — Spurious mode level in a uniform bend of a dielectric-coated guide. $2a = 2$ inches; $\epsilon = 2.5$; $\lambda = 5.4$ mm.

in the normal mode. The bending radius R is a function of position and an average bending radius,

$$\frac{1}{R_{\mathrm{Av}}^2} = \frac{1}{z} \int_0^z \frac{dz}{R^2}, \tag{29}$$

has to be used in (20).

All the attenuation terms (20) decrease with increasing coat thickness δ; the TE_{01} attenuation in the straight guide (10) and (14) increases with δ. Consequently there is an optimum thickness for which the total increase in attenuation is a minimum. This optimum thickness depends on the average radius of curvature. In Fig. 7 optimum thickness and the corresponding increase in attenuation have been plotted versus the average radius of curvature.

In gentle curvatures the normal mode is a mixture of TE_{01} and TM_{11} only and the attenuation increase as caused by the curvature is given by (27). In this case the optimum thickness and the corresponding attenuation increase are:

$$\delta_{opt} = \frac{1}{\sqrt[4]{2}} \frac{1}{p_{01}} \frac{\sqrt{\epsilon'}}{(\epsilon' - 1)^{3/4}} \sqrt{\frac{a}{R_{Av}}}, \tag{30}$$

$$\frac{\Delta \alpha}{\alpha_{01}} = \frac{\sqrt{2}}{\nu_{01}{}^2} \frac{\epsilon'}{\sqrt{\epsilon' - 1}} \frac{a}{R_{Av}}. \tag{31}$$

We note that δ_{opt} does not depend on frequency.

So far we have listed only the useful properties of the dielectric-coated guide. There is, however, one serious disadvantage. Serpentine bends caused by equally spaced discrete supports and the elasticity of the pipe are inherently present in any waveguide line. At critical frequencies, when the supporting distance l is a multiple of the beat wavelength λ_b between TE_{01} and a particular coupled mode, an increase in TE_{01} attenuation (23) and a spurious mode level (24) result from the mode conversion.

We evaluate (23) and (24) for a dielectric-coated copper pipe of 2.000-inch I.D. and 2.375-inch O.D. and a supporting distance $l = 15$ ft. The
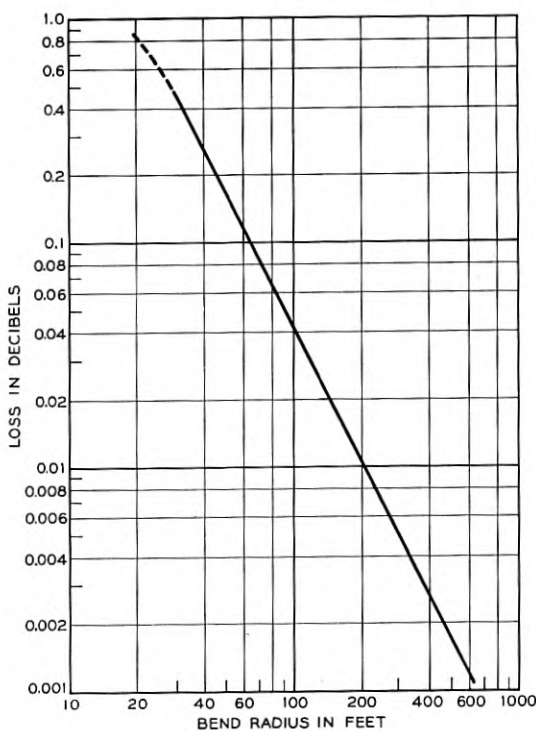

Fig. 6 — Bend conversion loss in a dielectric-coated guide of optimum design according to equation (28). $2a = 2$ inches; $\delta = 1.25\%$; $\epsilon = 2.5$; $\lambda = 5.4$ mm.

result is for coat thicknesses which cause the wavelength $\lambda = 5.4$ mm to be critical with respect to TE_{01}–TM_{11} coupling:

$$\delta = 0.002 \quad l = \lambda_b \quad \frac{\Delta\alpha_s}{\alpha_{01}} = 43.3 \quad 20 \log_{10}\left|\frac{E_2}{E_1}\right| = -1.29 \ db$$

$$= 0.004 \quad = 2\lambda_b \quad = 2.70 \quad = -13.32 \ db$$

$$= 0.006 \quad = 3\lambda_b \quad = 0.169 \quad = -25.37 \ db.$$

The values corresponding to $\delta = 0.002$ do not satisfy the condition (25). Therefore they cannot be considered as a quantitative result but only as an indication that the mode conversion is very high. We conclude from these values that the mode conversion is much too high for a coat thickness which makes the beat wavelength between TE_{01} and TM_{11} equal to the supporting distance or half of it.

If no other measures can be taken, such as removing the periodicity of the supports or inserting mode filters, the lowest critical frequencies of TE_{01}–TM_{11} coupling have to be avoided. A dielectric coat must be
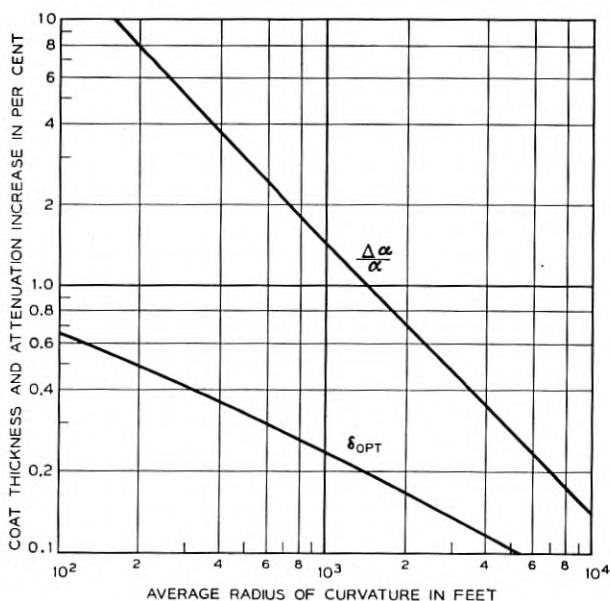

Fig. 7 — Optimum coat thickness and increase in TE_{01} attenuation of a dielectric-coated guide with random deviations from straightness. $2a = 2$ inches; $\lambda = 5.4$ mm; $\epsilon = 2.5$.

chosen, which is thin enough or thick enough to keep these critical frequencies out of the band.

Mode conversion from TE_{01} to the TE_{1m} modes in serpentine bends is not changed substantially by the presence of the dielectric coat. Generally these mode conversion effects decrease rapidly with the beat wavelength. When the curvature varies slowly compared to the difference in phase constant between coupled waves almost pure normal mode propagation is maintained.[7]

V. MODE CONVERSION AT TRANSITIONS FROM PLAIN WAVEGUIDE TO THE DIELECTRIC-COATED WAVEGUIDE

We consider a round waveguide, a section of which has a dielectric layer next to the walls. A pure TE_{01} wave incident on this dielectric-coated section will excite TE_{om} waves. For circular electric wave transmission it is important to keep low the power level of the higher circular electric waves which have low loss.

In an evaluation of Schelkunoff's generalized telegraphist's equations for the TE_{01} mode in a circular waveguide containing an inhomogeneous dielectric[1] S. P. Morgan describes the wave propagation in the dielectric-filled waveguide in terms of normal modes of the unfilled waveguide. The only restriction made in this analysis for the dielectric insert is

$$\frac{1}{S} \int_S |\,\epsilon - 1\,|\, dS \ll 1, \qquad (32)$$

where S is the cross-sectional area of the guide.

The dielectric-coated guide satisfies (32), and we may use the results of Morgan's evaluation here.

The round waveguide is considered as an infinite set of transmission lines, each of which represents a normal mode. Along the dielectric-coated section the TE_{0m} transmission lines are coupled mutually. The coupling coefficient d between TE_{01} and one of the TE_{0m} waves is obtained by taking Morgan's general formula and evaluating it for the dielectric coat:

$$d = p_{01}p_{0m} \frac{(\epsilon' - 1)\beta^2}{\sqrt{\beta_{01}\beta_{0m}}} \frac{\delta^3}{3}. \qquad (33)$$

We introduce this coupling coefficient into the coupled line equations (16). Since $d/\Delta\beta \ll 1$ for any of the coupled modes, the spurious mode level at the output of the dielectric-coated section is given by (21),

$$20 \log_{10} \left| \frac{E_{2\max}}{E_1} \right| = 20 \log_{10} \frac{2}{3} \frac{(\epsilon' - 1)p_{01}p_{0m}\beta^2}{(\beta_{01} - \beta_{om}) \sqrt{\beta_{01}\beta_{0m}}} \delta^3. \qquad (34)$$
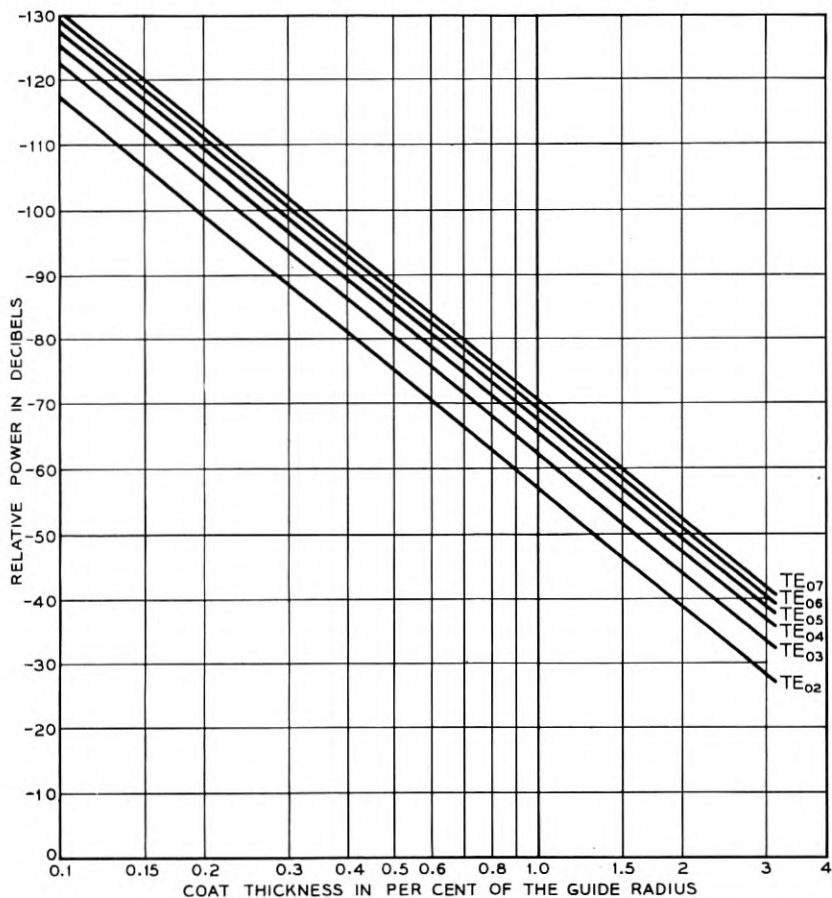
Fig. 8 — Higher circular electric waves at a transition from plain waveguide to the dielectric-coated guide. $\epsilon = 2.5$; $a/\lambda = 4.70$.

Fig. 8 shows an evaluation of (34) for $a/\lambda = 4.70$ and $\epsilon' = 2.5$ corresponding to a 2-inch pipe with a polystyrene coat at $\lambda = 5.4$ mm.

VI. SUMMARY

A theoretical analysis of wave propagation in the dielectric-coated guide is presented to provide information necessary for circular electric wave transmission in this waveguide structure. The normal modes of a waveguide with a thin dielectric coat are perturbed modes of the plain waveguide. While the perturbation of the phase constant is only of third order of the coat thickness for the circular electric waves, it is of first

order for all other modes. Thus, the degeneracy of equal phase constants of circular electric waves and TM_{1m} waves can be removed quite effectively. The additional attenuation to TE_{01} wave as caused by the dielectric loss in the coat and the increased wall current loss remains small as long as the coat is thin.

The dielectric-coated guide may be used for negotiating intentional bends or for avoiding extreme straightness requirements on normally straight sections. For intentional bends of as small a radius as possible, an optimum thickness of the coat makes the mode-conversion losses to TM_{11} and TE_{12} modes equal and minimizes the total conversion loss. For random deviations from straightness, an average radius of curvature is defined. For this average radius an optimum thickness of the coat minimizes the additional TE_{01} attenuation as caused by curvature and dielectric coat. In random deviations from straightness, propagation of only one normal mode is maintained as long as only the rate of change of curvature is small compared to the square of the difference in phase constant between TE_{01} and any coupled mode.

Serpentine bends, caused by equally spaced supports and the associated elastic deformation of the pipe, increase the TE_{01} attenuation substantially at certain critical frequencies, when the supporting distance is a multiple of the beat wavelength. The lowest critical frequencies of TE_{01}–TM_{11} coupling corresponding to a beat wavelength, which is equal to the supporting distance or half of it, have to be avoided by choosing the proper coat thickness.

At transitions from plain waveguide to dielectric-coated guide higher circular electric waves are excited by the TE_{01} wave. However, the power level of these spurious modes is low for a thin dielectric coat.

APPENDIX I

Approximate Solutions of the Characteristic Equation

In the following calculation we will use the definitions:

$$R_n(x, \rho x) = J_n(x) \, N_{n-1}(\rho x) - J_{n-1}(\rho x) N_n(x),$$
$$S_n(x, \rho x) = J_{n-1}(x) \, N_n(\rho x) - J_n(\rho x) \, N_{n-1}(x), \tag{35}$$

and their relation to the definitions (2);

$$\frac{W_n(x, \rho x)}{U_n(x, \rho x)} \equiv \rho x \frac{R_n(x, \rho x)}{U_n(x, \rho x)} + n \equiv -\rho x \frac{S_{n+1}(x, \rho x)}{U_n(x, \rho x)} - n,$$

$$\frac{V_n(x, \rho x)}{Z_n(x, \rho x)} \equiv \rho x \frac{x U_{n-1}(x, \rho x) + n R_n(x, \rho x)}{x S_n(x, \rho x) + n U_n(x, \rho x)} + n. \tag{36}$$

To find solutions of (1) for $1 - \rho \equiv \delta \ll 1$ we first substitute for the functions (36) their series expansions with respect to δ.

We have for instance

$$U_n(x, \rho x) = N_n(x) J_n(x - \delta x) - J_n(x) N_n(x - \delta x)$$

where we introduce

$$J_n(x - \delta x) = J_n(x) + \delta x J_n{}'(x) + \frac{(\delta x)^2}{2} J_n{}''(x) + \cdots$$

$$= J_n(x) + \delta x \left[J_{n+1}(x) - \frac{n}{x} J_n(x) \right]$$

$$+ \frac{(\delta x)^2}{2} \left[\frac{1}{x} J_{n+1}(x) + \left(\frac{n^2 - n}{x^2} - 1 \right) J_n(x) \right] + \cdots,$$

and

$$N_n(x - \delta x) = N_n(x) + \delta x \left[N_{n+1}(x) - \frac{n}{x} N_n(x) \right]$$

$$+ \frac{(\delta x)^2}{2} \left[\frac{1}{x} N_{n+1}(x) + \left(\frac{n^2 - n}{x^2} - 1 \right) N_n(x) \right] + \cdots.$$

Upon using the relation

$$J_{n+1}(x) N_n(x) - J_n(x) N_{n+1}(x) = \frac{2}{\pi x}$$

we get

$$U_n(x, \rho x) = \frac{2}{\pi} \delta \left[1 + \frac{\delta}{2} + \frac{\delta^2 x^2}{6} \left(\frac{n^2 + 2}{x^2} - 1 \right) \right] + 0(\delta^4), \tag{37}$$

and by the same procedure

$$R_n(x, \rho x) = \frac{2}{\pi x} \left[1 - (n - 1)\delta + \left(\frac{(n - 1)(n - 2)}{x^2} - 1 \right) \frac{(\delta x)^2}{2} \right.$$

$$\left. - \frac{n - 2}{x} \left(1 + \frac{(n - 1)(n - 3)}{x^3} \right) \frac{(\delta x)^3}{6} \right] + 0(\delta^4). \tag{38}$$

With these expressions the functions (36) are approximated by:

$$\frac{W_n(x, \rho x)}{U_n(x, \rho x)} = \frac{1}{\delta}\left(1 - \frac{\delta}{2}\right) + 0(\delta),$$

$$\frac{V_n(x, \rho x)}{Z_n(x, \rho x)} = \delta(x^2 - n^2) + 0(\delta^2), \tag{39}$$

and for $n = 0$ especially:

$$\frac{1}{\rho x^2}\frac{V_0(x, \rho x)}{Z_0(x, \rho x)} = -\frac{1}{x}\frac{U_1(x, \rho x)}{R_1(x, \rho x)}$$

$$= -\delta\left[1 + \frac{\delta}{2} + \delta^2\left(\frac{1}{3}x^2 + \frac{1}{2}\right)\right] + 0\ (\delta^4). \tag{40}$$

Since for $\delta = 0$ the roots of $J_n(\rho x_1) = 0$ and $J_n{}'(\rho x_1) = 0$ represent the solutions of (1) for the TM and TE waves respectively, we expand the Bessel functions of the argument ρx_1 in series around these roots:

$$\rho x_1 = (1 - \delta)(p_{nm} + \Delta x).$$

The result for TM waves is

$$J_n(p_{nm}) \equiv 0: \qquad \frac{J_n{}'(\rho x_1)}{J_n(\rho x_1)} = \frac{1}{\Delta x - \delta p_{nm}}; \tag{41}$$

for TE waves:

$$J_n{}'(p_{nm}) \equiv 0: \qquad \frac{J_n{}'(\rho x_1)}{J_n(\rho x_1)} = \frac{n^2 - p_{nm}{}^2}{p_{nm}{}^2}(x - \delta p_{nm}); \tag{42}$$

and for TE_{om} waves especially:

$$J_0{}'(p_{om}) = 0:$$

$$-\frac{J_0{}'(\rho x_1)}{J_0(\rho x_1)} = \Delta x - \delta p_{om} - \frac{1}{2p_{om}}(\Delta x^2 + \delta^2 p_{om}{}^2) - \frac{\delta^3}{6}p_{om}(3 + 2p_{om}{}^2). \tag{42}$$

Introducing (39 $\cdots$ 42) into the characteristic equation (1) and neglecting higher order terms in δ and Δx we get the following approximations for (1):

$$TM_{nm}\ \text{waves:} \qquad \Delta x = \left(p_{nm} - \frac{1}{\epsilon}\frac{x_2{}^2}{p_{nm}}\right)\delta$$

$$TE_{nm}\ \text{waves:} \atop {n \neq 0} \qquad \Delta x = \frac{x_2{}^2 - p_{nm}{}^2}{p_{nm}{}^2 - n^2}\frac{n^2}{\epsilon p_{nm}}\delta \tag{43}$$

$$TE_{om} \text{ waves:} \qquad \Delta x = -\frac{p_{om}}{3}(x_2^2 - p_{om}^2)\delta^3. \qquad (44)$$

If we write for the perturbed propagation constant

$$\gamma = \gamma_{nm} + \Delta\gamma,$$

we get with (3) and (4):

$$\Delta x = a^2 \frac{\gamma_{nm}}{p_{nm}} \Delta\gamma$$

$$= ja \frac{\sqrt{1 - \nu_{nm}^2}}{\nu_{nm}} \Delta\gamma,$$

and

$$x_2^2 = (\epsilon - 1 + \nu_{nm}^2) \frac{p_{nm}^2}{\nu_{nm}^2},$$

in which

$$\nu_{nm} = \frac{\lambda}{\lambda_{cnm}} = \frac{p_{nm}}{2\pi}\frac{\lambda}{a}.$$

Using these expressions in (43) and (44) we finally get approximate formulae for the perturbation of the propagation constant as caused by the dielectric coat:

$$\text{TM}_{nm} \text{ waves:} \qquad \frac{\Delta\gamma}{\gamma_{nm}} = \frac{\epsilon - 1}{\epsilon}\delta$$

$$\text{TE}_{nm} \text{ waves:} \qquad \frac{\Delta\gamma}{\gamma_{nm}} = \frac{n^2}{p_{nm}^2 - n^2}\frac{\epsilon - 1}{\epsilon}\frac{1}{1 - \nu_{nm}^2}\delta \qquad (45)$$
$$\phantom{\text{TE}_{nm} \text{ waves:}}_{n \neq 0}$$

$$\text{TE}_{0m} \text{ waves:} \qquad \frac{\Delta\gamma}{\gamma_{om}} = \frac{p_{om}^2}{3}\frac{\epsilon - 1}{1 - \nu_{om}^2}\delta^3.$$

The series expansions used so far hold only when $(1 - \rho)x \ll 1$. Approximate expressions which require only $(1 - \rho) \ll 1$ are:[8]

$$U_n(x, \delta x) = \frac{2}{\pi}\frac{\sin \dfrac{1 - \rho}{\sqrt{\rho}}\sqrt{\rho x^2 - n^2}}{\sqrt{\rho x^2 - n^2}},$$

$$S_n(x, \delta x) = \frac{2}{\pi}\frac{1}{(1 - \rho)x}\left[\sqrt{\rho}\cos\left(\frac{1 - \rho}{\sqrt{\rho}}\sqrt{\rho x^2 - (n - 1)^2}\right)\right.$$
$$\left. - \frac{1}{\sqrt{\rho}}\cos\left(\frac{1 - \rho}{\sqrt{\rho}}\sqrt{\rho x^2 - n^2}\right)\right].$$

If $x^2 \gg n^2$ these expressions may be further simplified:

$$U_n(x, \rho x) = \frac{2}{\pi} \frac{1}{\sqrt{\rho x}} \sin (1 - \rho)x,$$

$$S_n(x, \rho x) = -\frac{2}{\pi} \frac{1}{\sqrt{\rho x}} \cos (1 - \rho)x.$$

Substituting these values in (36) we get:

$$\frac{W_n(x, \rho x)}{U_n(x, \rho x)} = \rho x \cot (1 - \rho)x - n,$$

$$\frac{V_n(x, \rho x)}{Z_n(x, \rho x)} = -\rho x \tan (1 - \rho)x \frac{1 - \dfrac{n}{x} \dfrac{1 - \rho}{\rho} \cot (1 - \rho)x}{1 - \dfrac{n}{x} \tan (1 - \rho)x}.$$

With the restrictions $(1 - \rho)x < \pi/2$ and $n \ll x$ we may write:

$$\frac{W_n(x, \rho x)}{U_n(x, \rho x)} = \rho x \cot (1 - \rho)x,$$

$$\frac{V_n(x, \rho x)}{Z_n(x, \rho x)} = -\rho x \tan (1 - \rho)x. \tag{46}$$

With (46) the characteristic equation (1) is

$$n^2 \left[\frac{1}{x_1^2} - \frac{1}{x_2^2} \right]^2 - \rho^2 \frac{x_2^2 - x_1^2}{x_2^2 - \epsilon x_1^2} \left[\frac{1}{x_1} \frac{J_n{}'(\rho x_1)}{J_n(\rho x_1)} + \frac{\epsilon}{x_2} \cot \delta x_2 \right]$$
$$\cdot \left[\frac{1}{x_2} \frac{J_n{}'(\rho x_1)}{J_n(\rho x_1)} - \frac{1}{x_2} \tan \delta x_2 \right] = 0.$$

Solving this equation for $\cot \delta x_2$ we get:

$$\cot \delta x_2 = \frac{F}{2} + \sqrt{1 + \frac{F^2}{4}}, \tag{47}$$

in which

$$F = \frac{x_1}{x_2} \frac{J_n(\rho x_1)}{J_n{}'(\rho x_1)} \left[1 + \frac{n^2}{\epsilon \rho^2} \frac{(x_1^2 - x_2^2)(x_2^2 - \epsilon x_1^2)}{x_1^4 x_2^2} \right] - \frac{x_2}{\epsilon x_1} \frac{J_n{}'(\rho x_1)}{J_n(\rho x_1)}.$$

To evaluate (47) we specify a value of $\Delta\beta/\beta_{nm}$ and enter the right hand side of (47) with

$$x_1^2 = p_{nm}^2 - 2 \frac{\Delta\beta}{\beta_{nm}} \beta^2{}_{nm} a^2 \left(1 + \frac{1}{2} \frac{\Delta\beta}{\beta_{nm}} \right),$$

$$x_2^2 = (\epsilon - 1)\beta_{nm}^2 a^2 + x_1^2,$$

$$\rho = 1 - \delta_1$$

in which δ_1 is a first order approximation as given by (10) for a particular mode. Equation (47) then yields a value δ_2 which is usually accurate enough. To improve the accuracy the same calculation is repeated using δ_2. Since for small values of δ a change in δ affects the right hand side only slightly this method converges rapidly.

APPENDIX II

The TE_{01} Attenuation in the Dielectric-Coated Waveguide

The attenuation constant of a transmission line can be expressed as

$$\alpha = \frac{1}{2} \frac{P_M}{P}$$

in which P_M is the power dissipated per unit length in the line and P is the total transmitted power. For the dielectric-coated guide the power P_M is dissipated in the metal walls with finite conductivity σ.

For TE_{om} waves the wall currents are $i = H_z(a)$ (H_z axial component of the magnetic field) and therefore

$$P_M = \frac{1}{2} \int_0^{2\pi} \frac{ii^*}{t \cdot \sigma} a \, d\varphi$$

$$= \frac{\pi a}{t\sigma} H_z(a) H_z^*(a)$$

where $t =$ skin depth and $\sigma =$ conductivity.

The total transmitted power is

$$P = -\frac{1}{2} \int_0^{2\pi} \int_0^a E_\varphi H_r^* r dr \, d\varphi.$$

We introduce expressions for the field components, which are listed elsewhere[3, 4] and carry out the integration. Finally we express the wall current attenuation in terms of the functions (2) and (35);

$$\alpha_M = \frac{\alpha_{cm}}{p_{om}^2} x_2^2 \sqrt{\frac{x_2^2 - x_1^2}{x_2^2 - \epsilon x_1^2}} \left\{ 1 + \frac{\pi^2}{2} \rho x_2 \right.$$

$$\left. \cdot \left(\frac{x_2^2}{x_1^2} - 1 \right) \left(U_1(x_2, \rho x_2) + \frac{\rho x_2}{2} R_1(x_2, \rho x_2) \right) R_1(x_2, \rho x_2) \right\}^{-1} \tag{48}$$

To get an approximation for a thin dielectric coat we use the expressions (37) and (38) and obtain

$$\frac{\Delta \alpha_M}{\alpha_{om}} = \frac{\alpha_M - \alpha_{cm}}{\alpha_{om}} = (\epsilon - 1) \frac{p_{om}^2}{\nu_{om}^2} \delta^2. \tag{49}$$

REFERENCES

1. S. P. Morgan, Theory of Curved Circular Waveguide Containing an Inhomo-geneous Dielectric, pp. 1209–1251, this issue.
2. S. E. Miller, Coupled Wave Theory and Waveguide Applications, B.S.T.J., **33**, 661–719, May, 1954.
3. H. Buchholz, Der Hohlleiter von kreisförmigem Querschnitt mit geschichte-tem dielektrischen Einsatz, Ann. Phys., **43**, pp. 313–368, 1943.
4. H. M. Wachowski and R. E. Beam, Shielded Dielectric Rod Waveguides, Final Report on Investigations of Multi-Mode Propagation in Waveguides and Microwave Optics, Microwave Laboratory, Northwestern University, Ill., 1950.
5. S. P. Morgan and J. A. Young, Helix Waveguide, B.S.T.J., **35**, pp. 1347–1384, November, 1956.
6. H. G. Unger, Circular Electric Wave Transmission through Serpentine Bends, pp. 1279–1291, this issue.
7. J. S. Cook, Tapered Velocity Couplers, B.S.T.J., **34**, pp. 807–822, July, 1955; A. G. Fox, Wave Coupling by Warped Normal Modes, B.S.T.J., **34**, pp. 823–852, July, 1955; W. H. Louisell, Analysis of the Single Tapered Mode Coupler, B.S.T.J., **34**, pp. 853–870, July, 1955.
8. H. Buchholz, Approximation Formulae for a Well Known Difference of Prod-ucts of Two Cylinder Functions, Phil. Mag., Series 7, **27**, pp. 407–420, 1939.
9. A. E. Karbowiak, British Patent No. 751,322. H. G. Unger and O. Zinke, German Patent No. 935,677.

Circular Electric Wave Transmission Through Serpentine Bends

By H. G. UNGER

An otherwise straight waveguide line with equally spaced discrete supports may deform elastically into a serpentine bend under its own weight. The TE_{01} wave couples in such bends to the TM_{11} and TE_{1n} waves. The general solution of coupled lines with varying coupling coefficient is applied to a serpentine bend by an iterative process, and evaluated for the elastic curve resulting from a periodically supported line. TE_{01}-TM_{11} coupling causes only a small increase in TE_{01} attenuation. Mode conversion to TE_{1n} waves can become seriously high at certain critical frequencies when the supporting distance is a multiple of the beat wavelength. In a copper pipe of $2\frac{3}{8}$ inch O.D. and 2 inch I.D., the mode conversion to the TE_{12} wave at critical frequencies near 5-mm wavelength causes a TE_{01} attenuation increase of 90 per cent and a spurious mode level of -7 db. These mode conversion effects can be controlled effectively by inserting mode filters.

I. INTRODUCTION

In curved sections of round waveguide the TE_{01} - wave couples to the TM_{11} and TE_{1n} waves, and power is converted to these waves when the TE_{01} wave is transmitted through bends. A form of bend which is inherently present even in an otherwise straight and perfect line is the serpentine bend, Fig. 1. Between discrete supports the pipe is deflected by the force of its own weight. The resulting curve is well known from the theory of elasticity. The curvature varies along the axis following essentially a square law. The minimum bending radius occurs at the supports. For the practical example of a copper pipe of $2\frac{3}{8}$-inch O.D., 2.00-inch I.D. and a supporting distance of 15 ft, this minimum bending radius is 992 ft. A uniform bend of this radius would convert most of the power incident in the TE_{01} wave to the TM_{11} wave after a certain length of bend.

Fortunately a serpentine bend with the same order of bending radius does not affect circular electric wave transmission as seriously as does a
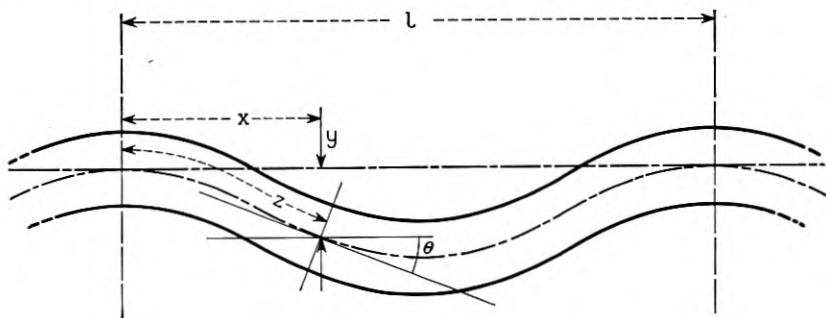
Fig. 1 — Serpentine bends.

uniform bend with the same bending radius. This will be shown in the following analysis.

A treatment of serpentine bends given previously by Albersheim[1] considers only circular and sinusoidal curvatures. Furthermore, it does not show all the effects of serpentine bends that we are interested in. We shall present a more general and complete analysis here. The only restriction we have to make is that the power exchanged in one section of the serpentine bend from the TE_{01} mode to any of the coupled modes or vice versa is small compared to the power in the mode from which it has been abstracted. The curvature may be any function of distance along the serpentine bend.

The general results indicate that normally a serpentine bend causes an additional attenuation to the TE_{01} mode. Part of the TE_{01} power which travels temporarily in one of the coupled modes suffers the higher attenuation of this coupled mode. Formulae for this increase in attenuation constant are obtained for periodically supported guides from the deflection curve given by the theory of elasticity.

The coupling between the TE_{01} and TM_{11} waves causes only a very slight increase in TE_{01} attenuation, since the difference in propagation constant for these two modes is very small. In fact, if there were no difference in propagation constant, as in the round guide of infinite wall conductivity, coupling between TE_{01} and TM_{11} waves in serpentine bends would not affect the TE_{01} transmission at all.

Coupled modes which have a larger difference in phase constant than TM_{11} but still are close to TE_{01} cause a serious increase in TE_{01} attenuation at certain critical frequencies. If a multiple of the beat wavelength between the TE_{01} mode and a particular coupled mode is equal to the supporting distance, power is converted continuously into the coupled

mode. For low attenuation in the coupled mode the power transfer may even be essentially complete.

II. SOLUTION OF THE COUPLED LINE EQUATIONS

In a curved round waveguide the TE_{01} mode couples to the TM_{11} mode and the infinite set of TE_{1n} waves. Consequently, the wave propagation is described by an infinite system of simultaneous first order linear differential equations. An adequate procedure is to consider only coupling between TE_{01} and one of the spurious modes at a time. Thus, the infinite system of equations reduces to the well known coupled line equations,[2]

$$\frac{dE_1}{dz} + \gamma_1 E_1 - k E_2 = 0,$$

$$\frac{dE_2}{dz} + \gamma_2 E_2 - k E_1 = 0; \tag{1}$$

in which

$E_{1,2}(z)$ = wave amplitudes in mode 1 (here always TE_{01}) and mode 2 (TM_{11} or one of the TE_{1n}), respectively;

$\gamma_{1,2}$ = propagation constant of modes 1 and 2, respectively, (The small perturbation of γ_1, γ_2 caused by the coupling may be neglected here); and

$k(z) = jc(z)$ = coupling coefficient between modes 1 and 2.

In the curved waveguide the coupling is proportional to the curvature;

$$c = \frac{c_0}{R} = c_0 \frac{d\theta}{dz}, \tag{2}$$

in which R = radius of curvature, and θ = direction of guide axis. (The various coupling coefficients are listed in the appendix.) Without loss of generality we start with $\theta(0) = 0$. We will use the average propagation constant γ,

$$\gamma = \tfrac{1}{2}(\gamma_1 + \gamma_2),$$

$$\Delta\gamma = \tfrac{1}{2}(\gamma_1 - \gamma_2). \tag{3}$$

Several coordinate transformations will change (1) to a form which can be solved approximately. A similar procedure has been used to solve the

related problem of the tapered mode coupler.[3] With the first transformation

$$
E_1(z) = \tfrac{1}{2}e^{-\gamma z}\,[u_1(z)e^{jc_0\theta} + u_2(z)e^{-jc_0\theta}],
$$
$$
E_2(z) = \tfrac{1}{2}e^{-\gamma z}\,[u_1(z)e^{jc_0\theta} - u_2(z)e^{-jc_0\theta}],
\tag{4}
$$

the new coordinates satisfy the equations:

$$
\frac{du_1}{dz} + \Delta\gamma e^{-j2c_0\theta}u_2 = 0,
$$
$$
\frac{du_2}{dz} + \Delta\gamma e^{j2c_0\theta}u_1 = 0.
\tag{5}
$$

With the second transformation

$$
u_1(z) = \tfrac{1}{2}[v_1(z)\,e^{-\Delta\gamma z} + v_2(z)\,e^{+\Delta\gamma z}],
$$
$$
u_2(z) = \tfrac{1}{2}[v_1(z)\,e^{-\Delta\gamma z} - v_2(z)\,e^{+\Delta\gamma z}],
\tag{6}
$$

$v_1(z)$ and $v_2(z)$ satisfy

$$
\frac{dv_1}{dz} - 2\Delta\gamma\,\sin^2 c_0\theta v_1 + j\Delta\gamma\,\sin 2c_0\theta e^{2\Delta\gamma z}v_2 = 0,
$$
$$
\frac{dv_2}{dz} + 2\Delta\gamma\,\sin^2 c_0\theta v_2 - j\Delta\gamma\,\sin 2c_0\theta e^{2\Delta\gamma z}v_1 = 0.
\tag{7}
$$

With the third transformation

$$
v_1(z) = w_1(z)\,\exp\left(2\Delta\gamma\int_0^z \sin^2 c_0\theta\,dz'\right),
$$
$$
v_2(z) = w_2(z)\,\exp\left(-2\Delta\gamma\int_0^z \sin^2 c_0\theta\,dz'\right).
\tag{8}
$$

We finally get the equations

$$
\frac{dw_1}{dz} + \xi_1(z)w_2 = 0,
$$
$$
\frac{dw_2}{dz} + \xi_2(z)w_1 = 0,
\tag{9}
$$

in which

$$\xi_{1,2}(z) = \pm j\Delta\gamma \sin 2c_0\theta \exp\left[\pm 2\Delta\gamma\left(z - 2\int_0^z \sin^2 c_0\theta \, dz'\right)\right]. \quad (10)$$

As long as we have the condition $\int_0^z |\xi_{1,2}(z')| \, dz' \ll 1$, approximate solutions of (9) can be written down which proceed essentially in powers of $\xi_{1,2}$ as follows,

$$w_1(z) = w_1(0) - w_2(0)\int_0^z \xi_1(z') \, dz'$$
$$+ w_1(0)\int_0^z \xi_1(z')\int_0^{z'} \xi_2(z'') \, dz'' \, dz',$$

$$w_2(z) = w_2(0) - w_1(0)\int_0^z \xi_2(z') \, dz' \qquad\qquad (11)$$
$$+ w_2(0)\int_0^z \xi_2(z')\int_0^{z'} \xi_1(z'') \, dz'' \, dz'.$$

The new coordinates are related to the wave amplitudes by:

$$E_1(z) = \frac{1}{2} e^{-\gamma z}\left\{w_1(z) \exp\left[-\Delta\gamma\left(z - 2\int_0^z \sin^2 c_0\theta \, dz'\right)\right]\cos c_0\theta\right.$$
$$\left. + jw_2(z) \exp\left[\Delta\gamma\left(z - 2\int_0^z \sin^2 c_0\theta \, dz'\right)\right]\sin c_0\theta\right\},$$

$$E_2(z) = \frac{1}{2} e^{-\gamma z}\left\{jw_1(z) \exp\left[-\Delta\gamma\left(z - 2\int_0^z \sin^2 c_0\theta \, dz'\right)\right]\sin c_0\theta\right. \qquad (12)$$
$$\left. + w_2(z) \exp\left[\Delta\gamma\left(z - 2\int_0^z \sin^2 c_0\theta \, dz'\right)\right]\cos c_0\theta\right\}.$$

The solution (12) in combination with (11) is general and may be applied to any form of curvature as long as the converted power remains small compared to the original power in either of the modes.

III. WAVE PROPAGATION IN SERPENTINE BENDS

If we apply (12) to a section of a serpentine bend with the length l we have $\theta(l) = 0$. The output amplitudes are related to the input amplitudes of both modes by a transmission matrix

$$E_i(l) = \| T \| E_i(0). \qquad (13)$$

The elements of $\| T \|$ are obtained from (11) and (12):

$$T_{11} = \left[1 + \int_0^l \xi_1(z) \int_0^z \xi_2(z') \, dz' dz \right]$$
$$\cdot \exp\left[-\gamma_1 l + 2\Delta\gamma \int_0^l \sin^2 c_0\theta \, dz \right],$$

$$T_{21} = -\int_0^l \xi_1(z) \, dz \exp\left[-\gamma_1 l + 2\Delta\gamma \int_0^l \sin^2 c_0\theta \, dz \right],$$

$$T_{12} = -\int_0^l \xi_2(z) \, dz \exp\left[-\gamma_2 l - 2\Delta\gamma \int_0^l \sin^2 c_0\theta \, dz \right], \tag{14}$$

$$T_{22} = \left[1 + \int_0^l \xi_2(z) \int_0^z \xi_1(z') \, dz' \, dz \right]$$
$$\cdot \exp\left[-\gamma_2 l - 2\Delta\gamma \int_0^l \sin^2 c_0\theta \, dz \right].$$

For a line of iterative serpentine bends we apply the rules of matrix calculus. If $E_{10} = 1$ and $E_{20} = 0$ at the input of the first section, then the output amplitudes of the nth section are:

$$E_{1n} = \frac{1}{2}\left[1 + \frac{T_{11} - T_{22}}{\sqrt{(T_{11} - T_{22})^2 + 4T_{12}T_{21}}} \right] e^{-n g_1}$$
$$+ \frac{1}{2}\left[1 - \frac{T_{11} - T_{22}}{\sqrt{(T_{11} - T_{22})^2 + 4T_{12}T_{21}}} \right] e^{-n g_2}, \tag{15}$$

$$E_{2n} = \frac{T_{12}}{\sqrt{(T_{11} - T_{22})^2 + 4T_{12}T_{21}}} [e^{-n g_1} - e^{-n g_2}],$$

where

$$e^{-g_{1,2}} = \tfrac{1}{2}[T_{11} + T_{22} \pm \sqrt{(T_{11} - T_{22})^2 + 4T_{12}T_{21}}]. \tag{16}$$

Two limiting cases for the expressions (15) and (16) are of special interest:

1. $|T_{11} - T_{22}|^2 \gg 4 |T_{12} T_{21}|$

$$e^{-g_1} = T_{11} + \frac{T_{12}T_{21}}{T_{11} - T_{22}}$$
$$E_{1n} = e^{-n g_1} - \frac{T_{12}T_{21}}{(T_{11} - T_{22})^2} [e^{-n g_1} - e^{-n g_2}] \tag{17}$$

$$e^{-g_2} = T_{22} - \frac{T_{12}T_{21}}{T_{11} - T_{22}} \qquad E_{2n} = \frac{T_{12}}{T_{11} - T_{22}} [e^{-n g_1} - e^{-n g_2}]$$

2. $4 |T_{12} T_{21}| \gg |T_{11} - T_{22}|^2$

$$e^{-g_{1,2}} = \frac{T_{11} + T_{22}}{2} \pm \sqrt{T_{12}T_{21}}$$
$$E_{1n} = \tfrac{1}{2}(e^{-n g_1} + e^{-n g_2}) \tag{18}$$
$$E_{2n} = \frac{1}{2}\sqrt{\frac{T_{12}}{T_{21}}} (e^{-n g_1} - e^{-n g_2}).$$

In case 1 the wave amplitude E_{1n} is only affected by a slight change of the propagation constant. The small additional term in the expression for E_{1n} can usually be neglected. The power in the wave E_{2n} is small compared to the E_{1n} power; T_{12} is usually of the same order of magnitude as T_{21}.

In case 2, however, a complete power transfer between E_{1n} and E_{2n} occurs cyclically if the loss is sufficiently low. Consequently, condition (18) has to be carefully avoided. Rather, condition (17) must always be satisfied.

IV. SERPENTINE BENDS FORMED BY ELASTIC CURVES

A section of the waveguide line between two supports deforms like a beam fixed at both ends. Under its own weight, w per unit length, such a beam will bend and form an elastic curve, Fig. 1, whose deflection from a straight line is given by:

$$ y = \frac{wl^4}{24EI} \frac{x^2}{l^2} \left(1 - \frac{x}{l} \right)^2, \tag{19} $$

in which $E =$ modulus of elasticity of the beam, and $I =$ moment of inertia of the beam. Since we are concerned with small deflections y only, we have $x = z$ and $\theta = dy/dx$. Hence,

$$ \theta = d \left(\frac{z}{l} - 3 \frac{z^2}{l^2} + 2 \frac{z^3}{l^3} \right), \tag{20} $$

in which $d = wl^3/12EI$. Introducing the elastic curve (20) into the transmission matrix (10) and (14) and performing the integrations with $\sin c_0\theta = c_0\theta$ we get for the elements of the transmission matrix:

$$ T_{11} = \exp \left[-\gamma_1 l + \Delta\gamma l \frac{c_0^2 d^2}{105} \right] \left\{ 1 + \frac{c_0^2 d^2}{4\Delta\gamma^6 l^6} \left[9 - 3\Delta\gamma^2 l^2 + \Delta\gamma^4 l^4 \right.\right. $$
$$ \left.\left. + \frac{2}{5} \Delta\gamma^5 l^5 - \frac{4}{105} \Delta\gamma^7 l^7 - (3 - 3\Delta\gamma l + \Delta\gamma^2 l^2)^2 e^{2\Delta\gamma l} \right] \right\}, $$

$$ T_{22} = \exp \left[-\gamma_2 l - \Delta\gamma l \frac{c_0^2 d^2}{105} \right] \left\{ 1 + \frac{c_0^2 d^2}{4\Delta\gamma^6 l^6} \left[9 - 3\Delta\gamma^2 l^2 + \Delta\gamma^4 l^4 \right.\right. \tag{21} $$
$$ \left.\left. - \frac{2}{5} \Delta\gamma^5 l^5 + \frac{4}{105} \Delta\gamma^7 l^7 - (3 + 3\Delta\gamma l + \Delta\gamma^2 l^2)^2 e^{-2\Delta\gamma l} \right] \right\}, $$

$$ T_{12} = T_{21} = j \frac{c_0 d}{2\Delta\gamma^3 l^3} [(3 - 3\Delta\gamma l + \Delta\gamma^2 l^2)e^{-\gamma_2 l} $$
$$ - (3 + 3\Delta\gamma l + \Delta\gamma^2 l^2)e^{-\gamma_1 l}]. $$

The expressions (21) are hard to evaluate, but for some special cases of interest they can be simplified greatly.

To compute the coupling effects between the TE_{01} wave and the TM_{11} wave we make use of $|\Delta\gamma l| \ll 1$ and get the following approximations:

$$T_{11} = \left[1 - \frac{c_0^2 d^2}{315} \Delta\gamma^3 l^3\right] \exp -\left(\gamma_1 - \frac{c_0^2 d^2}{105} \Delta\gamma\right) l,$$

$$T_{22} = \left[1 + \frac{c_0^2 d^2}{315} \Delta\gamma^3 l^3\right] \exp -\left(\gamma_2 + \frac{c_0^2 d^2}{105} \Delta\gamma\right) l, \qquad (22)$$

$$T_{12} = T_{21} = j \frac{c_0 d}{15} \Delta\gamma^2 l^2 e^{-\gamma l}.$$

In (22) the condition $|T_{11} - T_{22}|^2 \gg 4|T_{12}T_{21}|$ is satisfied; consequently the wave propagation is described by (17),

$$E_{1n} = \exp -\left(\gamma_1 - \frac{c_0^2 d^2}{105} \Delta\gamma\right) nl + \frac{c_0^2 d^2}{450} \Delta\gamma^2 l^2 \sinh \Delta\gamma nl e^{-\gamma nl},$$

$$\qquad (23)$$

$$E_{2n} = j \frac{c_0 d}{15} \Delta\gamma l \sinh \Delta\gamma nl e^{-\gamma nl}.$$

In addition to small oscillations, which are negligible, the wave amplitude E_1 suffers an additional attenuation

$$\Delta\alpha_s = -\frac{c_0^2 d^2}{105} \Delta\alpha. \qquad (24)$$

Physically this means that to a first approximation there is no net power transfer from E_1 to E_2. The power converted from E_1 to E_2 in one section of the iterative serpentine bends is all reconverted in the same section. But this power, which travels partly in the E_2 wave, suffers the E_2 attenuation and consequently changes the E_1 attenuation.

To evaluate (24) we introduce the coupling coefficient and the difference in attenuation constants between the TE_{01} and TM_{11} wave. Then, the relative increase of TE_{01} attenuation is:

$$\frac{\Delta\alpha_s}{\alpha_{01}} = 6.39 \times 10^{-3} d^2 \frac{a^2}{\lambda^2} \left(2.69 \frac{a^2}{\lambda^2} - 1\right), \qquad (25)$$

where α_{01} = attenuation constant of TE_{01},

a = inner radius of pipe,

λ = free-space wavelength.

A numerical example shows that the increase in TE_{01} attenuation caused by coupling to the TM_{11} wave in serpentine bends is small. For a copper pipe with 2.00-inch I.D. and $2\frac{3}{8}$-inch O.D. and a supporting length $l = 15$ ft, we have $d = 1.51 \times 10^{-2}$, and at $\lambda = 5.4$ mm we get $\Delta\alpha_s/\alpha_{01} = 0.19 \times 10^{-2}$.

For coupling between the TE_{01} wave and the waves of the TE_{1n} family the difference in propagation constant is no longer small; the approximation which was valid for the TM_{11} wave can not be made for TE_{1n} waves. Actually, the supporting distance is usually several beat wavelengths. Therefore, no essential simplifications of (21) are possible for the general case of coupling between TE_{01} and TE_{1n}. But closer examination of (21) shows that if

$$2\Delta\beta l = 2m\pi \qquad m = 1, 2, 3, \cdots \quad (26)$$

is satisfied, the difference $T_{11}-T_{22}$ becomes very small. The net power converted to any of the TE_{1n} modes may be small in each section of the iterative serpentine bends, but if (26) is satisfied the contributions from each section add in phase and in a long line with the square of distance more and more power is built up in the particular TE_{1n} wave. Only when the attenuation in this TE_{1n} wave is large enough to damp out the power as fast as it is converted will an undistorted TE_{01} propagation be maintained. This condition for the attenuation constant can be derived from $| T_{11} - T_{22} |^2 \gg 4 | T_{12}T_{21} |$. If $| \Delta\beta | \gg | \Delta\alpha |$ and $| \Delta\alpha l | \gg c_0^2d^2/10m\pi$ then $T_{11} - T_{22} = -2\Delta\alpha l e^{-\gamma_1 l}$, and since $T_{12}T_{21} = -9\, c_0^2d^2/m^4\pi^4\, e^{-2\gamma_1 l}$ the condition for undistorted TE_{01} propagation is:

$$| \Delta\alpha l |^2 \gg 9\, \frac{c_0^2d^2}{m^4\pi^4}. \qquad (27)$$

If (27) is satisfied the wave propagation is again described by (17). Neglecting all terms which are small because of (27) the wave amplitudes are:

$$E_{1n} = \left[1 + 9\, \frac{c_0^2d^2}{m^4\pi^4}\, \frac{1}{2\Delta\alpha l}\right]^n e^{-\gamma_1 n l} + 9\, \frac{c_0^2d^2}{m^4\pi^4}\, \frac{1}{4\Delta\alpha^2 l^2}[1 - e^{2\Delta\alpha n l}]e^{-\gamma_1 n l},$$

$$E_{2n} = -j3\, \frac{c_0 d}{m^2\pi^2}\, \frac{1}{2\Delta\alpha l}[1 - e^{2\Delta\alpha n l}]e^{-\gamma_1 n l}. \qquad (28)$$

For not too large values of n, the first term of E_{1n} may be written:

$$\left[1 + 9\, \frac{c_0^2d^2}{m^4\pi^4}\, \frac{1}{2\Delta\alpha l}\right]^n e^{-\gamma_1 n l} = \exp\left[-\left(\gamma_1 - 9\, \frac{c_0^2d^2}{m^4\pi^4}\, \frac{1}{2\Delta\alpha l^2}\right) nl\right].$$

The additional attenuation to the E_1 wave as caused by the continuous

power abstraction is seen from this expression to be

$$\Delta\alpha_s = -9 \frac{c_0^2 d^2}{m^4 \pi^4} \frac{1}{2\Delta\alpha l^2}. \tag{29}$$

The condition (27) may now be written

$$2\Delta\alpha_s \ll |\Delta\alpha|, \tag{30}$$

or, the rate of conversion loss has to be small compared to the difference between E_2 attenuation and E_1 attenuation.

When the wave is travelling through a large number of serpentine bends, power is built up gradually in the E_2 mode to a constant value,

$$\left|\frac{E_2}{E_1}\right| = 3 \frac{c_0 d}{m^2 \pi^2} \left|\frac{1}{2\Delta\alpha l}\right|. \tag{31}$$

Both the attenuation increase and the power level in spurious modes can seriously affect the E_1 transmission.

To evaluate (29) and (31) we rewrite them with $m\pi = \Delta\beta l$ and $d = wl^3/12EI$ as follows;

$$\frac{\Delta\alpha_s}{\alpha_{01}} = -\left[\frac{w}{EI} \frac{c_0}{(2\Delta\beta)^2 \alpha_{01}}\right]^2 \frac{\alpha_{01}}{2\Delta\alpha}, \tag{32}$$

$$\left|\frac{E_2}{E_1}\right| = \frac{w}{EI} \frac{c_0}{(2\Delta\beta)^2 \alpha_{01}} \left|\frac{\alpha_{01}}{2\Delta\alpha}\right|. \tag{33}$$

We note from (32) and (33) that the coupling effects cannot be controlled by changing the supporting distance. Only the number of critical frequencies in a given range decreases with decreasing supporting distance.

The previously cited numerical example of the 2 inch copper pipe yields the following values at the critical frequencies of the two lowest TE_{1n} waves near $\lambda = 5.4$ mm:

$$TE_{11} \quad \frac{\Delta\alpha_s}{\alpha_{01}} = 0.114 \qquad 20 \log\left|\frac{E_2}{E_1}\right| = -23.4 \; db,$$

$$TE_{12} \quad \frac{\Delta\alpha_s}{\alpha_{01}} = 0.855 \qquad 20 \log\left|\frac{E_2}{E_1}\right| = -6.85 \; db.$$

The mode conversion, especially to the TE_{12} wave, causes a seriously high additional attenuation and spurious mode level.

V. MODE FILTERS IN SERPENTINE BENDS

Periodically spaced supports are a condition for the critical case described by (32) and (33). Accordingly, the coupling effects can be controlled by removing the periodicity of the supports.
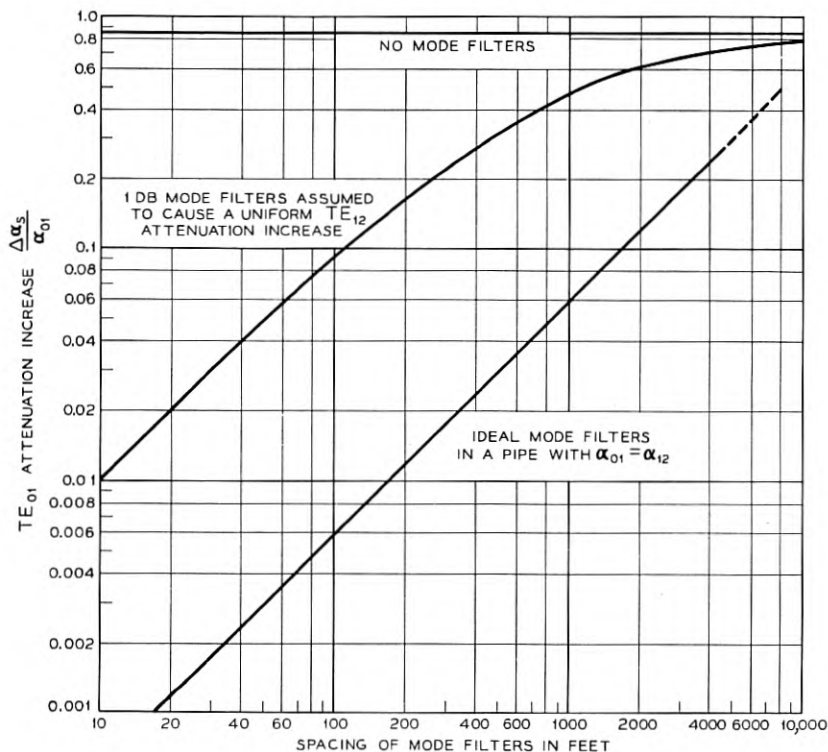
FIG. 2 — TE_{01} attenuation increase of TE_{01}–TE_{12} coupling in serpentine bends with mode filters; 2-inch I.D. $2\frac{3}{8}$-inch O.D., $\lambda = 5.4$ mm. Serpentine bends are caused by equally spaced supports and the elasticity of the copper pipe. The supporting distance is a multiple of the beat-wavelength between TE_{01} and TE_{12}.

An alternative to control the coupling effects is insertion of mode filters into the line. Mode filters which pass the TE_{on} waves without loss but attenuate all other modes have been developed in various forms. To estimate the amount of mode conversion control that can be achieved by mode filters, we make two different assumptions. Only the critical case of the supporting distance equal to a multiple of the beat wave-length is considered here.

A. The mode filters are ideal; they present infinite attenuation to all unwanted modes. At the input of a section between two mode filters we have a TE_{01} wave only and at the output the spurious mode level has risen to

$$\left| \frac{E_2}{E_1} \right| = \frac{w}{EI} \frac{c_0}{(2\Delta\beta)^2} L. \tag{34}$$
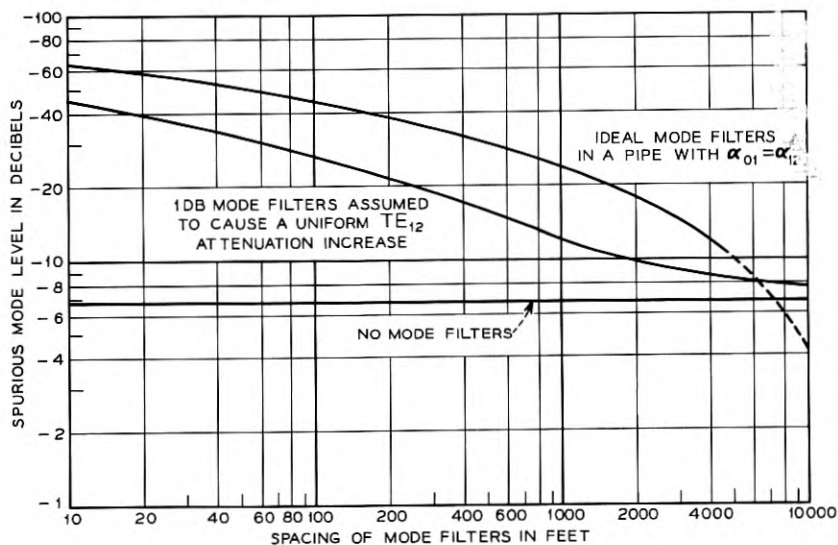
Fig. 3 — Spurious mode level of TE_{01}–TE_{12} coupling in serpentine bends with mode filters; 2-inch I.D. $2\frac{3}{8}$-inch O.D., $\lambda = 5.4$ mm. Serpentine bends are caused by equally spaced supports and the elasticity of the copper pipe. The supporting distance is a multiple of the beat-wavelength between TE_{01} and TE_{12}.

The loss to the TE_{01} wave caused by the mode conversion is equivalent to an increase in TE_{01} attenuation

$$\Delta\alpha_s = \frac{1}{2}\left[\frac{w}{EI}\frac{c_0}{(2\Delta\beta)^2}\right]^2 L. \tag{35}$$

L is the spacing between two successive mode-filters. In (34) and (35) the attenuation constants of E_1 and E_2 are assumed to be equal. Furthermore (34) and (35) hold only as long as the E_2 power level is small compared to the E_1 power level.

Ideal mode filters is a rather optimistic assumption. Practical mode filters present only a limited attenuation to the unwanted modes. Therefore a more realistic procedure is to represent the effect of the mode filters by a uniform increase of unwanted mode attenuation.

B. The mode filters with a loss A are considered to cause a uniform increase in E_2 attenuation $\Delta\alpha = A/L$. Equations (32) and (33) modified to include this attenuation increase are:

$$\frac{\Delta\alpha_s}{\alpha_{01}} = \left[\frac{w}{EI}\frac{c_0}{(2\Delta\beta)^2\alpha_{01}}\right]^2 \frac{\alpha_{01}}{|2\Delta\alpha| + \dfrac{A}{L}}, \tag{36}$$

$$\frac{E_2}{E_1} = \frac{w}{EI} \frac{c_0}{(2\Delta\beta)^2 \alpha_{01}} \frac{\alpha_{01}}{|\,2\Delta\alpha\,| + \dfrac{A}{L}} \cdot \qquad (37)$$

An evaluation of the TE_{01}-TE_{12} coupling in the previously described 2 inch copper pipe for critical frequencies near $\lambda = 5.4$ mm is shown in Figs. 2 and 3. The mode filter loss of 1 db can be achieved for the TE_{12} wave in an 18-inch long helix waveguide. A 100-foot spacing of the mode filters reduces the increase of TE_{01} attenuation to 9 per cent and the spurious mode level to -26 db.

APPENDIX

The coupling coefficient for the wave coupling between the TE_{01} wave and the TE_{11}, TE_{12}, TE_{13} waves as well as the TM_{11} wave have been calculated by S. P. Morgan.[4] If $c = c_0/R$, the factor c_0 is for the various waves

$$TM_{11} \; c_0 = 0.18454\beta a,$$

$$TE_{11} \; c_0 = \frac{0.09319(\beta a)^2 - 0.84204}{\sqrt{\beta_{01}a\beta_{11}a}} + 0.09319\sqrt{\beta_{01}a\beta_{11}a},$$

$$TE_{12} \; c_0 = \frac{0.15575(\beta a)^2 - 3.35688}{\sqrt{\beta_{01}a\beta_{12}a}} + 0.15575\sqrt{\beta_{01}a\beta_{12}a},$$

$$TE_{13} \; c_0 = \frac{0.01376(\beta a)^2 - 0.60216}{\sqrt{\beta_{01}a\beta_{13}a}} + 0.01376\sqrt{\beta_{01}a\beta_{13}a},$$

where a = radius of waveguide,

β = free-space phase constant,

β_{nm} = phase constant of TE_{nm} wave.

REFERENCES

1. W. J. Albersheim, Propagation of TE_{01} Waves in Curved Wave Guides, B.S.T.J., **28**, pp. 1–32, January, 1949.
2. S. E. Miller, Coupled Wave Theory and Waveguide Applications, B.S.T.J., **33**, pp. 661–719, May, 1954.
3. W. H. Louisell, Analysis of the Single Tapered Mode Coupler, B.S.T.J., **34**, pp. 853–870, July, 1955.
4. S. P. Morgan, Theory of Curved Circular Waveguide Containing an Inhomogeneous Dielectric, pp. 1209–1251, this issue.

Normal Mode Bends
for Circular Electric Waves

By H. G. UNGER

In dielectric-coated round waveguide the degeneracy or equality of phase constants of TE_{01} *and* TM_{11} *waves is removed. In such a non-degenerate waveguide, mode conversion in bends can be reduced by changing the curvature gradually instead of abruptly. With curvature tapers, which are of the order of, or longer than, the largest beat wavelength between* TE_{01} *and any of the coupled waves, propagation of only one normal mode is maintained throughout the bend. Linear curvature tapers can easily be made by bending the pipe within the limit of elastic deformation.*

Changes in the direction of a waveguide line can thus be made by inserting a dielectric-coated guide section which is elastically bent over a fixed center point. A thirty degree change of direction of a 2-inch I.D. pipe with 30 ft of a dielectric-coated guide yields a total bend loss at 5.4-mm wavelength that is twice the TE_{01} *loss in 30 ft of straight pipe. An optimum bend geometry is found which minimizes the total bend loss. The normal mode bend is a broadband device.*

I. INTRODUCTION AND SUMMARY

A major problem in circular electric wave transmission is the question of negotiating bends. In curved sections of a round waveguide the TE_{01} mode couples to the TE_{11}, TE_{12}, TE_{13} $\cdots$ modes and to the TM_{11} mode. The coupling to the TM_{11} mode presents the most serious problem, since the TE_{01} and TM_{11} modes are degenerate in that they have equal phase velocities in a perfectly conducting straight guide. TE_{01} power introduced at the beginning of the bend will be almost completely transferred to the TM_{11} mode at odd multiples of a certain critical bending angle. This power transfer can be reduced by removing the degeneracy of equal phase velocity of TE_{01} and TM_{11} modes. There are various methods to remove the degeneracy; a simple and a very effective one is a thin dielectric layer next to the walls of the waveguide. As a study of the dielectric-

coated waveguide has shown,[1] this dielectric layer changes the phase constant of the TM_{11} wave without appreciably affecting the propagation characteristics of the TE_{01} mode.

With removal of the TE_{01}-TM_{11} degeneracy the mode conversion which occurs when a TE_{01} wave passes through a bend of constant curvature may be considerably reduced, but it will not be completely eliminated. To design a bend with still lower mode conversion losses, we consider the effect of tapering the curvature along the guide.

Guided wave propagation is most easily explained in terms of normal modes. Normal modes are solutions of the wave equation in a particular waveguide structure, and represent waves propagating without loss of power except for dissipation. In the straight waveguide the normal mode, in which we are mainly interested here is the TE_{01} mode. The normal modes of the curved section are not as simple as the straight guide modes, but they can be expressed as the sum of the normal modes in the straight waveguide. Here the mode of our main concern is the one which, when represented as a sum of straight guide modes, has most of the power in the TE_{01} part of the sum; in other words, is most similar to the TE_{01} mode of the straight waveguide.

At a transition from a straight waveguide to a curved waveguide the normal (TE_{01}) mode of the straight waveguide will certainly excite this normal mode in the curved waveguide but it will also excite a series of other normal modes. All these modes propagate in the curved section, and at the other transition to the straight guide excite not only the TE_{01} mode but a series of other normal modes of the straight waveguide. All the power in the other normal modes represents mode conversion loss of the bend.

A transition which transforms the normal (TE_{01}) mode of the straight waveguide into only one of the normal modes of the curved guide and vice versa will avoid all mode conversion losses. Such a transition can be realized approximately by tapering the curvature. Beginning with zero curvature at the straight guide end of the taper, the curvature is increased gradually along the taper to the finite value of the bend. The normal (TE_{01}) mode incident from the straight guide will be gradually transformed into the particular normal mode of the bent guide which is most similar in field configuration to the circular electric wave. At each point along the taper there is essentially only one local normal mode corresponding in its configuration to the value of curvature at that point.

This taper, unless it is infinitely long, is however only an approximation of the ideal normal mode transition. There will still be other modes excited with a very low power level. In the next section we shall analyze

the propagation in the normal mode taper. We will find that the taper should have a certain minimum length to work properly. Usually it has to be long compared to the beat wavelength between the TE_{01} normal mode and any of the other normal modes into which power may be converted.

In the plain waveguide the degeneracy between TE_{01} and TM_{11} causes an infinitely long beat wavelength. Hence, the normal mode taper would not work there. A nondegenerate waveguide is an essential condition for the normal mode bend.

We shall confine our attention to the linear taper. This is not the optimum taper form, but it is most easily built.

The residual mode conversion in the bend is to be accounted for as bend loss. This loss and the loss caused by the normal mode attenuation in the bend add up to a total bend loss. We shall evaluate the total bend loss for bend configurations which might be useful in circular electric wave transmission. For specified waveguide dimensions the total bend loss can be minimized by choosing the proper bend geometry.

The normal mode bend is an inherently broadband device. The total bend loss shows the same order of frequency dependence as the loss in the straight waveguide.

II. ANALYSIS OF THE NORMAL MODE TAPER

In the curved waveguide, wave propagation can be described in terms of the normal modes of the straight waveguide. The relation between these modes is then given by an infinite system of simultaneous first order linear differential equations. It represents the mutual coupling of the straight guide modes in the curved waveguide. We are interested mainly in TE_{01} propagation and shall restrict ourselves to a low power level in all other modes. Consequently, an adequate procedure is to consider only coupling between TE_{01} and one of the coupled modes at a time. Thus, the infinite system of equations reduces to the well known coupled line equations:[2]

$$\frac{dE_1}{dz} = -\gamma_1 E_1 + jcE_2,$$

$$\frac{dE_2}{dz} = jcE_1 - \gamma_2 E_2,$$

(1)

in which

$E_{1,2}(z) =$ wave amplitudes in mode 1 (here always TE_{01}) and mode 2 (TM_{11} or one of the TE_{1m}), respectively;

$\gamma_{1,2} = j\beta_{1,2} + \alpha_{1,2}$ = propagation constants of modes 1 and 2, respectively, (the small perturbations of γ_1 and γ_2 caused by the coupling may be neglected here); and

$c(z)$ = coupling coefficient between modes 1 and 2.

In the curved waveguide the coupling coefficient is proportional to the curvature k:

$$c(z) = c'k(z) \equiv c' \frac{d\theta}{dz}, \qquad (2)$$

in which θ is the direction of the guide axis. The coupled line equations (1) with varying coupling coefficient have been solved by W. H. Louisell and we shall borrow freely from his treatment.[3]

We define local normal modes $w_1(z)$ and $w_2(z)$:

$$E_1 = [w_1 \cos \tfrac{1}{2} \xi - w_2 \sin \tfrac{1}{2} \xi] e^{-\gamma z},$$
$$E_2 = [w_1 \sin \tfrac{1}{2} \xi + w_2 \cos \tfrac{1}{2} \xi] e^{-\gamma z}, \qquad (3)$$

in which

$$\gamma = \frac{\gamma_1 + \gamma_2}{2},$$

$$\tan \xi = j2 \frac{c}{\gamma_2 - \gamma_1} \equiv j2 \frac{c}{\Delta\gamma}.$$

Substituting (3) into (1), we find that $w_1(z)$ and $w_2(z)$ must satisfy

$$\frac{dw_1}{dz} - \Gamma(z)w_1 = \frac{1}{2} \frac{d\xi}{dz} w_2,$$
$$\frac{dw_2}{dz} + \Gamma(z)w_2 = -\frac{1}{2} \frac{d\xi}{dz} w_1, \qquad (4)$$

where $\Gamma(z) = \frac{1}{2} \sqrt{\Delta\gamma^2 - 4c^2}$. In (4) the local normal modes are coupled only through the terms poportional to $d\xi/dz$. When ξ is constant they are uncoupled and true normal modes. For small values of $d\xi/dz$ or more specifically when

$$\left| \frac{1}{2\Gamma} \frac{d\xi}{dz} \right| \ll 1 \qquad (5)$$

approximate solutions of (4) can be written down, which proceed essentially in powers of $d\xi/dz$. These solutions are:

$$w_1(z) = e^{\rho(z)} \left[w_1(0) + \frac{1}{2} w_2(0) \int_0^z \frac{d\xi}{dz'} e^{-2\rho(z')} \, dz' \right.$$
$$\left. - \frac{1}{4} w_1(0) \int_0^z \frac{d\xi}{dz'} e^{-2\rho(z')} \int_0^{z'} \frac{d\xi}{dz''} e^{2\rho(z'')} \, dz'' \, dz' \right],$$
$$w_2(z) = e^{-\rho(z)} \left[w_2(0) - \frac{1}{2} w_1(0) \int_0^z \frac{d\xi}{dz'} e^{2\rho(z')} \, dz' \right.$$
$$\left. - \frac{1}{4} w_2(0) \int_0^z \frac{d\xi}{dz'} e^{2\rho(z')} \int_0^{z'} \frac{d\xi}{dz''} e^{-2\rho(z'')} \, dz'' \, dz' \right],$$

(6)

in which

$$\rho(z) = \int_0^z \Gamma(z') \, dz'.$$

The initial conditions in the normal mode taper are $E_1(0) = 1$ and $E_2(0) = 0$. The taper begins with zero curvature, $\xi(0) = 0$. Hence from (3) $w_1(0) = 1$ and $w_2(0) = 0$. The wanted local normal mode is w_1 while w_2 is an unwanted mode. At the end, z_1, of the taper the unwanted mode
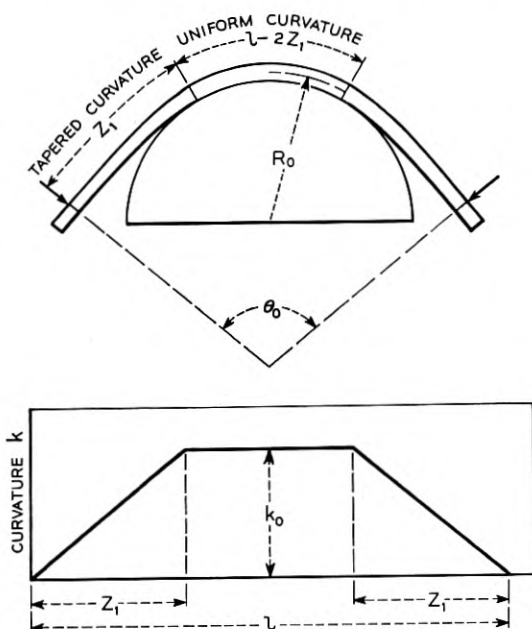

Fig. 1 — Normal mode bend with linear curvature taper.

amplitude is

$$| w_2(z_1) | = \frac{1}{2} \left| \int_0^{z_1} \frac{d\xi}{dz} e^{2\rho(z)} \, dz \right|. \tag{7}$$

This amplitude represents mode conversion loss and therefore has to be kept as small as possible.

In (7) the function $\xi(z)$, i.e., the taper function, is still undetermined. Obviously it can be chosen so as to optimize the taper performance. A taper of optimal design keeps the unwanted mode below a certain value with as short a taper length as possible. From (7) the relation between this optimizing problem and the problem of the transmission line taper of optimal design[4] is at once evident. The transmission line taper is a low reflection transition between lines of different characteristic impedances. To minimize the length of the transition for a specified maximal reflection, the characteristic impedance has to change along the transition according to a function which is essentially the Fourier transform of a Tschebyscheff polynomial of infinite degree. The same procedure can be applied here and it will result in a curvature taper of optimal design.

We are, however, at present not as much interested in a transition of optimal design as in a curvature taper which can easily be built. Suppose we bend the pipe to a bending radius R_o which causes only elastic deformation. We do this on a form of radius R_o, Fig. 1. The forces acting on both ends of the pipe cause a torque and hence a curvature of the pipe which increases approximately linearly from the pipe end ($z = 0$) to the point of contact ($z = z_1$) between pipe and form:

$$k = k_0 \frac{z}{z_1}. \tag{8}$$

The corresponding curve which the pipe forms along the taper is Cornu's spiral.

We shall evaluate (7) for a curvature as given by (8). In considering the mode conversion we may neglect all heat losses, that is $\gamma = j\beta$, etc. With

$$c = c_0 \frac{z}{z_1}, \tag{9}$$

we get

$$\frac{d\xi}{dz} = \frac{2c_0}{\Delta\beta z_1} \frac{1}{1 + 4 \dfrac{c_0^2 z^2}{\Delta\beta^2 z_1^2}}, \tag{10}$$

and

$$\rho(z) = j \frac{\Delta\beta^2 z_1}{4c_0} \left[\frac{c_0 z}{\Delta\beta z_1} \sqrt{1 + 4\left(\frac{c_0 z}{\Delta\beta z_1}\right)^2} + \frac{1}{2} \sinh^{-1} \frac{2c_0 z}{\Delta\beta z_1} \right]. \quad (11)$$

We introduce (10) and (11) into (7) and take advantage of

$$2\left|\frac{c_0}{\Delta\beta}\right| \ll 1, \quad (12)$$

which is satisfied for a gentle enough bend. The unwanted mode level is then given by

$$|w_2(z_1)| = \left| \frac{c_0}{\Delta\beta^2 z_1} (1 - e^{j\Delta\beta z_1}) \right| + 0\left(8 \frac{c_0^3}{\Delta\beta^3} \right). \quad (13)$$

The general restriction (5) for the solution (6) in case of the linear taper is

$$\frac{2c_0}{\Delta\beta^2 z_1} \left(1 + 4 \frac{c_0^2 z^2}{\Delta\beta^2 z_1^2} \right)^{-3/2} \ll 1,$$

and in view of (12) only

$$|\Delta\beta z_1| \geqq 1 \quad (14)$$

is required. The length of the transition has to be of the order or greater than the largest beat wavelength.

In addition to mode conversion loss the normal mode suffers heat loss along the taper. From (3) and (6) this heat loss is given by the real part of $[\gamma z - \rho(z)]$. If $\Delta\beta \gg \Delta\alpha$ we get

$$R[\gamma z - \rho] = \alpha_1 z + \Delta\alpha \int_0^z \frac{c^2}{\Delta\beta^2} dz'. \quad (15)$$

It follows from (15) that the attenuation of the coupled straight guide modes should not be too high for the normal mode bend to work properly.

III. THE TOTAL BEND LOSS

We will consider bends of the dielectric-coated waveguide only. The normal modes of the dielectric-coated waveguide have phase constants which are slightly different from the phase constants of the modes in the plain guide[1]

$$\mathrm{TM}_{nm} \quad \frac{\Delta\beta}{\beta_{nm}} = \frac{\epsilon' - 1}{\epsilon'} \delta,$$

$$\mathrm{TE}_{nm} \atop \text{with } n \neq 0 \quad \frac{\Delta\beta}{\beta_{nm}} = \frac{n^2}{p_{nm}^2 - n^2} \frac{\epsilon' - 1}{\epsilon'(1 - \nu^2)} \delta, \quad (16)$$

$$\mathrm{TE}_{0m} \quad \frac{\Delta\beta}{\beta_{0m}} = \frac{p_{0m}^2}{3} \frac{\epsilon' - 1}{1 - \nu_{0m}^2} \delta^3.$$

The losses in the dielectric coat increase the attenuation constants by:

$$\text{TM}_{nm} \ \frac{\alpha_D}{\beta_{nm}} = \frac{\epsilon''}{\epsilon'^2} \delta,$$

$$\underset{\text{with } n \neq 0}{\text{TE}_{nm}} \ \frac{\alpha_D}{\beta_{nm}} = \frac{n^2}{p_{nm}{}^2 - n^2} \frac{\epsilon''}{\epsilon'^2(1 - \nu_{nm}{}^2)} \delta, \tag{17}$$

$$\text{TE}_{0m} \ \frac{\alpha_D}{\beta_{0m}} = \frac{p_{0m}{}^2}{3} \frac{\epsilon''}{1 - \nu_{0m}{}^2} \delta^3.$$

For the circular electric waves the dielectric coat increases the wall current attenuation by

$$TE_{0m} \ \frac{\Delta\alpha}{\alpha_{0m}} = (\epsilon' - 1) \frac{p_{0m}{}^2}{\nu_{0m}{}^2} \delta^2. \tag{18}$$

The various symbols in (16), (17) and (18) are:

$\beta_{nm} = $ plain guide phase constants of TM_{nm} and TE_{nm} respectively;

$p_{nm} = $ mth root of $J_n(x) = 0$ for TM_{nm}, and mth root of $J_n'(x) = 0$ for TE_{nm} waves respectively;

$\nu_{nm} = \dfrac{\lambda}{\lambda_c} = \dfrac{p_{nm}\lambda}{2\pi a}$ cutoff factor in plain waveguide of radius a;

$\delta = \dfrac{d}{a}$ relative thickness of dielectric coat;

$\epsilon = \epsilon' - j\epsilon''$ relative dielectric permittivity of dielectric coat;

$\alpha_{0m} = $ attenuation constant of TE_{0m} in the plain waveguide.

The coupling coefficient between the straight guide modes in a curved waveguide is $c = c'/R$ in which:[5]

$$\text{TE}_{01} \rightleftarrows \text{TM}_{11} \ c' = 0.18454 \ \beta a,$$

$$\text{TE}_{01} \rightleftarrows \text{TE}_{11} \ c' = \frac{0.09319(\beta a)^2 - 0.84204}{\sqrt{\beta_{01}a\beta_{11}a}} + 0.09319 \ \sqrt{\beta_{01}a\beta_{11}a},$$

$$\text{TE}_{01} \rightleftarrows \text{TE}_{12} \ c' = \frac{0.15575(\beta a)^2 - 3.35688}{\sqrt{\beta_{01}a\beta_{12}a}} + 0.15575 \ \sqrt{\beta_{01}a\beta_{12}a}, \tag{19}$$

$$\text{TE}_{01} \rightleftarrows \text{TE}_{13} \ c' = \frac{0.01376(\beta a)^2 - 0.60216}{\sqrt{\beta_{01}a\beta_{13}a}} + 0.01376 \ \sqrt{\beta_{01}a\beta_{13}a},$$

where $\beta = $ free-space phase constant.

We consider the bend configuration of Fig. 1, with the curvature being a trapezoidal function of length. The maximum power loss due to conversion to one of the unwanted modes in the first transition is, by (13),

$$\mid w_2(z_1) \mid^2_{\max} = \frac{4}{(\Delta\beta z_1)^2} \frac{c_0{}^2}{\Delta\beta^2}.$$

By the law of reciprocity the same conversion loss occurs in the second transition. Both conversion parts phase with each other. To get an average total conversion we may add them in quadrature and the total conversion loss to one of the unwanted modes is, expressed in nepers,

$$A_c = \frac{4}{(\Delta\beta z_1)^2} \frac{c_0^2}{\Delta\beta^2}. \tag{20}$$

Under most unfavorable phase conditions the conversion loss may be twice this value, but it is very unlikely that such phase conditions will be satisfied for all coupled modes simultaneously.

Besides mode conversion loss the local normal mode suffers attenuation in the bend. This attenuation is larger than the straight guide attenuation. Each straight guide mode contained in the local normal mode of the bend causes an increase in attenuation. From (15) the loss caused by one of these straight guide modes is:

$$A_b = (\alpha_{1m} - \alpha_{01}) \int_0^l \frac{c^2}{\Delta\beta^2} \, dz. \tag{21}$$

Where α_{1m} is the attenuation constant of the TE_{1m} and TM_{11} waves respectively in the dielectric coated waveguide.

Introducing the trapezoidal curvature function of Fig. 1 into (21) we get

$$A_b = \frac{c_0^2}{\Delta\beta^2} (\alpha_{1m} - \alpha_{01}) \left(l - \frac{4}{3} z_1 \right). \tag{22}$$

The loss caused by the TE_{01} attenuation in the straight dielectric coated guide is from (17) and (18)

$$A_s = \alpha_{01} l \left[1 + (\epsilon - 1) \frac{p_{0m}^2}{\nu_{0m}^2} \delta^2 \right] + \frac{p_{01}^2}{3} \frac{\epsilon'' \beta_{01}}{1 - \nu_{01}^2} \delta^3 l. \tag{23}$$

The total bend loss is finally obtained by summing up all the terms of (20), (22), and (23),

$$A = A_s + \sum A_b + \sum A_c. \tag{24}$$

The summation signs indicate that all coupled modes (TM_{11} and TE_{1m}) have to be taken into account.

The effectiveness of the normal mode bend is best demonstrated by a practical example. A copper pipe now in experimental use at Bell Telephone Laboratories for circular electric wave transmission near 5.4 mm wavelength has 2-inch I. D. and $2\frac{3}{8}$-inch O.D. Suppose we want to change the direction of a waveguide line with this copper pipe bn an angle θ_0. We can do this most easily by inserting a dielectric-coated section, which

is bent around a fixed support in the center by forces acting on both ends. In order not to exceed elastic deformation the bending radius must not be smaller than

$$R_{\min} = \frac{E}{f_{\max}} a_1,$$ (25)

where $f_{\max} =$ flexural stress at elastic limit,
  $E =$ modulus of elasticity,
  $a_1 =$ outside radius of pipe.

This minimum bending radius requires a minimum length to change the pipe direction by a specified angle θ_0 given by

$$l_{\min} = 2\theta_0 R_{\min}.$$ (26)

The total bend loss (24) has been evaluated for a bend configuration as specified by (25) and (26). The result is shown in Fig. 2. The total additional bend loss is only of the order of the TE_{01} loss in the plain straight waveguide. For small bending angles the curvature taper becomes shorter and consequently the mode conversion loss increases. The mode conversion loss, however, does not go to infinity for zero bending angle. In this case (14) is no longer satisfied, and the mode conversion loss is no longer described by (20).

The level of the various unwanted modes which can be calculated from (20) is plotted in Fig. 2.

For a practical waveguide one would decide on a standard length of dielectric-coated pipe, one or several of which would be inserted whenever a change in direction has to be made. Take, in our example, a standard length of 15 feet. With one such section a change of direction up to 15° could be made. For a change in direction up to 30° two such sections would have to be inserted and bent around a fixed support at the center joint. The total loss of Fig. 2 is then a maximum value, which would only occur when the pipe is bent to the highest allowable bending angle.

IV. A NORMAL MODE BEND OF OPTIMUM DESIGN

The various terms of the total bend loss (24) depend on the bend geometry in quite different ways. It is therefore likely that for a given bending angle θ_0 a bend geometry can be found, which minimizes the total bend loss. The total bend loss can generally be written as:

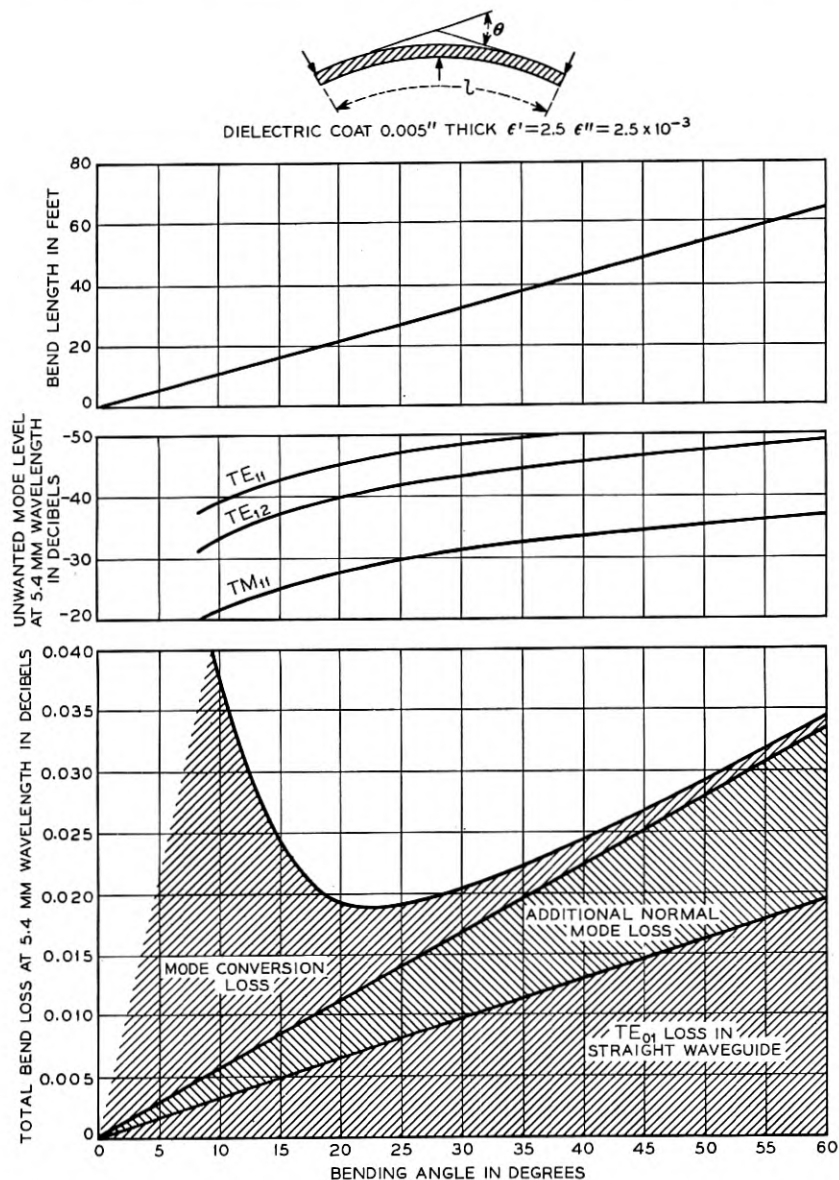$$A = Sl + B \frac{1 - \frac{4}{3} u}{l(1 - u)^2} + C \frac{1}{l^4(u - u^2)^2},$$ (27)

Fig. 2 — Normal mode bend. Dielectric-coated copper pipe with 2-inch I.D. and $2\frac{3}{8}$-inch O.D. deflected to limit of elastic deformation ($\lambda = 5.4$ mm).

in which

$$S = \alpha_{01}\left[1 + (\epsilon' - 1)\frac{p_{01}^2}{\nu_{01}^2}\delta^2\right] + \frac{p_{01}^2}{3}\frac{\epsilon''\beta_{01}}{1 - \nu_{01}^2}\delta^3,$$

$$B = \Sigma\frac{c'^2}{\Delta\beta^2}\theta_0^2(\alpha_{1m} - \alpha_{01}),$$

$$C = \Sigma\frac{c'^2}{\Delta\beta^4}\theta_0^2,$$

(28)

$$u = \frac{z_1}{l}.$$

Here again the summation signs indicate that all coupled modes have to be taken into account. The factors S, B, and C do not depend on the bend geometry, but only on the total bending angle, the waveguide properties, and the frequency. Necessary conditions for $A(u, l)$ to be a minimum are:

$$\frac{\partial A}{\partial u} \equiv \frac{2(1 - 2u)}{l(1 - u^3)}\left[\frac{B}{3} - \frac{C}{l^3 u^3}\right] = 0,$$

(29)

with the two roots

$$u = \frac{1}{2},$$

(30)

$$ul = \left(3\frac{C}{B}\right)^{\frac{1}{3}},$$

(31)

and

$$\frac{\partial A}{\partial l} \equiv S - B\frac{1 - \frac{4}{3}u}{(1 - u)^2}\frac{1}{l^2} - \frac{4C}{(u - u^2)^2}\frac{1}{l^5} = 0.$$

(32)

If $u = \frac{1}{2}$, the solutions of (32) are the roots of

$$S\,l^5 - \frac{4}{3}B\,l^3 - 64C = 0.$$

(33)

If $(lu)^3 = 3(C/B)$, the solutions of (32) are the roots of

$$l = \left(3\frac{C}{B}\right)^{\frac{1}{3}} \pm \left(\frac{B}{S}\right)^{\frac{1}{2}}.$$

(34)

Sufficient conditions for $A(u, l)$ to be a minimum are:

$$\frac{\partial^2 A}{\partial u^2}\frac{\partial^2 A}{\partial l^2} - \left(\frac{\partial^2 A}{\partial u\partial l}\right)^2 > 0,$$

(35)

$$\frac{\partial^2 A}{\partial u^2} > 0, \qquad \frac{\partial^2 A}{\partial l^2} > 0,$$

(36)

If $u = \frac{1}{2}$, we have:

$$\frac{\partial^2 A}{\partial u \partial l} \equiv 0,$$

$$\frac{\partial^2 A}{\partial l^2} = \frac{8}{l^3}\left(\frac{B}{3} + 40\,\frac{C}{l^3}\right), \tag{37}$$

$$\frac{\partial^2 A}{\partial u^2} = \frac{32}{l}\left(8\,\frac{C}{l^3} - \frac{B}{3}\right).$$

Substituting

$$x = \frac{1}{2}\left(\frac{S}{B}\right)^{\frac{1}{4}} l,$$

$$r = \left(3\,\frac{C}{B}\right)^{\frac{1}{4}}\left(\frac{S}{B}\right)^{\frac{1}{4}}, \tag{38}$$

we get instead of (33)

$$x^3(3x^2 - 1) - 2r^3 = 0, \tag{39}$$

and instead of (37)

$$\frac{\partial^2 A}{\partial u^2} = 16\,\frac{B}{l}\,(x^2 - 1).$$

The positive root of (39) is plotted in Fig. 3. It follows that if $r > 1$ we have $x > 1$, consequently $\partial^2 A/\partial u^2 > 0$; and if $r < 1$ we have $x < 1$, consequently $\partial^2 A/\partial u^2 < 0$. Consequently if, and only if, $r > 1$ the values $u = \frac{1}{2}$ and x from Fig. 3 minimize the total bend loss A.
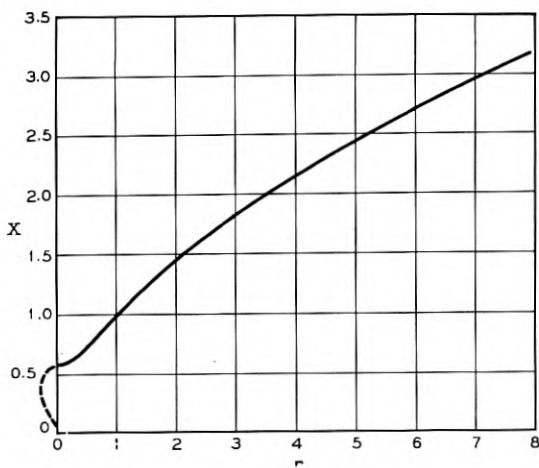

Fig. 3 — Positive root of $x^3(3x^2 - 1) - 2r^3 = 0$.

If $(ul)^3$ is equal to $3(C/B)$,

$$\frac{\partial^2 A}{\partial u^2}\frac{\partial^2 A}{\partial l^2} - \left(\frac{\partial^2 A}{\partial u \partial l}\right)^2 \equiv \frac{4B^2}{l^4 u}\frac{1-2u}{(1-u)^6},$$

and

$$\frac{\partial^2 A}{\partial u^2} \equiv \frac{2B}{lu}\frac{1-2u}{(1-u)^3}.$$

Hence, if $u < \frac{1}{2}$ or, because of (31) and (34) $r < 1$, a minimum of $A(u, l)$ is located at

$$(ul)^3 = 3\frac{C}{B}, \qquad l = \left(3\frac{C}{B}\right)^{\frac{1}{3}} + \left(\frac{B}{S}\right)^{\frac{1}{3}}.$$
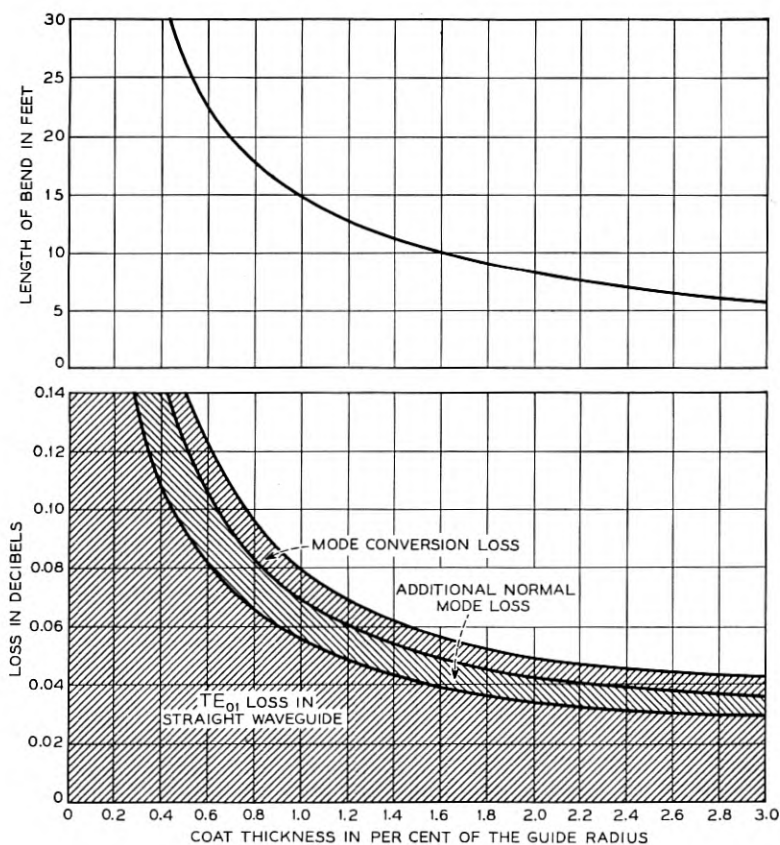

Fig. 4 — 90° normal mode bend of $\frac{7}{8}$-inch I.D. copper pipe with a dielectric coat of $\epsilon' = 2.5$, $\epsilon'' = 2.5 \times 10^{-3}$. Optimum design for 5.4-mm wavelength.

To find the optimum bend geometry for a given dielectric coated guide and a specified bending angle we calculate r from (38). If $r > 1$ the optimum geometry is

$$l = 2 \sqrt{\frac{B}{S}}\, x \quad \text{and} \quad z_1 = \sqrt{\frac{B}{S}}\, x$$

with x from Fig. 3. If $r < 1$,

$$l = \left(3\frac{C}{B}\right)^{\frac{1}{4}} + \left(\frac{B}{S}\right)^{\frac{1}{2}}, \quad \text{and} \quad z_1 = \left(3\frac{C}{B}\right)^{\frac{1}{4}}.$$

A numerical example, the 90° bend of a $\frac{7}{8}$-inch I. D. copper pipe, is shown in Fig. 4. The total bend loss in the optimally designed bend decreases steadily with increasing thickness of the dielectric coat. This indicates that there is also an optimum coat thickness, which minimizes the total loss of the normal mode bend of optimum total length and taper length. Unfortunately, however, several approximations made in calculating phase constants and coupling coefficients in the dielectric-coated
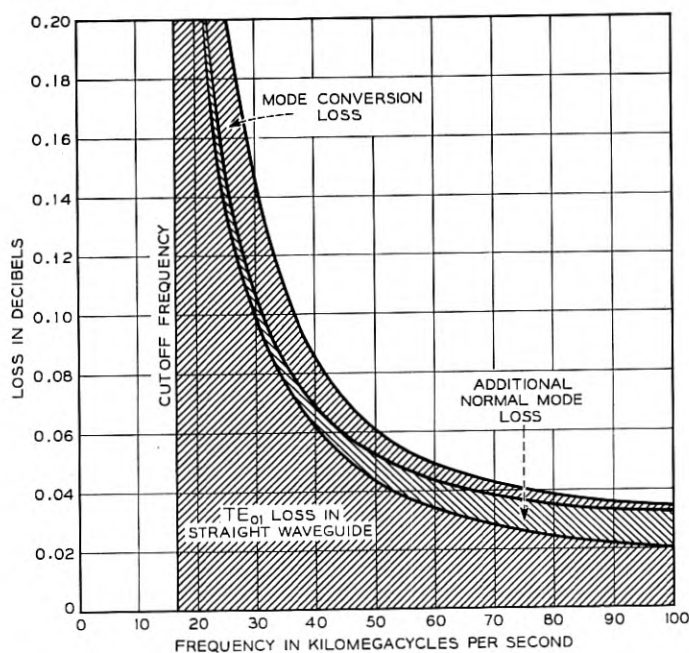

Fig. 5 — 90° normal mode bend of $\frac{7}{8}$-inch I.D. copper pipe with a dielectric coat 0.0075 inch thick ($\epsilon' = 2.5$, $\epsilon'' = 2.5 \times 10^{-3}$), designed for optimum performance at $\lambda = 5.4$ mm (55.5 kmc).

waveguide usually break down at smaller than optimum values of the coat thickness.

It should be mentioned finally that the normal mode bend is an inherently broad band device. Except for the oscillations of the mode conversion portion of the total loss as caused by spurious mode phasing, there is only a gradual change of the loss with frequency.

Some terms contributing to the total loss decrease with frequency, others increase. The over-all frequency dependence is of the same order as the frequency dependence of the loss in the straight waveguide. As an example, in Fig. 5 the bend loss has been plotted versus frequency for the normal mode bend of Fig. 4.

ACKNOWLEDGMENT

REFERENCES

1. H. G. Unger, Circular Electric Wave Transmission in the Dielectric Coated Waveguide, pp. 1253–1278, this issue.
2. S. E. Miller, Coupled Wave Theory and Waveguide Applications, B.S.T.J., 33, pp. 661–719, May, 1954.
3. W. H. Louisell, Analysis of the Single Tapered Mode Coupler, B.S.T.J., 34, pp. 853–870, July, 1955.
4. R. W. Klopfenstein, A Transmission Line Taper of Improved Design, Proc. I.R.E., 44, pp. 31–35, January, 1956.
5. S. P. Morgan, Theory of Curved Circular Waveguide Containing an Inhomogeneous Dielectric, pp. 1209–1251, this issue.

Bell System Technical Papers Not Published in This Journal

ASHKIN, A.[1]

Electron Beam Analyzer, J. Appl. Phys., **28,** p. 564, May, 1957.

BECK, A. C.[1]

Communications Superhighways, Trans. I.R.E., **PGMTT, MTT-5,** pp. 81–82, April, 1957.

BECKER, G. E.[1]

Dependence of Magnetron Operation on the Radial Centering of the Cathode, Trans. I.R.E., **PGED, ED-4,** pp. 126–131, April, 1957.

BOOTHBY, O. L., see Williams, H. J.

BOWERS, F. K.[1]

What Use is Delta Modulation to the Transmission Engineer? Commun. & Electronics, **30,** pp. 142–147, May, 1957.

BROWN, S. C., see Rose, D. J.

BROYER, A. P., see Schlabach, T. D.

BUCK, T. M.,[1] and McKIM, F. S.[1]

Experiments on the Photomagnetoelectric Effect in Germanium. Phys. Rev., **106,** pp. 904–909, June 1, 1957.

BUEHLER, E.[1]

Contribution to the Floating Zone Refining of Silicon, Rev. Sci. Instr., **28,** pp. 453–460, June, 1957.

CHILBERG, G. L.[2]

Buried Cable Telephone Systems, Commun. & Electronics, **30,** pp. 130–135, May, 1957.

---

[1] Bell Telephone Laboratories, Inc.
[2] American Telephone and Telegraph Company.

CHYNOWETH, A. G.,[1] and McKAY, K. G.[1]

Internal Field Emission in Silicon P-N Junctions, Phys. Rev., **106,** pp. 418–426, May 1, 1956.

CLEMENCY, W. F.,[1] ROMANOW, F. F.,[1] and ROSE, A. F.[2]

The Bell System Speakerphone, Commun. & Electronics, **30,** pp. 148–153, May, 1957.

COMPTON, K. G.[1]

Variability in Working Copper Sulfate Half Cells, Corrosion, **13,** pp. 19–20, March, 1957.

COWAN, F. A.[2]

Transmission of Color Over Nationwide Television Networks, S.M.P.T.E., **66,** pp. 278–283, May, 1957.

DRENICK, R.[1]

An Operational View of Equipment Reliability, Trans. Annual Convention, Am. Soc. Quality Control, **11,** pp. 603–611, May 22, 1957.

EASLEY, J. W.[1]

The Effect of Collector Capacity on the Transient Response of Junction Transistors, Trans. I.R.E., **PGED, ED-4,** pp. 6–14, Jan., 1957.

EMLING, J. W.[1]

General Aspects of Hands-Free Telephony, Commun. & Electronics, **30,** pp. 201–205, May, 1957.

FAGEN, R. E., see Hall, A. D.

FELDMANN, W. L., see Pearson, G. L.

FORD, B. W.[5]

Demand Increasing for Special Uses of Telephone Facilities, Telephony, **152,** pp. 22–24, 44, 48, June 8, 1957.

FREERICKS, L.[1]

Semiconductors in Switching Circuits, General Engineering Bulletin (N. Y. Tel. Co.), **7,** pp. 21–25, May, 1957.

---

[1] Bell Telephone Laboratories, Inc.
[2] American Telephone and Telegraph Company.
[5] Illinois Bell Telephone Company, Chicago.

FREUDENSTEIN, F.,[1] WARTHMAN, K. L.,[1] and WATROUS, A. B.[1]

Designing Gear-Train Limit Stops for Control of Shaft Rotation, Machine Design, **11,** pp. 84–86, May 30, 1957.

GALT, J. K.[1]

Losses in Ferrites — Single Crystal Studies, J. Inst. Elec. Engrs. (London), **104,** pp. 189–197, June, 1957.

GELLER, S.[1]

Comments on Pauling's Paper on Effective Metallic Radii for Use in the β-Wolfram Structure, Acta Cryst., **10,** pp. 380–382, May 10, 1957.

GERARD, H. B.[1]

Some Effects of Status, Role Clarity and Group Goal Clarity Upon the Individual's Relations to Group Process, J. Personality, **25,** pp. 475–488, June, 1957.

GREEN, E. I.[1]

Evaluating Scientific Personnel, Elec. Engg., **76,** pp. 578–584, July, 1957.

GUPTA, S. S.,[1] HUYETT, M. J.,[1] and SOBEL, M.[1]

Selection and Ranking Problems with Binomial Populations, Trans. Annual Convention, Am. Soc. Quality Control, **11,** pp. 635–718, May 22, 1957.

HAKE, E. A.[1]

A 10-Kw Germanium Rectifier for Automatic Power Plants, A.I.E.E. Conf. Publication "Rectifiers in Industry", **T-93,** p. 119, June, 1957.

HALL, A. D.,[1] and FAGEN, R. E.[1]

Definition of System, Yearbook Soc. Advancement of General Systems Theory, **1,** pp. 18–28, April, 1957.

HARKER, K. J.[1]

Non-Laminar Flow in Cylindrical Electron Beams, J. Appl. Phys., **28,** pp. 645–650, June, 1957.

HENNESSEY, T. M.[6]

A Dial Service and Community Relationships. Telephony, **152,** pp. 22–24, 40, June 1, 1957.

---

[1] Bell Telephone Laboratories, Inc.
[6] New England Telephone and Telegraph Company, Boston, Mass.

HERRMANN, G.[1]

Transverse Scaling of Electron Beams, J. Appl. Phys., **28,** pp. 474–478, April, 1957.

HUYETT, M. J., see Gupta, S. S.

LEVENBACH, G. J.[1]

Accelerated Life Testing of Capacitors, Trans. I.R.E., **PGRQC, RQC-10,** pp. 9–20, June, 1957.

LLOYD, S. M.[3]

A New Water Rheostat for Testing Exchange Power Plants, Telephony, **152,** pp. 32–34, May 25, 1957.

LUMSDEN, G. Q.[1]

Wood Poles for Communication Lines, A.S.T.M. Bulletin, **222,** pp. 19–24, May, 1957.

McCALL, D. W.[1]

Cell for the Determination of Pressure Coefficients of Dielectric Constant and Loss of Liquids and Solids to 10,000 psi, Rev. Sci. Instr., **28,** pp. 345–351, May, 1957.

McCALL, D. W., see Slichter, W. P.

McKAY, K. G., see Chynoweth, A. G.

McKIM, F. S., see Buck, T. M.

McSKIMIN, H. J.[1]

Use of High Frequency Ultrasound for Determining the Elastic Moduli of Small Specimens, Proc. National Electronics Conf., **12,** pp. 351–362, April 15, 1957.

MILLER, W. A.[7]

A Narrow-Band Experimental FM Mobiletelephone System, Commun. & Electronics, **30,** pp. 98–100, May, 1957.

MONTGOMERY, H. C.[1]

Field Effect in Germanium at High Frequencies, Phys. Rev., **106,** pp. 441–445, May 1, 1957.

[1] Bell Telephone Laboratories, Inc.
[3] Western Electric Company, Inc.
[7] Pacific Telephone and Telegraph Company, Los Angeles, Calif.

O'BRIEN, J. A.[1]

Unit Distance Binary-Decimal Code Translators, Trans. I.R.E., PGEC, EC-6, pp. 122–123, June, 1957, Letter to the Editor.

PEARSON, G. L.,[1] READ, W. T., JR.,[1] and FELDMANN, W. L.[1]

Deformation and Fracture of Small Silicon Crystals, Acta Met., 5, pp. 181–191, April, 1957.

PEDERSON, C. W.[1]

Crystal Clock for Airborne Computer, Electronics, 30, pp. 196–198, June 1, 1957.

READ, W. T., JR., see Pearson, G. L.

RIDER, D. K., see Schlabach, T. D.

ROMANOW, F. F., see Clemency, W. F.

ROSE, A. F., see Clemency, W. F.

ROSE, D. J.,[1] and BROWN, S. C.[4]

Microwave Gas Discharge Breakdown in Air, Nitrogen, and Oxygen, J. Appl. Phys., 28, pp. 561–563, May, 1957.

SCHLABACH, T. D.,[1] WRIGHT, E. E.,[1] BROYER, A. P.,[1] and RIDER, D. K.[1]

Testing of Foil-Clad Laminates for Printed Circuitry, Bull A.S.T.M., 222, pp. 25–30, May, 1957.

SHENITZER, A.[1]

On the Problem of Chebyshev Approximation of a Continuous Function by a Class of Functions, J. Assoc. Computing Machinery, 4, pp. 30–35, Jan., 1957.

SHERWOOD, R. C., see Williams, H. J.

SNOKE, L. R.[1]

Some Needed Basic Research on Wood Deterioration Problems, Appl. Microbiology, 5, pp. 188–193, May, 1957.

SOBEL, M., see Gupta, S. S.

---

[1] Bell Telephone Laboratories, Inc.
[4] Massachusetts Institute of Technology, Cambridge.

VAN UITERT, L. G.[1]

Effects of Annealing on the Saturation Induction of Ferrites Containing Nickel and/or Copper, J. Appl. Phys., **28,** pp. 478–481, April, 1957.

WARTHMAN, K. L., see Freudenstein, F.

WATROUS, A. B., see Freudenstein, F.

WHITTEMORE, L. E.[2]

The Institute of Radio Engineers — Forty-five Years of Service, Proc. I.R.E., **45**, pp. 597-635, May, 1957.

WILLIAMS, H. J.,[1] and SHERWOOD, R. C.[1]

Magnetic Domain Patterns on Thin Films, J. Appl. Phys., **28,** pp. 548–555, May, 1957.

WILLIAMS, H. J.,[1] SHERWOOD, R. C.[1] and BOOTHBY, O. L.[1]

Magnetostriction and Magnetic Anisotropy of MnBi, J. Appl. Phys., **28,** pp. 445–447, April, 1957.

WRIGHT, E. E., see Schlabach, T. D.

[1] Bell Telephone Laboratories, Inc.
[2] American Telephone and Telegraph Company.

Recent Monographs of Bell System Technical Papers Not Published in This Journal*

BENNETT, W. R.

Synthesis of Active Networks, Monograph 2816.

DEWALD, J. F.

Formation of Anode Films on Single-Crystal Indium Antomonide, Monograph 2802.

DITZENBERGER, J. A., see Fuller, C. S.

EIGLER, J. H., see Sullivan, M. V.

* Copies of these monographs may be obtained on request to the Publication Department, Bell Telephone Laboratories, Inc., 463 West Street, New York 14, N. Y. The numbers of the monographs should be given in all requests.

VAN UITERT, L. G.[1]

Effects of Annealing on the Saturation Induction of Ferrites Containing Nickel and/or Copper, J. Appl. Phys., **28,** pp. 478–481, April, 1957.

WARTHMAN, K. L., see Freudenstein, F.

WATROUS, A. B., see Freudenstein, F.

WHITTEMORE, L. E.[2]

The Institute of Radio Engineers — Forty-five Years of Service, Proc. I.R.E., **45,** pp. 597-635, May, 1957.

WILLIAMS, H. J.,[1] and SHERWOOD, R. C.[1]

Magnetic Domain Patterns on Thin Films, J. Appl. Phys., **28,** pp. 548–555, May, 1957.

WILLIAMS, H. J.,[1] SHERWOOD, R. C.[1] and BOOTHBY, O. L.[1]

Magnetostriction and Magnetic Anisotropy of MnBi, J. Appl. Phys., **28,** pp. 445–447, April, 1957.

WRIGHT, E. E., see Schlabach, T. D.

[1] Bell Telephone Laboratories, Inc.
[2] American Telephone and Telegraph Company.

Recent Monographs of Bell System Technical Papers Not Published in This Journal*

BENNETT, W. R.

Synthesis of Active Networks, Monograph 2816.

DEWALD, J. F.

Formation of Anode Films on Single-Crystal Indium Antomonide, Monograph 2802.

DITZENBERGER, J. A., see Fuller, C. S.

EIGLER, J. H., see Sullivan, M. V.

* Copies of these monographs may be obtained on request to the Publication Department, Bell Telephone Laboratories, Inc., 463 West Street, New York 14, N. Y. The numbers of the monographs should be given in all requests.

FLASCHEN, S. S., see Garn, P. D.

FULLER, C. S., and DITZENBERGER, J. A.
Effect of Defects in Germanium on Diffusion and Acceptance of Copper, Monograph 2803.

FULLER, C. S., and MORIN, F. J.
Diffusion and Electrical Behavior of Zinc in Silicon, Monograph 2789.

GARN, P. D., and FLASCHEN, S. S.
Analytical Applications of a Differential Thermal Analysis Apparatus, Monograph 2769.

GEBALLE, T. H., see Kunzler, J. E.

GEBALLE, T. H., see Morin, F. J.

GOHN, G. R., see Torrey, M. N.

GOULD, H. L. B., and WENNY, D. H.
Supermendur: A New Rectangular-Loop Magnetic Material, Monograph 2780.

GREEN, E. I.
Nature's Pulses, Monograph 2770.

GREEN, E. I.
Science and Liberal Education, Monograph 2765.

GREEN, E. I.
Telephone, Monograph 2806.

HAGSTRUM, H. D.
Auger Ejection of Electrons from Tungsten by Noble Gas Ions, Monograph 2715.

HAGSTRUM, H. D.
Effect of Monolayer Adsorption on Ejection of Electrons from Metals, Monograph 2804.

HAGSTRUM, H. D.

Thermionic Constants and Sorption Properties of Hafnium, Monograph 2790.

HERRING, C., see Morin, F. J.

HULL, G. W., see Kunzler, J. E.

KLEMM, G. H.

Automatic Protection Switching for TD-2 Radio System, Monograph 2772.

KOHN, W.

Effective Mass Theory in Solids from a Many-Particle Standpoint, Monograph 2791.

KUNZLER, J. E., GEBALLE, T. H., and HULL, G. W.

Germanium Resistance Thermometers Suitable for Low-Temperature Calorimetry, Monograph 2792.

LLOYD, S. P., and McMILLAN, B.

Linear Least Squares Filtering and Prediction of Sampled Signals, Monograph 2815.

LUNDBERG, C. V., see Vacca, G. N.

McMILLAN, B., see Lloyd, S. P.

MENDIZZA, A.

Standard Salt-Spray Test — Is It A Valid Acceptance Test?, Monograph 2807.

MESZAR, J.

Full Stature of the Crossbar Tandem Switching System, Monograph 2750.

MILLER, S. L.

Ionization Rates for Holes and Electrons in Silicon, Monograph 2794.

MORIN, F. J., see Fuller, C. S.

MORIN, F. J., GEBALLE, T. H., and HERRING, C.

Temperature Dependence of Piezoresistance of High-Purity Silicon, Germanium, Monograph 2797.

MORIN, F. J., and REISS, H.

Formation of Ion Pairs and Triplets Between Lithium and Zinc in Germanium, Monograph 2795.

REISS, H., see Morin, F. J.

ROSE, D. J.

Microplasmas in Silicon, Monograph 2796.

SMITH, K. D., see Veloric, H. S.

SUHL, H.

Theory of Ferromagnetic Resonance at High Signal Powers, Monograph 2817.

SULLIVAN, M. V., and EIGLER, J. H.

Electroless Nickel Plating for Making Ohmic Contacts to Silicon, Monograph 2808.

SULLIVAN, M. V., and EIGLER, J. H.

Five Metal Hydrides as Alloying Agents on Silicon, Monograph 2775.

TORREY, M. N., and GOHN, G. R.

A Study of Statistical Treatments of Fatigue Data, Monograph 2778.

VACCA, G. N., and LUNDBERG, C. V.

Aging of Neoprene in a Weatherometer, Monograph 2809.

VAN HORN, R. H.

Experimental Evaluation of Reliability of Solderless Wrapped Connections, Monograph 2810.

VELORIC, H. S., and SMITH, K. D.

Silicon Diffused Junction "Avalanche" Diodes, Monograph 2811.

VOGEL, F. L., JR.

Dislocations in Plastically Bent Germanium Crystals, Monograph 2763.

WEBER, L. A.

Influence of Noise on Telephone Signaling Circuit Performance, Monograph 2812.

WEIBEL, E. S.

An Electronic Analog Multiplier Using Carriers, Monograph 2813.

WENNY, D. H., see Gould, H. L. B.

YOUNKER, E. L.

A Transistor-Driven Magnetic-Core Memory, Monograph 2814.

Contributors to This Issue

C. H. ELMENDORF, B.S., California Institute of Technology, 1935; M.S., 1936; Bell Telephone Laboratories, 1936–. Mr. Elmendorf was concerned with the development of coaxial cable transmission systems from 1936 to 1955, except for the period from 1941–1945 when he worked on airborne radar systems. In 1952 he started an exploratory program on submarine cable systems. As Assistant Director of Transmission Systems Development since 1955, he has been responsible for development of submarine cable systems. He is a senior member of the I.R.E.

BRUCE C. HEEZEN, B.A., University of Iowa, 1948; M.A., Columbia University, 1952; Ph.D. 1956. After participating in a cruise of the Woods Hole research vessel *Atlantis* in the summer of 1948, Mr. Heezen held a fellowship in geology at Columbia, where he joined the staff of the Lamont Geological Observatory when it was founded in 1949. As submarine geologist, and now as senior scientist in charge of the submarine geology program, he has been a member of numerous deep-sea expeditions. In addition, he teaches a graduate course in submarine geology on the Columbia campus. His work includes deep-sea topography, sediments, and sedimentation processes; submarine photography and deep-sea research instrumentation; and geologic, geophysical, and oceanographic exploration of the deep sea.

VOGEL, F. L., JR.

Dislocations in Plastically Bent Germanium Crystals, Monograph 2763.

WEBER, L. A.

Influence of Noise on Telephone Signaling Circuit Performance, Monograph 2812.

WEIBEL, E. S.

An Electronic Analog Multiplier Using Carriers, Monograph 2813.

WENNY, D. H., see Gould, H. L. B.

YOUNKER, E. L.

A Transistor-Driven Magnetic-Core Memory, Monograph 2814.

Contributors to This Issue

C. H. ELMENDORF, B.S., California Institute of Technology, 1935; M.S., 1936; Bell Telephone Laboratories, 1936–. Mr. Elmendorf was concerned with the development of coaxial cable transmission systems from 1936 to 1955, except for the period from 1941–1945 when he worked on airborne radar systems. In 1952 he started an exploratory program on submarine cable systems. As Assistant Director of Transmission Systems Development since 1955, he has been responsible for development of submarine cable systems. He is a senior member of the I.R.E.

BRUCE C. HEEZEN, B.A., University of Iowa, 1948; M.A., Columbia University, 1952; Ph.D. 1956. After participating in a cruise of the Woods Hole research vessel *Atlantis* in the summer of 1948, Mr. Heezen held a fellowship in geology at Columbia, where he joined the staff of the Lamont Geological Observatory when it was founded in 1949. As submarine geologist, and now as senior scientist in charge of the submarine geology program, he has been a member of numerous deep-sea expeditions. In addition, he teaches a graduate course in submarine geology on the Columbia campus. His work includes deep-sea topography, sediments, and sedimentation processes; submarine photography and deep-sea research instrumentation; and geologic, geophysical, and oceanographic exploration of the deep sea.

SAMUEL P. MORGAN, B.S., 1943; M.S. and Ph.D., 1947, California Institute of Technology; Bell Telephone Laboratories, 1947–. A research mathematician, Mr. Morgan has been concerned with the application of electromagnetic theory to microwave problems, and has also made studies in other fields of mathematical physics. Member American Physical Society, Tau Beta Pi, Sigma Xi and I.R.E.

LLOYD R. SNOKE, B.S. in For., 1948, Pennsylvania State University; Bell Telephone Laboratories, 1948–. Since joining the Laboratories, Mr. Snoke has specialized in the timber products used in the Bell System and their preservative treatment. He has been specifically engaged in the study of timber treatment theory, the application of radioactive isotopes to fundamental problems and the bioassay of wood preservatives. For the past four years Mr. Snoke has been concerned with microbiological testing of materials including laboratory bacteriological studies and actual marine tests. He heads the Environmental Protection Group of the Outside Plant Development Department. Member American Association for the Advancement of Science, the Society for Industrial Microbiology, American Wood Preservers' Association, American Society for Testing Materials, Materials Advisory Board — Technical Panel on Miscellaneous Materials, Steering Committee of Microbiological Deterioration Section — Gordon Research Conferences and Zi Sigma Pi.

HANS-GEORG UNGER, Dipl. Ing., 1951, Dr. Ing., 1954, Technische Hochschule Braunschweig (Germany); Bell Telephone Laboratories 1956–. Mr. Unger's work at the Laboratories has been in waveguides, especially circular electric wave transmission. He holds several foreign patents on waveguides and has published in German technical magazines. Member I.R.E.

E. E. ZAJAC, B.M.E., 1950, Cornell University; M.S.E., 1952, Princeton University; Ph.D., 1954, Stanford University; Bell Telephone Laboratories, 1954–. Since joining the Laboratories, Mr. Zajac's work has been in theoretical and applied mechanics in the Mathematical Research Department. Member of the American Society of Mechanical Engineers, Tau Beta Pi, Pi Tau Sigma, Phi Kappa Phi and Sigma Xi.